

CRITERION-III
EVIDENCE(S), AS PER SOP

METRIC No. 3.7.1	Number of collaborative activities with other institutions/ research establishment/industry for research and academic development of faculty and students per year
<ul style="list-style-type: none">• Copies of documents indicating the collaboration/related documents indicating the nature of collaboration and activities year-wise	

Review

Allantoin: A Potential Compound for the Mitigation of Adverse Effects of Abiotic Stresses in Plants

Rasleen Kaur¹, Jipsi Chandra², Bobby Varghese^{3,*} and S. Keshavkant¹ 

¹ School of Studies in Biotechnology, Pt. Ravishankar Shukla University, Raipur 492 010, India; rasleen.kaur000@gmail.com (R.K.); skeshavkant@gmail.com (S.K.)

² Center for Basic Sciences, Pt. Ravishankar Shukla University, Raipur 492 010, India; jipsi.biotech@gmail.com

³ Centre for Academic Success in Science and Engineering, University of KwaZulu-Natal, Durban 4001, South Africa

* Correspondence: varghese@ukzn.ac.za

Abstract: Stress-induced alterations vary with the species of plants, the intensity and duration of the exposure, and stressors availability in nature or soil. Purine catabolism acts as an inherent defensive mechanism against various abiotic stresses and plays a pivotal role in the stress acclimatisation of plants. The intermediate metabolite of purine catabolism, allantoin, compensates for soil nitrogen deficiency due to the low carbon/nitrogen ratio, thereby maintaining nitrogen homeostasis and supporting plant growth and development. Allantoin accounts for 90% of the total nitrogenous compound in legumes, while it contributes only 15% in non-leguminous plants. Moreover, studies on a variety of plant species have reported the differential accumulation of allantoin in response to abiotic stresses, endowing allantoin as a stress modulator. Allantoin functions as signalling molecule to stimulate stress-responsive genes (*P5CS*; pyrroline-5-carboxylase synthase) and ROS (reactive oxygen species) scavenging enzymes (antioxidant). Moreover, it regulates cross-talk between the abscisic acid and jasmonic acid pathway, and maintains ion homeostasis by increasing the accumulation of putrescine and/or spermine, consequently enhancing the tolerance against stress conditions. Further, key enzymes of purine catabolism (xanthine dehydrogenase and allantoinase) have also been explored by constructing various knockdown/knockout mutant lines to decipher their impact on ROS-mediated oxidative injury in plants. Thus, it is established that allantoin serves as a regulatory signalling metabolite in stress protection, and therefore a lower accumulation of allantoin also reduces plant stress tolerance mechanisms. This review gives an account of metabolic regulation and the possible contribution of allantoin as a photo protectant, osmoprotectant, and nitrogen recycler to reduce abiotic-stress-induced impacts on plants.

Keywords: abscisic acid; allantoin; antioxidants; mutants; reactive oxygen species; ureide metabolism



Citation: Kaur, R.; Chandra, J.; Varghese, B.; Keshavkant, S.

Allantoin: A Potential Compound for the Mitigation of Adverse Effects of Abiotic Stresses in Plants. *Plants* **2023**, *12*, 3059. <https://doi.org/10.3390/plants12173059>

Academic Editor: Ferenc Fodor

Received: 8 June 2023

Revised: 14 August 2023

Accepted: 17 August 2023

Published: 25 August 2023



Copyright: © 2023 by the authors. Licensee MDPI, Basel, Switzerland. This article is an open access article distributed under the terms and conditions of the Creative Commons Attribution (CC BY) license (<https://creativecommons.org/licenses/by/4.0/>).

1. Introduction

Environmental stresses are unpredictable, irregular, and ever-changing. Plants are exposed to several complex environmental variables, including temperature, radiation, precipitation, humidity, wind, and soil factors. When a plant experiences less/more than optimum environmental conditions (stress), either through climatic change or human interference, this ultimately affects its survival [1]. Abiotic-stress-induced injuries result in stress-specific responses through distinct modes, and irrespective of the type of stress factor plants elicits a universal response mechanism [2]. Plants can evoke a myriad of responses (morphological, physiochemical, and molecular) to oscillating environmental (stress) conditions [3]. In general, stress conditions stimulate the generation of reactive oxygen species (ROS) such as hydrogen peroxide (H₂O₂), singlet oxygen (¹O₂), hydroxyl radical (•OH), superoxide (O₂^{•−}) anion, and cytotoxic compounds like methylglyoxal (MG), which disturbs cellular redox homeostasis [4]. The generation of ROS is unavoidable, even under optimal conditions. During normal cellular metabolism, plants can produce



Mechanistic prospective and pharmacological attributes of quercetin in attenuation of different types of arthritis

Anita Bhoi¹ · Shradha Devi Dwivedi² · Deependra Singh² · S. Keshavkant¹ · Manju Rawat Singh²

Received: 14 June 2023 / Accepted: 8 September 2023
© King Abdulaziz City for Science and Technology 2023

Abstract

Arthritis is a frequent autoimmune disease with undefined etiology and pathogenesis. Scientific community constantly fascinating quercetin (QUR), as it is the best-known flavonoid among others for curative and preventive properties against a wide range of diseases. Due to its multifaceted activities, the implementation of QUR against various types of arthritis namely, rheumatoid arthritis (RA), osteoarthritis (OA), gouty arthritis (GA) and psoriatic arthritis (PsA) has greatly increased in recent years. Many research evidenced that QUR regulates a wide range of pathways for instance NF- κ B, MAK, Wnt/ β -catenine, Notch, etc., that are majorly associated with the inflammatory mechanisms. Besides, the bioavailability of QUR is a major constrain to its therapeutic potential, and drug delivery techniques have experienced significant development to overcome the problem of its limited application. Hence, this review compiled the cutting-edge experiments on versatile effects of QUR on inflammatory diseases like RA, OA, GA and PsA, sources and bioavailability, therapeutic challenges, pharmacokinetics, clinical studies as well as toxicological impacts. The use of QUR in a health context would offer a tearing and potential therapeutic method, supporting the advancement of public health, particularly, of arthritic patients worldwide.

Keywords Inflammation · Gout arthritis · Osteoarthritis · Psoriatic arthritis · Rheumatoid arthritis · Quercetin

Abbreviations

AIM2	Absent in melanoma 2	COX	Cyclooxygenase
ADME	Absorption, distribution, metabolism, and excretion	E-ADA	Ectoadenosine deaminase
ADA	Adenosine deaminase	ENM	Electrospun nanofiber membrane
AIA	Adjuvant-induced arthritic	ECM	Extracellular matrix
ALP	Alkaline phosphatase	FLS	Fibroblast like synovium
ASC	Apoptosis-associated speck-like protein containing CARD	GATA6	GATA transcription factor 6
CaC ₂ O ₄	Calcium oxalate	GO	Gene ontology
CCL	C–C motif chemokine ligand	GA	Gout arthritis
JNK	C-Jun N-terminal kinase	HO	Heme oxygenase
CD14	Cluster of differentiation 14	H	Hydrogen
CoPP	Cobalt protoporphyrin IX	HIF-1	Hypoxia-inducible factor-1
CIA	Collagen-induced arthritic	iNOS	Inducible nitric oxide synthase
C3	Complement protein 3	IL	Interleukin
CFA	Complete Freund adjuvant	KOA	Knee-OA
		KEGG	Kyoto Encyclopedia of Genes and Genomes
		LII	Limb idleness index
		LOX	Lipoxygenase
		LPS	Lipopolysaccharides
		M1	Secretes pro-inflammatory cytokines
		M2	Secretes anti-inflammatory cytokines
		MMPs	Matrix metalloproteinases
		MTX	Methotrexate
		mPEG-PA	Methyl-poly(ethylene glycol)-l-poly(alanine)
		MIA	Monoiodoacetate

✉ Manju Rawat Singh
manjursu@gmail.com

¹ School of Studies in Biotechnology, Pt. Ravishankar Shukla University, Raipur 492 010, India

² University Institute of Pharmacy, Pt. Ravishankar Shukla University, Raipur 492 010, India



Antibacterial Activity of CdTe/ZnS Quantum Dot- β Lactum Antibiotic Conjugates

Sandeep K. Vaishnav² · Jyoti Korram¹ · Tikendra K. Verma⁵ · S. K. Jadhav³ · Rekha Nagwanshi⁴ · Manmohan L. Satnami¹

Received: 4 April 2023 / Accepted: 13 June 2023 / Published online: 30 June 2023
© The Author(s), under exclusive licence to Springer Science+Business Media, LLC, part of Springer Nature 2023

Abstract

β -Lactum antibiotics are broad class of antibiotics which kills bacteria by inhibiting the formation of peptidoglycan that constitutes the bacterial cell wall. The resistance that develops in bacteria for antibiotics led the scientific world to think about the future aspects for modifying the way through which antibiotics are acted on the bacteria and become lethal for them. In this consequence, the potential of latest marketed antibiotics e.g. Amoxiciline (I), ceftazidim (II) have been evaluated after being conjugated with quantum dots. The surface of quantum dots has been conjugated with antibiotics by carbodiimide coupling with the help of 1-ethyl-3-(3-dimethylaminopropyl) carbodiimide (EDC) and N-hydroxysuccinimide (NHS) as conjugating agent between antibiotic and functionalized quantum dots. The antibacterial properties of QD-conjugated antibiotics have been determined by disc diffusion assay. The potency of QD-conjugated antibiotics has been estimated by determining their MIC₅₀ for the selected strain of Gram-negative (*Escherichia coli*) and Gram-positive (*Staphylococcus aureus*) bacteria. Minimum inhibitory concentration study, minimum bactericidal concentration and growth pattern analysis revealed that QD-antibiotic conjugates showed slightly more prospective than pure native antibiotics against both Gram-negative (*Escherichia coli*) and Gram-positive (*Staphylococcus aureus*) bacteria.

Keywords β -Lactum antibiotics · QD-antibiotics conjugates · MIC₅₀ · Antibacterial Activity

Introduction

Since the invention of penicillin, β -lactam antibiotics have developed as the most essential spectrum of antibacterial agents [1, 2]. However, the experimental treatment and wide utilization of these agents have made the bacteria to

generate various types of β -lactamases (β -Lases), which could prompt the spread of bacterial resistance [3–6]. Thus clinical viability of β -lactam antibiotics was negotiated. β -lactam antibiotics resistance has turned out to be a serious issue that encounters the human health [7–10]. Thus, progressively more demand has been put on pharmaceutical investigators and medical researchers to develop new antibiotics [11]. Some strategies have been accounted for disabling the bacterial resistance. One was to change the structure of β -lactam to reduce its sensitivity to the hydrolysis by β -Lases [12]. Another technique was to utilize double activity cepheems; if bacteria have resistance to one of them, the other antibacterial agent would destroy them in another way [13–16]. Vergauwe and coworkers utilized reagents, for example, 3 clavulanic acid to inactivate the β -Lases [17]. In all these techniques, reagents added to conquer the bacterial resistance were organic compounds. Inorganic components were occasionally utilized as a part of the antimicrobial industry. Though, it is notable that inorganic nanomaterials are great antimicrobial agents. Currently, there were some research work reported, which

✉ Manmohan L. Satnami
manmohanchem@gmail.com

Sandeep K. Vaishnav
fsl.sandeep16@gmail.com

¹ School of Studies in Chemistry, Pt. Ravishankar Shukla University, Raipur, C.G. 492010, India

² State Forensic Science Laboratory, Police line Campus, Tikrapara, Raipur, C.G. 492001, India

³ School of Studies in Biotechnology, Pt. Ravishankar Shukla University, Raipur, C.G. 492010, India

⁴ Department of Chemistry, Govt. Madhav P. G. Science College, Ujjain, M. P. 456010, India

⁵ Laxman Prasad Baidh Govt. Girls College, Bemetera, C.G. 491335, India

started to investigate the antimicrobial impacts of combination of β -lactam and inorganic nanomaterials. This investigation would be invaluable for designing novel antimicrobial agents.

Over the previous decades, nanoparticles with exclusive chemical and physical properties have demonstrated a growing significance in biological, biomedical, and pharmaceutical applications. Inorganic nanomaterials have large surface to volume ratio and pronounced bioactivity which made them great candidate to displace conventional organic antimicrobial agents that are enormously irritant and toxic. Currently, various nanoparticles have been appeared to have antimicrobial activities [18, 19] and among them the silver nanoparticles have been very much examined and reported to accrue in the *Escherichia coli* (*E. coli*) membrane to have efficaciously antibacterial effects [20]. Titanium dioxide (TiO_2), Silicon dioxide (SiO_2) and zinc oxide (ZnO) nanoparticles, also demonstrate encouraging biocidal properties against both Gram-positive and Gram-negative bacteria [21]. All these assemblies are observed to be photosensitive and can create reactive oxygen species (ROS) under high intensity light at a particular wavelength. TiO_2 can be utilized as an important antibacterial agent although when sunlight is applied as the excitation source. In contrast with different nanoparticles, quantum dots (QDs) have superior size-dependent optical properties. They are essentially nanoscale crystals fabricated from semiconducting materials [22, 23]. QDs have turned out to be more significant research subjects in present years [24] because of their exceptional physical properties including photostability, narrow emission, and wide excitation range, high photoluminescence and potential applications in recent biosensors [25], cell imaging [26] and in vivo tracking of living being [27]. QDs can indicate sizes and numbers of atoms between the molecular level and bulk solids with a band-gap relying upon different factors, for example, strength and type of bond with adjacent atoms. Usually, narrow fluorescent emission peaks are witnessed for separated atoms. It has been accounted for that a nanoparticle of roughly 100–10000 atoms indicates distinctive narrow optical line spectra. On the premise of this data, QDs can be characterized as artificial atoms [28].

It has been demonstrated that under UV illumination, QDs produce free radicals, of which the quality and type are controlled by their center core materials [29]. The high extent of free radicals is hurtful to microorganisms. The release of free metal ions from QDs could also be hazardous to microbes. There are only few reports on antimicrobial activity of QDs can be established [30, 31]. For instance, Kloepper et al. demonstrated that cadmium selenium (CdSe) QDs can prevent bacterial growth [32]. To diminish the lethality and toxicity of QDs, core/shell structure and core/

shell materials are commonly utilized. Scientists develop various types of center/shell QDs (CdTe/ZnSe , CdTe/ZnS , and CdSe/ZnS), core/shell/shell QDs (CdTe/CdS/ZnS , CdSe/CdTe/ZnSe), and condition cordial QDs (CuInSe , Ag_2S , and Si QDs) for different purposes [33–41].

In the present study, CdTe/ZnS core/shell QDs were selected as one of the most robust and highly fluorescent QDs which are synthesized through a green way or environment-friendly way using water as a solvent. The CdTe/ZnS core/shell QDs can be applied in various biological fields because the high Cd toxicity of CdTe QDs is supposed to be reduced by forming a shell of ZnS . In the present study, CdTe/ZnS core/shell QDs were conjugated with amoxicillin (Amox) and ceftazidime (CZ) and subsequently characterized with spectroscopic and microscopic techniques. The potency of antibacterial activities of these CdTe/ZnS -antibiotic conjugates was evaluated against *E. coli* and *S. aureus* which is commonly used as a model in microbiological research.

Experimental Section

Materials

Amoxicillin, ceftazidime, 1-ethyl-3-(3-dimethylaminopropyl) carbodiimide (EDC) and N-hydroxysuccinimide (NHS), cadmium acetate ($(\text{CH}_3\text{COO})_2\text{Cd}$), tellurium powder, sodium borohydride (NaBH_4), zinc acetate ($(\text{CH}_3\text{COO})_2\text{Zn}$), thiourea (NH_2CSNH_2), manganese acetate tetrahydrate ($(\text{CH}_3\text{COO})_2\text{Mn}\cdot 4\text{H}_2\text{O}$), glutathione (GSH), acetone (CH_3COCH_3) and all other chemicals were purchased from Sigma Aldrich, Bangaluru, India. All the chemicals used were of analytical grade and millipore water was used in all experiments.

The strains which were employed in this study are the Gram-negative bacterium *E. coli* (MTCC 1687) and the Gram-positive bacterium *S. aureus* (MTCC 3160), purchased from the Microbial Type Culture Collection, Institute of Microbial Technology (Chandigarh).

Synthesis of CdTe/ZnS Core/Shell Quantum Dots

Core-shell CdTe/ZnS quantum dots were synthesized by slight modification of reported method [42]. Briefly, a NaHTe solution was prepared by dissolving Te powder (1 mM) and NaBH_4 (4 mM) in 2 mL of nitrogen bubbled millipore water which was stirred for a few hours at 4 °C. The Cd^{2+} precursor solution was prepared by dissolving GSH (10 mM) and Cd ($(\text{CH}_3\text{COO})_2$ (4.0 mM) in 100 mL millipore water. Subsequently, the pH was adjusted to 10.5 by adding 0.1 M NaOH followed by the addition of NaHTe solution into N_2 saturated Cd^{2+} precursor solution. The colour of the solution immediately changed from colourless to yellow.

The molar ratio of Cd^{2+} : NaHTE: GSH was maintained at 4:1:10. Then, the reaction mixture was heated at 100 °C, and aliquots of the mixture (0.5 mL) were collected after every 10 minutes. After desired growth the reaction was quenched by rapidly cooling down to 0 °C in an ice-bath. The core nanocrystals were precipitated by adding acetone (1:1 v/v), followed by centrifugation at 5000 rpm for 2 h. For ZnS shell coating, a Zn^{2+} precursor solution was prepared by dissolving GSH (0.2 mM) and $\text{Zn}(\text{CH}_3\text{COO})_2$ (0.1 mM) in 25 mL of Millipore water with adjusting pH to 7.0. For the synthesis of CdTe/ZnS core/shell QDs, the purified CdTe nanocrystals (0.025 $\mu\text{mol/L}$) and thiourea (0.1 mM) were added to the Zn^{2+} precursor solution, and the pH was adjusted to 11.0. The molar ratio of Cd^{2+} /thiourea (TU)/GSH in the reaction mixture was 1:1:2. Afterwards, the reaction mixture was kept at 90 °C, and aliquots (0.5 mL) were collected in a glass vial at a series of different times. Each reaction was quenched by cooling to 0 °C in an ice bath. The core/shell QDs were precipitated by adding equal volume of acetone (1:1 v/v), followed by centrifugation at 4000 rpm for 1.5h. The precipitate was used for further studies.

Conjugation of Antibiotics with CdTe/ZnS Core/Shell Quantum Dots

One milligram of CdTe/ZnS QDs was dissolved in 10 mL of 50 mM PBS buffer (pH 7.40). Then 10 mg of NHS and 20 mg of EDC were added to the QD solution, and stirred for 30 min to activate the carboxylate groups on QDs. Then various amounts of antibiotics (amoxicillin/ ceftazidime) (1 $\mu\text{g/ml}$ -300 $\mu\text{g/ml}$) was dissolved in PBS buffer, and added to the activated QD solution. After reaction overnight, the antibiotic-conjugated QDs were separated from the solution by an ultracentrifugation.

Characterization

UV-Visible spectra were recorded by using ThermoScientific evolution-300spectrophotometer operated at a resolution of 2 nm. Fluorescence spectra were recorded using an Agilent fluorescence spectrophotometer (G9800AA). The fourier-transform infrared (FTIR) spectral analysis was performed within the wave number ranges from 4000-600 cm^{-1} were measured using FTIR spectrometer (DRS-FTIR) set with deuterated, L-alanine doped triglycine sulfate (DLaTGS) detector (Model: Nicolet iS10, Thermofisher Scientific Instrument, Madison, USA). The size of the CdTe/ZnS QDs were assessed by transmission electron microscopy (TEM) on a JEOL, JEM-2100F model instrument operated an accelerating voltage of 200kV. The samples were prepared by adding drops of sample solution on carbon-129 coated copper grids and allowed to dry in air. The resulting images

were analyzed by gatan micrograph software. X-Ray diffraction study has been performed on PANalytical 3 kW X'pert Powder XRD–Multifunctional.

Antibacterial Activity

The antibacterial activities of QD-antibiotics conjugates were investigated against Gram-negative bacteria *Escherichia coli* (*E. coli*) MTCC 1687 and Gram-positive bacteria *Staphylococcus aureus* (*S. aureus*) MTCC 3160 by two methods: well diffusion and broth dilution method. The strains were cultured in Nutrient agar medium (NAM) plates in an incubator overnight at 37 °C. A single colony was inoculated in 20 ml of NAM Broth (TSB) and grown statically overnight at 37 °C. Then, 100 μl of this bacterial suspension was transferred into 100ml of NAM in a conical flask and grown in a shaker incubator at 150 rpm at 37 °C.

Well Diffusion Method

The antibacterial activity of QD-antibiotics conjugates were assessed in vitro against two pathogenic bacterial strains using well diffusion method. NAM plates were prepared by pour plate method. For agar well diffusion, 100 μl of the bacterial suspension was inoculated on semi solidified NAM plates and spread properly. Small wells about 5 mm diameter of size were made into semisolid NAM plates. Different dosages (5-150 $\mu\text{g/ml}$) of QDs, 50-300 $\mu\text{g/ml}$ and 1-30 $\mu\text{g/ml}$ of amoxicillin and its corresponding QD-amox conjugates for *E.coli* and *S. aureus* were added in to each well. Similarly, 5-50 $\mu\text{g/ml}$ and 1-30 $\mu\text{g/ml}$ of ceftazidime and its corresponding QD-CZ conjugates for *E.coli* and *S. aureus* QD- were added in to each well. The plates were placed in a 37 °C incubator for 24 h. Test was done in triplicate, then inhibitory action of tested samples on the growth of the bacteria was determined by measuring diameter of inhibition zone in mm around each well. *Streptomycin* was used as a positive control while water is used as negative control to test the bioactivity of compounds.

Broth Dilution Method

Nutrient broth medium inoculated in different test tubes plugged with sterile cotton and autoclaved. The 100 μl bacterial suspensions were inoculated in two set of test tubes containing different dosages of different dosages (5-150 $\mu\text{g/ml}$) of QDs, 50-300 $\mu\text{g/ml}$ and 1-30 $\mu\text{g/ml}$ of amoxicillin and its corresponding QD-amox conjugates for *E.coli* and *S. aureus*. Similarly, 5-50 $\mu\text{g/ml}$ and 1-30 $\mu\text{g/ml}$ of ceftadizime and its corresponding QD-CZ conjugates for *E.coli* and *S. aureus* QD- were used. The final volume in the tubes was 10 ml. The tubes were incubated in a shaker incubator at 100 rpm at 37 °C for overnight. Growth of inoculums in the test tube was observed by determining the optical density (OD) at 600

nm by colorimeter. For standard comparison a control sample was prepared by a similar method exclusive of QD-antibiotic conjugates. The experiments were carried out in triplicate to confirm reproducibility. The percentage of growth inhibition was calculated using the following formula:

$$\% \text{ Growth Inhibition} = - \left[\frac{OD_c - OD_t}{OD_c} \right] \times 100 \quad (1)$$

where OD_c and OD_t correspond to the optical density of the control and test sample of nanocomposite, respectively.

Results and Discussion

Spectral Characterization of CdTe/ZnS QDs and CdTe/ZnS QDs Antibiotic Conjugates

Figure 1 represents usual evolution of both absorption and fluorescence spectra of GSH-topped CdTe/ZnS QDs synthesized in the aqueous phase. Although successfully synthesizing CdTe QDs with an inclusive range of sizes, current study emphases on CdTe core with emission maxima at 556 nm and study the evolvement of the optical, electronic and structural properties as a function of ZnS coating. The size and concentration of the CdTe core are 3.78 nm and 4.7×10^{-6} M, respectively, which is determined by utilizing the empirical formula (Eq. 2): [43]

$$A = \varepsilon cl, \varepsilon = 10043(D)^{2.12}$$

$$D = (9.8127 \times 10^{-7})\lambda^3 - (1.7147 \times 10^{-3})\lambda^2 + (1.0064)\lambda - (194.84) \quad (2)$$

Here A is the absorbance of the first excitonic absorption peak for CdTe QDs, c is the molar concentration (mol/L) of the CdTe QDs, l is the path length (cm) of the radiation beam, D is the

diameter of the QDs, ε is the molar absorptivity of CdTe QDs and λ (nm) is the wavelength of the first excitonic absorption peak of the CdTe QDs. Heating the solution containing glutathione, Zn^{2+} and core CdTe QDs results in gradual red shift in the absorption and fluorescence spectra (Fig 1a), which infers that a ZnS shell is gradually developing in situ on the CdTe core. With the refluxing, the excitonic absorption peak of QDs shifts toward longer wavelength from 565 nm to 620 nm as the QDs grow to bigger size. This phenomenon is observed due to quantum confinement effect. The corresponding fluorescence emission wavelengths and QYs of the CdTe/ZnS NCs are 585 nm 40%, 600 nm 48 %, 610 nm 42 %, 620 nm 39 %, and 635 nm 36 %, respectively. After the 15 min of refluxing, the best fluorescence QY (48 %) of the CdTe/ZnS QDs achieved is 1.4 times greater than that of the CdTe core QDs. At the same time, the diameter of the core-shell QDs rises to 4.7 nm (core CdTe = 3.8 nm), which displays that the thickness of ZnS shell is around 0.9 nm. After 30 min. of refluxing, the fluorescence wavelength increases with decrease in the QY of CdTe/ZnS to 42 %. Further refluxing to 50 min, the increasing rate fluorescence wavelength diminishes with the decrease in the QY to 39 %. Lastly, after 90 min. of refluxing, the fluorescence emission wavelength of the QDs shifts up to 635 nm, however the QY reduced to just 36 %. These results show that during refluxing, the QDs are grown to their final size, as well as the fluorescence emission of the core-shell CdTe/ZnS QDs can be tuned in color with the refluxing time.

As appeared in the Fig. 1a, the absorption band shifts towards longer wavelength with increase in the fluorescence intensity as the ZnS shell grows. The increased intensity is due to the *in situ* formation of ZnS shell causing in the considerable decrease in the surface deformities of core CdTe QDs and the dropping down of confinement energy of exciton after coating core QDs with greater band gap shells [43–49]. Interfacial strain play an essential role which emerges from the extensive lattice mismatch between the ZnS shell and CdTe core (cross section parameters for ZnS $c = 6.257 \text{ \AA}$ and for CdTe $c =$

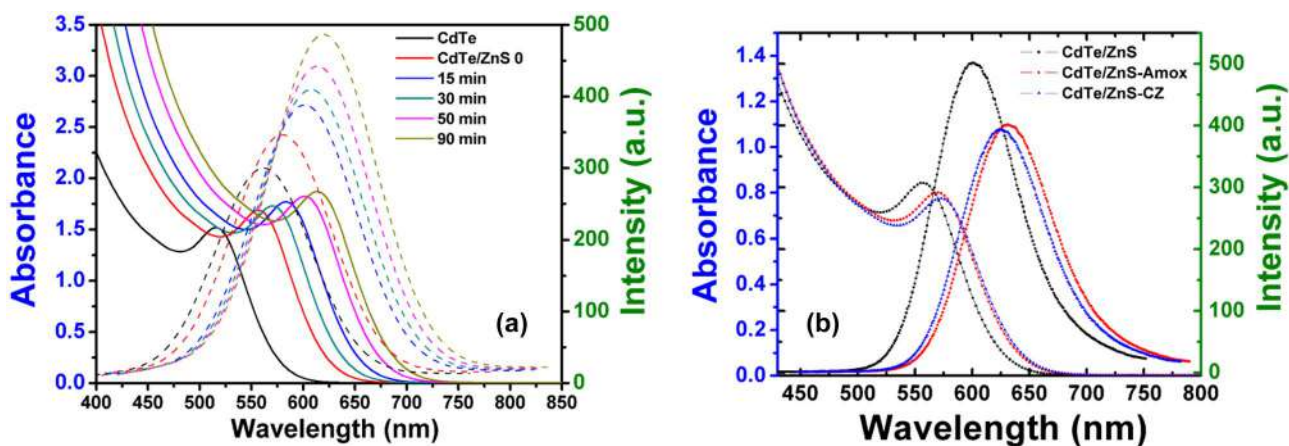


Fig. 1 Absorption and corresponding fluorescence spectra of CdTe and CdTe/ZnS QDs with refluxing time Absorption and corresponding FL spectra of CdTe/ZnS QDs and CdTe/ZnSamox and CdTe/ZnS CZ conjugates

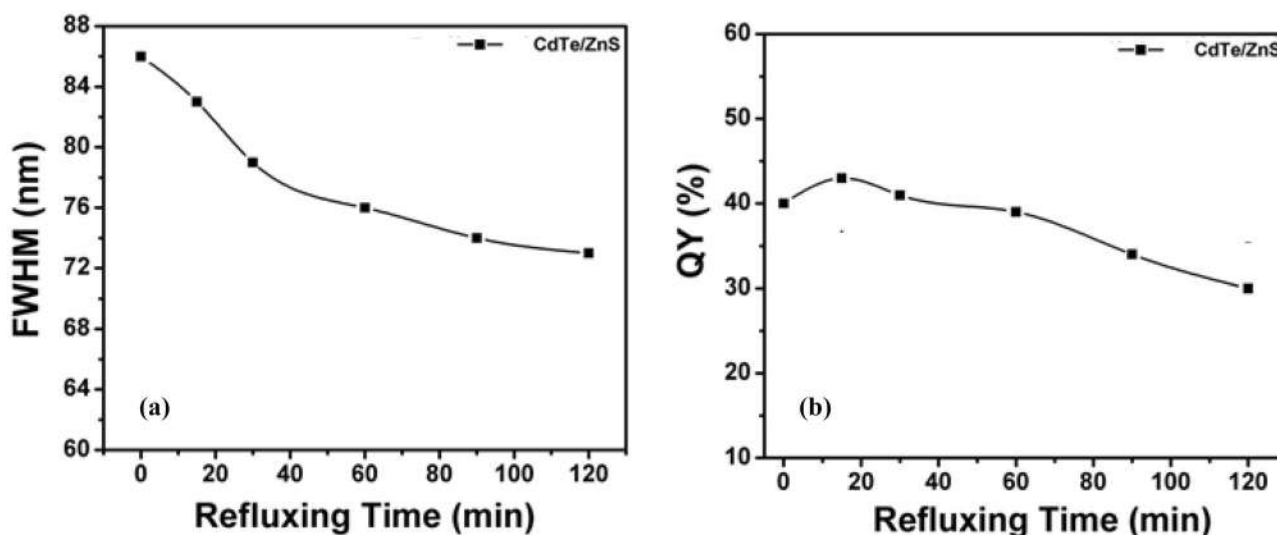


Fig. 2 Variation of FWHM (a) and Quantum Yield (b) of CdTe/ZnS QDs with refluxing time

6.477 Å) [50]. On the other hand, it can be found in Figs. 1a and 2 that the sizes of QDs grow in aqueous phase accomplished by the fluorescence full width at half most extreme (FWHM) decreasing. FWHM of the fluorescence emission peak rapidly changes from 86 nm to 76 nm during refluxing for 15–90 min. The narrow FWHM of the fluorescence emission peak reveals the narrow size distribution, which is a proficient way to explore the size focusing. Furthermore, the conjugation of CdTe/ZnS with Amox and CZ also monitored with absorption and fluorescence spectral measurements (Fig. 1b). The absorption and corresponding fluorescence spectra of amox and CZ CdTe/ZnS conjugates shifts towards longer wavelength with considerable decrease in intensity suggest the conjugation of CdTe/ZnS QDs with amox and CZ.

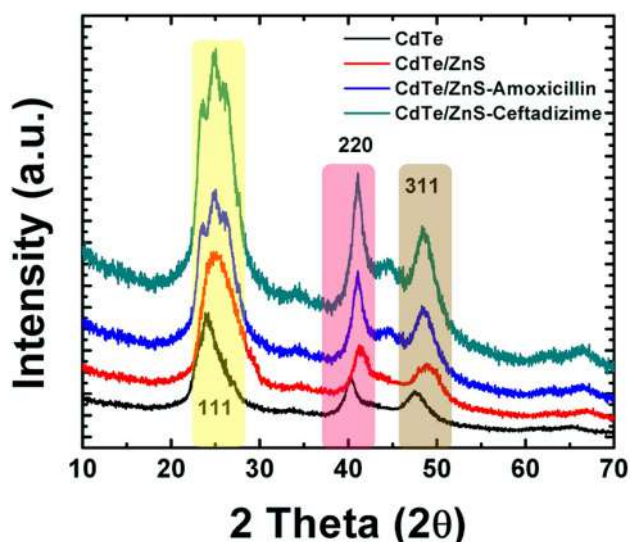


Fig. 3 XRD of CdTe/ZnS QDs and CdTe/ZnS -Amox and CdTe/ZnS CZ conjugate

The powder XRD diffractogram for the CdTe, CdTe/ZnS, CdTe/ZnS-Amox and CdTe/ZnS CZ conjugates are depicted in Fig. 3. The typical zinc blend planes of 111, 220, and 311 positioned at 24.40° , 41.60° , and 47.90° for CdTe and at 24.94° , 41.72° , and 48.76° for CdTe/ZnS in the range of $10\text{--}70^\circ$ have been observed. The position of the diffraction peaks of CdTe cores is well matched with those of the bulk CdTe cubic structure (JCPDSNO. 15-0770) [42]. After formation of ZnS shell on CdTe core, diffraction peak position shifted to greater angles towards the positions of bulk ZnS cubic structure (JCPDS NO. 05-0566) [42], which is confirmed the formation of CdTe/ZnS. Furthermore, the diffraction peaks of CdTe/ZnS Amox and CdTe/ZnS CZ conjugates also appears to be at 24.94° , 41.72° , and 48.76° , but the peaks at 24.95° shows a small splitting. The splitting of peaks might be due to slight loss in crystalline structure at 111 planes due to conjugation. The TEM and HRTEM images in Fig. 4 show that the CdTe/ZnS NCs possess a good dispersed crystalline structure, and have an average diameter of about 4.7 nm, consistent with the results calculated from the absorption spectrum. The structural characterizations show a

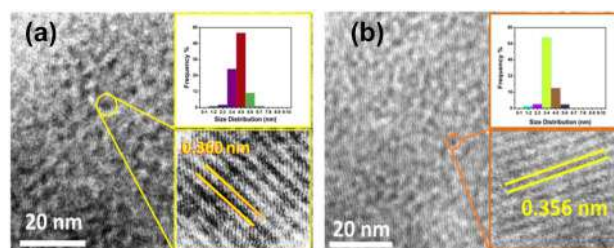


Fig. 4 TEM image of CdTe (a) and CdTe/ZnS QDs (b) Inset: Histogram of CdTe and CdTe/ZnS QDs and HRTEM showing interplaner distance

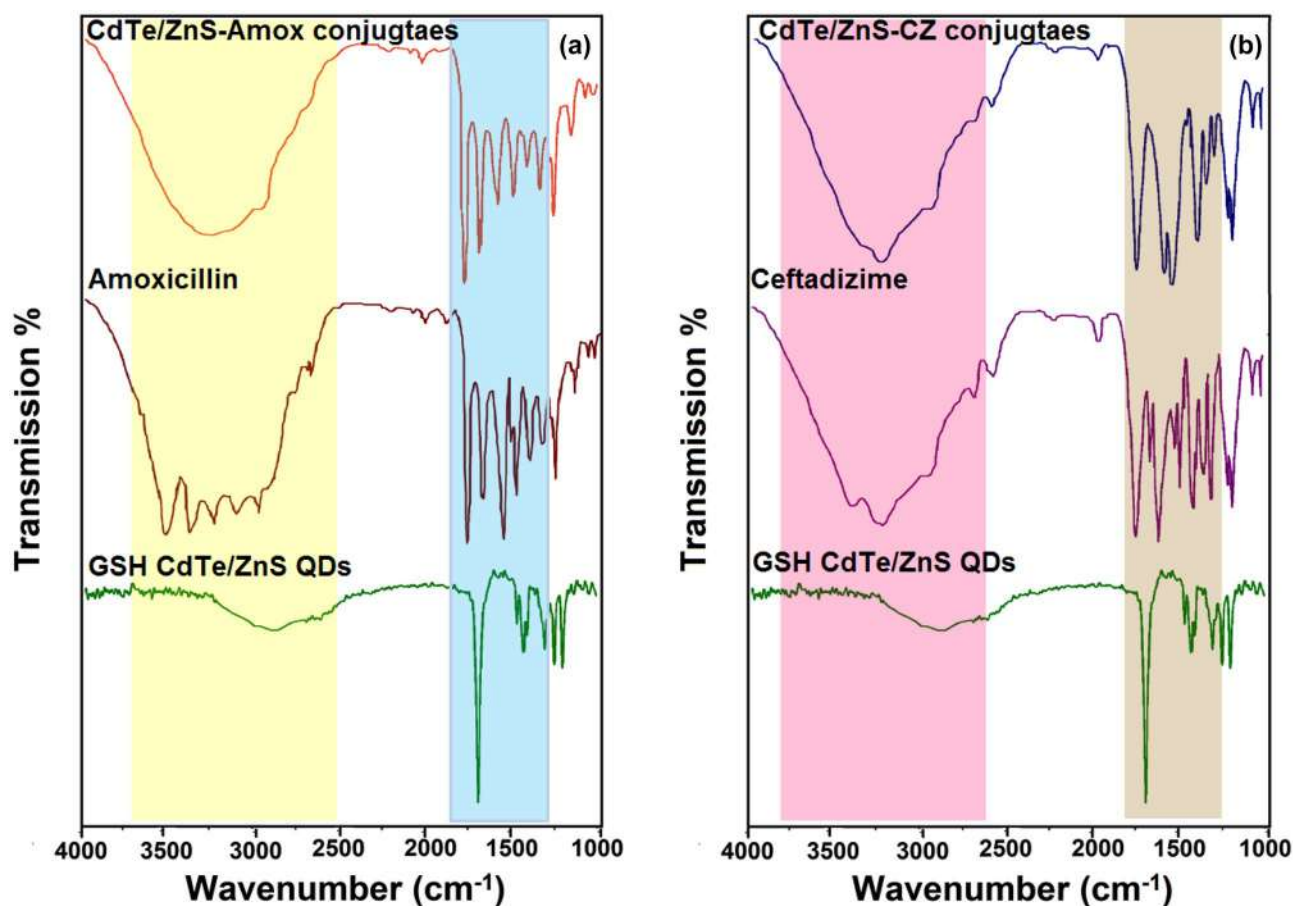


Fig. 5 FTIR spectra of (a) free Amox and Amox-CdTe/ZnS conjugate (b) CZ and CZ-CdTe/ZnS conjugates

continuous growth of the crystallographic planes without a distinct boundary at the core-shell interface. Energy-dispersive X-ray spectroscopy (EDS) was also used to examine the composition of CdTe/CdS/ZnS (Fig. S1). Zn and S were both clearly visible in the EDS pattern,

and the atomic ratio of S:Zn: Cd:Te was determined to be 1.38:1:1.64: 2.84. The FTIR spectrum of CdTe/ZnS antibiotics conjugates and free antibiotics (amox and CZ) reveals the conjugation of CdTe/ZnS with antibiotics as evident in the FTIR spectrum (Fig. 5) Curve 2 (Fig. 5a) represent

Table 1 List of some of the previously reported antibacterial activity studies of Quantum dots and corresponding bacterial strain

S. No.	Quantum Dot Nanaomaterial	Bacterial Strain	Reference
1	CdTe QDs CdS/Ag ₂ S QDs	Escherichia coli Escherichia coli, Pseudomonas aeruginosa, Staphylococcus aureus	[51] [52]
2	CdTe–Rocephin QD complex	Escherichia coli	[53]
3	Thioglycolic acid (TGA) and mercapto-acetohydrazide (TGH) lysine-capped	Staphylococcus aureus	[54]
4			
5	Ciprofloxacin-Carbon dot conjugate	Escherichia coli, Pseudomonas aeruginosa, Staphylococcus aureus Bacillus subtilis	[55]
6	CdTe/ZnS-Amoxicilline And Ceftadizime	Escherichia coli, Staphylococcus aureus	Current study

Table 2 MIC₅₀ values of pure antibiotics and antibiotics CdTe/ZnS conjugates for *E.coli* and *S. aureus*

Tested Sample	MIC ₅₀ (µg/ml)	
	<i>E.coli</i>	<i>S. aureus</i>
CdTe/ZnS	> 700	> 600
Amox	140±2.5	4.8±0.5
Amox-CdTe/ZnS	102 ±1.5	3.0±0.8
CZ	12.5 ±0.5	4.6±0.8
CZ-CdTe/ZnS	9.5±0.5	3.6±0.5

the free amox which show characteristic absorption bands of cephalosporin compounds, such as 3660-3250 cm⁻¹ (N-H group axial deformation), 1750-1725 cm⁻¹ and 1540 cm⁻¹ (carboxylic acid function C=O stretching), 1475-1600 cm⁻¹ (aromatic ring C=C axial deformation), 1350-1300 cm⁻¹ (C-N axial deformation) and 1680-1630 cm⁻¹ (amide group C=O axial deformation). Curve 3 (Fig. 5a) amox-CdTe/ZnS conjugates which shows quite characteristics changes in their amide stretching vibration such as splitting of 1680 cm⁻¹ (amide group C=O axial deformation) bands which suggest the formation of conjugates through amide bond formation. Similarly, Curve 2 (Fig. 5b) represent the free CZ which show broad absorption bands of N-H group axial deformation at 3660-3250 cm⁻¹, 1748 cm⁻¹ (carboxylic acid function C=O stretching), 1480 cm⁻¹ (aromatic ring C=C axial deformation), 1382 cm⁻¹ (C-N axial deformation) and 1678 cm⁻¹ (amide group C=O axial deformation). The stretching band at 1678 cm⁻¹ splits in to two peaks suggested the formation of new amide bond as well as the conjugation of CdTe/ZnS QDs with CZ.

Antibacterial Activity Tests

To evaluate the antibacterial efficacy of CdTe/ZnS antibiotics conjugates, the activity were tested at different concentrations against *E.coli* and *S. aureus*. The micro dilution method was employed to evaluate their antibacterial activity

and minimum inhibitory concentration (MIC₅₀). The evaluation included also the different concentrations of bare CdTe/ZnS, pure antibiotics and CdTe/ZnS-antibiotic conjugates to compare and analyze the antibacterial behavior contributed from each component of the conjugates. Moreover, the current study has been compared with that of previous reports and best of our literature survey we found that no such attempts have been made till now (Table 1)

Tables 2, 3 and 4 summarizes the percentage inhibition and MIC₅₀ values of bare CdTe/ZnS, pure antibiotics (Amox, CZ) and CdTe/ZnS-antibiotic conjugates, to inhibit both bacterial strains. The obtained data show that the percentage inhibition of bacterial growth increases with increasing concentration of CdTe/ZnS, Amox, CZ, and its conjugates. The percentage inhibition of Amox-CdTe/ZnS conjugates (50, 100, 150, 200 and 300 µg/ml) against *E.coli* is found to be 32.06, 49.94, 69.01, 85.69 and 94.63% which is greater than the percentage inhibition of free Amox which shows 20.14, 40.40, 61.85, 79.73 and 89.27 % after 6h treatment at 37 °C (Fig. 6a). Similarly, the percentage inhibition of Amox-CdTe/ZnS conjugates (1, 3, 5, 10 and 20 µg/ml) against *S. aureus* found to be 33.25, 51.13, 71.39, 85.31 and 95.01 % which is greater than the percentage inhibition of free Amox Table (2 and 3) (Fig. 6c). Similar trends were observed for CZ-CdTe/ZnS conjugates and pure CZ against both the bacterial strain (Fig. 6b, d) (Tables 5 and 6). Furthermore, the MIC₅₀ of 102.0 and 3.0 µg/mL of Amox-CdTe/ZnS conjugates and 9.5 and 3.6 µg/mL of CZ-CdTe/ZnS conjugates are required to kill 50 % of *E. coli* and *S. aureus* bacteria, respectively (Table 2). On the other hand, the MIC₅₀ corresponding to bare CdTe/ZnS, CZ and Amox were found to be above the Amox-CdTe/ZnS and CZ-CdTe/ZnS conjugates for *E. coli* and *S. aureus* bacteria (i.e., 700 µg/ml and 500 µg/ml for CdTe/ZnS, 140 µg/mL and 4.8 µg/ml for Amox, 12.5 µg/ml and 4.8 µg/ml for CZ). It is clear that there is a significant enhancement and a strong antibacterial activity associated with CdTe/ZnS-antibiotic conjugates, as compared to bare CdTe/ZnS and pure antibiotics.

Table 3 Inhibition percentage of Amox, Amox-QD conjugates after 6 h treatment.

Tested Sample				Inhibition Percentage			
<i>E.coli</i> MTCC1687		<i>S. aureus</i> MTCC 3180		<i>E.coli</i> MTCC1687		<i>S. aureus</i> MTCC 3180	
Amox (µg/ml)	Amox-QD (µg/ml)	Amox (µg/ml)	Amox-QD (µg/ml)	Amox	Amox-QD	Amox	Amox-QD
50	50	1	1	20.14±1.93	32.06±1.83	27.29±1.97	33.25±1.82
100	100	3	3	40.40±1.84	49.94±1.89	42.78±2.33	51.13±2.16
150	150	5	5	61.85±2.23	69.01±2.13	64.24±1.91	71.39±1.85
200	200	10	10	79.73±1.94	85.69±1.69	80.12±1.74	85.31±1.78
300	300	20	20	89.27±1.86	94.63±1.79	90.70±1.96	95.01±1.91

Table 4 Inhibition percentage of CZ, CZ-QD conjugates after 6 h treatment.

Tested Sample				Inhibition Percentage			
<i>E. coli</i> MTCC1687		<i>S. aureus</i> MTCC 3180		<i>E. coli</i> MTCC1687		<i>S. aureus</i> MTCC 3180	
CZ ($\mu\text{g/ml}$)	CZ-QD ($\mu\text{g/ml}$)	CZ ($\mu\text{g/ml}$)	CZ-QD ($\mu\text{g/ml}$)	CZ	CZ-QD	CZ	CZ-QD
5	5	1	1	24.91 \pm 2.13	36.82 \pm 2.22	15.37 \pm 1.85	22.52 \pm 1.98
10	10	3	3	48.15 \pm 1.84	52.32 \pm 1.87	39.21 \pm 1.54	43.98 \pm 1.86
15	15	5	5	64.97 \pm 2.23	76.73 \pm 2.12	55.89 \pm 2.11	64.24 \pm 1.92
20	20	10	10	85.08 \pm 1.94	89.46 \pm 1.69	73.77 \pm 1.74	77.35 \pm 2.41
30	30	20	20	93.82 \pm 1.86	96.30 \pm 1.81	89.27 \pm 1.96	95.23 \pm 1.92

The antimicrobial effectiveness of CdTe/ZnS-Amox and CdTe/ZnS-CZ conjugates, dose-dependent growth kinetics curves of *E. coli* and *S. aureus* were used to assess the relative rate and extent of antibacterial activity of CdTe/ZnS-Amox and CdTe/ZnS-CZ conjugates. Figure 7 display the growth profiles of *E. coli* treated with various concentrations of pure antibiotics and CdTe/ZnS-antibiotic conjugates. Figure 7a, b shows a strong inhibition of *E. coli* and

S. aureus when treated with Amox and CZ. The interaction between CdTe/ZnS-antibiotics conjugates (Amox and CZ) and *E. coli* was stronger than pure antibiotics (Amox and CZ), and the inhibition was significantly high (Fig. 7a, b). The lowest concentration of 50 $\mu\text{g/ml}$ of Amox exerts a delay of 4 h in the growth rate of *E. coli* and 5 $\mu\text{g/ml}$ of CZ exerts a delay of 6 h in the growth rate of *E. coli*. On the other hand, CdTe/ZnS-antibiotic conjugates displayed a slightly

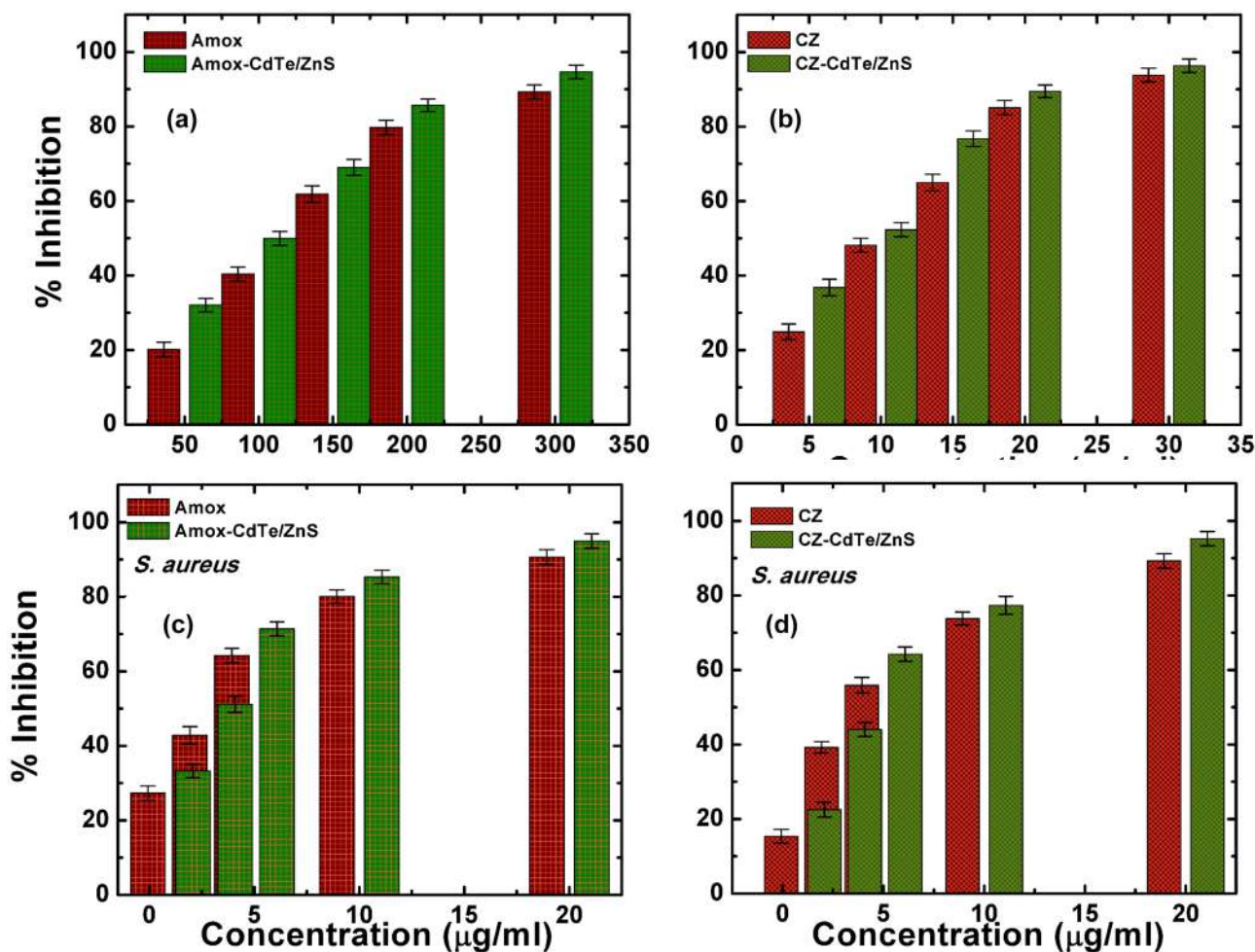
**Fig. 6** Inhibition percentage profile of Amox, Amox-CdTe/ZnS CZ and CZ-CdTe/ZnS conjugates against *E. coli* and *S. aureus*

Table 5 Inhibition zone of Amox, Amox-QD conjugates after 24 h treatment

Tested Sample				Inhibition Zone (mm)			
<i>E. coli</i> MTCC1687		<i>S. aureus</i> MTCC 3180		<i>E. coli</i> MTCC1687		<i>S. aureus</i> MTCC 3180	
Amox (µg/ml)	Amox-QD (µg/ml)	Amox (µg/ml)	Amox-QD (µg/ml)	Amox	Amox-QD	Amox	Amox-QD
50	50	1	1	14.0±1.93	18.0±1.93	13.0±1.93	18.0±1.93
100	100	3	3	25.0±1.93	29.0±1.93	20.0±1.93	24.0±1.93
150	150	5	5	30.0±1.93	34.0±1.93	26.0±1.93	29.0±1.93
200	200	10	10	36.0±1.93	44.0±1.93	32.0±1.93	35.0±1.93
300	300	20	20	45.0±1.93	56.0±1.93	35.0±1.93	41.0±1.93

Table 6 Inhibition zone of CZ, CZ-QD conjugates after 24 h treatment.

Tested Sample				Inhibition Zone (mm)			
<i>E. coli</i> MTCC1687		<i>S. aureus</i> MTCC 3180		<i>E. coli</i> MTCC1687		<i>S. aureus</i> MTCC 3180	
CZ (µg/ml)	CZ-QD (µg/ml)	CZ (µg/ml)	CZ-QD (µg/ml)	CZ	CZ-QD	CZ	CZ-QD
5	5	1	1	16.0±1.93	17.0±1.93	15.0±1.93	18.0±1.93
10	10	3	3	23.0±1.93	28.0±1.93	21.0±1.93	24.0±1.93
15	15	5	5	27.0±1.93	32.0±1.93	26.0±1.93	29.0±1.93
20	20	10	10	31.0±1.93	37.0±1.93	31.0±1.93	35.0±1.93
30	30	20	20	41.0±1.93	46.0±1.93	38.0±1.93	43.0±1.93

strong antibacterial behavior at lower concentrations than pure antibiotics. Similar bacterial population growth kinetics experiments have been carried out for pure antibiotics and QD-antibiotic conjugates with *S. aureus* (Fig. 7a, b). Similar to the *E. coli*, pure Amox and CZ displayed strong antibacterial activity against *S. aureus*, where the bacterial growth rate becomes slower when increasing the antibiotic

(Amox and CZ) concentrations. Nonetheless, an increase in the antibacterial effect of CdTe/ZnS-antibiotic conjugates was observed.

Furthermore, we used the well diffusion method to evaluate the ability of QDs-antibiotic conjugate to inhibit the formation of bacterial biofilms (Figs. 8 and 9). Tables 5 and 6 summarizes the diameter of the inhibition zones exhibited by

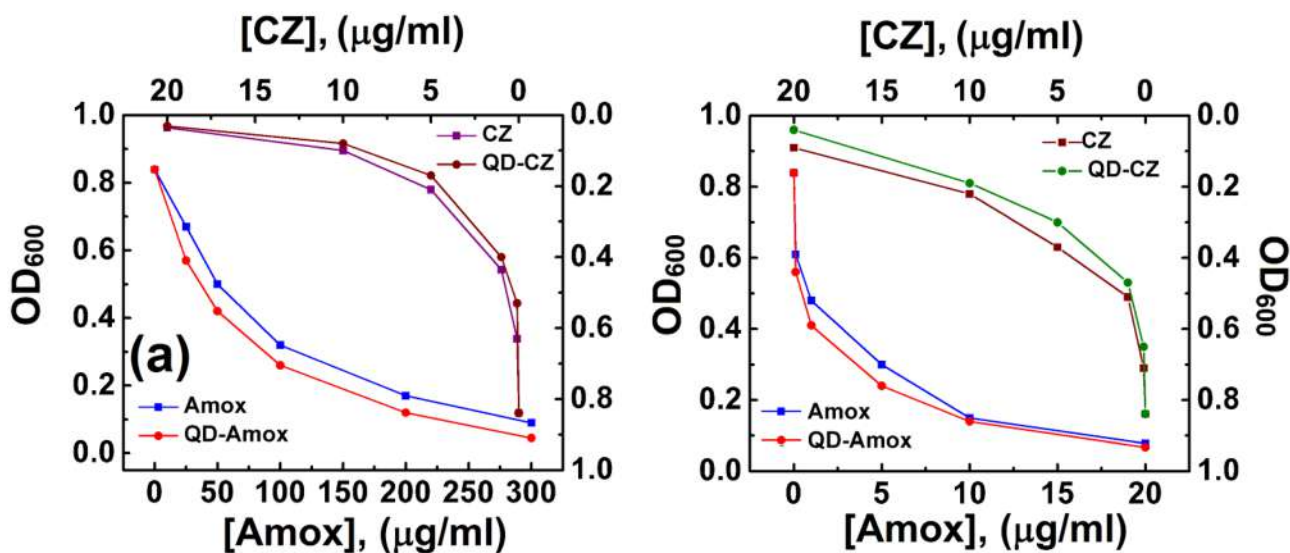


Fig. 7 Bacterial growth inhibition curve of (*E. coli* and *S. aureus*) at different concentration of pure antibiotics and its corresponding QD-conjugates

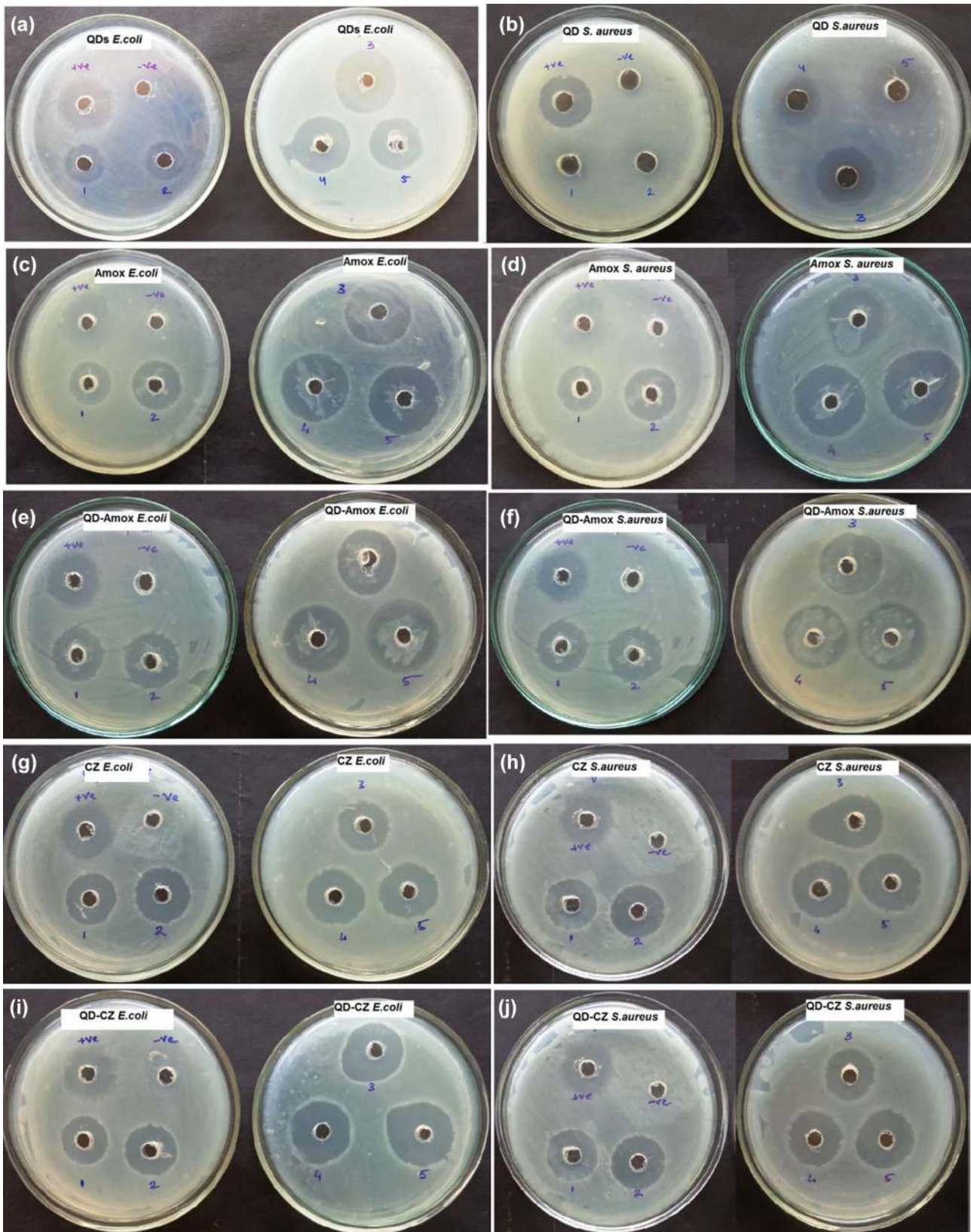


Fig. 8 Disc diffusion assay for *E. coli* and *S. aureus* (a–b) QDs against *S. aureus* and *E. coli*, (c–d) Amox against *S. aureus* and *E. coli*, (e–f) QDs-Amox conjugates against *S. aureus* and *E. coli*, (g–h) CZ against *S. aureus* and *E. coli*, (i–j) QDs-CZ conjugates against *S. aureus* and *E. coli*

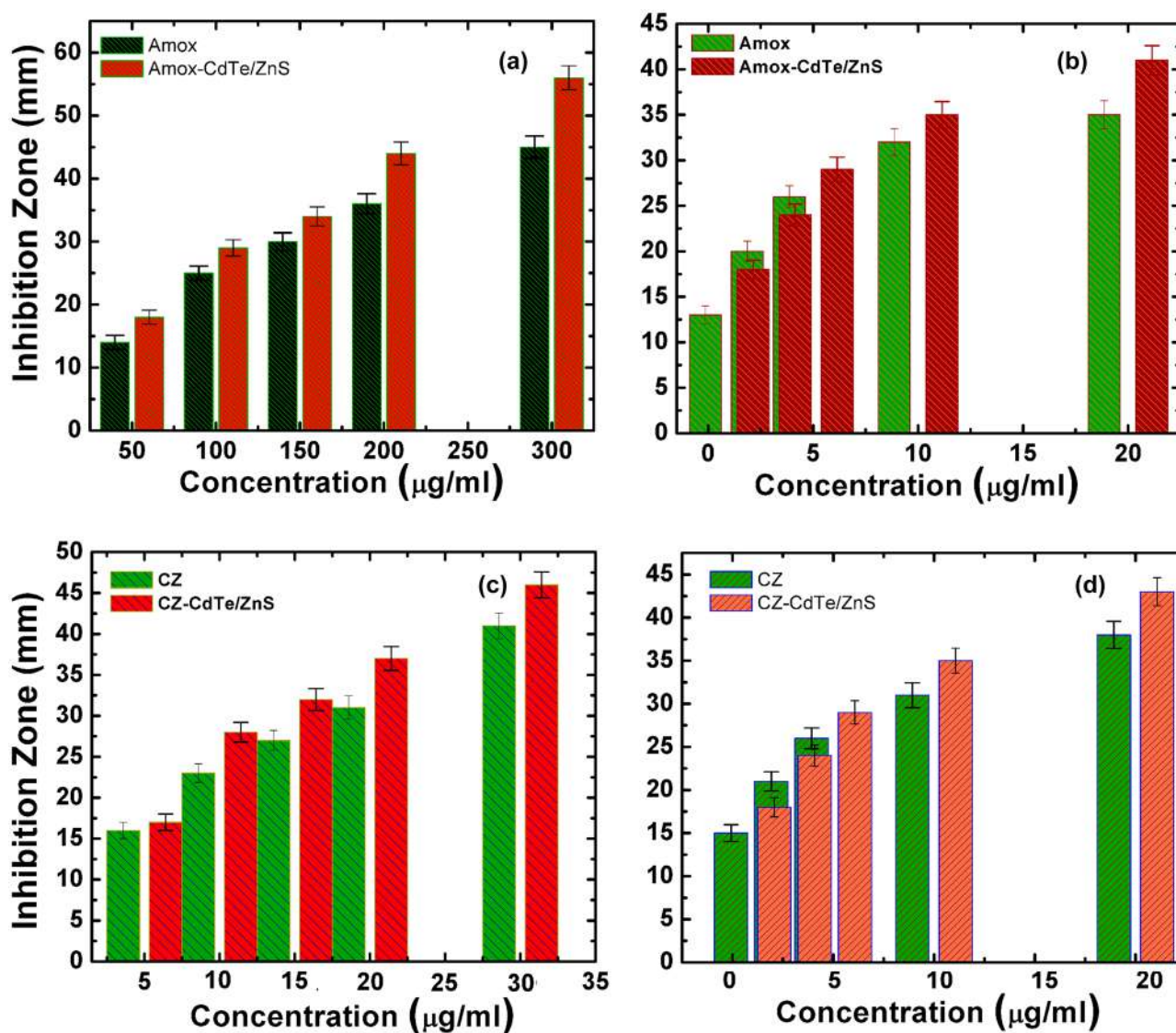


Fig. 9 Inhibition Zone profile of Amox, Amox-CdTe/ZnS, CZ and CZ CdTe/ZnS conjugates against *E. coli* (a-c) and *S. aureus* (b-d)

the diffusion of bare QDs, pure antibiotics and QD-antibiotic conjugates. The diameter of inhibition zone by Amox-CdTe/ZnS conjugates (50, 100, 150, 200 and 300 $\mu\text{g/ml}$) against *E. coli* is found to be 18.0, 29.0, 34.0, 44.0 and 56.0 mm which is greater than the diameter of inhibition zone created by free Amox which shows 14.0, 25.0, 30.0, 36.0 and 45.0 mm after 24 h treatment at 37 °C. Similarly, the inhibition zone produced by Amox-CdTe/ZnS conjugates (1, 3, 5, 10 and 20 $\mu\text{g/ml}$) against *S. aureus* is found to be 18.0, 24.0, 29.0, 35.0 and 41.0 mm which is greater than the inhibition zone produced by free Amox (Tables 5 and 6). Similar trends were observed for CZ-CdTe/ZnS conjugates and pure CZ against both the bacterial strain. In contrast, bare CdTe/ZnS exhibited very low inhibition against both bacterial strains while antibiotics showed quite strong inhibition for both the

bacterial strain. Moreover, the Amox-CdTe/ZnS and CZ-CdTe/ZnS conjugates displayed greater inhibition than the pure antibiotics.

The observed antibacterial efficacy of Amox-CdTe/ZnS and CZ-CdTe/ZnS conjugates can be explained on the basis of earlier studies. We proposed that β -Lactam antibiotics exhibit bactericidal properties by disrupting the formation of bacterial cell walls through covalent binding to crucial penicillin-binding proteins (PBPs). These enzymes are responsible for the final stages of peptidoglycan cross-linking in both Gram-negative and Gram-positive bacteria. Furthermore, The QDs insert into the cell membrane to cause membrane stress; and heavy metal ions are released into the cells to decline the gene expression of superoxide dismutase (SOD) [51]. In addition, the QD-antibiotic

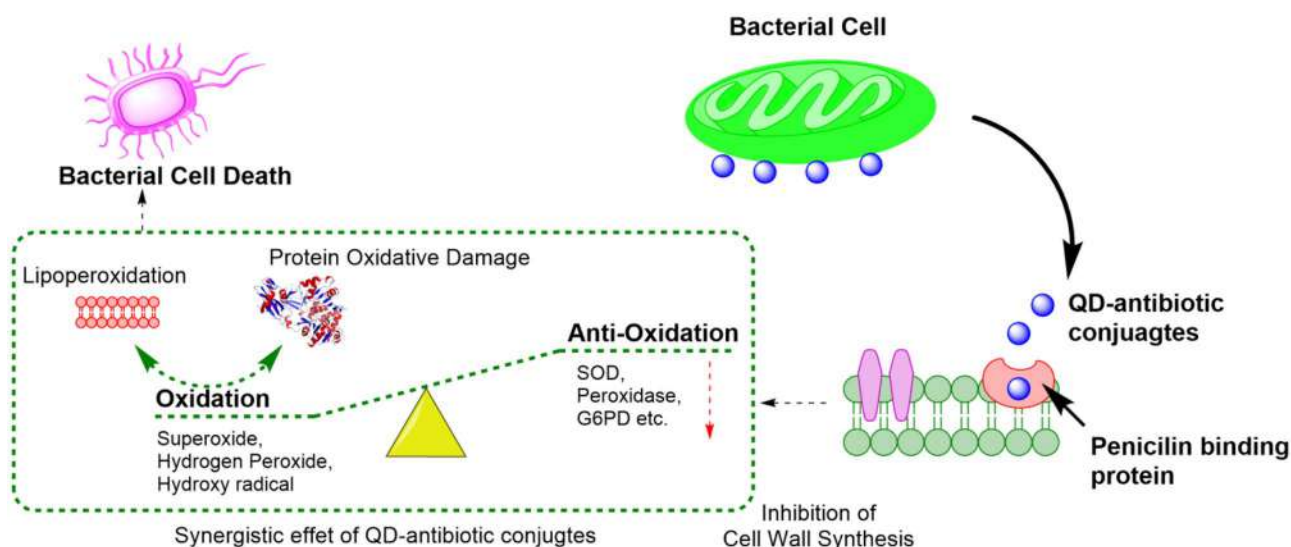


Fig. 10 Mechanism of antibacterial activity

conjugates attach to nuclear material and interfere with protein synthesis or nucleic acid replication (Fig 10) [52]. The synergistic effect of a CdTe/ZnS-antibiotic conjugates can contribute to the superior antibacterial efficacy of CdTe/ZnS-Amox and CdTe-CZ conjugates compared to that of bare CdTe/ZnS quantum dots and antibiotic.

Conclusions

The CdTe/ZnS core shell quantum dots with high quantum yield up to 48% were successfully synthesized. Furthermore, the GSH functionalized CdTe/ZnS core shell QDs was successfully conjugated with amoxicillin and ceftazidime to form QDs-antibiotics conjugates. The Amox-CdTe/ZnS and CZ-CdTe/ZnS conjugates showed enhanced antibacterial activity against *E.coli* and *S. aureus* bacteria, which are used as Gram-negative and Gram-positive model bacteria, respectively. The results showed that the conjugation of CdTe/ZnS QDs with Amox and CZ antibiotics fosters a small synergistic effect and reduces the concentrations of antibiotics required to inhibit both bacterial strains. This research can provide helpful insights to the development of new kind of antimicrobial agents.

Supplementary Information The online version contains supplementary material available at <https://doi.org/10.1007/s10895-023-03316-x>.

Acknowledgment We are thankful to sophisticated analytical instrument research facility (AIRF) Jawaharlal Lal Nehru University (JNU), New Delhi for TEM analysis. We are also grateful to Prof. M.K. Deb, School of Studies in Chemistry, Pt. Ravishankar Shukla University, Raipur for FTIR analysis. Authors are thankful to the head, School of Studies in Chemistry, Pt. Ravishankar Shukla University, Raipur for providing laboratory facilities. Authors are thankful to the head, School

of Studies in Biotechnology, Pt. Ravishankar Shukla University, Raipur for providing laboratory facilities.

Authors' Contributions S.K.V.: experiment, data interpretation and drafting of the manuscript; J.K.: some measurement of fluorescence; R.N.: correction and review of manuscript; T.V.: helped in performing the antibacterial activity experiment and interpretation; S.K.J.: supervise all the antibacterial activity experiment and interpretation; M.L.S.: supervise all the experiment, interpretation of data and manuscript writing.

Funding Financial assistance from DST-FIST and SAP is acknowledged with appreciation.

Data Availability All the data and materials from this manuscript will be made available on request.

Declarations

Ethical Approval Not Applicable.

Consent to Participate Not Applicable.

Consent for Publication Not Applicable.

Conflict of Interests The authors declare no competing interest.

References

1. Imming P, Klar B, Dix D (2000) Hydrolytic stability versus ring size in lactams: Implications for the development of lactam antibiotics and other serine protease inhibitors. *J Med Chem* 43:4328–4331
2. Taggi AE, Hafez AM, Wack H, Young B, Drury WJ, Lectka T (2000) Catalytic, asymmetric synthesis of β -lactams. *J Am Chem Soc* 122:7831–7832
3. Garrity JD, Bennett B, Crowder MW (2005) Direct evidence that the reaction intermediate of metallo- β -lactamase L1 is metal bound. *Biochem* 44:1078–87

4. Farina V, Hauck SI, Firestone RA (1996) Synthesis of cephems bearing olefinic sulfoxide side chains as potential β -lactamase inhibitors. *Bioorg Med Chem Lett* 6:1613–1618
5. Liu YC, Huang WK, Huang TS, Kunin CM (1999) Detection of antimicrobial activity in urine for epidemiologic studies of antibiotic use. *J Clinical Epidem* 52:539–545
6. Zhang HZ, Hackbarth CJ, Chansky KM, Chambers HF (2001) A proteolytic transmembrane signaling pathway and resistance to β -lactams in staphylococci. *Science* 291:1962–1965
7. Neu HC (1992) The crisis in antibiotic resistance. *Science* 257:1064–1073
8. Helena B, Andrea L, Sylvia J, Wolfgang MP, Janka K, Peter M, Milan K (1998) Study of β -lactam resistance in ceftazidime-resistant clinical isolates of Enterobacteriaceae. *Int J Antimicrob Agents* 10:135–141
9. Pitout JD, Sanders CC, Sanders WE Jr (1997) Antimicrobial resistance with focus on β -lactam resistance in gram-negative bacilli. *Am J Med* 103:51–59
10. Craig WA (1996) Antimicrobial resistance issues of the future. *Diagn Microbiol Infect Dis* 25:213–217
11. Miethke M, Pieroni M, Weber T, Brönstrup M, Hammann P, Halby L, Arimondo PB, Glaser P, Aigle B, Bode HB, Moreira R (2021) Towards the sustainable discovery and development of new antibiotics. *Nature Reviews Chemistry* 5:726–749
12. Souli M, Wennersten CB, Eliopoulos GM (1998) In vitro activity of BAY 12–8039, a new fluoroquinolone, against species representative of respiratory tract pathogens. *Int J Antimicrob. Agents* 10:23–30
13. Fonzé E, Vanhove M, Dive G, Sauvage E, Frere JM, Charlier P (2002) Crystal Structures of the Bacillus licheniformis BS3 Class A β -Lactamase and of the Acyl– Enzyme Adduct Formed with Cefoxitin. *Biochemistry* 41:1877–1885
14. Georg GI (1993) *The Organic Chemistry of β -Lactamas* (New York: VCH publishers) 121–96
15. Buynak JD, Doppalapudi VR, Adam G (2000) The synthesis and evaluation of 3-substituted-7-(alkylidene) cephalosporin sulfones as β -lactamase inhibitors. *Bioorg Med Chem Lett* 10:853–857
16. Jones RN, Marshall SA, Varnam DJ (1998) Activity of a broad-spectrum cephalosporin (Ro 48–8391) alone and in combination with two novel β -lactamase inhibitors (Ro 48–5545 and Ro 48–8724). *Diagn Microbiol Infect Dis* 32:85–89
17. Vergauwe A, Van Geldre E, Inzé D, Van Montagu M, Van den Eeckhout E (1996) The use of amoxicillin and ticarcillin in combination with a β -lactamase inhibitor as decontaminating agents in the Agrobacterium tumefaciens-mediated transformation of Artemisia annua L. *J Biotechnology* 52:89–95
18. Sondi I, Salopek-Sondi B (2004) Silver nanopartikel som antimikrobiellt medel: en fallstudie på E. coli som modell för gram-negativa bakterier. *J Colloid Interface Sci* 275:177–182
19. Lyon DY, Adams LK, Falkner JC, Alvarez PJ (2006) Antibacterial activity of fullerene water suspensions: effects of preparation method and particle size. *Environ Sci Tech* 40:4360–4366
20. Lok CN, Ho CM, Chen R, He QY, Yu WY, Sun H, Che CM (2007) Silver nanoparticles: partial oxidation and antibacterial activities. *J Biological Inorg. Chem.* 12:527–534
21. Heinlaan M, Ivask A, Blinova I, Dubourguier HC, Kahru A (2008) Toxicity of nanosized and bulk ZnO, CuO and TiO₂ to bacteria Vibrio fischeri and crustaceans Daphnia magna and Thamnocephalus platyurus. *Chemosphere* 71:1308–1316
22. Cao X, Li CM, Bao H, Bao Q, Dong H (2007) Fabrication of strongly fluorescent quantum dot– polymer composite in aqueous solution. *Chem Mater* 19:3773–3779
23. Li R, Li CM, Bao H, Bao Q, Lee VS (2007) Stationary current generated from photocycle of a hybrid bacteriorhodopsin/quantum dot bionanosystem. *App Phys Lett* 91:223901
24. Zhu C, Chen Z, Gao S, Goh BL, Samsudin IB, Lwe KW, Wu Y, Wu C, Su X (2019) Recent advances in non-toxic quantum dots and their biomedical applications. *Progress in Natural Science: Mater Int* 29:628–640
25. Constantine CA, Gattás-Asfura KM, Mello SV, Crespo G, Rastogi V, Cheng TC, DeFrank JJ, Leblanc RM (2003) Layer-by-layer biosensor assembly incorporating functionalized quantum dots. *Langmuir* 19:9863–9867
26. Heger Z, Cernei N, Blazkova I, Kopel P, Masarik M, Zitka O, Adam V, Kizek R (2014) γ -Fe₂O₃ Nanoparticles Covered with Glutathione-Modified Quantum Dots as a Fluorescent Nanotransporter. *Chromatographia* 77:1415–1423
27. Voura EB, Jaiswal JK, Mattoussi H, Simon SM (2004) Tracking metastatic tumor cell extravasation with quantum dot nanocrystals and fluorescence emission-scanning microscopy. *Nature Medicine* 10:993–998
28. Alivisatos AP (1996) Perspectives on the Physical Chemistry of Semiconductor Nanocrystals. *J. Phys. Chem.* 100:13226–13239
29. Rhyner MN, Smith AM, Gao X, Mao H, Yang L, Nie S (2006) Quantum dots and multifunctional nanoparticles: new contrast agents for tumor imaging. *Nanomedicine* 1:209–217
30. Dwarakanath S, Bruno JG, Athmaram TN, Bali G, Vattam D, Rao P (2017) Antibody-quantum dot conjugates exhibit enhanced antibacterial effects vs. unconjugated quantum dots. *Folia Microbiologica* 52:31–34
31. Ananth DA, Rameshkumar A, Jeyadevi R, Jagadeeswari S, Nagarajan N, Renganathan R, Sivasudha T (2015) Antibacterial potential of rutin conjugated with thioglycolic acid capped cadmium telluride quantum dots (TGA-CdTe QDs). *Spectrochim. Acta A: Molecul Biomol Spectro* 138:684–692
32. Klopfer JA, Mielke RE, Nadeau JL (2005) Uptake of CdSe and CdSe/ZnS quantum dots into bacteria via purine-dependent mechanisms. *Appl Environ Microbiol* 71:2548–2557
33. Allen PM, Bawendi MG (2008) Ternary I– III– VI quantum dots luminescent in the red to near-infrared. *J Am Chem Soc* 130:9240–9241
34. Blackman B, Battaglia D, Peng X (2008) Bright and water-soluble near IR-emitting CdSe/CdTe/ZnSe type-II/type-I nanocrystals, tuning the efficiency and stability by growth. *Chem Mater* 20:4847–4853
35. Jensen KF, Bawendi MG (1997) (CdSe)ZnS Core–Shell Quantum Dots: Synthesis and Characterization of a Size Series of Highly Luminescent Nanocrystallites. *J. Phys. Chem. B* 101:9463–9475
36. Du Y, Xu B, Fu T, Cai M, Li F, Zhang Y, Wang Q (2010) Near-infrared photoluminescent Ag₂S quantum dots from a single source precursor. *J Am Chem Soc* 132:1470–1471
37. Hewa-Kasakarage NN, Gurusinge NP, Zamkov M (2009) Blue-shifted emission in CdTe/ZnSe heterostructured nanocrystals. *J Phys Chem C* 113:4362–4368
38. Shen S, Zhang Y, Peng L, Du Y, Wang Q (2011) Matchstick-Shaped Ag₂S–ZnS Heterostructures Preserving both UV/Blue and Near-Infrared Photoluminescence. *Angew Chem Int Ed* 50:7115–7118
39. Tsay JM, Pflughoeft M, Bentolila LA, Weiss S (2004) Hybrid approach to the synthesis of highly luminescent CdTe/ZnS and CdHgTe/ZnS nanocrystals. *J Am Chem Soc* 126:1926–1927
40. Zhang C, Ji X, Zhang Y, Zhou G, Ke X, Wang H, He Z (2013) One-pot synthesized aptamer-functionalized CdTe: Zn²⁺ quantum dots for tumor-targeted fluorescence imaging in vitro and in vivo. *Anal Chem* 85:5843–5849
41. Erogbogbo F, Yong KT, Roy I, Hu R, Law WC, Zhao W, Ding H, Wu F, Kumar R, Swihart MT, Prasad PN (2011) In vivo targeted cancer imaging, sentinel lymph node mapping and multi-channel imaging with biocompatible silicon nanocrystals. *ACS Nano* 5:413–423

42. Liu YF, Yu JS (2010) In situ synthesis of highly luminescent glutathione-capped CdTe/ZnS quantum dots with biocompatibility. *J Colloid Interface Sci* 351:1–9
43. Yu WW, Qu LH, Guo WZ, Peng XG (2003) Experimental determination of the extinction coefficient of CdTe, CdSe, and CdS nanocrystals. *Chem. Mater* 15:2854–2860
44. Bao H, Gong Y, Li Z, Gao M (2004) Enhancement effect of illumination on the photoluminescence of water-soluble CdTe nanocrystals: toward highly fluorescent CdTe/CdS core–shell structure. *Chem Mater* 16:3853–3859
45. He Y, Sai LM, Lu HT, Hu M, Lai WY, Fan QL, Wang LH, Huang W (2007) Microwave-assisted synthesis of water-dispersed CdTe nanocrystals with high luminescent efficiency and narrow size distribution. *Chem Mater* 19:359–365
46. He Y, Lu HT, Sai LM, Lai WY, Fan QL, Wang LH, Huang W (2006) Microwave-assisted growth and characterization of water-dispersed CdTe/CdS Core–Shell nanocrystals with high photoluminescence. *J Phys Chem B* 110:13370–13374
47. Dobrovolskaia MA, Clogston JD, Neun BW, Hall JB, Patri AK, McNeil SE (2008) Method for analysis of nanoparticle hemolytic properties in vitro. *Nano Lett* 8:2180–2187
48. Ostomel TA, Shi Q, Stoimenov PK, Stucky GD (2007) Metal oxide surface charge mediated hemostasis. *Langmuir* 23:11233–11238
49. Liu YF, Yu JS (2010) In situ synthesis of highly luminescent glutathione-capped CdTe/ZnS quantum dots with biocompatibility. *J Colloid Interface Sci* 333:690–698
50. Trindade T, O'Brien P, Pickett NL (2001) Nanocrystalline semiconductors: synthesis, properties, and perspectives. *Chem. Mater* 13:3843–3858
51. Lu Z, Li CM, Bao H, Qiao Y, Toh Y, Yang X (2008) Mechanism of antimicrobial activity of CdTe quantum dots. *Langmuir* 24:5445–5452
52. Neelgund GM, Oki A, Luo Z (2012) Antimicrobial activity of CdS and Ag₂S quantum dots immobilized on poly(amidoamine) grafted carbon nanotubes. *Colloids Surf. B Biointerfaces* 100:215–221
53. Luo Z, Wu Q, Zhang M, Li P, Ding Y (2011) Cooperative antimicrobial activity of CdTe quantum dots with Rocephin and fluorescence monitoring for Escherichia coli. *J. Colloid Interface Sci.* 362:100–106
54. Dhar R, Singh S, Kumar A (2015) Effect of capping agents on optical and antibacterial properties of cadmium selenide quantum dots. *Bull. Mater. Sci.* 38:1247–1252
55. Thakur M, Pandey S, Mewada A, Patil V, Khade M, Goshi E, Sharon M (2014) Antibiotic conjugated fluorescent carbon dots as a theranostic agent for controlled drug release, bioimaging, and enhanced antimicrobial activity. *J. Drug Delivery* 2014:1–9

Publisher's Note Springer Nature remains neutral with regard to jurisdictional claims in published maps and institutional affiliations.

Springer Nature or its licensor (e.g. a society or other partner) holds exclusive rights to this article under a publishing agreement with the author(s) or other rightsholder(s); author self-archiving of the accepted manuscript version of this article is solely governed by the terms of such publishing agreement and applicable law.



Low-temperature storage in dark condition improved the *in vitro* regeneration of *Plumbago zeylanica* synthetic seeds: a medicinally valuable species

Ravishankar Chauhan^{1,2} · Priya Banjare² · Subir Kumar Parey² · Afreen Anjum² · Afaque Quraishi²

Received: 26 June 2023 / Accepted: 1 February 2024 / Editor: Raj Deepika
© The Society for In Vitro Biology 2024

Abstract

Medicinal applications of *Plumbago zeylanica* and its metabolites on various diseases and low viability and inconsistent germination of its seeds are the reasons behind the loss of its genetic diversity. Hence, an efficient protocol for the short-term storage of *P. zeylanica* synthetic seeds, which is an overexploited medicinally valuable plant, was developed. Initially, *in vitro* culture was performed from nodal explants to develop synthetic seeds from its proliferated shoots. Murashige and Skoog (MS) medium augmented with 0.5 mg L⁻¹ 6-benzylaminopurine (BAP) resulted in the best morphogenetic response. Thereafter, the developed synseeds were stored for 2 wk at a temperature of 10 or 25°C in different conditions and further evaluated for regeneration. Higher re-growth rate (80%) and the identical morphogenetic response were recorded for the *P. zeylanica* synthetic seeds, which were stored at a temperature of 10°C in dark condition after its storage period. As per the available literature, this is the first report pertaining to *in vitro* low-temperature storage of synthetic seeds of *P. zeylanica* and can further be utilized for the conservation of elite clones for the study of medicinally potent species.

Keywords Cold storage · Encapsulation · *In vitro* conservation · Micropropagation · Synseed

Introduction

Plumbago zeylanica L. is an herbaceous species generally known as Chitrak, which is widely distributed across the subtropics of the world, more particularly southern and central India (Jain *et al.* 2018; Santra and Ghosh 2023). Previous reports have shown its medicinal and pharmacological impacts on hemorrhoids, rheumatism, and skin diseases, and it exhibited anti-cancer, anti-microbial, central nervous system stimulatory, and hepato-protective properties due to the presence of an important bioactive—plumbagin (Edwin *et al.* 2009; Sharma and Agrawal 2018; Zheng *et al.* 2023). These impacts cause an increase in market demand for the targeted species, resulting in constant overexploitation, which ultimately results in the loss of future genetic

diversity (Mittal *et al.* 2010; Pandey *et al.* 2023). *P. zeylanica* propagation through seeds is not reliable due to low viability and inconsistent germination (Chaplot *et al.* 2006). Hence, in order to preserve *P. zeylanica*, an efficient *in vitro* conservation strategy is needed.

In comparison to field-grown plants, *in vitro* regenerated cultures required limited care for their conservation over time (Alzubi *et al.* 2019; Sota *et al.* 2023). However, tissue culture-grown plants need successive subcultures that are economically not feasible and may induce off-types *via* somaclonal variations (Quraishi *et al.* 2017). There are several efficient techniques to preserve elite germplasm of clonally propagated plants. Among them, the slow-growth conservation technique allows the conservation of plant materials for short to long periods of time (Reed *et al.* 2011) in a small area and at a low cost by slowing down the plant's physiological metabolism (Deepa and Thomas 2020; Lacerda *et al.* 2021). Production of synseeds is also one of the chief approaches for conservation and transportation with high germination and bears immense potential as a substitute for true seed (Jain *et al.* 2018). It can be defined as the artificial encapsulation of totipotent cells or tissues, which can grow under both *in vivo* and *in vitro* conditions

✉ Ravishankar Chauhan
ravi18bt@gmail.com

¹ Department of Botany, Pandit Ravishankar Tripathi
Government College, Bhaiyathan, Surajpur 497231, India

² School of Studies in Biotechnology, Pt. Ravishankar Shukla
University, Raipur 492010, India

Targeting Pathways and Integrated Approaches to Treat Rheumatoid Arthritis

Shradha Devi Dwivedi,^a Krishna Yadav,^a Anita Bhoi,^b Keshav Kant Sahu,^b Neelam Sangwan,^c Deependra Singh,^a & Manju Rawat Singh^{a,*}

^aUniversity Institute of Pharmacy, Pt. Ravishankar Shukla University, Raipur (C.G), 492010, India; ^bSchool of studies in biotechnology, Pt. Ravishankar Shukla University, Raipur (C.G), 492010, India; ^cDepartment of Biochemistry, School of Interdisciplinary and Applied Sciences, Central University of Haryana, Mahendergarh, 123031, India

*Address all correspondence to: Dr. Manju Rawat Singh, Asst. Professor, University Institute of Pharmacy, Pt. Ravishankar Shukla University, Raipur (C.G.)492010, India; Tel.: +91-7712262832 (Telefax); Mobile: 8109797927, E-mail: manjursu@gmail.com

ABSTRACT: Rheumatoid arthritis (RA) is a chronic symmetrical systemic disorder that not only affects joints but also other organs such as heart, lungs, kidney, and liver. Approximately there is 0.5%–1% of the total population affected by RA. RA pathogenesis still remains unclear due to which its appropriate treatment is a challenge. Further, multitudes of factors have been reported to affect its progression i.e. genetic factor, environmental factor, immune factor, and oxidative factor. Therapeutic approaches available for the treatment of RA include NSAIDs, DMARDs, enzymatic, hormonal, and gene therapies. But most of them provide the symptomatic relief without treating the core of the disease. This makes it obligatory to explore and reach the molecular targets for cure and long-term relief from RA. Herein, we attempt to provide extensive overlay of the new targets for RA treatment such as signaling pathways, proteins, and receptors affecting the progression of the disease and its severity. Precise modification in these targets such as suppressing the notch signaling pathway, SIRT 3 protein, Sphingosine-1-phosphate receptor and stimulating the neuronal signals particularly efferent vagus nerve and SIRT 1 protein may offer long term relief and potentially diminish the chronicity. To target or alter the novel molecules and signaling pathway a specific delivery system is required such as liposome, nanoparticles and micelles and many more. Present review paper discusses in detail about novel targets and delivery systems for treating RA.

KEY WORDS: rheumatoid arthritis, causative factor, notch signaling, sirtuin, sphingosine-1-phosphate, neuronal signals, delivery system

I. INTRODUCTION

Rheumatoid arthritis (RA) is a chronic systemic autoimmune disorder that systematically affects the whole body. RA chronicity is manifested as destruction of cartilage lining by synovial capsule, the formation of pannus, morning stiffness, and intolerable pain particularly in cold conditions.¹ Globally, around 1% of the total world population suffer from RA.² The incidence of RA in women is two to three-times higher than men. At any age, RA can occur but it generally occurs at the age of 40–60 years in women while in men it is 60 years.³ Along with these, 40% of RA patients suffer from extra-articular symptoms such as glomerulonephritis, atherosclerosis, and small vascular vacuities. This deteriorates the quality of patient life both socially and economically which results



A comprehensive report on valorization of waste to single cell protein: strategies, challenges, and future prospects

Sharda Devi Rajput¹ · Neha Pandey¹ · Keshavkant Sahu¹

Received: 10 June 2023 / Accepted: 16 March 2024

© The Author(s), under exclusive licence to Springer-Verlag GmbH Germany, part of Springer Nature 2024

Abstract

The food insecurity due to a vertical increase in the global population urgently demands substantial advancements in the agricultural sector and to identify sustainable affordable sources of nutrition, particularly proteins. Single-cell protein (SCP) has been revealed as the dried biomass of microorganisms such as algae, yeast, and bacteria cultivated in a controlled environment. Production of SCP is a promising alternative to conventional protein sources like soy and meat, due to quicker production, minimal land requirement, and flexibility to various climatic conditions. In addition to protein production, it also contributes to waste management by converting it into food and feed for both human and animal consumption. This article provides an overview of SCP production, including its benefits, safety, acceptability, and cost, as well as limitations that constrains its maximum use. Furthermore, this review criticizes the downstream processing of SCP, encompassing cell wall disruption, removal of nucleic acid, harvesting of biomass, drying, packaging, storage, and transportation. The potential applications of SCP, such as in food and feed as well as in the production of bioplastics, emulsifiers, and as flavoring agents for baked food, soup, and salad, are also discussed.

Keywords Microbial protein · Microorganisms · Fermentation · Downstream processing · Food source · Green protein

Introduction

The global population is predicted to increase to nine billion by 2050. In light of the present pattern of food consumption, we may probably require 1250 million tonnes of dairy and meat products per year to fulfill the demand of animal-derived proteins (Verstraete et al. 2016). In the future, requirement of additional proteins cannot be fulfilled with the existing food production strategies such as agriculture. However, the proteins are quite essential for cellular and metabolic activities and serves as a source of nitrogen for animals and humans to form their functional and structural components for survival. In recent decades, protein-calorie malnutrition (PCM) has been reported to affect children, resulting in poor mental growth and weak immunity (Junaid et al. 2020). The nutritional value of proteins depends on

their constituent amino acids. Due to their inability to be synthesized by the cells, animal populations typically require essential amino acids (EAAs) from external food sources to achieve their daily demand (Junaid et al. 2020). Proteins derived from different fruits, vegetables, and typical grains are often out of reach of the average person; therefore, microbial protein can be an alternate source of food for economically deprived population worldwide. Hence, this is high time to concentrate on deriving alternate, innovative, affordable, and unconventional protein sources to satisfy the nutritional requirements of the growing population. In regard, single-cell proteins (SCPs), cultured meat, plant-based new proteins, macroalgae, seaweed, and insects are some of the examples of sources of alternate proteins. Production of SCP is one of such potential approaches.

Single-cell protein mainly consists of a dried mass of microorganisms with high protein content, carbohydrates, lipids, minerals, and vitamins. The term SCP was coined by Carol L. Wilson in 1966 to define microbial biomass products (Suman et al. 2015). It can be total biomass or proteins isolated from pure culture or a mixed culture of microbial populations such as bacteria, algae, and fungi. The SCP has countless significant advantages over other protein sources:

Responsible Editor: Ta Yeong Wu

✉ Keshavkant Sahu
skeshavkant@gmail.com

¹ School of Studies in Biotechnology, Pt. Ravishankar Shukla University, Raipur, Chhattisgarh 492 010, India



Nano zinc oxide mediated resuscitation of aged *Cajanus cajan* via modulating aquaporin, cell cycle regulatory genes and hormonal responses

Rasleen Kaur¹ · Bhumika Yadu² · Nagendra Singh Chauhan³ · Arun Singh Parihar³ · S. Keshavkant¹

Received: 5 December 2023 / Accepted: 19 March 2024

© The Author(s), under exclusive licence to Springer-Verlag GmbH Germany, part of Springer Nature 2024

Abstract

Key message Nanoparticle pretreatment improved the health of aged *Cajanus cajan* seeds viz., regulation of redox status, gene expression, and restoration of hormonal homeostasis.

Abstract Ageing deteriorates the quality of seeds by lowering their vigor and viability, and terminating with loss of germination. These days, nanotechnology has been seen to revolutionize the agricultural sectors, and particularly nano zinc oxide (nZnO) has gained considerable interests due to its distinctive properties. The aim of the present work was to decipher the possibilities of using nZnO to rejuvenate accelerated aged (AA) seeds of *Cajanus cajan*. Both chemically (CnZnO) and green (GnZnO; synthesized using *Moringa oleifera*) fabricated nZnOs were characterized via standard techniques to interpret their purity, size, and shape. Experimental results revealed erratic germination with a decline in viability and membrane stability as outcomes of reactive oxygen intermediate (ROI) buildup in AA seeds. Application of nZnO substantially rebated the accrual of ROI, along with enhanced production of antioxidants, α -amylase activity, total sugar, protein and DNA content. Higher level of zinc was assessed qualitatively/ histologically and quantitatively in nZnO pulsed AA seeds, supporting germination without inducing toxicity. Meantime, augmentation in the gibberellic acid with a simultaneous reduction in the abscisic acid level were noted in nZnO invigorated seeds than that determined in the AA seeds, suggesting possible involvement of ROI in hormonal signalling. Furthermore, nZnO-subjected AA seeds unveiled differential expression of aquaporins and cell cycle regulatory genes. Summarizing, among CnZnO and GnZnO, later one holds better potential for a revival of AA seeds of *Cajanus cajan* by providing considerable tolerance against ageing-associated deterioration via recouping the cellular redox homeostasis, hormonal signaling, and alteration in expression patterns of aquaporin and cell cycle regulatory genes.

Communicated by Om Parkash Parkash Dhankher.

✉ S. Keshavkant
skeshavkant@gmail.com

¹ School of Studies in Biotechnology, Pt. Ravishankar Shukla University, Raipur 492 010, India

² School of Life and Allied Science, ITM University, Raipur 492 002, India

³ Drug Testing Laboratory and Research Centre, Raipur 490 024, India



Role and uptake of metal-based nanoconstructs as targeted therapeutic carriers for rheumatoid arthritis

Shradha Devi Dwivedi¹ · Anita Bhoi² · Madhulika Pradhan³ · Keshav Kant Sahu² · Deependra Singh¹ · Manju Rawat Singh¹

Received: 8 December 2023 / Accepted: 15 April 2024
© King Abdulaziz City for Science and Technology 2024

Abstract

Rheumatoid Arthritis (RA) is a chronic autoimmune systemic inflammatory disease that affects the joints and other vital organs and diminishes the quality of life. The current developments and innovative treatment options have significantly slowed disease progression and improved their quality of life. Medicaments can be delivered to the inflamed synovium via nanoparticle systems, minimizing systemic and undesirable side effects. Numerous nanoparticles such as polymeric, liposomal, and metallic nanoparticles reported are impending as a good carrier with therapeutic properties. Other issues to be considered along are nontoxicity, nanosize, charge, optical property, and ease of high surface functionalization that make them suitable carriers for drug delivery. Metallic nanoparticles (MNPs) (such as silver, gold, zinc, iron, titanium oxide, and selenium) not only act as good carrier with desired optical property, and high surface modification ability but also have their own therapeutical potential such as anti-oxidant, anti-inflammatory, and anti-arthritis properties, making them one of the most promising options for RA treatment. Regardless, cellular uptake of MNPs is one of the most significant criteria for targeting the medication. This paper discusses the numerous interactions of nanoparticles with cells, as well as cellular uptake of NPs. This review provides the mechanistic overview on MNPs involved in RA therapies and regulation anti-arthritis response such as ability to reduce oxidative stress, suppressing the release of proinflammatory cytokines and expression of LPS induced COX-2, and modulation of MAPK and PI3K pathways in Kupffer cells and hepatic stellate cells. Despite of that MNPs have also ability to regulates enzymes like glutathione peroxidases (GPxs), thioredoxin reductases (TrxRs) and act as an anti-inflammatory agent.

Keywords Rheumatoid arthritis · Metallic nanoparticle · Targeting · Cellular uptake

✉ Manju Rawat Singh
manjursu@gmail.com

Shradha Devi Dwivedi
shradhadwivedi9@gmail.com

Anita Bhoi
anitabhohi0001@gmail.com

Madhulika Pradhan
madhulika.pradhan1@gmail.com

Keshav Kant Sahu
skeshavkant@gmail.com

Deependra Singh
deependraiop@gmail.com

¹ University Institute of Pharmacy, Pt. Ravishankar Shukla University, Raipur, Chhattisgarh 492010, India

² School of Studies in Biotechnology, Pt. Ravishankar Shukla University, Raipur, C.G 492010, India

³ Gracious College of Pharmacy, Abhanpur Raipur, Chhattisgarh 493661, India

Introduction

Rheumatoid Arthritis (RA) is a chronic systemic autoimmune disorder. It is characterized by the destruction of bone and cartilage inflammation at a synovial site, leading to enhanced mortality disability and reduced quality of life. (Song et al. 2021; Devi Dwivedi et al. 2023) Out of 100,000 of the total population, 40 persons are affected by RA, more significant than 0.5 to 1%. It commonly starts at the age of 40 to 60 years (Zheng et al. 2021). According to the Global Burden of Disease 2010, the prevalence of RA in women is almost three times greater than in males which is usually one female in 28 and one male in 59. RA can develop at any stage of life. Women between the ages of 30 and 60 are more likely than males to acquire RA (Brennan-Olsen et al. 2017). Advancement in RA therapy was associated with the joint damage, inhibition, control the progression of disease

***“Design and Characterization of Hybrid photodetector
based on Polypyrrole and silicon”***



*A Dissertation Submitted in Partial
Fulfillment of the requirements*

For the degree of

MASTER OF TECHNOLOGY

in

Optoelectronics and Laser Technology

Submitted by

Drishty Singh

(2210196002)

Under the Guidance of

Supervision of

Dr. Sesa Vempati

Assistant professor, Department of Physics,
Indian Institute of Technology
Bhilai, Chhattisgarh.

Co-Supervision of

Dr. Kavita Thakur

Professor & Course Coordinator
S.O.S Electronics and Photonics
PRSU, Raipur, Chhattisgarh

Work carried out at



Department of Physics, Indian Institute of Technology, Bhilai

Bhilai – 491001

Chhattisgarh

Jan-june 2024



School of Studies in Electronics and Photonics
Pt. Ravishankar Shukla University
Raipur - 492010
Chhattisgarh

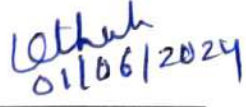
Dissertation Approval For M.Tech

Session 2023-24

This dissertation work entitled, "*Design and Characterization of Hybrid Photodetector based on Polypyrrole and silicon*" submitted by *Ms. Drishty Singh* at the *Department of Physics, Indian Institute of Technology Bhilai* during the period *Jan 2024 to June 2024* is Approved for the degree of *Master of Technology (4th Semester)* in *Optoelectronics and Laser Technology*, Pt. Ravishankar Shukla University, Raipur, Chhattisgarh


EXTERNAL EXAMINER

Dr. H.S. Tewari
professor
Department of pure &
Applied physics.
Guru Ghasidas University
Bilaspur - 495009


INTERNAL OF EXAMINER

Dr Kavita Thakur
Professor & Course Coordinator
S.o.S in Electronics and Photonics
Pt. Ravishankar Shukla University, Raipur
Chhattisgarh-492010

Date :

Place :



Department of Physics, Indian Institute of Technology Bhilai
Bhilai – 491001
Chhattisgarh

CERTIFICATE

This is to certify that the dissertation work entitled, *“Design and Characterization of Hybrid Photodetector based on Polypyrrole and Silicon”* submitted by **Ms Drishty Singh**, is a credible work carried out by her at the *Department of Physics, Indian Institute of Technology Bhilai* during the period *Jan 2024 to June 2024*. The work has been presented in a manner suitable to affirm acceptance towards the partial fulfillment of the requirement for the degree of *Master of Technology in Optoelectronics and Laser Technology, Pt. Ravishankar Shukla University, Raipur, Chhattisgarh*, is the candidate’s work carried out by her under my supervision. Her dedication and sincerity are praiseworthy.

V.S.Pavan Kumar

Signature of Supervisor

Dr. Sesa Vempati

Assistant Professor

Department of Physics,

Indian Institute of Technology, Bhilai,

Chhattisgarh

Date: 27/05/2024

Place: Bhilai





School of Studies in Electronics and Photonics
Pt. Ravishankar Shukla University
Raipur - 492010
Chhattisgarh

CERTIFICATE

This is to certify that the dissertation work entitled, ***“Design and Characterization of Hybrid Photodetector based on Polypyrrole and silicon”*** submitted by ***Ms. Drishty Singh*** is a credible work carried by her at the ***Department of Physics, Indian Institute of Technology Bhilai*** during the period ***Jan 2024 to June 2024***. The work has been presented in a manner suitable to affirm acceptance towards the partial fulfilment of the requirement for the degree of ***Master of Technology in Optoelectronics and Laser Technology, Pt. Ravishankar Shukla University, Raipur, Chhattisgarh.***

K. Thakur
01/06/2024

INTERNAL SUPERVISOR

Dr. Kavita Thakur

Professor & Course Coordinator
S.o.S in Electronics and Photonics
Pt. Ravishankar Shukla University,
Raipur

K. Thakur
01/06/2024

HEAD OF DEPARTMENT

Dr. Kavita Thakur
Head

Date :

Place:

DECLARATION

I hereby declare that the dissertation entitled "*Design and Characterization of Hybrid Photodetector based on Polypyrrole and silicon*" submitted to the *School of Studies in Electronics & Photonics, Pt. Ravishankar Shukla University, Raipur, Chhattisgarh* for the degree of *Master of Technology in Optoelectronics & Laser Technology* is an original record of work done by me at the *Department of Physics, Indian Institute of Technology Bhilai* under the guidance of *Dr. Sesa Vempati, Assistant Professor, Department of Physics, Indian Institute of Technology, Bhilai*. I also declare that I have adhered to all principles of academic honesty and integrity.

I further declare that to the best of my knowledge; my dissertation does not contain any part of any work that has been submitted for the award of any degree either in this institute or in any other university without proper citation.



Drishty Singh

(Roll No: **2210196002**)

Enrollment No: AH/00514

MTech (OELT), 4th, Semester, Pt. Ravi Shankar
Shukla University

ACKNOWLEDGMENT

I would like to express my deep sense of gratitude to my project supervisor **Dr. Sessa Vempati**, Assistant Professor at the Department of Physics, IIT Bhilai for his encouragement, guidance, and motivation for providing me with all the required facilities for my project work. I feel proud to have the opportunity to work with such exceptionally experienced professors. His insightful comments and valuable suggestions have contributed significantly to my work and improved my understanding of the subject matter. Without his encouragement and guidance, this project would not have materialized. I am extremely exhilarated to have completed this report under his able and inspiring guidance.

I sincerely wish to express my gratefulness to **H.O.D Prof. Kavita Thakur** (Head of the department, SoS in Electronics and Photonics, PRSU, Raipur) for her suggestions, help, coordination, and support for giving me her precious time to improve the quality of this project work.

I would also like to express my sincere thanks to **Mr. Narayan Prasad, Ms. Smita Singh, Mrs Subhalaxmi Nayak**, and all the **members of the Department of Physics lab, IIT Bhilai** for their valuable recommendations, remarkable support, and assistance in carrying out many experimental projects.

I would also like to express my sincere thanks to my fellow Batch mate **Mr. Sandeep Sahu** and the faculty of my department, **Mr. Mohnish Kumar Sahu, Mr. K. Anil, and Mr. Madhu Allalla** who helped me during this work, I also extend my gratitude to lab coordinators and all technical-non-technical staff of the department for their support. Last but not least, I express my thanks to my parents for providing me congenial atmosphere for me to work on the project report.

Drishty Singh

ABSTRACT

This thesis presents a comprehensive study on designing, current-voltage (I-V) characteristics, and Raman spectral analysis of the photodetector with a focus on the utilization of novel and advanced materials such as Polypyrrole (Ppy) polymer and silicon. Photodetectors are one of the components in optoelectronic devices and has been a topic of research in the last few years because of the advancements made in optoelectronics. Optoelectronics devices are introduced as an essential component of photonics and sensor technology, ranging from optical communication to renewable energy. The I-V characteristics of the photodetectors are systematically studied under different illumination and dark conditions, revealing the device's response to different wavelength. Raman spectroscopy is employed to investigate the polymer and semiconductor material's structural characteristics and vibration modes. This spectral analysis provides valuable insights into the molecular interactions, crystallinity, and quality of the materials, aiding in optimizing the device's performance.

KEYWORDS Raman Spectroscopy, I-V Characteristics, Photodetector, Polypyrrole, Silicon

Table of Contents

Chapter-1

OPTOELECTRONIC DEVICES AND MATERIALS.....	1
1.1 Research Objective.....	2
1.2 Introduction.....	3
1.3 Carrier photon interaction	4
1.3.1 Emission and absorption rates & the Einstein relation.....	5
1.3.2 Direct and Indirect gap.....	7
1.3.3 Population inversion.....	8

Chapter-2

HYBRID AND ADVANCE FUNCTIONAL MATERIALS.....	10
2.1 Introduction.....	10
2.2 Fundamentals of Hybrid Materials.....	11
2.2.1 Definition and Category of Hybrid Material.....	11
2.3 Inorganic/ Organic Hybrids.....	12
2.3.1 Polypyrrole-Silicon Hybrid Material.....	13
2.3.2 Synthesis method preparation of Polypyrrole-silicon as Hybrid Material	14
2.3.3 Characterization of Hybrid Material.....	15

Chapter-3

POLYPYRROLE CONDUCTING POLYMER FORMATION AND SPECTROSCOPY.....	17
3.1 Synthesis of Polypyrrole.....	17
3.1.1 Electro polymerization of Pyrrole.....	18
3.1.2 Chemical polymerization of Pyrrole.....	18
3.2 Raman spectroscopy of Polypyrrole.....	20

3.2.1 Raman spectrum.....	20
3.3 Conducting nature of Polypyrrole.....	21
3.3.1 Temperature dependence of conductivity.....	21
3.3.2 Frequency dependence of conductivity.....	22
Chapter-4	
PHOTODETECTOR.....	25
4.1 Photodetector Requirement.....	26
4.2 Photodetection Theory.....	26
4.3 Photonic Detection Parameter.....	27
4.4 Assessment of detectors parameter.....	29
Chapter-5	
RAMAN SPECTROSCOPY AND SPECTRAL ANALYSIS.....	30
5.1 Raman Spectroscopy-Principles & instrumentation	31
5.2 Analysis of Raman Spectra and Spectral Analysis.....	31
Chapter-6	
EXPERIMENTAL.....	32
6.1 Introduction.....	33
6.2 Material and Components.....	33
6.3 Instrumentation.....	34
6.4 Image Result.....	36
6.5 Procedure for Device Preparation.....	37
6.6 Experimental Method.....	39
6.7 Result.....	41
6.7.1 Raman Spectroscopy Result.....	45

6.7.2 IV characterization Result.....	45
6.8 Amplifier Design.....	51
6.9 Conclusion.....	52
References.....	

List of Figures

Figure:1-Schematic diagram of Absorption, Spontaneous Emission, Stimulated Emission

Figure:2-Population inversion state of semiconductor

Figure:3-Morphology in Inorganic/Organic Hybrids (a) Polymer Modified Silicate Type

(b) Clay/ polymer Layer type (c) Silica Particle polymer matrix

Figure:4-Difference between Inorganic/Organic Hybrids and Inorganic-Organic

Nanocomposites with examples of clay-nylon

Figure:5-Oxidative polymerization of pyrrole to Polypyrrole

Figure:6-Chemical structure of Polypyrrole in aromatic and quinoid forms and in

oxidized polaron and bipolaron forms

Figure:7-Raman Spectra of Polypyrrole

Figure:8-(a) Comprehensive data analysis of Raman data (a) Raman spectra (b) Curve

fitting by Raman fit (c) Origin plot of the data

Figure:9-Raman images of (a) Silicon (b) composite (Ppy75%+Si25%) (c) Polypyrrole (d)

composite (Ppy25%+Si75%) (e) composite (Ppy+Si) 50% (f) composite (Ppy+Si) 50%

Figure:10-(a) Device in Probe station for testing (b) Ppy (c) Ppy25%+Si25% (d)

Ppy75%+Si25% (e) Ppy+Si=50% (f) Red Laser illumination over a device

Figure:11- Device image of Hybrid Photodetector

Figure:12- Raman spectra of Polypyrrole under Dark and UV illumination conditions

(a)40um,0v,0uA,dark,(b)35um,0.07v,71.1uA,uv,(c)35um,1Hz,120-300uA-dark,(d)

35um,500mHz,170-250uA,uv.

Figure:13- Raman spectrum of Ppy75%+25% UV and Dark illumination

Figure:14- Analysis of silicon peak of composites under dark and UV conditions

Figure:15- I-V Characteristics curve of polypyrrole

Figure:16- I-V Characteristics curve of silicon

Figure:17- I-V Characteristics curve of Ppy50%+si50%

Figure:18- I-V Characteristics curve of Ppy75%+25%

Figure 19:- I-V Characteristics curve of Ppy25%+si75%

List of abbreviations

SE	Spontaneous Emission
CB	Conduction Band
VB	Valence Band
CD	Compact Disk
DVD	Digital Versatile Disk
SRH	Shockley Read Hall
Cdep	Capacitor of Depletion Region
Rdep	Resistance of Depletion Region
Cdiff	Capacitor of Diffusion Region
Rdiff	Resistance of Diffusion Region
VIS	Visual Detector
RMS	Root Mean Square
PCB	Printed Circuit Board
DC	Dication
RC	Radical Cation
LWIR	Long Wavelength Infrared

Chapter-1

OPTOELECTRONIC DEVICES AND MATERIAL

1.1 Research Objective

The necessity to increase the capabilities of polypyrrole and Silicon-based photodetectors in response to modern problems and demands in optoelectronic applications is the driving force behind this study. Despite their widespread use, photodetectors have several restrictions that limit their adoption and ideal performance. This study aims to solve these constraints by concentrating on critical areas for development. One primary goal is to improve the sensitivity and responsivity of these photodetectors. We need to improve their performance, particularly in low-light circumstances, experiment with new materials, optimize device architecture, and combine cutting-edge technology. Furthermore, the project intends to address the concerns about the stability and dependability of polymer-based photodetectors by investigating techniques to decrease degradation over time and increase long-term functionality. Energy efficiency is also a major factor, and the thesis seeks to investigate strategies for optimizing photodetector energy usage. This could include improving device architecture, investigating energy harvesting methods, and using advanced signal processing techniques to provide optimal performance while minimizing power consumption. This research not only contributes to the integration of polymer and silicon-based photodetectors by addressing these problems and investigating options for improvement. It also has the potential to impact different industries that rely on precise and efficient light-detecting technologies.

1.2 Introduction

This chapter introduces the fundamental theory and operational concepts of semiconductor optoelectronic devices. Nowadays, there are a lot of optoelectronic devices that are used in many different applications. Among these are light-emitting diodes (LEDs), optical amplifiers, photodetectors, laser diodes, and optical modulators. Let's begin this chapter by dealing with the physical interactions that occur between electrons and photons in semiconductors and how this phenomenon is used to create a wide range of devices. Whether its in solid-state lighting, computers, televisions, LED indicator lights, or countless other items, optoelectronic devices are everywhere in modern life. They can also be found in bar-code scanning systems at supermarkets, compact disc (CD), digital versatile disc (DVD), and Blu-ray players at home, office laser printers, phone systems, and cable television sets. There has been an information explosion in the last ten or so years, making it simple for anyone with an internet-enabled device to access information from anywhere in the world. Semiconductor-based optoelectronic devices are essential parts of the system in each of these applications. Compact size is one of the main advantages of semiconductor devices. A common edge-emitting laser, for example, has dimensions of $500 * 250 * 100 \mu m^3$. A single wafer can produce thousands of such devices. As a result, after packaging, these devices are exceedingly compact coherent radiation sources. The application of semiconductor devices in telecommunications stands out as having the greatest impact on modern living. When compared to older, analog-based systems, digital-based data transmission allows information to be delivered across long distances with considerably less erosion in signal quality. With short optical pulses lasting less than 100 ps, optical telecommunications may transmit data at speeds greater than 10 Gbit/s, making them appropriate for use in digital systems. It is common to attain bit error rates of less than one in every 10^9 bits, even at this extraordinarily fast data transfer rate.

These capabilities are the direct result of extensive research and development work put into manufacturing semiconductor devices for light emission and detection. In the next part, we provide a brief history of this evolution before delving into the key physics and technological aspects of device operation. Optoelectronic devices are manufactured mostly of III-V semiconductor compounds, as well as their alloys because of their direct-band gap. Hybrid materials are composites of two or more different types of materials with distinct properties. They can give better results than separate materials like Polypyrrole, which is a conducting polymer, and Silicon, which is a semiconductor; composites of these two materials are capable of giving favorable outcomes in the optoelectronic industry. Understanding the characteristics of these materials is critical in the development of optoelectronic devices. (Sweeney 2006), [14]

1.3 Carrier-Photon Interaction

There are three conceivable processes for electrons under interaction with a photon.

1. Absorption
2. Spontaneous Emission
3. Stimulated Emission

When an electron in the conduction band CB with energy E_2 recombines with a hole in the valence band VB with energy E_1 , spontaneous emission SE takes place. A photon is produced when the energy differential ($E_2 - E_1$) is released. As the name suggests, photons can be emitted in any direction and with any polarisation throughout this random process. The electron density in the conduction band CB (n) and the hole density in the valence band VB (p) are directly related to the probability of spontaneous emission SE. An electron is excited from the valence band VB to the conduction band CB through the absorption of a photon with energy equal to or greater than the optical band gap. Stimulated emission produces nearly identical photons as SE spontaneous emission, resulting in monochromatic light and coherence. An electron is

excited from the valence band VB to the conduction band CB through the absorption of a photon with energy equal to or greater than the optical band gap. Stimulated emission produces nearly identical photons to SE spontaneous emission, but produces monochromatic light with coherence instead. The conduction band CB has much fewer electrons than the valence band VB at ambient temperature in an undoped semiconductor. As a result, absorption is much more likely than emission. It is feasible to inject electrons into the CB and holes into the VB by delivering an electrical current (electrical pumping) or injecting light with photon energies greater than the transition energy (optical pumping). (Sweeney, 2006), [14]

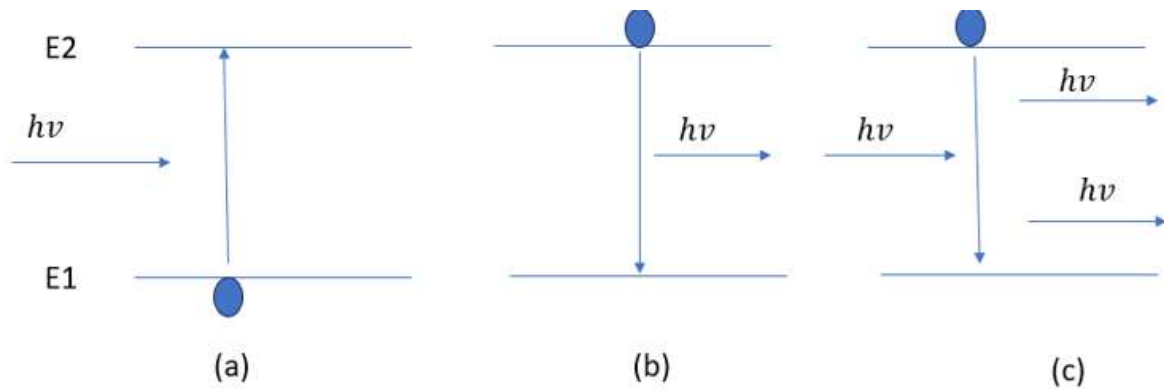


Fig: 1 Diagram of (a) absorption, (b) spontaneous Emission, and (c) stimulated Emission

1.3.1 Emission and Absorption Rates and the Einstein Relations

The densities of states and the Fermi-Dirac occupancy probability determine the populations of electrons and holes in the CB and VB, respectively. Electron-electron and hole-hole scattering speed in a semiconductor are typically nearly equal to 100 fs, while electron-hole recombination periods are nearly equal to 1 ns. As a result, we may assume that the electrons and holes are thermally equilibrated and can be represented using a Fermi-Dirac distribution. It is useful to distinguish between two quasi-Fermi levels. These are denoted as f_c and f_v ,

respectively, and correspond to the energy at which the occupation probability equals 1/2 for electrons in the CB and VB. $f_c = f_v$ in thermal equilibrium. The associated energy-dependent Fermi functions is:

$$f_c(E) = \frac{1}{1 + \exp\left(\frac{E - E_c}{k_B T}\right)}$$

$$f_v(E) = \frac{1}{1 + \exp\left(\frac{E - E_v}{k_B T}\right)}$$

If we label states in the VB as 1 and states in the CB as 2, the *absorption rate*, r_{12} , for photons of energy $h\nu$ is given by

$$r_{12} = B_{12} \rho_\nu f_v (1 - f_c) \rho_c P(h\nu)$$

where f_c and f_v are the CB and VB densities of states, respectively. $P(h\nu)$ is the photon density at energy $h\nu$ and B_{12} is the Einstein coefficient for the absorption process. Similarly, the stimulated emission rate,

$$r_{21} = B_{21} \rho_c f_c (1 - f_v) \rho_\nu P(h\nu)$$

r_{12} , may be written as

where B_{21} is the Einstein coefficient for the stimulated emission process. For the spontaneous emission SE rate.

$$r_{21} = A_{21} \rho_c f_c (1 - f_v) \rho_\nu$$

A_{21} is the Einstein coefficient for the SE process. Note that, since SE does not require a photon to initiate the process, $r_{\text{spont}_{21}}$ does not depend on $P(h\nu)$. Under steady-state

conditions, the total upward transition rate must equal the total downward transition rate, thus

$$r_{12} = r_{21} + r_{21}^{\text{spont}}$$

Thus, by combining Equations:

$$B_{12}\rho_v f_v (1 - f_c)\rho_c P(h\nu) = B_{21}\rho_c f_c (1 - f_v)\rho_v P(h\nu) + A_{21}\rho_c f_c (1 - f_v)\rho_v$$

In thermal equilibrium ($f_c = f_v$)

$$P(h\nu) = \frac{A_{21}}{B_{12} \exp\left(\frac{h\nu}{k_B T}\right) - B_{21}}$$

The standard expression for black-body radiation is given by Planck's law as:

$$P(h\nu) = \frac{8\pi^3 n^3 (h\nu)^2}{(hc)^3} \frac{1}{\exp\left(\frac{h\nu}{k_B T}\right) - 1}$$

Here, n is the refractive index of the semiconductor. For simplicity, here we assume that the medium is non-dispersive. From these two expressions of $P(h\nu)$, we obtain the result that

$$B_{12} = B_{21} = B$$

And

$$A_{21} = B \frac{8\pi^3}{(hc)^3} n^3 (h\nu)^2$$

1.3.2 Direct and indirect gap

Semiconductors can be classified into two types based on whether the band gap is direct or indirect. The choice of whether the band gap is direct or indirect has a significant impact on their suitability for use in optoelectronic devices and indirect-band gap semiconductors. For direct band gap material, the conduction band CB energy minimum occurs at the same k -value as the valence band VB maximum in contrast, the CB minimum for the indirect-band gap

material is at a different k-value than that of the VB maximum. The energy and momentum must be conserved for any electron transfer. The magnitude of the photon wavevector is defined by $2\frac{\pi}{\lambda}$, λ - wavelength of the photon (order of 100's of nm). The magnitude of the electron wavevector ranges between $-\frac{\pi}{a}$ and $+\frac{\pi}{a}$ within the first Brillouin zone, where a is the lattice spacing of (order of 1Å). The photon wavevector is much less than that of various electron wavevectors, and if a photon interacts with an electron, the transition must occur with virtually little change in wavevector; thus, only vertical transitions are permitted. Such transitions are possible in the direct-band gap semiconductor. In the case of indirect semiconductors, however, such transitions are only achievable through the interaction of phonon. It is now a three-particle interaction, the transition probability is greatly lowered. Direct band gap semiconductor is typically employed to manufacture photo-emissive devices such as LEDs and lasers. Notably indirect band gap semiconductor are particularly effective semiconductor materials for detection.(Sweeney, 2006), [14]

1.4.3 Population Inversion

Population inversion is a fundamental concept in the field of laser physics and quantum electronics. It refers to the condition where the number of atoms or molecules in an excited energy state exceeds the number in a lower energy state, contrary to what is typically observed in thermal equilibrium. This non-equilibrium distribution of population levels is essential for the operation of lasers, as it enables the amplification of light through stimulated emission.

1.4.3.1 Theoretical Background

In thermal equilibrium, the distribution of particles among different energy states follows the Boltzmann distribution, where the population of a higher energy state N_2 is less than that of a lower energy state N_1 , mathematically expressed as:

$$\frac{N_2}{N_1} = e^{-\frac{E_2 - E_1}{KT}}$$

Where, E_2 and E_1 are the energies of higher and lower states, respectively, K is the Boltzmann constant and T is the absolute Temperature.

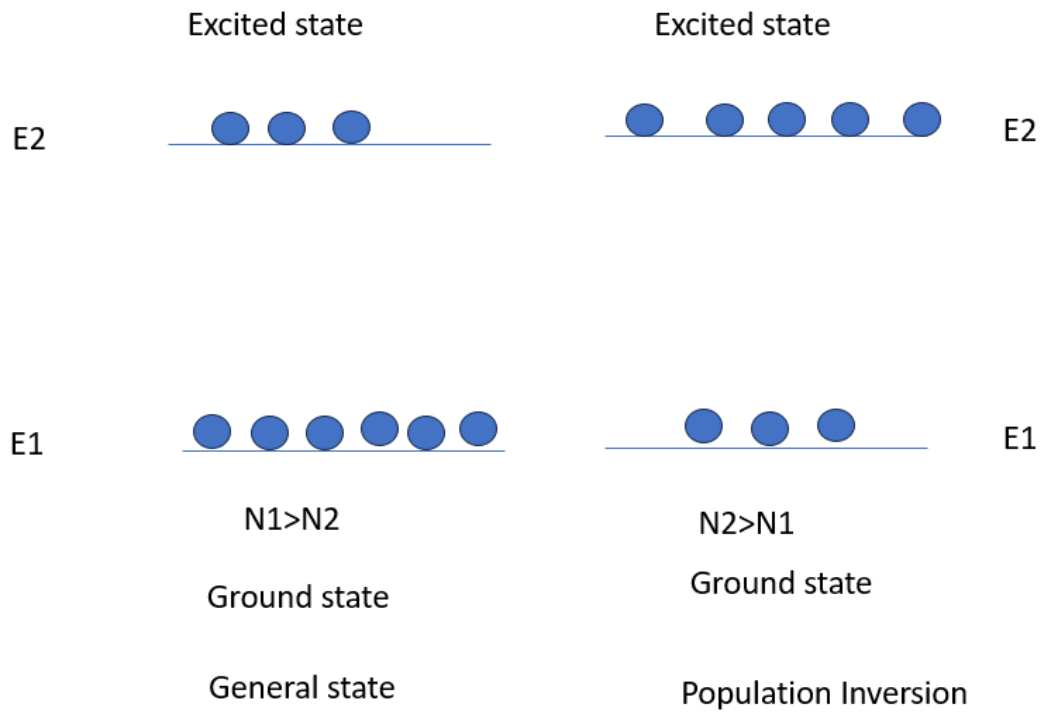


Fig: 2 Population inversion state of semiconductor

Chapter-2

Hybrid and Advance Functional Materials

Hybrid materials are emerging as a powerful and promising class of materials. In recent times, multifunctional materials have emerged as the most sophisticated and advanced engineering materials. They possess the capacity to endure mechanical loads, high fatigue and heat stability, and enhanced chemical and environmental resistance. Advanced functional materials are materials that are developed to perform specific tasks in addition to their standard tasks. These materials frequently have distinct physical, electrical, chemical, or mechanical properties adapted to specific uses. They are created at the atomic or molecular level to have desired properties including superconductivity, self-healing, and shape memory.

2.1 Introduction

Natural hybrid materials often possess complex architectures at sizes ranging from a few nm to several micro- to mm. Their collective qualities are determined by the mix of composition and structure on each length scale. Different dimensions and levels of complexity are intentionally designed hierarchical architectures of organic-inorganic hybrid materials.(Yamada et al., 1989),[17] Inspired by nature, this idea can provide a simple, versatile, and cost-effective method for fabricating multifunctional nanostructures for technological applications through the self-assembly of functional hybrid materials. However, understanding the fundamental principles of self-assembly and applying this approach to a variety of combinations of organic-inorganic materials is a major challenge in current materials science and engineering.(Makisima, 2004),[5]

2.2 Fundamentals of Hybrid Materials

Recent advancements in materials science and engineering have been encouraged by the need for new materials with customized properties and multifunctional capabilities. Hybrid materials stand out among the wide range of materials that have grown up as a potential class that combines different characteristics of various elements to produce improved functionality and performance.(Yamada et al., 1989),[17] By elucidating the basic ideas, importance, and applicability of hybrid materials in current research and application fields, this introduction chapter lays a foundation for an in-depth analysis of these materials.

2.2.1 Definition and Category of Hybrid Material

Hybrid materials are a mixture of two or more materials with different properties caused by modified molecular orbital structure formed between each material, such as the covalent bond between polymer and silanol molecular in an organic/inorganic hybrid.(Makisima, 2004),[5] Substances are classified into three materials based on the type of chemical bond : metal, organic materials, and their polymers, and ceramics. This categorization of hybrid material and their related material was proposed as follows:

- i. Composites: Mixture of materials consisting of matrix and micron-level dispersion.
- ii. Hybrids: Sub-micron level mixture of different kinds of material.
- iii. Nanocomposites: Sub-micron level mixture of similar kinds of material.
- iv. Nanohybrid: Atomic or molecular level mixture of different materials with chemical bonds between their different material.

(Sanchez, 2004) classified hybrid materials as organic/inorganic hybrid materials or inorganic biomaterials. They also stated that the characteristic size of hybrid materials was less than 10^3 nm. They did not provide a formal description of hybrid material, nor did they discuss the formation of new electron orbitals or chemical bonds. On the other hand, (Brechet, 2001), [18] described hybrid materials as a combination of two or more materials in an integrated shape and scale that optimally serves for engineering use. (Suzuki, 2000), [13] identified hybrid materials as a deliberate mixture of two or more elements complementing each other to have super-functions or novel functions that the component materials did not have. based on hybridization the hybrid material is categorized into three categories.

1. Structurally-hybridized material
2. Materials hybridized in chemical bond
3. Functionally-hybridized material

2.3 Inorganic/Organic Hybrids

Inorganic/organic hybrids have drawn a lot of interest from a variety of disciplines and have been hot subjects in material science engineering. (Suyama, 2004), [12] categorized hybrid materials into three categories based on structural differences. The first example of inorganic/organic hybrid is the organically modified silicates fabricated by sol-gel processing shown in figure: 3 (a) This possesses outstanding mechanical properties because of a strong covalent bond between silica and organic molecules. Hybrid materials are fabricated in such a way not only include dispersed silica in polymer but also categorized by the chemical bond between them in comparison to traditional composites. There are many types of hybrids clay/polymer is one among them as shown in Figure: 3 (b). The strong chemical bond between silicate monolayer and polymer molecules provides enhanced mechanical properties and lower gas permeability than those of polymer material as shown in Figure: 4 (usuki, 2001) provides

a comprehensive explanation of the structural differences between hybrid materials and nanocomposites made up of clay and polymer material.

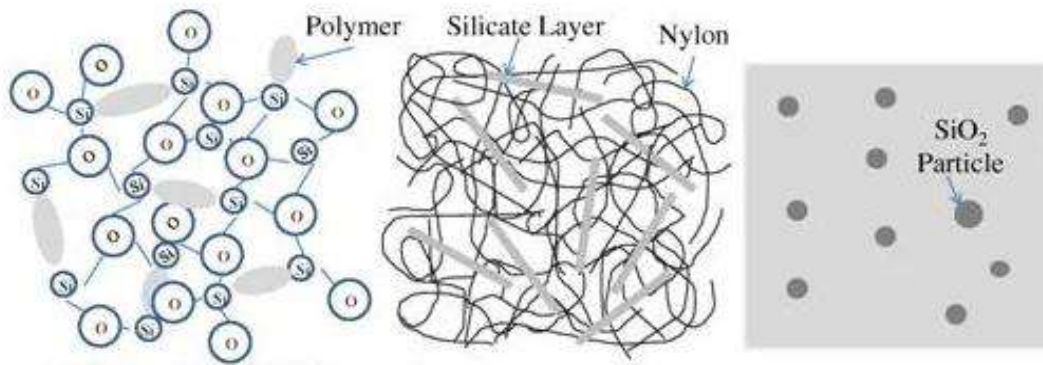


Fig:3 Morphology in Inorganic/ Organic Hybrids (a)Polymer-modified Silicate Type (b)Clay/polymer Layer type (c)Silica Particle-Polymer Matrix Type.(Nanko, 2009),[6]

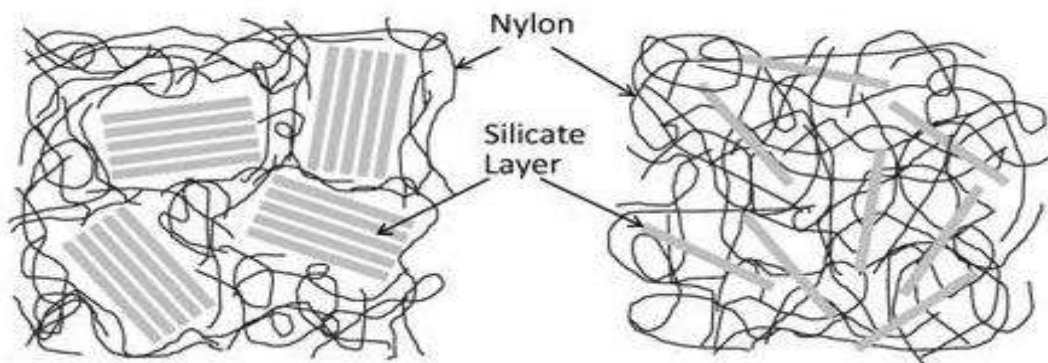


Fig:4 Differences between Inorganic-Organic Hybrids and Inorganic-Organic Nanocomposites with example of Clay-Nylon.(Nanko, 2009),[6]

2.3.1 Polypyrrole-Silicon Hybrid Materials

A hybrid material with various proportions of silicon and polypyrrole composites is used for the project. The polypyrrole P type purchased from Sigma-Aldrich for the research work is doped with sulfonic acid; its conductivity ranges from 10 to 50 S/cm, and it is stable in organic solvents up to 290°C and silicon (Si), acquired from SK Novel Materials and Technologies, is

of the N-type with a resistivity of 1–10 Ohm–cm and thickness of 300um. Polypyrrole and silicon are two different classes of materials with different properties and uses. Polypyrrole is a conductive polymer with high electrical conductivity and chemical stability. On the other hand, silicon is a semiconductor that is abundant in nature and widely used in electronics and photovoltaic devices. Combining these materials into a hybrid structure will allow for the effective combination of their properties, which could lead to new applications in biomedical devices, sensors, and energy storage devices.

2.3.2 Synthesis Method: Preparation of Polypyrrole-Silicon as Hybrid Material

To produce close contact and a strong binding between the two components. The procedures listed below are used in the production of polypyrrole silicon as a hybrid material. Using this method, the hybrid material's shape, composition, and properties can be altered to satisfy the needs of a particular application.(Kickelbick, 2007),[4]

1. Preparation of the Synthesis: To prepare a composites with variations in terms of quantity, such as 50% Ppy and 50% silicon, 25% Ppy and 75% silicon, 75 %Ppy and 25% silicon, pure Ppy and silicon . The first step is to gather all the raw materials needed for the synthesis of the hybrid material, such as the pelletizer, die, Ppy and silicon wafer.

2. Grinding: A mortar and pestle crystal is used to crush silica to produce a fine powder form. The surface-to-volume ratio is increased during the grinding process.

3. Mixing of materials: Mortar and pestle crystal are used to achieve homogeneity and tune the characteristics of new material.

4. Die: Place the silicon and polypyrrole mixture in the Die in measured quantity for the various composites as stated above.

5. Pelletization of material: A pelletizer is used in the pelletizing process to exert pressure of one and one and a half tonnes over the die, resulting in compact pellets with increased density of 10mm diameter of various composites.

2.3.3 Characterization of Hybrid Material

The hybrid material of Polypyrrole and silicon is synthesized and utilized in designing a photodetector. To understand the structural and electrical properties of the material, and to optimize its performance Raman spectroscopy and I-V Characterization are performed. Raman spectroscopy an effective technique for analyzing molecular vibrational modes and material crystal structures is Raman spectroscopy. Using Raman spectroscopy on the PPy/Si hybrid material, information related to the following is collected. Molecular Structure and Composition: Raman spectra identified characteristic peaks corresponding to PPy and Si. These peaks confirm the presence and distribution of both components within the hybrid material. Doping and Interaction Effects: The doping of PPy with sulphonic acid leads to shifts in the Raman peaks, indicating changes in the electronic structure. By examining these shifts, it is possible to understand the interaction between the dopant and the polymer, as well as any charge transfer effects between PPy and si. Material Quality and Defects: Raman spectroscopy reveals about defects or disorders within the material. For instance, the presence of additional peaks or changes in peak intensity and width can indicate structural imperfections or variations in crystallinity. I-V characterization involves measuring the current response of the photodetector as a function of applied voltage. This technique provides critical information about the electrical performance of the hybrid material. Photocurrent Response: By measuring the current under illumination (405nm,532nm,655nm,905nm), the photocurrent generated by the photodetector is evaluated. This helps in determining the device's sensitivity to light and its efficiency in converting light to electrical signals. Dark Current: The current measured in the

absence of light (dark current) is an important parameter. A low dark current is desirable as it indicates minimal leakage and noise, leading to higher signal-to-noise ratios in the photodetector. Voltage Dependence: The I-V curve reveals how the current changes with applied voltage, providing insights into the charge transport mechanisms within the hybrid material. Stability and Repeatability: Repeated I-V measurements can assess the stability and repeatability of the device's performance, ensuring its reliability for practical applications.(Kickelbick, 2007),[4]

Chapter-3

Polypyrrole conducting polymer, Formation and Spectroscopy

Conducting polymers have significant attention due to their unique combination of electrical conductivity and the intrinsic properties of polymers, such as flexibility, processability, and lightweight characteristics. Among these materials, Polypyrrole (PPy) is a promising conducting polymer due to its relatively high conductivity, ease of synthesis, environmental stability, and versatile applications. Polypyrrole, a polymer of the heterocyclic compound pyrrole, was first discovered in the 1960s but gained widespread recognition in the late 1970s when the potential of conducting polymers became evident. The conductivity of PPy arises from the presence of conjugated π -electron systems along the polymer backbone, which can be doped with various anions to enhance its electrical properties. This doping process involves the oxidation of the polymer, leading to the creation of charge carriers that facilitate electrical conduction.(Saville, 2005),[11]

3.1 Synthesis of Polypyrrole

Pyrrole monomer can be oxidatively polymerized to create polypyrrole chemically or electrochemically. The absolute form of polypyrrole, as depicted in Figure, is a long-conjugated backbone polymer with resonance structures resembling those of the quinoid or aromatic forms. In its neutral state, the polymer is non-conductive; it only turns conductive when it undergoes oxidation..(Olmedo, 1997),[7]

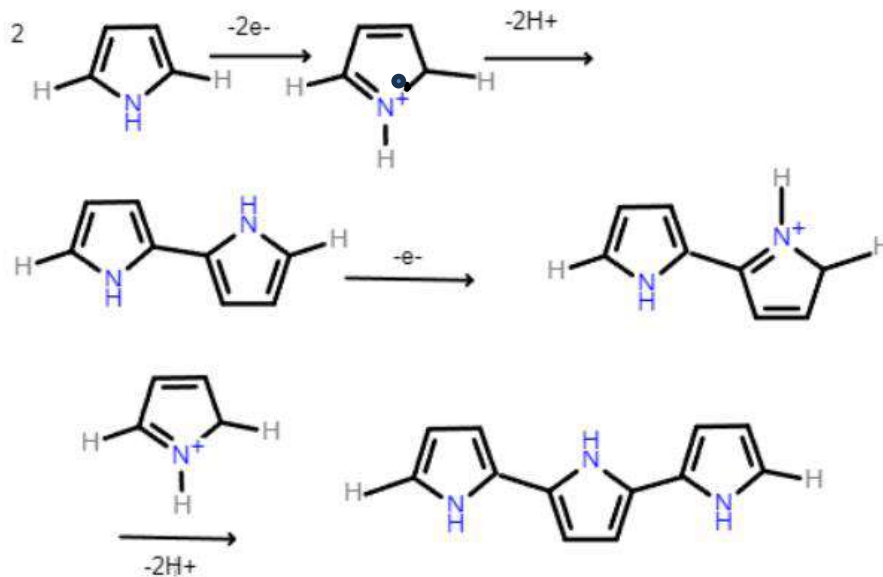


Fig:5 Oxidative polymerization of pyrrole to Polypyrrole(Saville, 2005),[11]

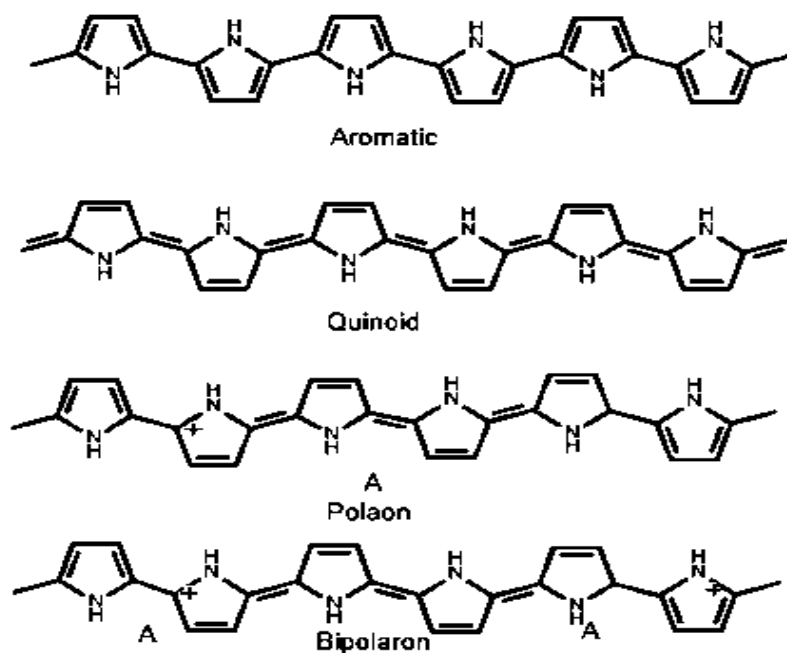


Fig: 6 chemical structure of Polypyrrole in aromatic and quinoid forms and in oxidized polaron and bipolaron forms.(Saville, 2005),[11]

A dication (bipolaron) or a radical cation (polaron) can be formed when the charge linked to the oxidized state delocalizes over several pyrrole units. Polypyrrole can be physically represented as an insoluble film through electro-polymerization or as an unstable powder through chemical polymerization.

3.1.1 Electro polymerization of Pyrrole

A conducting polymer coating is formed by the electrochemical oxidation of pyrrole. Electro-polymerization of pyrrole to Polypyrrole is shown in the figure. The process begins with the electrochemical oxidation that produces radical cations, and it proceeds through the combining of two radical cation monomers that result in the loss of two hydrogen ions. 2,2'-bi-pyrrole is created when an interaction is formed at two places within the pyrrole ring. 2-Monosubstituted pyrroles only form dimmers, but 2,5-disubstituted pyrroles do not polymerize. Reoxidation of the pyrrole and further radical combination are the means of propagation. When there is no more monomer available for oxidative polymerization, termination takes place. The stability of the radical through charge delocalization and the ease of oxidation are key factors in polymerization success. Since the loss of hydrogen ions renders oligomer formation irreversible, the proton acceptor facilitates electro-polymerization.(Saville, 2005),[11]

3.1.2 Chemical Polymerization of Pyrrole

The process involved in the chemical synthesis of pyrrole is the oxidation of pyrrole with an oxidant such as ferric chloride. The conductivities and processes are identical to those found in the electropolymerization of pyrrole. The resultant polymer is conducting in its oxidized state because FeCl_4^- provided charge compensation. The conductivity of Polypyrrole formed from different ferric salts has been related to the $\text{Fe}^{2+}/\text{Fe}^{3+}$ redox potential because of its strong acid anions forming capacity provides the most oxidizing ferric species. Weaker acid anions typically coordinate Fe^{3+} ions more strongly, reducing its oxidizing potential and if the reaction

occurs because of the solvents, it changes the redox potential whereas if the redox potential increases an irreversible dissolution of Polypyrrole can occur. As the synthesis temperature is lowered, Polypyrrole's conductivity rises, which is assumed to be the result of fewer side reactions. The conductivity of Polypyrrole is analysed concerning reflectivity and divided into 3 regions i.e .metallic, critical, and insulating.(Saville, 2005) ,[11]

3.2 Raman spectroscopy of Polypyrrole

Raman spectroscopy has been used in the past to investigate conducting polymers and is an effective means of examining the local structure. It is a good tool for performing microscopic structural analysis. The doping method directly affects the Raman modes, but the doping level modifies the polymer's electrical structure. For this reason, Raman spectroscopy is a helpful tool for learning about the characteristics of charge carriers. The doping method directly affects the Raman modes, but the doping level modifies the polymer's electrical structure. For this reason, Raman spectroscopy is a helpful tool for learning about the characteristics of charge carriers. Sulphonic acid is present in the samples being examined as a dopant ion together with a silicon composite. A 532 nm laser is used to stimulate the sample being studied.(Mikat, 2002),[2]

3.2.1 Raman spectrum

Peaks that appeared in the Raman spectra of Polypyrrole are divided into 3 groups, the first group represents peaks due to change in ring deformation second group represents peaks due to symmetry in C-H, and the third group represents peaks due to C=C stretching. Each group further consists of two bands, radical cation and dication.(Mikat, 2002)

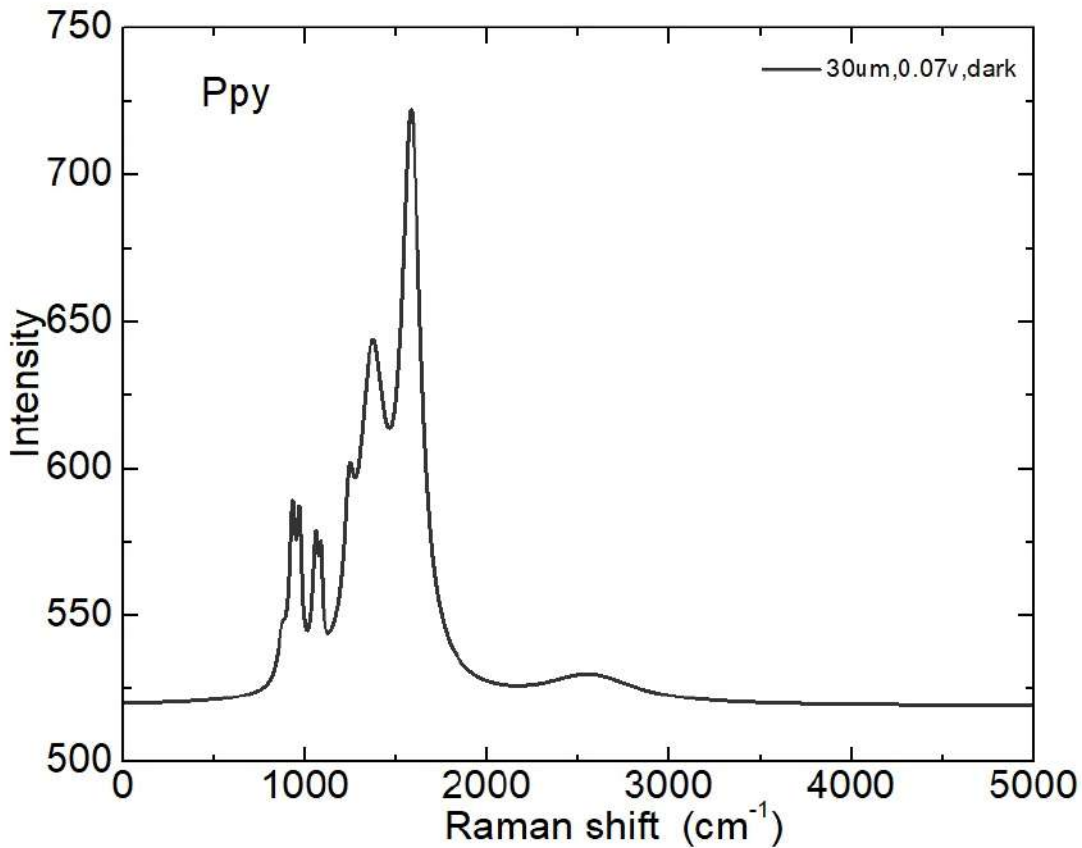


Fig:7 Raman spectra of Polypyrrole

3.3 Conducting Nature of Polypyrrole

In polypyrrole, polaron or bipolaron states result from the oxidation of a non-conducting polymer, which generates charge carriers. Though there are a few exceptions, conducting polymers are generally believed to be disordered materials. In the undoped condition ($\sigma_{dc} = 0$), there are no conduction channels. As the polymer becomes partially doped, oxidized spots on the polymer chains, or islands of conducting material, emerge. These sites are primarily isolated from one another and are typically repaired by structural disorders and dopants. (Furukawa et al., 1988), [1] As charge carriers tunnel or hop

across sites (islands) in the polymer, the variable range hopping model (VRH) explains the ac conductivity or intra/interchain conduction observed at higher frequencies. A small fraction of the sites will network together throughout the material, producing a small, finite DC static conductivity.

3.3.1 Temperature Dependence of Conductivity

The temperature dependence of the dc conductivity of conducting polymers tends to follow the Variable Range Hopping model's prediction of (Saville, 2005), [11]

$$\sigma = \sigma_0 \exp\left[-\left(\frac{T_0}{T}\right)^{1/4}\right] \quad 1$$

Where

$$\begin{aligned} \sigma_0 &= e^2 R^2 \nu_{ph} N(E_F) \\ T_0 &= \frac{\lambda a^3}{kN(E_F)} \end{aligned} \quad 2$$

and T_0 is the characteristic temperature, e is the electronic charge (1.602×10^{-19} C), k is Boltzmann's constant (8.616×10^{-5} eV/K), R is the average hopping distance (cm) ν_{ph} is the phonon frequency ($\sim 10^{13}$ Hz), $N(E_F)$ is the density of localized states at the fermi level ($\text{cm}^{-3} \text{eV}^{-1}$), λ is the dimensional constant (~ 18.1) and α is the coefficient of exponential decay of the localized states (cm^{-1}).

3.3.2 Frequency Dependence

Low-frequency methods ($10^{-2} - 10^7$ Hz) of measuring electrical relaxations in a material yield the equivalent parallel conductance, G , and capacitance, C . These terms then define the complex permittivity, ε^* , conductivity, σ^* , resistivity, ρ^* , and complex modulus, M^* .

$$\varepsilon^* = \varepsilon' - i\varepsilon'' = \frac{1}{M^*} = \frac{\sigma^*}{i\omega\varepsilon_0} = C - \frac{iG}{\omega\varepsilon_0}$$

$$3\sigma^* = \frac{1}{\rho^*} = G + i\omega\varepsilon_0 C \quad 4$$

$$\rho^* = \rho' - i\rho'' = \frac{G}{G^2 + \omega^2 \varepsilon_0^2 C^2} - i \frac{\omega \varepsilon_0 C}{G^2 + \omega^2 C^2} \quad 5$$

$$M^* = \frac{\omega^2 \varepsilon_0^2 C}{G^2 + \omega^2 \varepsilon_0^2 C^2} + i \frac{\omega \varepsilon_0 C}{G^2 + \omega^2 \varepsilon_0^2 C^2} \quad 6$$

A frequency-dependent contribution to permittivity is likely to originate from the mobile charge carriers based on dielectric relaxation studies on these mobile charge carriers. (Saville, 2005)

$$\varepsilon'' = \frac{\sigma_{DC}}{\omega \varepsilon_0} \quad 7$$

where σ_{DC} is the low-frequency conductivity of the material and accounts for long-range charge transport.

$$\varepsilon^* = \varepsilon' - i \left(\varepsilon'' - \frac{\sigma_{DC}}{\omega \varepsilon_0} \right) \quad 8$$

This expression assumes that the complex permittivity is solely dependent on the contribution from equation (6) and is unaffected by the transport process that results in long-range DC conductivity. This suggests that one relaxation time, τ_σ , can characterize the conductance process.

$$\tau_\sigma = \frac{\varepsilon_0 \varepsilon_s}{\sigma_{DC}} \quad 9$$

For a disordered system such as a conducting polymer, or conducting composite, a distribution of relaxation times (τ) is more appropriate.

$$\sigma_{DC} = \frac{\varepsilon_0 \varepsilon_s}{(\tau)} = \frac{\varepsilon_0}{M_s(\tau)} \quad 10$$

where M_s is the static modulus or the reciprocal of the static permittivity.

It is apparent from previous assessments of the conduction mechanisms that frequency and doping level impact polypyrrole's conductivity. A material's total conductivity is the sum of its ac and dc components.(Saville, 2005),[11]

$$\sigma_{Total} = \sigma_{ac} + \sigma_{dc} \quad 11$$

As hopping transitions enable conduction, for lightly doped polypyrrole films, the ac conductivity is larger than the dc conductivity at high frequencies. The charge carriers have more time to cross the sample after the percolation network at low frequencies, which causes the dc conductivity to be bigger and dominate charge transport. The overall conductivity is frequency-independent and the dc conductivity predominates at high dopant levels. The equation relates the imaginary part of permittivity to the ac and dc conductivity.

$$\varepsilon'' = \frac{\sigma_{ac} + \sigma_{dc}}{\omega \varepsilon_0} \quad 12$$

Chapter-4

PHOTODETECTOR

Photodetectors serve as vital parts of many technological applications, such as electronic appliances, communication systems, environmental monitoring, and medical imaging. The creation of hybrid materials that can improve photodetectors' performance beyond what can be achieved with conventional materials is becoming more and more popular as the need for more efficient, sensitive, and flexible photodetectors increases. The superior sensitivity, wider spectrum response, and increased flexibility of hybrid photodetectors are the outcomes of combining the beneficial properties of inorganic and organic materials. The fundamental mechanisms that enable the better performance of hybrid photodetectors, as well as the ideas underlying them, are explored in this chapter along with various kinds of hybrids. Photodetectors operate on the principle of converting light into an electrical signal. When photons are absorbed by the photodetector material, they generate electron-hole pairs. These charge carriers are then separated and collected by an internal electric field, producing a measurable current or voltage. The efficiency of this process depends on the material's ability to absorb light and transport charge carriers effectively. Photodetector performance is the primary factor of most optoelectronic devices' performance. It functions as an optical receiver's main front-end component as well. High speed and the best achievable signal-to-noise ratio are requirements for many applications. Consequently, it ought to possess minimal dark current and noise, elevated quantum efficiency, enhanced adaptability, and a quick response time. In addition, they are valued for their long lifespan, exceptional adaptability, low production costs, lightweight, tiny size, and low power consumption in practical applications.(Sweeney, 2017)

,[14]

4.1 Photodetector Requirements

Numerous factors must be considered while designing photodetectors. These can be broadly divided into the following categories: Sensitivity, Speed, Noise, Physical size (footprint), Reliability, Temperature sensitivity, Ease of use, and finally cost.

4.2 Photodetection Theory

For semiconductor optical detector band structures, the active area's band gap must be smaller than the amount of photon energy that has to be absorbed. An applied or built-in field that is present in the active zone separates the electron-hole pair that is produced when a photon is absorbed. If the field causes the electron and hole to move apart by a distance, x , the charge that is induced to flow in the external circuit that is connected to the detector is qx . In a basic photoconductive detector, where conducting electrodes and a bulk semiconductor are the components, l is the separation between the electrodes.(Sweeney, 2017),[14]. When thinking about a detector's band structure, several things need to be considered. Initially, the light to be detected's absorption depth needs to match the active zone's width. This will increase the possibility that photogenerated carriers will be formed inside the active region or shorter than the minority-carrier diffusion length from it. Since the dark current in the device establishes the minimum signal strength that can be detected, one must also take the band structure into account. Three important effects can give rise to the generation of electron-hole pairs even when no light is falling on the device. These are:

- (a) Thermal generation
- (b) Band-to-band tunneling
- (c) Avalanche breakdown.

4.3 Detector Parameter

In this section, the basic parameters of photodetectors will be defined

Detector Signal

The detector signal is typically the voltage or current value seen at the detector output as a result of incident radiation. The signal value is determined by the detector bias voltage V , modulation frequency f , wavelength λ , radiant flux ϕ_e , active area A of the detector, and temperature T .

Radiation Power

The characteristics of the detector must be properly defined to calculate the incident radiation power, sometimes referred to as radiant flux, and its spectral and spatial distribution. The energy of source radiation per unit of time is known as the radiant flux and can be described as follows:

$$\phi_e = \frac{dQ_e}{dt}$$

Active Area

The physical portion of a photodetector that converts incoming optical light into an electric output signal is known as the active area. In the case of circular detectors, the diameter is often stated; in the case of rectangular or square detectors, the length and breadth are specified.

Bias Voltage

A lot of detectors need a low-noise DC power supply. Two factors that affect the detector output signal and noise are the radiation modulation frequency and bias. The ideal signal-to-noise ratio circumstances ought to be produced by the bias.

Breakdown Voltage

The breakdown voltage is the highest reverse voltage that may be supplied to a detector without damaging it. Current-limiting protection is also necessary since the photodiode conducts current over its breakdown voltage very quickly.

Photocurrent

A photocurrent is a current created by a photodetector when it is exposed to optical radiation.

The photocurrent is proportional to the incident radiation for a tiny radiation signal.

$$I_{ph} = q\eta A\phi_e g$$

where q – is the elementary charge, η is the quantum efficiency, and g is the photoelectric current gain. In general, the photoelectric current gain in a typical photovoltaic detector is equal to unity.

Photoelectric Current Gain

The electron leaves the sample quickly after producing electron and hole pairs, reaching the positively charged electrode far quicker than the hole does, and leaving the sample quickly.

For the sample to remain electrically neutral, an additional electron needs to enter it from the negative electrode. This new electron quickly approaches the electrode and leaves the sample, but the hole keeps moving slowly through the sample. To maintain neutrality, thus, another electron needs to enter the sample; this process continues until the hole either reaches the negative electrode or recombines with one of these arriving electrons.

Dark Current Voltage Equation

The dark current-voltage (I-V) equation describes a photodiode's behaviour in the absence of incident light. When reverse-biased, a modest saturation current, I_s , flows in the circuit. Adding

a forward bias causes the current to grow exponentially.

It's connected to the dark current.

$$I_d = I_s \left[\exp\left(\frac{qV}{\beta kT}\right) - 1 \right]$$

where q is the electron charge, β is the ideality factor of the junction, k is the Boltzmann constant and T is temperature.

Response Time

A key variable determining how fast a detector reacts to a shift in the incident signal is its response time. and when a certain percentage (usually between 90% and 95%) of the detector's final value is reached. Depending on the application's needs and the speed of the detector, it is commonly measured in milliseconds (ms) or microseconds (μ s).

4.4 Detector Parameter Assessment

In addition to the electrical measuring instruments, the following are required to measure detector parameters: a monochromatic radiation source, a blackbody, an adjustable frequency modulated radiation source, and a reference detector. The bias voltage V_b , incident radiation power ϕ_e , detector active area A_d , wavelength λ , signal modulation frequency f , and temperature T all affect the detector signal.(Sweeney, 2017),[15]

$$V_s(V_b, \phi_e, A_d, \lambda, f, T) = u(V_b, \phi_e, A_d, T)u(\lambda)u(f)$$

Assuming that the incident radiation power, the detector area, and temperature are constant, then the above expression takes the form of:

$$V_s(V_b, \lambda, f) = uV_b u(\lambda)u(f)$$

Thus, three independent characteristics of $u(V_b)$, $u(\lambda)$ (called spectral) and $u(f)$ (called frequency) are obtained, which can be measured independently.

Chapter-5

Raman Spectroscopy and Data Analysis

The study of how electromagnetic radiation interacts with matter is known as spectroscopy. Spectroscopic techniques can be based in several phenomena, including scattering, fluorescence, emission, and absorption. According to Mikat et al. (2002),[2], Raman spectroscopy in particular concentrates on scattering phenomena to offer comprehensive molecular information. To characterize a broad variety of samples, various spectroscopic techniques are applied. Quantitative and qualitative analyses of samples are conducted using these techniques. The Qualitative analysis is performed to establish the identity of the sample while quantitative analysis is performed to estimate the concentration of analyte in the sample(Furukawa, 1988),[1] A versatile technique for analyzing a variety of materials is Raman spectroscopy. It overcomes many drawbacks of previous spectroscopic methods and has qualitative and quantitative research applications.

5.1 Raman spectroscopy: Principles & Instrumentation

Raman spectroscopy is an effective method for examining a material's rotational, vibrational, and other low-frequency modes. The basic principle lies in the Raman effect, which is the inelastic scattering of monochromatic light interacting with phonons or molecular vibrations in a sample. This light is usually generated by a monochromatic source. In 1928, Sir C.V. Raman made the first observation of this effect.(Mikat et al., 2002),[2]. The Raman Effect is defined as the majority of light that interacts with molecules being elastically scattered, or Rayleigh scattered, with no energy change. A small amount of light, on the other hand, is scattered inelastically and results in an energy gain or loss. The term "anti-Stokes scattering" refers to an instance in which the scattered photon has more energy than the incident photon, causing a

shift to a shorter wavelength (higher energy), while "Stokes scattering" is used when the scattered photon has less energy than the incident photon. (Paul Rostron, 2016),[8] The Raman shift is the energy difference, expressed in wavenumbers (cm^{-1}), between the incident and scattered photons. This shift yields a distinct vibrational fingerprint that is exclusive to the sample's molecular structure and environment.

5.2 Instrumentation of Raman Spectroscopy

The light source used to excite the sample is a monochromatic green laser of 532 nm. Using lenses or microscope objectives, the laser beam is directed onto the sample. The sample's scattered light is collected, usually at a 90-degree angle. The scattered light is detected using a sensitive detector, like a charge-coupled device (CCD) or photodiode array. The optical signal is transformed into an electronic signal by the detector so that it can be processed and analyzed further. The electronic signals are processed by specialized software to create a Raman spectrum, which graphs the scattered light's intensity against the Raman shift. The analysis of this spectrum reveals the molecular vibrations and structural information of the sample. (Mikat, 2002),[2]

5.3 Raman Spectrum, Data Analysis, and Curve Fitting

The composites' Raman spectra were analyzed to look into the material's molecular interactions and vibrational modes. The purpose of the Raman spectrum analysis was to look at possible changes in the vibrational modes of the composites under different circumstances. Raman spectroscopy is an effective technique for identifying alterations in molecular vibrations, which reveals information on compositional and structural changes in the material. Comprehensive Data Analysis of composites under Varied conditions is achieved by comparing The composite data of Ppy50%+si50%, Ppy75%+si25%, and Ppy25%+si75%, as well as the PPy and Silicon data, to analyze the Raman spectra under various AC (1Hz,10Hz, 100Hz) and DC (0,0.07,0.15 voltage) and for different Laser power for both UV and dark conditions. Raman spectra

obtained include background signals or noise that obscure the actual Raman peaks. Curve fitting procedures are required for baseline correction, which removes these unwanted components, ensuring that the analysis focuses on the true Raman signal. To adequately identify the position, width, and intensity of each identified peak, an appropriate model was fitted, with a Lorentzian model. This fitting procedure was made easier by the Raman FITS program, which offered both automated and manual fitting options to get the ideal fit. Using Origin plot software, an additional examination of the fitted Raman spectra was carried out. This included Data Import and Visualisation: After importing the fitted data from Raman FITS into Origin, extensive visualization capabilities allowed for the production of graphs suited for publication.

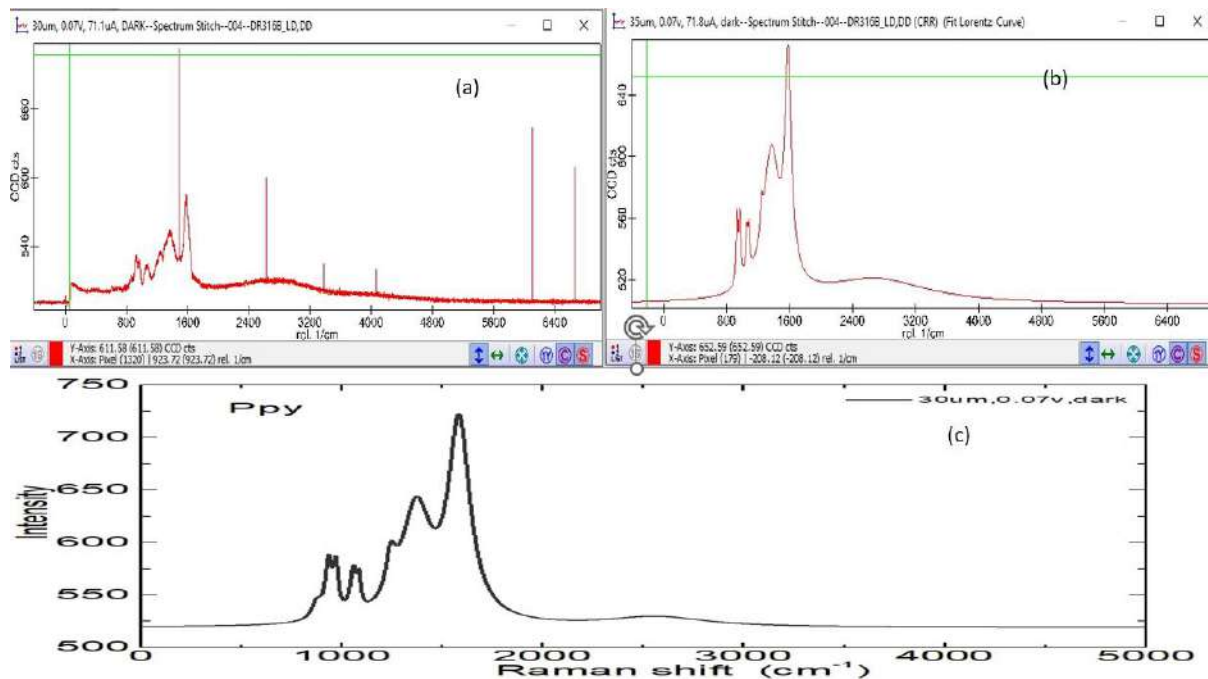


Fig: 8 (a) Comprehensive data analysis of Raman data (a) Raman spectra (b) Curve fitting by Raman fit (c) Origin plot of the data

CHAPTER-6

EXPERIMENTAL

6.1 Introduction

Chemical or electrochemical doping of conjugated polymers can result in extremely conductive materials. By altering the doping quantities, the magnitude of the conductivity can be changed. Examples of conducting polymers are polyacetylene, Polypyrrole, and polyaniline. Among these polymers, Polypyrrole is most significant due to its strong resistance to environmental impacts and high conductivity, which makes it an ideal choice for potential uses. The local electronic structure is strongly influenced by the charge carriers' electron-phonon interaction with the polymer. The interaction's strength affects the degree of distortion. Raman spectroscopy has been used to investigate conducting polymers before and is an effective way to investigate the local structure. The samples under evaluation contain materials Polypyrrole which is doped with sulphonic acid and silicon used to form a composite of different variations such as Ppy50%+si50%, Ppy75%+si25%, Ppy25%+si75%. The Raman Analysis of composites and pure Ppy was carried out with a 532 nm laser excitation wavelength. Instruments provide great resolution as well as good differentiation between bands allocated to different types of vibration in the evolution of the Raman spectrum, with a focus on changes in relative intensities and band shifts, and their relationship to possible changes in charge carrier type.

6.2 Materials and Components

All reagents used for experimental work are of research-grade quality, which is as follows: Polypyrrole (organic sulfonic acid is used as a dopant-P type) whose conductivity: 10-50 S/cm (pressed pellet), organic solvent: insoluble, stability up to 290 °C in air purchased from Sigma.-

Aldrich Polypyrrole is easily mixed with other materials to make composite structures with improved characteristics. This adaptability enables the material to be customized to specific performance needs in photodetector applications., Silicon (N type), resistivity: 1-10 Ohm-cm, thickness:300um, surface: SSP purchased from SK Novel Materials and Technologies. Silicon has very high electron and hole mobility, charge carriers can travel through it efficiently. This is required for photodetectors to have fast response times and great sensitivity and it has electrical properties that remain constant across a wide temperature range, making it ideal for applications that demand consistent performance in different environmental circumstances. Silver paste, diluent: Isoamyl acetate, adhesive electrodes the application of silver paste aids in the reduction of contact resistance at the electrode interface. Low contact resistance is critical for efficient charge injection and extraction, especially in devices like photodetectors where light-to-electrical signal conversion is a critical function and silver paste binds effectively to a variety of substrates used in electrical devices, including silicon wafers and other semiconductor materials. This high adherence is critical for keeping the electrode in excellent electrical contact with the underlying substance. Glass substrate is an underlying material on which the photodetector material is placed. PCB (printed circuit board) enable electrical components to be laid out in a compact and orderly manner. This is critical in photosensor design, because various components, such as photodiodes, amplifiers, and signal processing circuits, must be integrated into a small space.

6.3 Instrumentation

6.3.1 Raman spectrometer

The WITec Raman Alpha300 Series, which is equipped with a 532 nm laser, is a comprehensive and powerful equipment that is widely used for material analysis in scientific

research. The underlying principle of this instrument involves the inelastic scattering of monochromatic light, commonly laser, by electrons. This provides useful insights into molecular vibrations, and crystal structures, of materials. polypyrrole and silicon are the materials utilized to make the device, and both have high market expectations for device fabrication in terms of reliability and quality. WITec imaging technology is employed to understand their physical and chemical properties.

6.3.2 Probe Station

A probe station is an essential equipment used in semiconductor testing and characterization. It allows precise positioning and connecting probes to a device under test (DUT) to measure various electrical parameters. coupled with a Source Measurement Unit (SMU) and controlled via LabVIEW software, provides a comprehensive and automated solution for testing the IV characteristics of a designed photodetector using hybrid material under different illumination and dark conditions. The source used for illumination is 532nm Red laser, 655nm Green laser, 405 UV, 905 IR. To evaluate the performance and quality of a device at different wavelengths.

6.4 Images of Composites

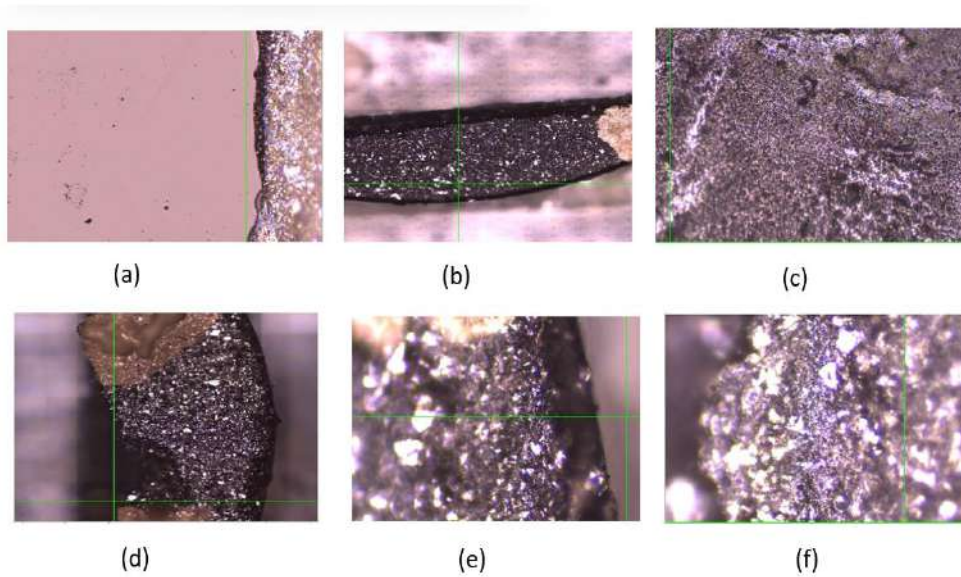


Fig:9 Raman images of (a) Silicon (b) composite (Ppy75%+Si25%) (c) Polypyrrole (d) composite (Ppy25%+Si75%) (e) composite (Ppy+Si) 50% (f) composite (Ppy+Si) 50%

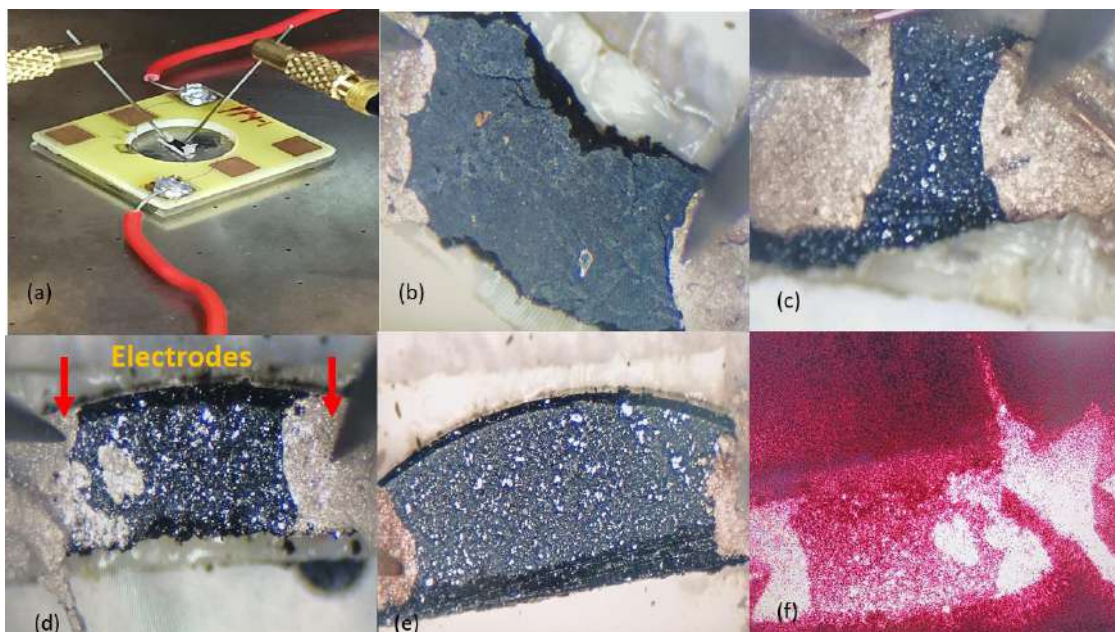


Fig:10 (a) Device in Probe station for testing (b) Ppy (c) Ppy25%+Si25% (d) Ppy75%+Si25% (e) Ppy+Si=50% (f) Red Laser illumination over a device

6.5 Procedure for Device Preparation

6.5.1 Preparation of the Substrate:

1. Preparation of the Synthesis: Prepare composites with variations measurements, such as 50% Ppy and 50% silicon, 25% Ppy and 75% silicon, 75 %Ppy and 25% silicon, pure Ppy and silicon. The first step is to gather all the raw materials needed for the synthesis of the hybrid material and make sure the substrate surface is clean and free of contaminants before beginning the process of designing of device as cleanliness is critical for establishing reliable and uniform device performance.

2 Grinding

A mortar and pestle crystal is used to crush silica to produce a fine powder form. The surface-to-volume ratio is increased during the grinding process.

3 Mixing of materials

Mortar and pestle crystal are used to achieve homogeneity and tune the characteristics of new material.

4 Die

Place the silicon and polypyrrole mixture in the Die in measured quantity for the various composites as stated above.

5 Pelletization of material

A pelletizer is used in the pelletizing process to exert pressure of one and one and a half tons over the die, resulting in the formation of compact pellets with an increased density of 10mm in diameter.

6 Silver Paste Application

To connect electrodes and test the device's conductivity, silver paste is applied to the extremities of the composites.

7 Electrode Integration

Fix electrodes to the extremities of the composites to test the device.

8 Curing and drying:

Allow the applied silver paste to dry before proceeding with the next step. This process assists in the removal of solvents and the good adherence of the silver paste to the substrate. The particular drying and curing conditions are determined by the properties of the silver paste.

9 Assembling

Assemble the components of the device into their final shape, to perform further analysis to check its various AC and DC variable electrical parameters.

10 Storage:

The device is kept in a box to keep it moist and dust-free.



Fig:11: Device images of Hybrid Photodetector

6.6 Experimental method

To understand the properties of unique combinations of materials, a device of a varied composite of Polypyrrole and silicon is made such as Polypyrrole 25% and Silicon 75%, Polypyrrole 75% and Silicon 25%, Polypyrrole 50% and Silicon 50%, 100% Polypyrrole and 100% Silicon. In this study, both Raman spectroscopy and IV characterization were performed on the photodetector device to comprehensively evaluate its material properties and electrical performance. Initially, Raman spectroscopy was utilized to analyze the molecular vibrations with Raman spectrometer WiTec alpha 300 series equipped with a charge-coupled device CCD detector. The Raman spectra were excited with the 532 nm diode laser. A CCD camera system with a monitor was utilized to select the location of the sample for the Raman spectra. An internal in-built lamp is used for calibration. The bands under discussion are large and asymmetric, and they overlap with adjacent bands. Various fitting approaches, such as WiTec Raman fits and Origin are used. Fitting methods can enhance the resolution of Raman spectra by breaking overlapping peaks. This is critical when dealing with complicated samples with closely spaced peaks or peaks hidden by other spectral features. The spectra were taken over ten accumulations and recorded with an integration time of 10 seconds. Every spectrum was obtained multiple times for comparison. To better understand how a sample's molecular vibrations react to changes in external circumstances, Raman spectra are recorded under different kinds of illumination conditions, such as in the dark and under ultraviolet (UV) light, and spectrum is also recorded at different laser power intensities. AC and DC analysis of the circuit provides insights into electronic transport. DC analysis focuses on the steady-state behaviour of circuits when exposed to constant voltage or current and also provides insights into the rate of change of voltages or currents and the response time of electronic systems. AC analysis focuses on understanding how a system responds to changing frequencies of electrical impulses requires conducting an AC analysis. Following the Raman analysis, the device

underwent IV characterization to assess its electrical behaviour under various illumination conditions. The photodetector was mounted on a probe station, which is coupled with a Source Measurement Unit (SMU) and controlled via LabVIEW software, providing a comprehensive and automated solution for this testing. The probe station is equipped with a high-magnification microscope for accurate visual alignment of probes on the photodetector's contact points. The device under test was securely placed on the chuck, which often includes a vacuum system to hold the device in place. Fine probe arms X, Y, and Z were capable of delicate and accurate movements, which were used to establish electrical contact with the device. For the IV characterization of the photodetector, an advanced setup incorporated with a probe station is a Source Measurement Unit (SMU) and LabVIEW software was employed to ensure automated electrical measurements. The SMU, is renowned for its ability to source voltage or current and simultaneously measure the corresponding electrical response. This integration allowed for highly accurate and sensitive detection of current-voltage characteristics. To streamline the testing process, LabVIEW software was used to control the SMU, automating the voltage and current sweeps and enabling real-time data acquisition and analysis. LabVIEW's customizable interface facilitated the setup of measurement parameters and the transition between different illumination conditions, including complete darkness. This combination of SMU and LabVIEW within the probe station setup provided a robust and efficient solution for comprehensive electrical characterization of the photodetector.

6.7 Results

6.7.1 Raman spectroscopy results

Peaks that appeared in the Raman spectra of polypyrrole are divided into 3 groups, the first group represents peaks due to change in ring deformation second group represents peaks due to symmetry in C-H, and the third group represents peaks due to C=C stretching. Each group further consists of two bands, radical cation and dication. (Furukwa, 1988)

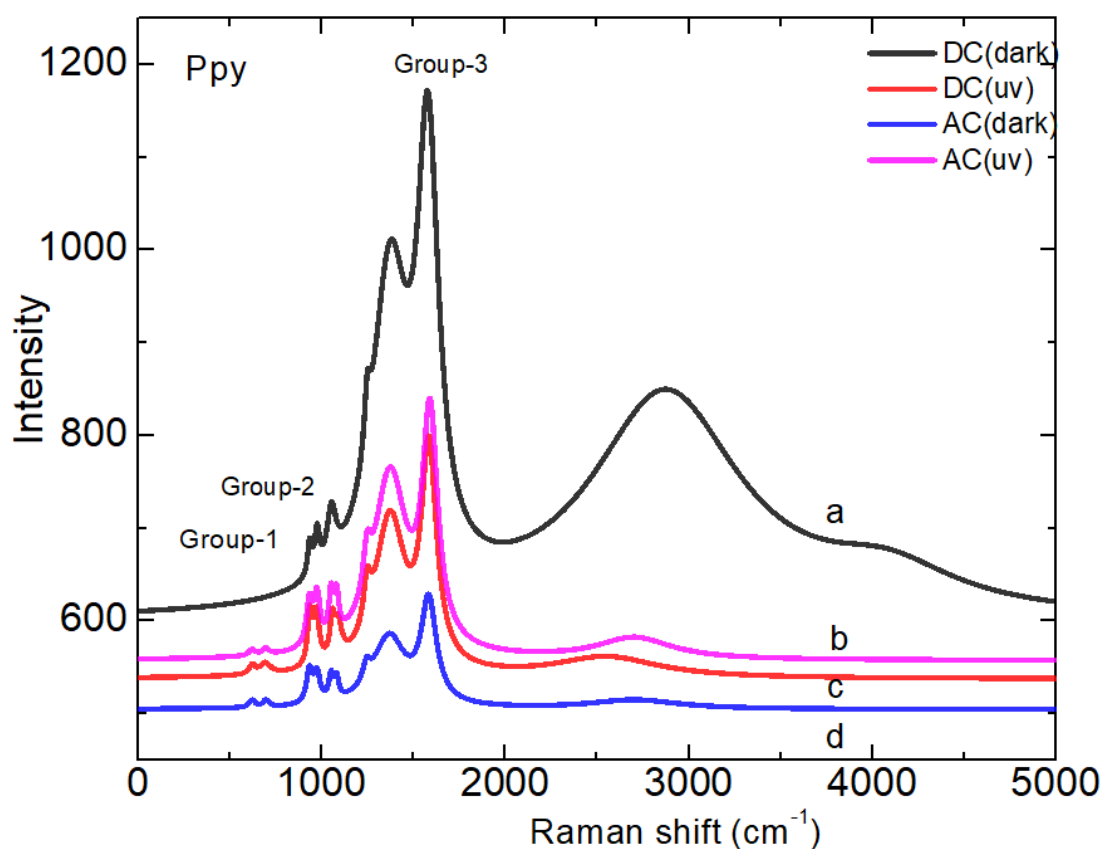


Fig:12 Raman spectra of Polypyrrole under Dark and UV illumination conditions
(a)40um,0v,0uA,dark,(b)35um,0.07v,71.1uA,uv,(c)35um,1Hz,120-300uA-dark,(d)
35um,500mHz,170-250uA,uv.

Group-1	Group-2	Group-3
Ring deformation	Symmetrical CH	C=C stretching
Dication~937 cm ⁻¹	Radical cation~1055 cm ⁻¹	1591 cm ⁻¹
Radicalcation~974 cm ⁻¹	Dication~1090 cm ⁻¹	1616 cm ⁻¹

Table: 1 Division of peaks into three different groups

While analyzing Raman spectra of polypyrrole and composites some shifts are visible these shifts provide valuable insights into the interactions and modifications within the material. In polypyrrole, the shifts in Raman bands often indicate the formation of polarons and bipolarons, which are charge carriers in conducting polymers or due to doping, which introduces charge carriers into the polymer. Doping levels can alter the position of the Raman bands, typically causing shifts to higher or lower wavenumbers depending on the nature and concentration of the dopant

Shifts in Polypyrrole Composites Raman Spectra: These shifts may result from the molecular interactions between the polypyrrole and silicon, or they may be caused by stress or strain induced in the polypyrrole matrix, which influences the Raman bands through the incorporation of silicon. The broadening of the peak near 1200 cm⁻¹ and the shifts in the Raman spectra around the silicon region (519–524 cm⁻¹) that are visible in figure 13 provide important insights into the interactions and modifications that occur within polypyrrole composites. These spectral features highlight the changes in electronic properties, stress and strain effects, and structural disorder induced by the composite formation.

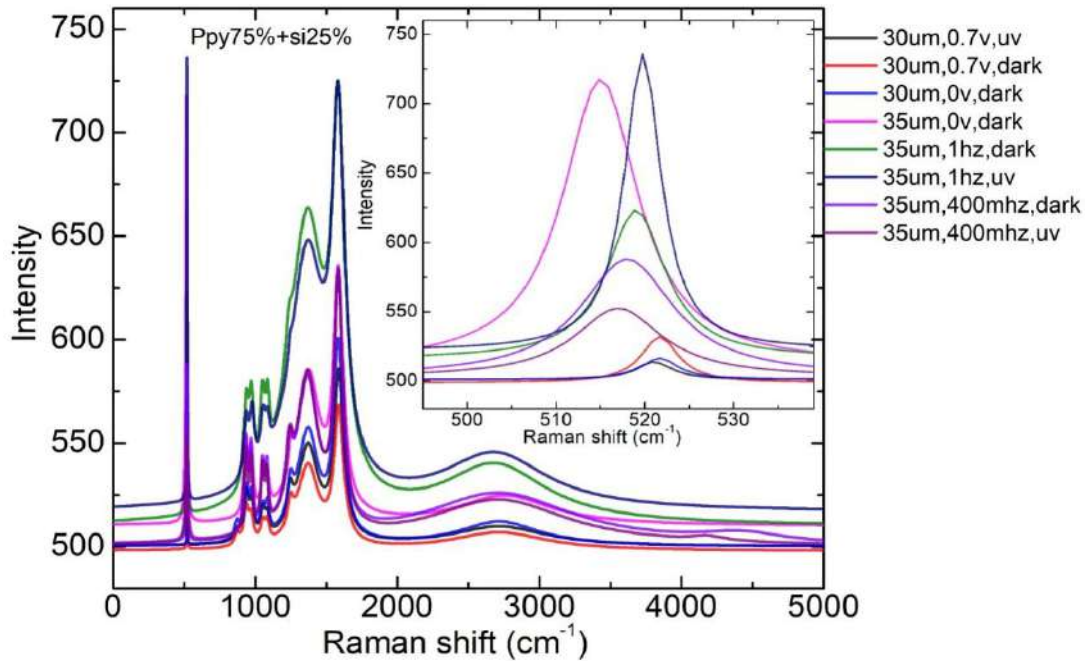


Fig: 13 Raman spectrum of Ppy75%+si25% UV and Dark illumination

Silicon Peaks Results

As for pure silicon, the peak appears at 520 cm^{-1} , but since I used composites of Ppy and silicon of different variations, I can see a wide range appearing for silicon from $(519\text{-}524)\text{ cm}^{-1}$. This is because of the interaction of monochromatic light with the lattice. It is described as the first-order scattering on the phonon at the center of the Brillouin zone (Γ) that satisfies the selection criterion $|k| \approx 0$. Feynman explains the scattering mechanism process in two ways. First, the excited photon forms an electron and a hole that interact with the lattice, changing their energy before recombining as an anti-Stokes or Stokes-like radiative transition and another one is After producing a phonon, the stimulating photon radiates as a Stokes or anti-Stokes photon. Strong Raman peaks are produced by the unique wave vectors of the phonons in crystalline semiconductors. Small crystallite sizes or crystal defects result in asymmetric peak widening

and a shift to lower frequencies. Therefore, the Raman spectrum provides exact details about the materials' crystallinity. The amorphous silicon, crystalline silicon, and polycrystalline silicon, Raman spectra appear to differ from one another. The polycrystalline silicon Raman peak exhibits an asymmetric broadening towards the low-frequency side when compared with the crystalline silicon Raman peak. The absorption coefficient of polycrystalline Silicon is higher than that of crystalline Silicon, the intensity of the peak is also associated with the crystal's sizes. (Kadlečíková et al., 2018), [[3]]

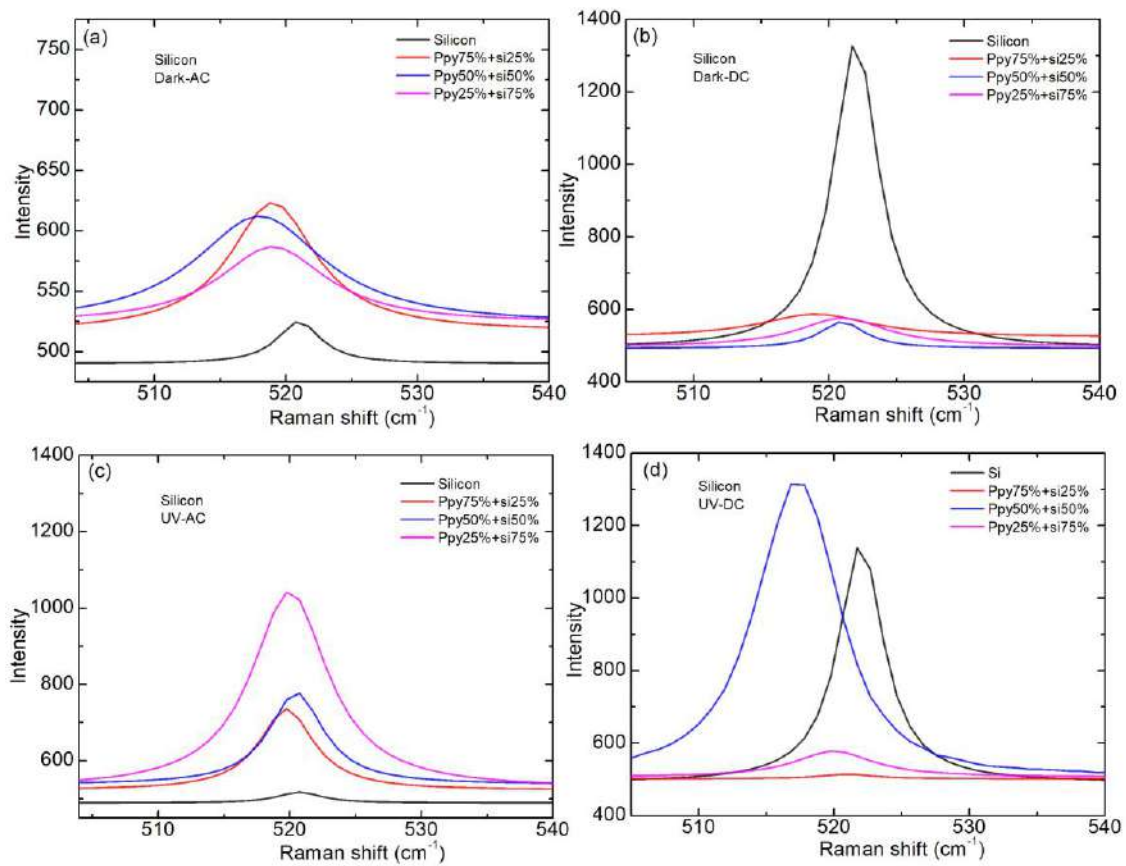


Fig:14 Analysis of Silicon Peaks of composites under dark and UV illumination. (a) silicon dark-AC (b) silicon dark-DC (c) silicon UV-AC (d) silicon UV-DC

6.7.2 I-V Characterization Result

IV characteristics of the device were obtained in both dark and illumination at room temperature. The device has been evaluated under various illumination conditions. It is tested by shining 100% of its light at two different wavelengths: 532 nm Green Laser and 655 nm Red Laser. The working voltage for UV light with a wavelength of 405 nm is 10.4 V, whereas the operating voltage for IR (infrared) light with a wavelength of 905 nm is 2 V. We measured the current-voltage (IV) of silicon, Polypyrrole (PPy), and their composites under identical illumination conditions. To make sure that the measurements were stable and consistent, there was a 10-minute waiting period after each illumination interval. The resulting I-V Characteristics of Polypyrrole, silicon, Ppy75%+si25%, Ppy50%+si50%, and Ppy25%+si75% are shown in the figure.

The IV curves for PPy were tested under dark conditions and illuminated with various wavelengths (532 nm, 655 nm, 405 nm, and 905 nm) up to an applied voltage of 2V. The IV curve for PPy under dark conditions shows a linear behaviour, indicating ohmic conduction. This suggests that the current through the PPy is directly proportional to the applied voltage, and consistency of the material exhibiting stable resistive properties. 532 nm and 655 nm IV curves exhibit a minor increase in current when compared to the dark condition, suggesting a photoconductive response, compared to the other wavelengths, the IV curve for 405 nm illumination shows the least rise in current, indicating that photoconductive enhancement is not very strong at this wavelength. The most significant rise in current is seen in the IV curve for illumination at 905 nm, which suggests a high photoconductive response. This implies that PPy is more sensitive to light in the near-infrared range. This could be because of improved absorption or more efficient charge carrier generation at this wavelength. Figure 15

The IV curves for silicon were tested under dark conditions and various illumination conditions up to an applied voltage of 10V. IV response of Silicon shows low conductivity when not

lighted, as indicated by the nonlinear, step-wise IV curve under dark conditions. There appears to be limited charge carrier movement in silicon due to low intrinsic carrier concentration, as indicated by the current that is in the microampere range up to 10V. The significant rise in current under infrared illumination suggests that infrared light absorption enhances silicon's conductivity. According to the photoconductive response, infrared light produces more charge carriers, which raises the conductivity overall.

The IV curves for the composite material, which is composed of 50% silicon and 50% PPy, were examined at 2.5V applied voltage under both dark and different illumination conditions (UV, 532 nm, 655 nm, and IR). The summarized result we got from this composite is IV curve in the dark exhibits a significant current response, suggesting better conductivity. The IV curve illuminated by UV light is similar to the dark condition, indicating that UV light does not appreciably change the composite's conductivity. There is a considerable increase in current compared to the dark condition in the IV curves for 532 nm and 655 nm illumination, suggesting some photoconductive response to visible light. The IV curve under IR illumination displays a reduced current response in contrast to the dark and visible light circumstances. This suggests that the composite is less sensitive to near-infrared light photoconductivity.

The IV curves were analyzed in both dark and different illumination conditions (UV, 532 nm, 655 nm, and IR) up to a 15V applied voltage for the composite material made up of 25% PPy and 75% silicon. The summarized result we got from this composite in dark conditions, the current increases with applied voltage, indicating a nonlinear relationship between complex charge transport within the composite. The apparent variations imply variations in conductivity. A similar increase and significant fluctuations under UV, 532nm, and 655nm illumination are observed. IR is stable but low conductivity is examined. The composite consisting of 75% Polypyrrole (PPy) and 25% silicon shows a linear response of up to 2 volts at different wavelengths. Under all circumstances, the current and voltage are Linear up to 2

volts for wavelengths of 532nm, 655nm, and IR, the conductivity is comparable. Under UV light, the conductivity is at its lowest the composite performs consistently in a variety of lighting conditions, with noticeable variations in conductivity occurring mostly in UV light. The experiments were carried out up to 3 volts, however, the linear trend is visible up to 2 volts

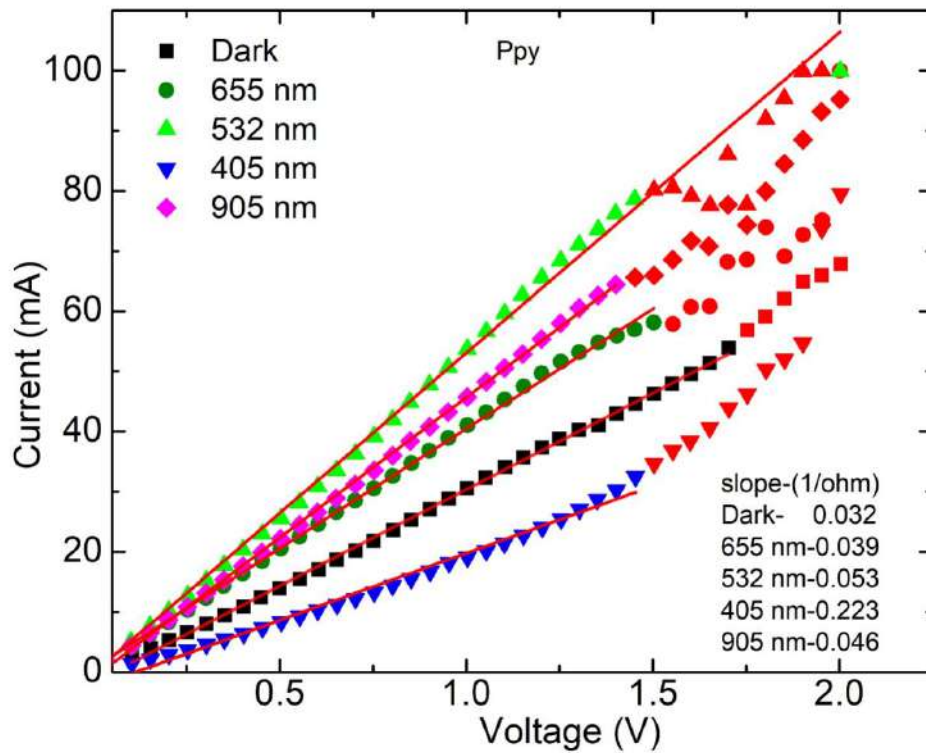


Fig:15 IV Characterization curve of polypyrrole

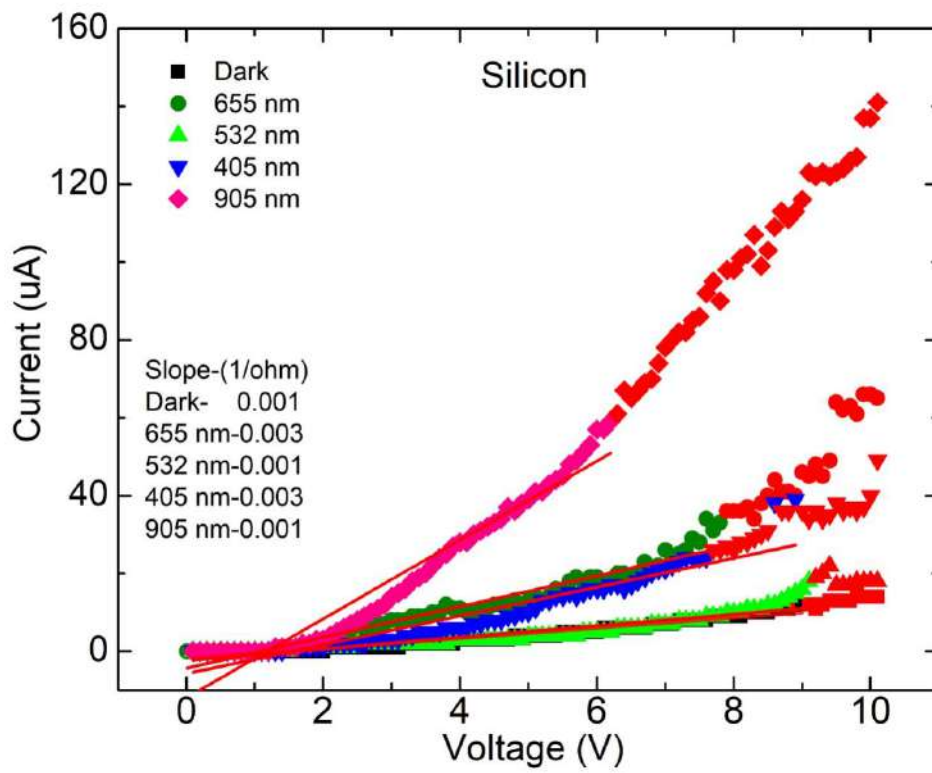


Fig:16 IV Characterization curve of Silicon

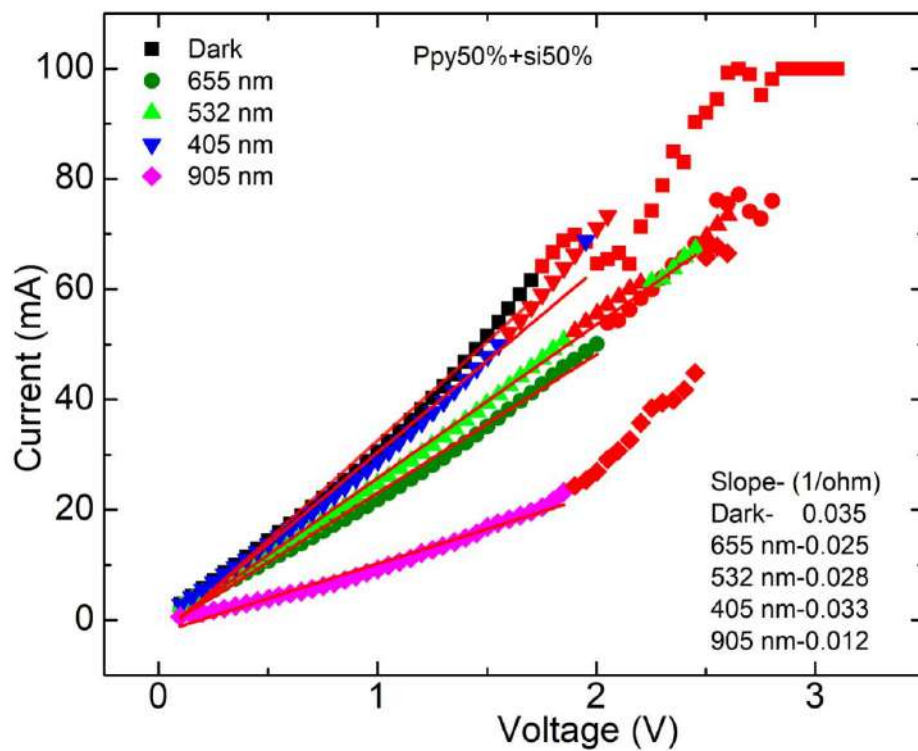


Fig:17 IV Characterization curve of Ppy50%+50%

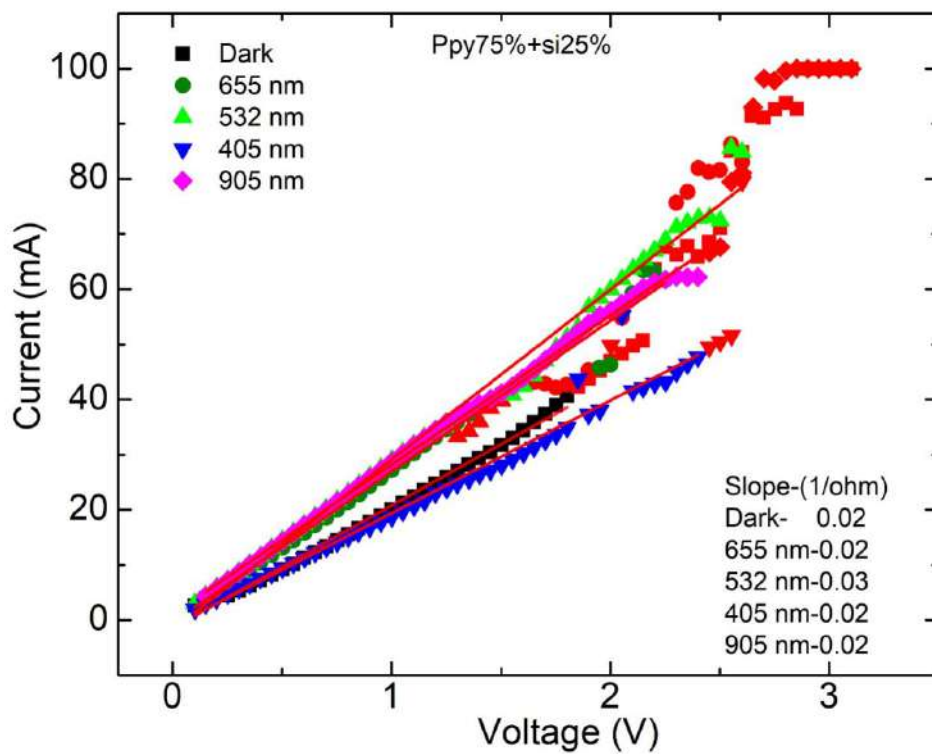


Fig:18 IV Characterization curve of Ppy75%+si25%

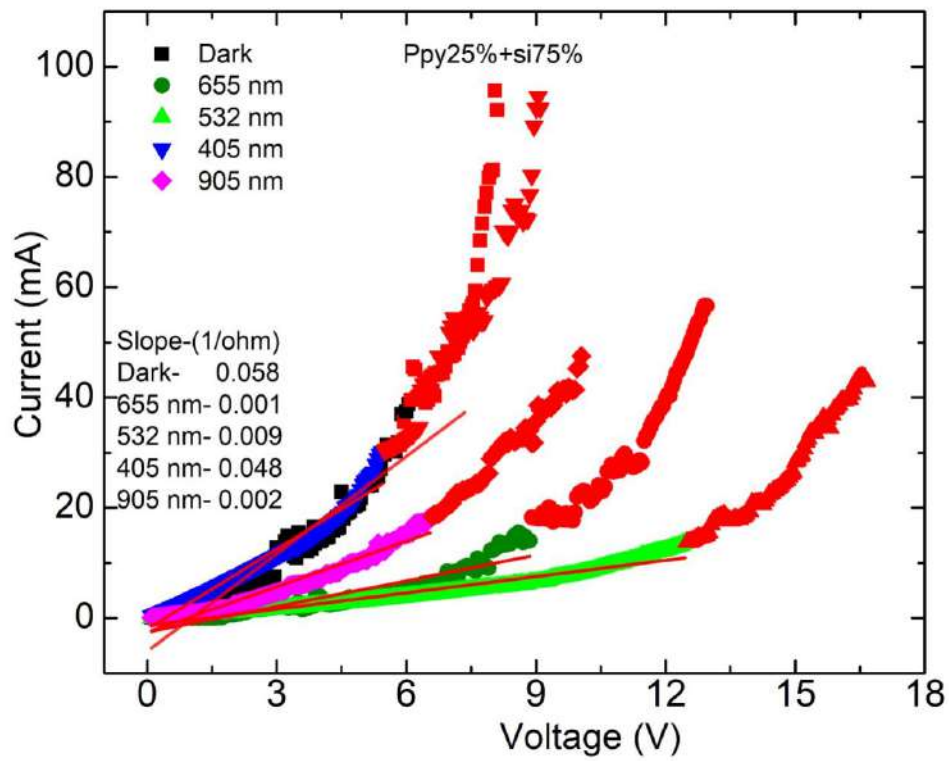
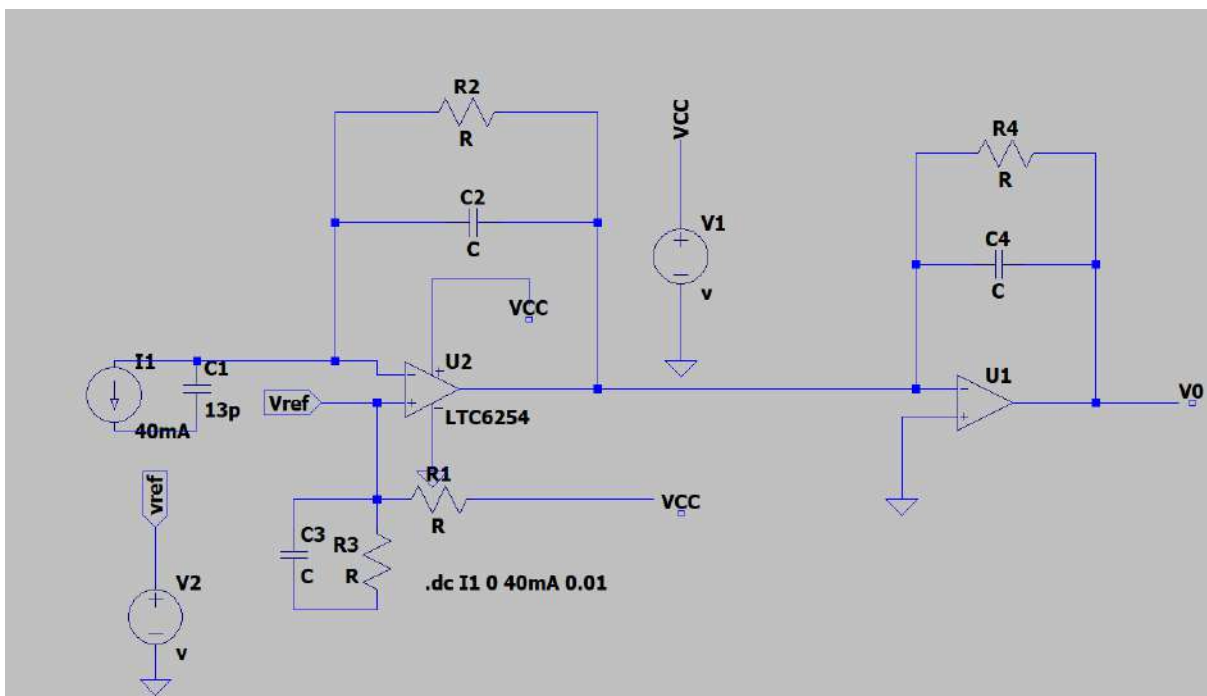


Fig:19 IV Characterization Curve of Ppy25%+si75%

6.8 Amplifier circuit Design



6.9 Conclusion

This thesis comprehensively investigates the structural and electrical properties of polypyrrole (PPy), silicon, and their composites, utilizing Raman spectroscopy and current-voltage (IV) measurements to elucidate their behaviours under various conditions. The Raman spectra provided valuable insights into the vibrational modes and interactions within these materials. The Raman spectra of PPy revealed characteristic peaks corresponding to the C=C and C–C stretching modes, indicative of its conjugated polymer structure. The intensity and position of these peaks confirmed the successful synthesis of PPy with a high degree of conjugation. The Raman spectrum of silicon displayed a prominent peak at around 520 cm^{-1} , This peak is characteristic of crystalline silicon. The interaction between PPy and silicon was evidenced by shifts in peak positions and changes in intensity. IV measurements were carried out to look at the electrical properties of silicon, PPy, and their composites in both dark and various illumination conditions this gives us insight into the functioning and potential of the photodetector and its future optimization.

REFERENCES

- [1] Furukawa, Y., Tazawa, S., Fujii, Y., & Harada, I. (1988). Raman spectra of polypyrrole and its 2, 5-¹³C-substituted and C-deuterated analogues in doped and undoped states. *Synthetic metals*, 24(4), 329-341
- [2] Mikat, J., Orgzall, I., & Hochheimer, H. (2002). Raman spectroscopy of conducting polypyrrole under high pressure. *Physical Review B*, 65(17), 174202.
- [3] Kadlečíková, M., Breza, J., Vančo, L., Mikolášek, M., Hubeňák, M., Racko, J., & Greguš, J. (2018). Raman spectroscopy of porous silicon substrates. *Optik*, 174, 347-353.
- [4] Kickelbick, G. (2007). Hybrid Material: Synthesis, Characterization, and Application. *Wiley-VCH*.
- [5] Makisima, A. (2004). Possibility of Hybrids Material *Ceramic Japan*.
- [6] Nanko, M. (2009). definition and Categories of Hybrid Materials. *Advances in Technology of Materials and Materials Processing*, 11.
- [7] Olmedo, L., Hourquebie, P., Buvat. (1997). An illustration of Dielectric Properties of Conductive Polymers. *Technical papers of the annual Technical Conference Society of the plastic Engineer corporation*.
- [8] Paul Rostron, S. G., Dina Gaber. (2016). Raman Spectroscopy, Review. *Research gate*.
- [9] Rostron, P., Gaber, S., & Gaber, D. (2016). Raman spectroscopy, review. *laser*, 21, 24.
- [10] Sanchez, P. G.-R. a. C. (2004). Functional Hybrid Material. *Wiley-VCH Verlag GmbH & Co*.
- [11] Saville, P. (2005). *Polypyrrole, formation and use*. Defence Research & Development Canada, Defence R & D Canada-Atlantic.
- [12] Suyama, Y. (2004). "Research and Development of Organic-inorganic Nanohybrids Materials" *Ceramics Japan*. *Research gate*.
- [13] Suzuki, Y. H. a. H. (2000). Fracture Mechanics. *Ohmsha, Japan*.
- [14] Sweeney, S., Adams, A. . (2006). *Optoelectronic Devices and Materials*,
- [15] Sweeney, S. J., Mukherjee, Jayanta. (2017). *Optoelectronics and Photonics Material*.
- [16] A.usuki, A. (2001). Organic-Inorganic Hybrid Materials. *Expected material for the Future*.
- [17] Yamada, A., Sasabe, H., Osada, Y., Shiroda, Y., & Yamamoto, I. (1989). Concepts of hybrid materials. *Hybrid Materials–Concept and Case Studies, ASM International, OH, USA*.
- [18] Brechet, M. F. A. a. Y. J. M. (2001). Designing Hybrid Material. *Acta Mater*.



**51st National Symposium on Acoustics
(NSA-2024)
27-28 Sep 2024 at NSTL, Visakhapatnam**



This is to certify that

*NEHA DEWANGAN, Kavita Thakur, Urawashi sahu, Sunandan Mandal
Bikesh Kumar Singh*

has presented paper titled
A Study on Cross Corpus Cross Lingual Speech Emotion Recognition

at National Symposium on Acoustics 2024 (51st NSA) held at Naval Science &
Technological Laboratory, Visakhapatnam during 27-28 September 2024

(Dr Mahavir Singh)
General Secretary
Acoustical Society of India

(Dr V Ramakrishna)
Convener
NSA-2024

(Er PVS Ganesh Kumar)
Organising Chairman
NSA-2024

“Improvement in the system developed for abrasion testing of solar glass coating & durability testing of coating”



*A Dissertation Submitted in Partial Fulfilment of the Requirements
for the Degree of*
MASTER OF TECHNOLOGY

in
Optoelectronics and LASER Technology
Submitted by

Sandeep Kumar
(2210196003)

Under the Guidance of

Supervisor

Prof. Anil Kottantharayil

Professor
Department of Electrical Engineering,
IIT Bombay, Maharashtra

Co-Supervisor

Dr. Kavita Thakur

Professor & Course Coordinator
S.O.S Electronics and Photonics
PRSU, Raipur, Chhattisgarh

Work carried out at



National Centre for Photovoltaic Research and Education (NCPRE)
Indian Institute of Technology, Bombay (IITB)

400076, Maharashtra

Jan- Jun 2024

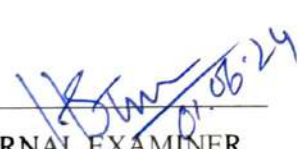


School of Studies in Electronics and Photonics
Pt. Ravishankar Shukla University
Raipur - 492010
Chhattisgarh

Dissertation Approval for MTech

Session 2023-24

This dissertation work entitled, *“Improvement in the system developed for abrasion testing of solar glass coating & durability testing of coating”* submitted by *Sandeep Kumar* at *NCPRE, IIT Bombay* during the period *Jan-Jun 2024* is approved for the degree of *Master of Technology (IVth Semester)* in *Optoelectronics and LASER Technology*, Pt. Ravishankar Shukla University, Raipur, Chhattisgarh.


EXTERNAL EXAMINER

Dr. H.S. Tewari

Professor

Department of Pure & Applied

Physics

Guru Ghasidas University, Bilaspur,
Chhattisgarh - 495009

Date: 01-06-2024

Place: Raipur


INTERNAL EXAMINER

Dr. Kavita Thakur

Professor & Course Coordinator

S.o.S in Electronics and Photonics

Pt. Ravishankar Shukla University, Raipur

Chhattisgarh-492010



Indian Institute of Technology, Bombay (IITB)
400076, Maharashtra

CERTIFICATE

This is to certify that the dissertation work entitled, *“Improvement in the system developed for abrasion testing of solar glass coating & durability testing of coating”* submitted by *Sandeep Kumar*, is a credible work carried out by him at NCPRE, IIT Bombay during the period *July 2023 to June 2024*. The work has been presented in a manner suitable to affirm acceptance towards in the partial fulfilment of the requirement for the degree of *Master of Technology in Optoelectronics and LASER Technology, Pt. Ravishankar Shukla University, Raipur, Chhattisgarh*, is candidate’s own work carried out by him under my supervision. His dedication and sincerity are praiseworthy.

Date: 24 May 2024

Place: Mumbai

Signature of Supervisor

Prof. Anil Kottantharayil

Professor,

Department of Electrical Engineering,
IIT Bombay, M.H.

PROFESSOR
Department of Electrical Engineering
Indian Institute of Technology Bombay,
Powai, Mumbai 400 076



School of Studies in Electronics and Photonics
Pt. Ravishankar Shukla University
Raipur - 492010
Chhattisgarh

CERTIFICATE

This is to certify that the dissertation work entitled, *“Improvement in the system developed for abrasion testing of solar glass coating & durability testing of coating”* submitted by *Sandeep Kumar* is a credible work carried by him at *NCPRE, IIT Bombay* during the period *Jan-Jun 2024*. The work has been presented in a manner suitable to affirm acceptance towards in the partial fulfilment of the requirement for the degree of *Master of Technology in Optoelectronics and LASER Technology, Pt. Ravishankar Shukla University, Raipur, Chhattisgarh.*

Dr. Kavita Thakur
01/06/2024

INTERNAL SUPERVISOR

Dr. Kavita Thakur

Professor & Course Coordinator

S.o.S in Electronics and Photonics

Pt. Ravishankar Shukla University, Raipur
Chhattisgarh-492010

Dr. Kavita Thakur
01/06/2024

HEAD OF DEPARTMENT

Dr. Kavita Thakur
Head

Date:

Place: Raipur

DECLARATION

I hereby declare that the dissertation entitled "*Improvement in the system developed for abrasion testing of solar glass coating and durability testing of coating*" submitted to the School of Studies in Electronics & Photonics, Pt. Ravishankar Shukla University, Raipur, Chhattisgarh for the degree of *Master of Technology in Optoelectronics & LASER Technology* is an original record of work done by me at *NCPRE, IIT Bombay* under the supervision of Prof. Anil Kottantharayil Department of Electrical Engineering, IIT Bombay, Maharashtra and co-supervision of Dr. Kavita Thakur Professor Department of Electronics and Photonics PRSU, Raipur, Chhattisgarh. I also declare that I have adhered to all principles of academic honesty and integrity.

I declare that this written submission represents my ideas in my own words and where other's ideas or words have been included; I have adequately cited and referenced the original source.



Sandeep Kumar

(Roll No: 2210196003)

Enrollment No: AC/22785

MTech (OELT), 4th - Semester

Date: 1-6-24

ACKNOWLEDGMENT

I want to sincerely thank my project supervisor, **Prof. Anil Kottantharayil**, (Professor, EE Department, IIT Bombay) for all of his support, direction, and inspiration in getting me all the resources I needed for my project work.

I would like to take this opportunity to thank my co-supervisor, **Prof. Kavita Thakur** (Professor, SoS in Electronics and Photonics, PRSU, Raipur), for granting me permission to work at IITB and for her encouragement and advice on this project.

Additionally, I would like to sincerely thank **Prof. Narendra Shiradkar** (EE Department, IITB) and **Prof. Sudhanshu Mallick** (MEMS Department, IITB) for their helpful advices. Sincere thanks to **Mr. Pavan Fuke, Mr. Shoubhik De, Mr. Karan Rane** and all the **NCPRE Module Lab members** for their insightful advice, help, and support in completing this project.

Furthermore, I would like to sincerely thank the faculties of my department **Mr. Madhu Allalla, Mr. K Anil Kumar**, and **Mr. Mohnish Kumar Sahu**. Thank you to my colleague **Ms Drishty Singh** for her encouraging words during my moments of low self-esteem.

Finally, but just as importantly, I want to thank my **Parents**, for giving me a comfortable environment and support.

SANDEEP KUMAR

ABSTRACT

Photovoltaic (PV) modules are susceptible to soiling, that is the accumulation of dust and other particles on the surface of the solar module (PV module). Soiling can reduce the efficiency of the PV module, leading to a loss in energy production and revenue. Anti-soiling (AS) coatings are promising solution for mitigating soiling losses. Commercial AS coatings are typically hydrophobic, meaning they repel water, however hydrophilic coatings are also available in the market. The durability of AS coatings in real-world environmental conditions is a challenge. This because the high humidity, temperature, and other weather parameter can cause the coating to degrade over time. An indoor accelerated testbed is developed at the IIT Bombay which emulates outdoor stressors. Modifications have been made to the system to make its performance more reliable and precise. Furthermore, a load measurement system is introduced to measure the loads applied by the brush during cleaning. In this study, we have also studied the durability of ASC for different cleaning loads and their cleaning efficacy. The result of the experiment can help for better compromise between cleaning load and cleaning efficacy.

Keywords: PV, Soiling, ASC, Durability, Efficacy.

Table of Contents

ACKNOWLEDGMENT	v
ABSTRACT	vi
List of figures	ix
List of Tables.....	xi
List of abbreviations.....	xii
Chapter 1	1
Solar Market.....	1
1.1) Worldwide Solar Power Installation	1
Chapter 2	2
PV Technology.....	2
2.1) Introduction	2
2.2) Main Components of a PV Module.....	2
Chapter 3	3
Soiling	3
3.1) Reasons for being concerned about PV output.....	3
3.2) Effect of Soiling on PV modules.....	3
3.3) Soiling Mitigation Approaches.....	4
Chapter 4	6
Anti Soiling Coating and Literature Review.....	6
4.1) Introduction	6
4.1.1) Hydrophilic coating.....	6
4.1.2) Hydrophobic coating.....	6
4.2) Characteristic Parameters of ASC	7
4.3) Challenges with Anti-Soiling Coatings	7
4.4) Accelerated Stress Test.....	9
4.4.1) UV exposure and damp heat test.....	9
4.4.2) Abrasion test.....	10
4.4.3) Combination of stressors	10
Chapter 5	12
Cleaning Cycle Simulator (CCS)	12
5.1) Introduction	12
Chapter 6	13
Modifications in system	13
6.1) Introduction	13
6.2) Temperature uniformity.....	13
6.3) Real time temperature.....	14
6.3.1) Testing.....	14

6.3.2) Observation	15
6.3.3) MAX6675 K-type thermocouple	16
6.4) Support structure	16
6.5) Load measurement system	18
6.5.1) Measuring the load: Experimental Setup	18
Chapter 7	20
Effect of Different Cleaning loads on Coating and Cleaning Efficacy	20
7.1) Introduction	20
7.2) Effect of Different Cleaning Loads on Coating.....	20
7.2.1) Sample preparation, characterization and CCS programming:.....	20
7.2.2) Brush characteristics	20
7.2.3) Experiment Process:.....	21
7.2.4) Result and discussion	22
7.3) Statistical Analysis (Hypothesis testing)	23
7.3.1) Wilcoxon Signed Rank Test.....	23
7.3.2) Result and discussion	23
7.4) Efficacy of different cleaning loads	25
7.4.1) Fundamental approach.	25
7.4.2) Experimental setup.....	25
7.4.3) Process followed:	27
7.4.4) Result and discussion	29
7.5) Conclusion.....	29
Chapter 8	30
Summary and Future Objective	30
8.1) Summary.....	30
8.2) Future work	30
References	31

List of figures

Figure 1: Evolution of Annual PV Installations (Note: X-year, Y-GWp)	1
Figure 2: Cumulative PV Installations (Note: X-year, Y-GWp)	1
Figure 3: Components of c-Si module	2
Figure 4: Soiling on PV modules	3
Figure 5: factors affecting soiling on PV module	4
Figure 6: Vertical mounted bifacial PV modules (left soiled, right clean)	5
Figure 7: Contact angle for different types of coating	6
Figure 8: Optical and hydrophobic performance of outdoor sample	7
Figure 9: WCA measurements for coated coupons over time	8
Figure 10: (a) The coated black panel maintained its power production even after snowfall. (b) The coated panel (right) stayed clean, residues left on an uncoated panel (left).....	8
Figure 11: Optical and hydrophobic performance during UV Exposure	9
Figure 12: “WCA and RA of the hydrophobic coating after damp heat.....	10
Figure 13: Hydrophobic-coating performance before and after abrasion with CS10 and Felt Pad.....	10
Figure 14: The effectiveness of coatings following exposure to a combination of four stressors and three stressors	11
Figure 15: Cleaning Cycle Simulator at NCPRE module lab, IITB	12
Figure 16: (a) Non uniform cooling of Cu plate (b) Non uniform heating of Cu plate	13
Figure 17: (a) 20*20cm ² copper plate, (b) 11*8cm ² copper plate	14
Figure 18: (a) 20*20cm ² plate heating non uniformly, (b) 11*8cm ² plate heating nearly uniform.....	14
Figure 19: (a) Dallas temperature sensor DS18B20 (b) FLIR E75 (c) Fluke 52II thermometer with k-type thermocouple wire	15
Figure 20 : K-type thermocouple wire with MAX6675 amplifier	16
Figure 21: Cu plate screwed over carriage (a) top view, (b) side view (c) reduced Cu plate	16
Figure 22: Construction of the acrylic sheet support structure. (a) Bottom layer, (c) Middle layer, and (e) Top layer and (d), (e), and (f) shows the assembly steps for the acrylic sheets.	17
Figure 23: (a) framed loadcell side view, (b) top view	18
Figure 24: Load applied by different designs of brush	19

Figure 25: a) CA after applying coating, b) CA after coating degraded.....21

Figure 26: Effect of different cleaning loads on coating.....22

Figure 27: WSRT for Dataset pair1 for loads 300g, 600g, 900g, 1010g (clockwise from top left corner).24

Figure 28: WSRT for Dataset pair2 for loads 300g, 600g, 900g, 1010g compared at their degradation cycle (65, 70, 85 and 100) clockwise from top left corner.....24

Figure 29: packaged mini solar module25

Figure 30: a), b) and c) represents I_{sc} measurement setup without dust, with dust and after cleaning the dust respectively.26

Figure 31: a) $0.2\text{mg}/\text{cm}^2$, b) $0.6\text{mg}/\text{cm}^2$ dust deposition on glass samples.....28

List of Tables

Table 1: Different cleaning techniques for solar PV.....	4
Table 2: Different Device (Temperature Sensing) and Temperature.....	15
Table 3: Brush design specification	19
Table 4: Current and Temperature References	27
Table 5: Measured average I_{SC} values of mini module.....	28
Table 6: Soiling Loss	28

List of abbreviations

ASC	Anti-Soiling Coating
AST	Accelerated Stress Test
CA	Contact Angle
CCS	Cleaning Cycle Simulator
Cu	Copper
DDDC	Dew Dust Dry Clean
DI	Di-Ionised Water
EVA	Ethylene-Vinyl-Acetate
FF	Fill Factor
IEA	International Energy Agency
IEC	International Electrotechnical Commission
IR	Infrared
PM	Particulate Matter
PV	Photovoltaic
RA	Roll Off Angle
RH	Relative Humidity
SPI	Serial Peripheral Interface
TW	Tera Watt
UK	United Kingdom
UV	Ultra Violet
WCA	Water Contact Angle
WSRT	Wilcoxon's Signed Rank Test

Chapter 1

Solar Market

1.1) Worldwide Solar Power Installation

According to the International Energy Agency (IEA), 231GW of solar power was installed worldwide in 2022, increasing the total to 1.2 TW. Photovoltaic (PV) has shown to be a significant, long-term contributor to the energy sectors, carbon reductions and cost-competitive electricity generation. Over 66% of new renewable energy capacity added in 2022, producing over 50% of power generation from new renewable energy[1].

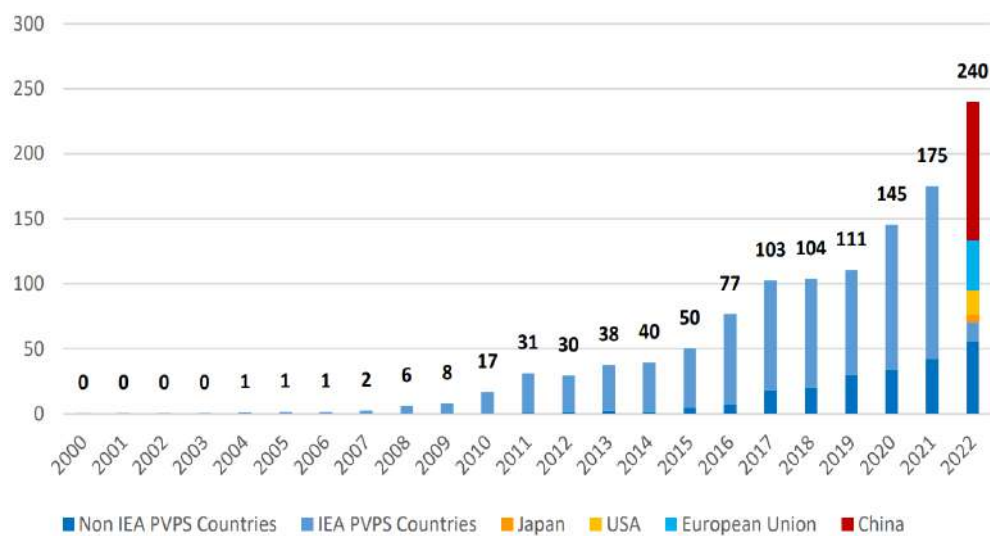


Figure 1: Evolution of Annual PV Installations (Note: X-year, Y-GWp)

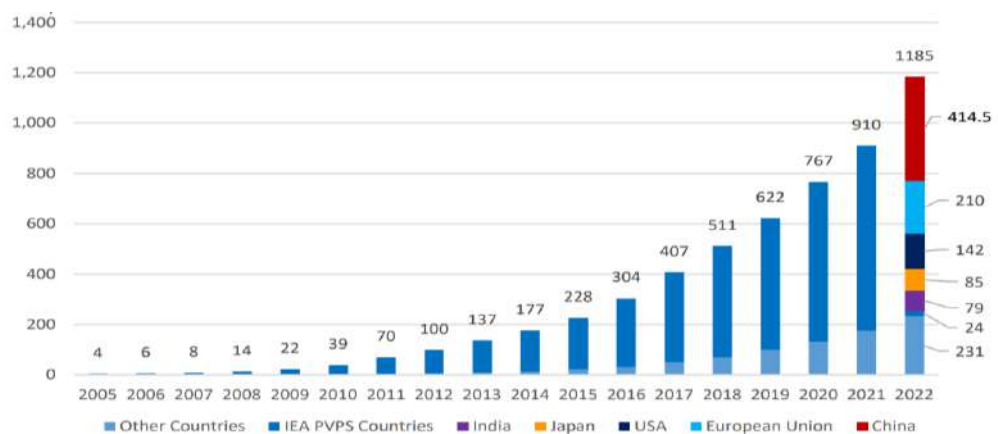


Figure 2: Cumulative PV Installations (Note: X-year, Y-GWp)

Above figures highlight the evolution of PV installations and impact of the Chinese PV market, rapidly expanding PV markets in India and other emerging nations. [1].

Chapter 2

PV Technology

2.1) Introduction

The most adaptable type of energy we have is electricity. Since the 1970s, solar electricity has demonstrated that a significant amount of the world's electrical power can be produced without the use of nuclear fission reactions or the burning of fossil fuels like coal, oil, or natural gas. The technology known as photovoltaics uses photons to illuminate semiconductors to produce electrical direct current (DC). The solar cell, which is the name for each individual PV element is a precisely engineered semiconductor diode that effectively absorbs and transforms solar light energy into electrical energy [2][3]. Characteristic parameters (mainly) of solar cells are short circuit current density (J_{sc}), Open circuit voltage (V_{oc}), Fill factor (FF) and Conversion efficiency (η) [2].

2.2) Main Components of a PV Module

- A **Low Iron Glass** front layer, which provides mechanical stability and is transparent to light.
- A layer of **Ethylene-Vinyl-Acetate (EVA) Encapsulant**, which protects the solar cells from moisture and other environmental stresses.
- A **back layer** made of **PVF-polyester-PVF**, which protects from the humidity and other stresses.
- An **Aluminium frame**, which enhances the mechanical stability of the module.
- A **Junction box**, which contains electrical connections to the solar cells.

These components are stacked together in a specific order to create a durable and efficient PV module [3].

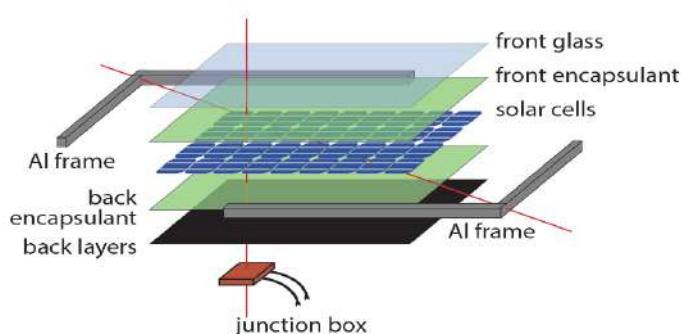


Figure 3: Components of c-Si module

Chapter 3

Soiling

3.1) Reasons for being concerned about PV output

A power output of a PV system is affected by various environmental factors that includes temperature, irradiance, type of technology used (monocrystalline, multi-crystalline, multijunction etc.), design and selection of necessary equipment (batteries, chargers, power electronic devices, wiring etc). After installing solar PV systems, a few major problems arise, for example, the amount of energy produced by the systems is significantly reduced by shading, **soiling** etc. that are caused by various factors [4], [5].



Figure 4: Soiling on PV modules [6]

3.2) Effect of Soiling on PV modules

Soiling results from the accumulation of either organic or inorganic dirt particles, which reduces light transmission and attenuates solar radiation. This directly affects the PV module's electrical output [6]. Soiling is a phenomenon that is location-dependent and it influenced by a variety of environmental factors [7]. Power output reduction is the short-term effect of soiling, while the formation of a cement-like coating on the PV module's surface is the long-term effect which forms a strong bond with module surface [8], [9].

Dust deposition on PV module can affect the energy generation down to 50% if it is not cleaned for 4 months in Mumbai, India (warm and humid climate) [10]. Losses due to dust deposition on solar modules can go as high as 0.4%/day [11], [12]. Three significant factors that influences deposition of dust on PV modules are depicted in figure 5.

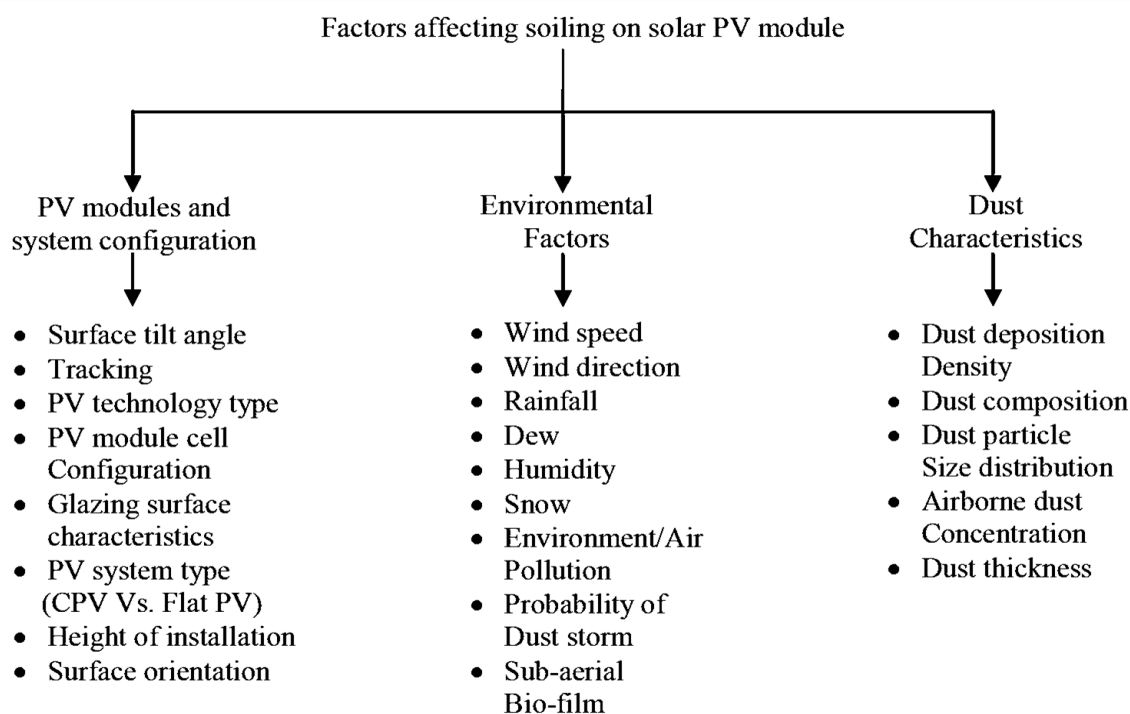


Figure 5: factors affecting soiling on PV module

According to Ilse et al., the soiling can reduce the global solar production by at least 3-4% in optimized clean-up scenarios. This translates into annual revenue losses of between €3 billion and €5 billion. High particulate matter (PM) counts in countries like China, India, and the Middle East result in high soiling losses of up to 1% per day, which is estimated to cause financial losses of 1 billion euros annually by 2023 [13].

3.3) Soiling Mitigation Approaches

Mitigation techniques are essential to deal with the soiling issue in PV systems, to remove dust deposition to ensure higher conversion efficiencies and, also to improve the economic viability of solar PV projects[14]. The number of PV cleaning methods are described in the table below with their pros and cons:

Table 1: Different cleaning techniques for solar PV.

Method	Pros	Cons
Manual cleaning	<ul style="list-style-type: none"> ✓ Reliable cleaning method ✓ Possibility of removing even difficult deposits 	<ul style="list-style-type: none"> ➤ Challenging and drastic manpower required for huge size solar plants ➤ Huge amount of Water needed ➤ High risk ➤ Needs to be scheduled periodically for good results

High water spray cleaning	<ul style="list-style-type: none"> ✓ Cost effective ✓ Commercial and available in the market 	<ul style="list-style-type: none"> ➤ Can damage panels due to high pressure exerted ➤ Huge amount of water needed
Electrostatic precipitator (active method)	<ul style="list-style-type: none"> ✓ No physical contact ✓ No mechanical damage, scratch & scar marks on panel 	<ul style="list-style-type: none"> ➤ High energy consumption ➤ Dissatisfactory maintenance
Microfiber – cloth wiper and vacuum cleaning	<ul style="list-style-type: none"> ✓ Relatively low capital cost 	<ul style="list-style-type: none"> ➤ Ineffective as dust particles remain on the surface ➤ Requires power source for vacuum cleaning.
Silicon rubber brush	<ul style="list-style-type: none"> ✓ Lightweight compared to robotic system ✓ Low cost ✓ Easy to automate 	<ul style="list-style-type: none"> ➤ Not commercial, pilot projects implemented only ➤ May not be effective to remove heavy dirt.
Robotic system	<ul style="list-style-type: none"> ✓ Automatic and flexible in design ✓ Able to clean efficiently 	<ul style="list-style-type: none"> ➤ Some requires charging separate ➤ Heavy load on panel's surface ➤ Expensive technique
Self-cleaning mechanism (nano film coating)	<ul style="list-style-type: none"> ✓ Avoids deposition of dust on the panel ✓ Rainwater gets scattered ✓ No power required (passive method) 	<ul style="list-style-type: none"> ➤ Not commercial method yet, various research is to be held

There are other techniques available that can be used to mitigate the soiling on modules. Research indicates that as the tilt angle increases, the amount of soiling loss decreases [15]. Sonali B. investigated that mounting bifacial module vertically, soiling losses may be reduced and consequently, frequent panel cleaning may be avoided [12].



Figure 6: Vertical mounted bifacial PV modules (left soiled, right clean)

Chapter 4

Anti Soiling Coating and Literature Review

4.1) Introduction

Soiling can cause PV modules to lose a significant amount of their power output. One efficient technique to reduce soiling losses is to apply anti-soiling coatings (ASC) on the glass surface of PV module. ASC is nano or micro-layer coating [10]. Based on their contact angle, ASCs are categorized as super-hydrophilic, hydrophilic, hydrophobic, and super-hydrophobic [16].

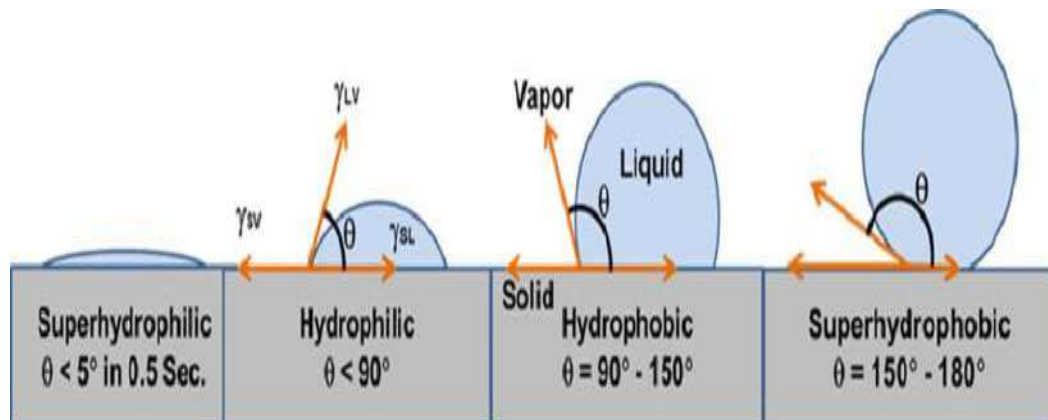


Figure 7: Contact angle for different types of coating

4.1.1) Hydrophilic coating

Water is necessary for hydrophilic coatings to completely wet the glass and remove dust particles as the water flows down-slope to the panel's bottom. They are made of high surface energy materials. Perfectly clean Titanium surface with unsaturated chemical bonds represent a high-energy surface and show hydrophilic properties[16].

4.1.2) Hydrophobic coating

They prevent water droplets from wetting the surface and serve as a sort of cleaning mechanism by rolling off the droplet with dust particles together. Hydrophobic coatings are made of a low surface energy, chemically inert material, they stop chemical reactions between soil and the glass surface. Materials with low surface energy, like fluorinated materials or the addition of silicone compounds, are super-hydrophobic [16]. When compared to hydrophilic surfaces, soiling rates are 42% lower on hydrophobic coatings [17].

4.2) Characteristic Parameters of ASC

Important characteristics for describing anti-soiling coatings are **roughness** and **contact angle** [18]. The **roll-off angle** - the angle at which a water droplet would begin to roll off the coated surface [19] and **Surface energy** - defines the hydrophobicity of the coating can also be used for characterization [20].

4.3) Challenges with Anti-Soiling Coatings

It is a concern that under severe operating conditions, the ASC, which is applied to the PV module's outer surface, may degrade [17]. There is less dependability of the anti-soiling coating in actual environmental circumstances. Therefore, it is necessary to validate the ASC in an actual outdoor field setting. Furthermore, there isn't presently a standard or methodology available to test the ASC durability (pass/fail) for commercial applications. In order to measure the durability of the commercially available coatings and to make it easier to develop new, long-lasting ASC. A standard testing procedure would serve as a baseline [21]. Few studies have examined these coatings performance and durability in-depth for PV applications:

- A study is conducted in Hydrophobic coating for 6 months (Jul-Feb) in Nottingham, UK (Climate zone – Oceanic climate). With temperature (21.3°C to -0.5°C), Rainfall 85.1 to 46.2 mm each month, Sunshine duration per month 178.5 to 54.9 hours Facing south at an angle of 45°. Water contact angle (WCA) showed ~31% degradation and Roll-off-angle (RA) increased by ~64° to 84° [22].

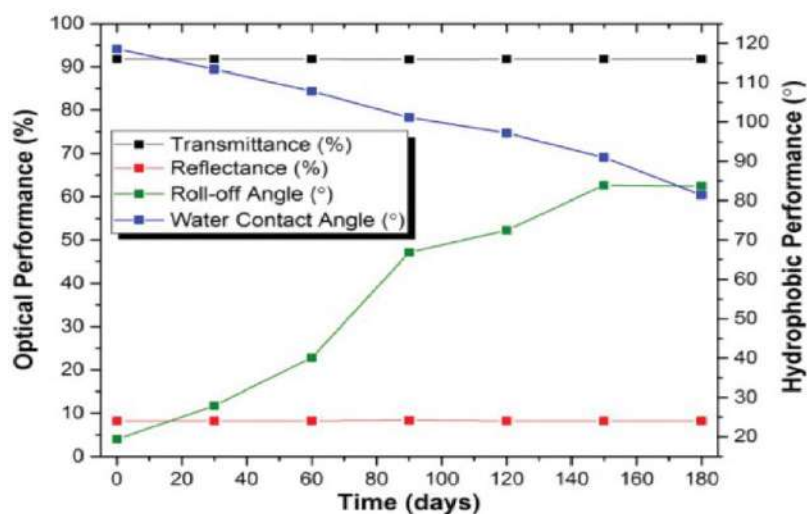


Figure 8: Optical and hydrophobic performance of outdoor sample

- Another study (5 months) in winter for two hydrophobic coatings (A and B) is conducted in Denmark (Climate zone –high oceanic) and Colorado (Climate zone– Tropical, and Subtropical). samples were exposed to sub-zero temperatures, rainfall, and high humidity in the first two weeks. High rate of initial degradation of contact angle observed for both coatings A and B in the first two weeks of exposure. The coated module was fully operational after the snowfall, while the not-coated module retained snow coverage and thus produced no power. Numerous factors, such as solvent release, fluorine loss, coating thinning, and increased surface macro-roughness, contributed to degradation [19].

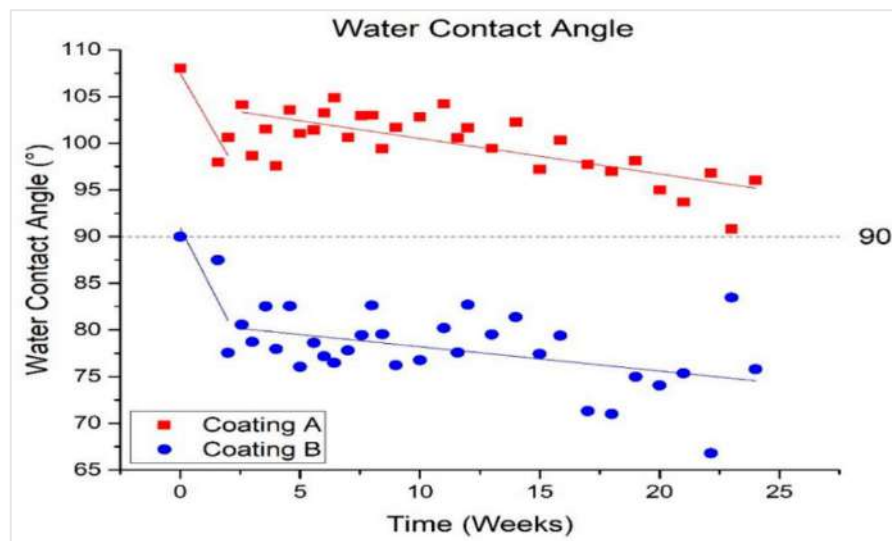


Figure 9: WCA measurements for coated coupons over time

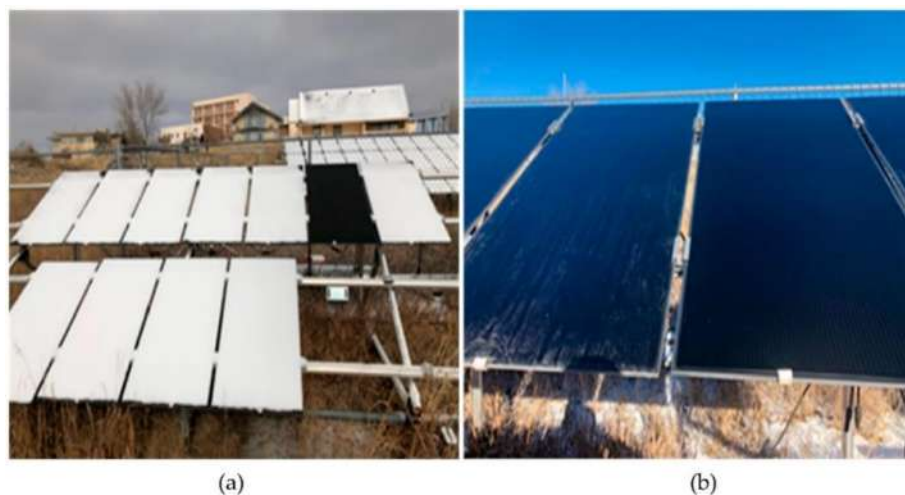


Figure 10: (a) The coated black panel maintained its power production even after snowfall. (b) The coated panel (right) stayed clean, but residues were left on the uncoated panel (left).

4.4) Accelerated Stress Test

Accelerated stress testing (AST) exposes anti-soiling coatings to a variety of environmental stresses for a shorter amount of time compared to what they would be exposed to in the real world in order to determine how durable the coatings are. This makes it possible to quickly evaluate a coating's durability to the challenging conditions like UV radiation, high humidity, and extreme temperatures, that solar modules are commonly exposed to [22].

4.4.1) UV exposure and damp heat test

- Based on the IEC 61215-2:2016, Kenan Isbilir et al. [22] reported that hydrophobic ASC shows no sign of degradation after 1000 hours of exposure to damp heat at 85°C/85% relative humidity (RH) and after 4,000 hours of immersion in DI water. However, after the UV exposure tests, the WCA dropped to 87° and the RA increased to 60.5°. UV exposure had a major negative effect on the coating because it was not meant to be used in the sun and its resistance to the sun was not specified. Using X-ray photoelectron spectroscopy, they detected a decrease in fluorine concentration following the UV exposure.

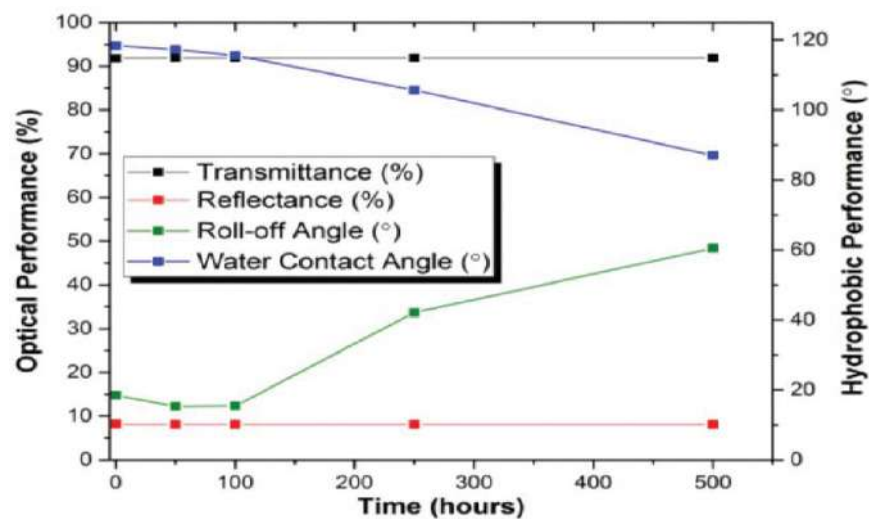


Figure 11: Optical and hydrophobic performance during UV Exposure [35].

- Based on IEC16215-17, S. F. Bukhari et al. [23] demonstrated that the WCA holds steady even after a 1000-hour UV exposure test. Nevertheless, due to solvent/moisture capture, damp heat testing revealed a decrease in the WCA after 500 hours of exposure.

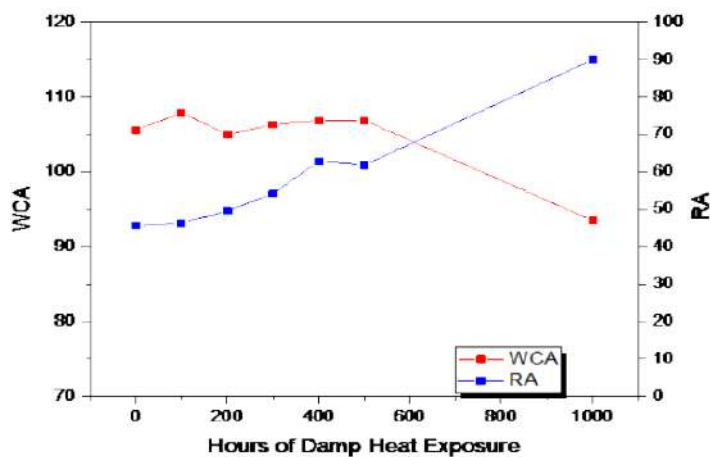


Figure 12: “WCA and RA of the hydrophobic coating after damp heat

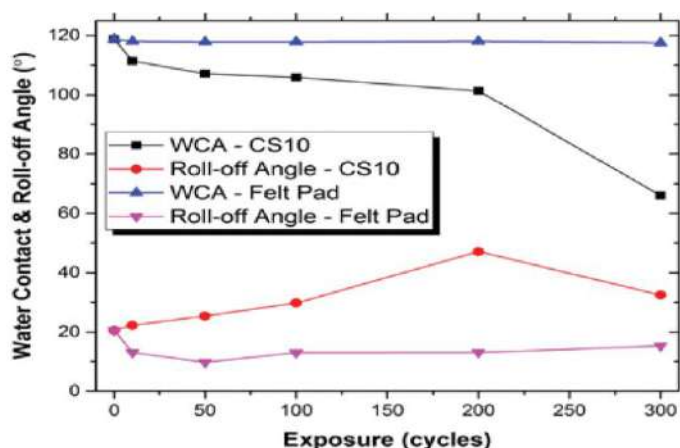


Figure 13: Hydrophobic-coating performance before and after abrasion with CS10 and Felt Pad

4.4.2) Abrasion test

- During the abrasion test, no notable abrasion caused by soft material, such as a felt pad [22]. Nevertheless, the coating suffered serious damage when using abrasive materials that are commonly used in the industry, like CS10. The gentle abrasive effect of CS-10 wheels replicates the effects of polishing and cleaning.

4.4.3) Combination of stressors

- Few studies have investigated the impact of stresses emulating real-world settings. [24]. S. Bhaduri [21] developed an indoor accelerated stress tests methodology to investigate the impact of various stressors on ASC for a reasonable period, at IIT Bombay. In [25] she identified the significant stressors that reduce the performance commercial hydrophobic ASC during outdoor testing, conducted on solar glass coupons and PV modules. Her research finding states, hydrophobic coatings have

poor reliability in warm and humid climate zones (when taking 25-year module lifetimes into account). Coating shows lower life-time as combination of stressors increases.

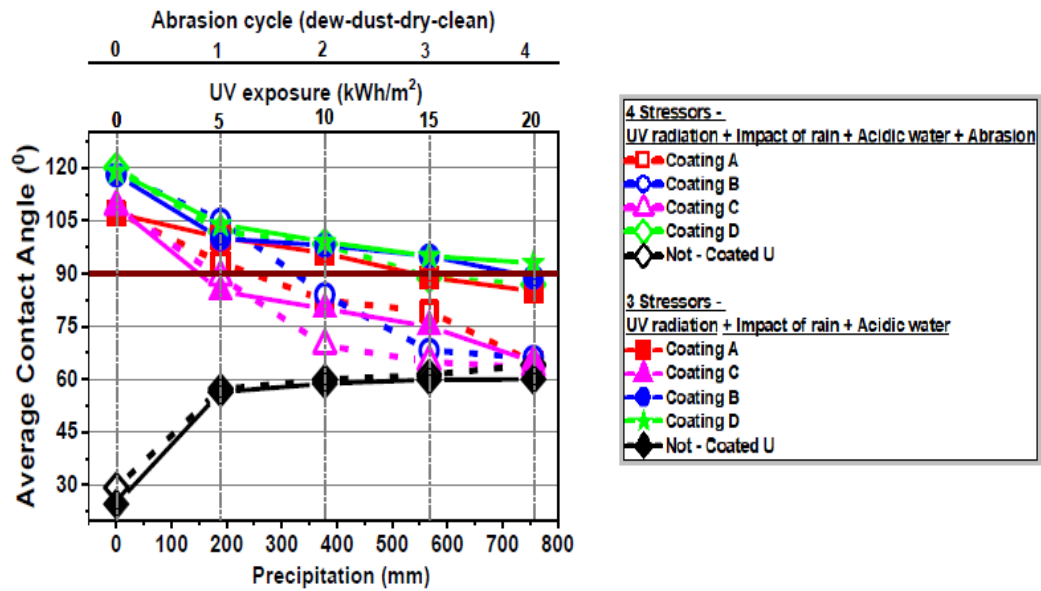


Figure 14: The effectiveness of coatings following exposure to a combination of four stressors and three stressors

Chapter 5

Cleaning Cycle Simulator (CCS)

5.1) Introduction

The process of natural dust deposition involves the accumulation of dust along with cycles of cooling during the night, dew in the early morning, and heating during midday. Due to this procedure, the dust is able to stick to the PV modules' surface more firmly. CCS is an accelerated test bed wherein the sample undergoes cleaning, soiling and heating-cooling. An indoor abrasion testbed CCS is built at IIT Bombay to mimic the following conditions that influence abrasion damage in outside field circumstances., relevant for PV application:

- (a) Thermal cycling,
- (b) Dust deposition and
- (c) Cleaning cycle via brush.



Figure 15: Cleaning Cycle Simulator at NCPRE module lab, IITB

Chapter 6

Modifications in system

6.1) Introduction

The CCS system is capable to emulate the outdoor condition for ASC testing, however, some considerable issues observed that has to resolve for better performance and accuracy of the system. Some modifications have been done in the system which is listed below:

- A. Temperature uniformity
- B. Real time temperature
- C. Support structure
- D. Load measurement system

6.2) Temperature uniformity

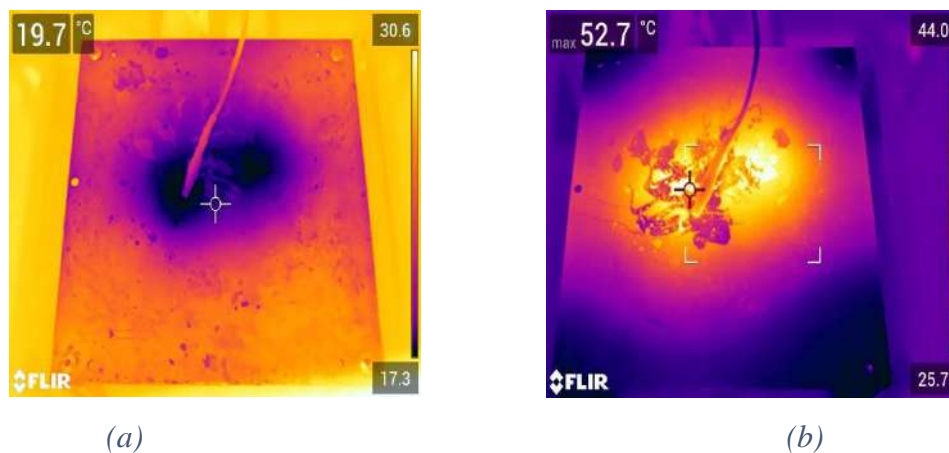


Figure 16: (a) Non uniform cooling of Cu plate (b) Non uniform heating of Cu plate

A 20x20cm² copper plate were in use to keep samples for testing. Issue with this plate was that plate was not heating/cooling uniformly, as shown in below IR images (fig: 16a and 16b). The temperature difference between the centre of the plate and the edges were significant. In such case, for defined minimum and maximum temperature, the placement of the temperature sensor is critical to obtaining the desired output. One possible reason for this nonuniformly heating/cooling was the large size of the copper plate (20x20 cm²) compared to the size of the two Peltier modules (4x4 cm² each) [26]. Size reduction of plate is done as per requirement the area of Cu plate from 20*20cm² to 11*8cm². Which results in uniform distribution of temperature.

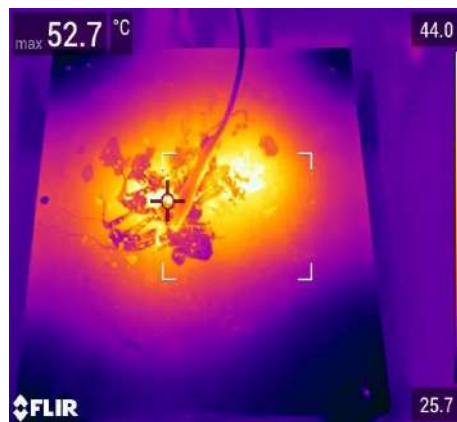


(a)



(b)

Figure 17: (a) 20*20cm² copper plate, (b) 11*8cm² copper plate



(a)



(b)

Figure 18: (a) 20*20cm² plate heating non uniformly, (b) 11*8cm² plate heating nearly uniform

6.3) Real time temperature

The copper plate is attached with a digital temperature sensor, the DS18B20. This temperature sensor is essential to preserve the target temperature range. An experiment performed to investigate the real time output from different temperature sensing electronic components.

6.3.1) Testing

In our experimental setup, the Arduino Mega is programmed 21°C (minimum) to 64°C (maximum) temperature of peltier modules. When any of the targeted temperature achieved, the Arduino sends a signal to deactivate the relay, thereby stopping the operation. A comparison of the temperature readings obtained from different sensors indicates that the responsiveness of the DS18B20 is noticeably slower in contrast to the K-type thermocouple.



Figure 19: (a) Dallas temperature sensor DS18B20 (b) FLIR E75 (c) Fluke 52II thermometer with k-type thermocouple wire

Table 2: Different Device (Temperature Sensing) and Temperature

	DS18B20 Temperature displayed on lcd screen (°C)	FLIR thermal camera (°C)	Fluke thermometer (°C)
Minimum	21	12	11
	25	21	21
Maximum	64	80	79
	33	64	64

6.3.2) Observation

- Direct contact that the thermocouple establishes with the copper plate whereas the DS18B20 is encased in plastic.
- In DS18B20 the temperature conversion process depends on a series of commands to request and retrieve temperature readings that takes a comparatively longer duration of 750 milliseconds [27].

This multi-step process causes the Peltier module to become hotter than the temperature registered by the temperature sensor at any given moment. If this assumption holds true, it could lead to more frequent damage to the Peltier module, potentially exceeding its specified temperature limits. Moreover, it may introduce variations in the achieved temperature range, which is critical for our intended experiments.

6.3.3) MAX6675 K-type thermocouple

We transitioned from the DS18B20 to the MAX6675 K-type thermocouple. The MAX6675 incorporates a temperature sensor for reference junction compensation, amplifying the voltage for microcontroller readings. The MAX6675 effectively compensates for changes in ambient temperature using cold-junction compensation. The MAX6675 provides temperature data directly over serial peripheral interface (SPI), providing it more responsive than the DS18B20, and also accuracy and responsiveness [28].



Figure 20 : K-type thermocouple wire with MAX6675 amplifier

6.4) Support structure

Previously, we employed a 20x20 cm² copper plate to place the samples, utilizing both a support base and top. Within the sample holder chamber, a carriage equipped with springs maintained a gap between the carriage base and the coolant chamber, allowing for the conveyor belt to operate smoothly. Additional electronic and mechanical components were also present. The copper plate served to press against the Peltier modules and springs, ensuring that all components remained in their respective positions during the back-and-forth motion of carriage.

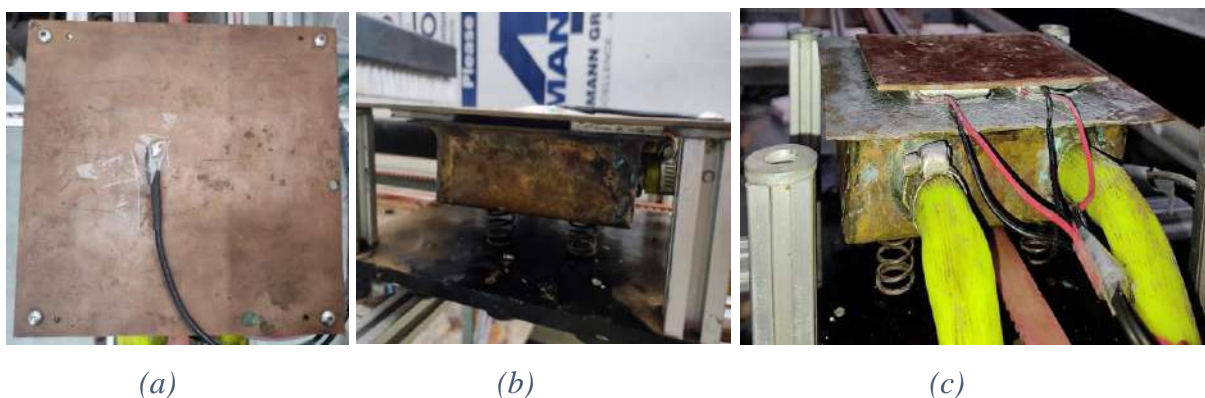


Figure 21: Cu plate screwed over carriage (a) top view, (b) side view (c) reduced Cu plate

Upon reducing the copper plate's area to 11x8 cm², a support structure became necessary to prevent loose contacts between components. We added three acrylic sheets, each 2 mm thick and measuring 20x20 cm². The bottom sheet covers the thickness of the Peltier module and restricts its movement with a narrow-cropped area. The middle sheet covers the thickness of the copper plate and also creates a channel for the thermocouple wire. During the carriage's motion, it helps the thermocouple experience less stress. To hold the samples and shield the thermocouple wire from the top, slots are incorporated into the *top layer* of the acrylic sheet. After this arrangement, the chamber becomes comparable in rigidity to how it was before when the copper plate was larger.

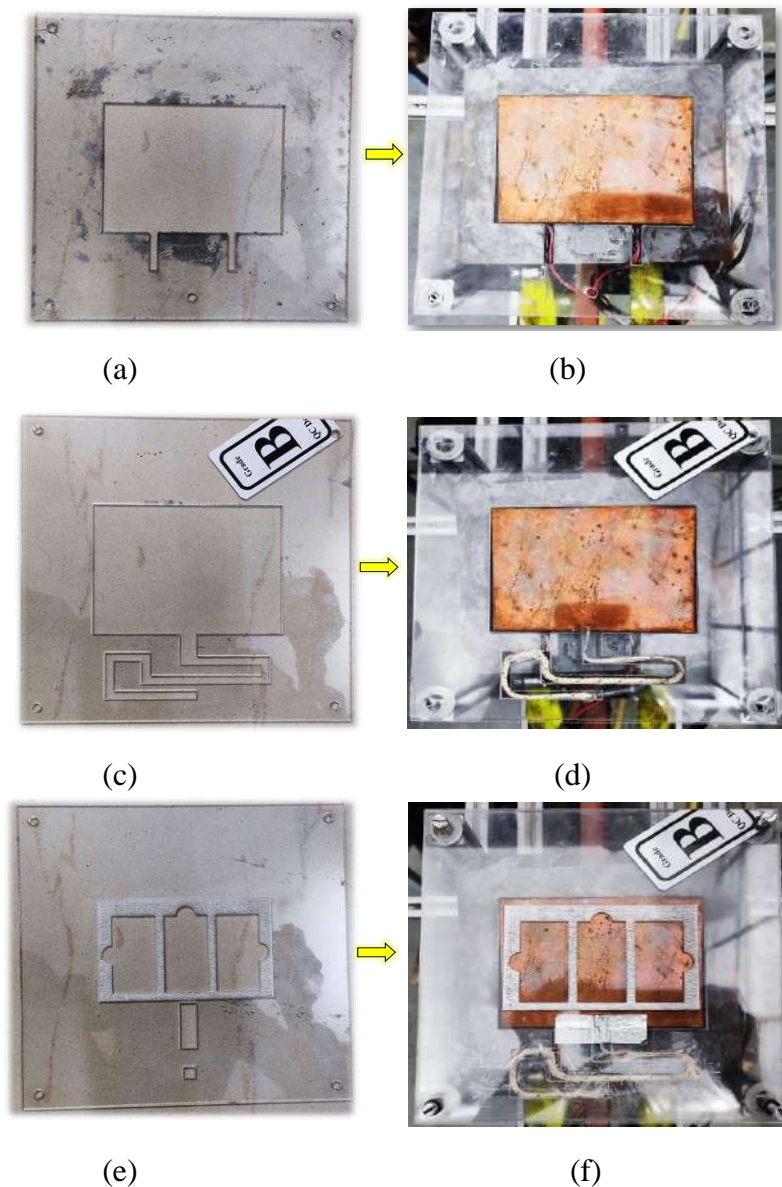


Figure 22: Construction of the acrylic sheet support structure. (a) Bottom layer, (c) Middle layer, and (e) Top layer and (d), (e), and (f) shows the assembly steps for the acrylic sheets.

6.5) Load measurement system

Measuring the load applied by the brush during cleaning is one additional feature that can be added to CCS. Depending on the magnitude of the applied load, the coating's degradation can vary greatly. Including force applied by the brush on the surface with number of cycles of cleaning could help in predicting the durability of the coating more precisely. To address this, it became essential to measure the load acting on the glass surface by brush. To achieve this, we have incorporated a load-cell based instrument in our experiment. The load cell chosen for our application is a 4-wire load cell equipped with a full Wheatstone bridge. Four specialized resistors, known as strain gauges, are affixed to the load cell. When force is applied to one side of the metal block, two of the strain gauges experience compression, while the other two undergo stretching. This differential strain in the strain gauges results in a potential difference within the Wheatstone bridge, which can be accurately measured. To ensure proper deformation of the load cell's middle section due to the force applied from top, a frame has been constructed around the load cell. This frame serves to facilitate the deformation of the load cell under load



Figure 23: (a) framed loadcell side view, (b) top view

6.5.1) Measuring the load: Experimental Setup

In the cleaning system of CCS, a brush is mounted on a metallic block. This metallic block can be moved up and down vertically using a threaded rod with a pitch of 2 mm. One complete rotation of the rod moves the block either 2 mm upwards or 2 mm downwards, depending on the direction of rotation. Since the brush is attached to the block, its position is also adjusted by 2 mm. To measure the load exerted by the brush on a surface, a frame equipped with a load cell is moved back and forth under the brush in 90-degree intervals, corresponding to a displacement of 0.5 mm. The force in grams is recorded by the Arduino. The force in newtons can be calculated using the formula:

$$F = m * g$$

where F is the force in newtons, m is the mass (load value) in Kilograms, and g is the acceleration due to gravity, approximately 9.8 m/s^2 . The force exerted by the brush varies depending on its design parameters, such as density, tuft and length. To investigate this relationship, we measured the force for different brush designs. The results demonstrate that the force is indeed sensitive to these design parameters.

Table 3: Brush design specification

Brush Design	Bristle Count (tips/tufts)	Total Tufts	Area (mm ²)	tuft density (tufts/mm)
Commercial	120	140	62 x 370	0.38
IEC 62788-7-3 Standard	160	59	40 x 85	0.88
IEC 62788-7-3 Standard Modified	160	171	40 x 230	0.88

Brush material is nylon 6,12 (poly-amide)

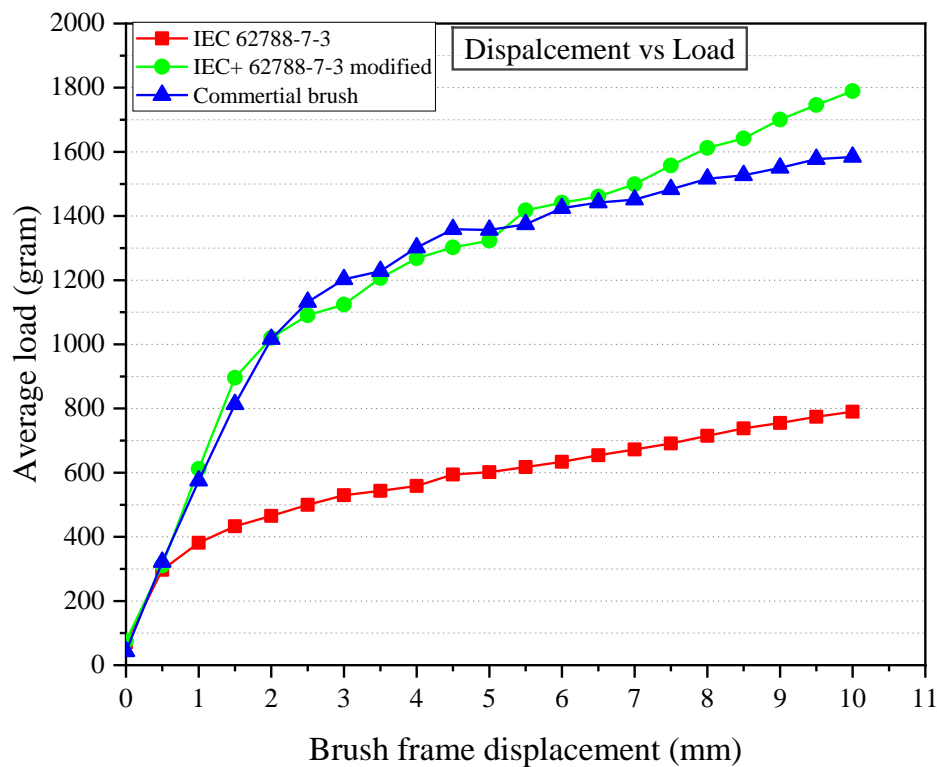


Figure 24: Load applied by different designs of brush

The above graph shows that different brush designs exert different loads during cleaning on the surface of glass and this can affect the coating lifetime.

Chapter 7

Effect of Different Cleaning loads on Coating and Cleaning Efficacy

7.1) Introduction

This chapter looks into how different loads affect coatings when they are being cleaned. The main goal is to find the ideal load that finds a compromise between coating durability and cleaning efficacy. We experimented with glass coupons using a Cleaning Cycle Simulator (CCS) to accomplish this goal. A total of four different loads: 300g, 600g, 900g, and 1010g were applied. It is believed that the study's conclusions would provide light on the most effective way to clean coated surfaces. The experiment consists two parts: in first effect of cleaning load on coating is performed and in second the cleaning efficacy of different cleaning load is experimented.

7.2) Effect of Different Cleaning Loads on Coating

7.2.1) Sample preparation, characterization and CCS programming:

The surface of 2.5*5cm² borosil glass coupons is coated with a superhydrophobic fluoropolymer-based coating. Using a cotton cloth soaked in the coating solution, gently wipe the glass surface until the solution dried completely. The coated glass coupons are then left to air dry for two hours. To characterize the hydrophobicity of the coating, the contact angle is measured. For CA measurement, Data-Physics Instruments' model OCA SEC15 is utilized. Measurement utilized a 2µl dosing volume (DI water) with a 1µl/s dosing rate. CA is measured at ten distinct coupon points on each sample and the measurement is held off for one second post the droplet deposition onto the surface. CCS is programmed for temperature range of 15°C (minimum) to 70°C (maximum). Dust deposition is set to 0.2mg/cm² which is 2 weeks of soiling measured at IIT Bombay[29]. Cleaning velocity is set to 3m/s as per IEC 62788-7-3 standard recommends.

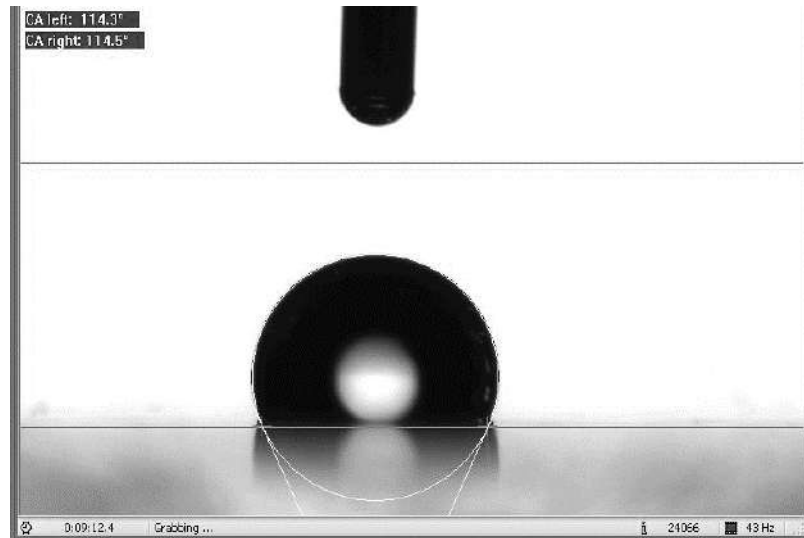
7.2.2) Brush characteristics

We used a specially designed brush based on the IEC 62788-7-3 standard for this investigation. The brush is made of nylon (polyamide 612) and has 0.23mm-diameter bristles. The brush has 171 tufts, 160 tips/tuft, with a tuft density of 0.88 tufts/millimetre. Load variation (300g, 600g, 900g, and 1010g) for this brush can be adjusted based on the brush frame's displacement.

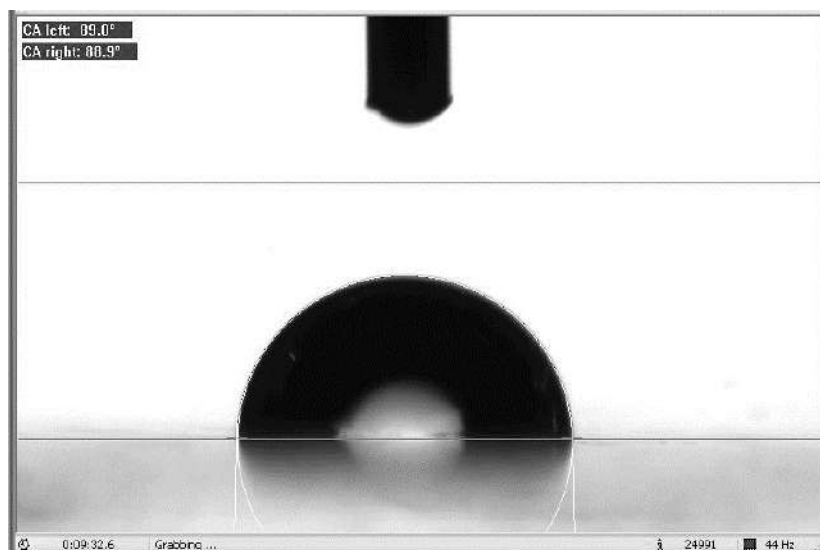
7.2.3) Experiment Process:

The following procedure is used to carry out the Dew-Dust-Dry-Clean (DDDC) cycle operation on the five identical glass samples for each load (a total of 20 samples):

- Placed 5 samples on CCS sample stage, adjusted the load to 300g, and ran 5-DDDC cycles.
- After completion of 5-DDDC cycles, adjusted the load to 600g and ran the 5-DDDC again with fresh samples.
- Above process is continued in the same manner, increasing the load to 900g and then 1010g while completing five samples of the 5-DDDC each time.
- CA of all samples were now measured (10 distinct points on every sample).
- The above process is repeated after each 5-DDDC cycle and CA measurement.



a. CA after coating the glass



b. CA after coating failure.

Figure 25: a) CA after applying coating, b) CA after coating degraded.

7.2.4) Result and discussion

The coating failure, defined as a CA reduction below 90° ($\theta < 90^\circ$), did not exhibit a direct proportional relationship with cleaning load shown in figure 27. Surprisingly, a 900g cleaning load caused earlier degradation (~ 63 DDDC) followed by 600g, 1010g and then 300g. The bristle tips of the brush and their bending angle may be the cause of this performance. The sharp tips have the ability to scratch the surface more than a circular tips. When we apply 300g cleaning load it forms a very light contact on the surface, and because the glass is coated, it allows bristles to slide over the surface without significantly harming the coating. Further applying 600g or 900g of cleaning load on coated surface causes the bristles to bend at some angle and damage the coating surface more severely than when using 300g of cleaning load, which accelerates degradation. In comparison to smaller cleaning loads, the brush frame will bend more if we apply a 1010g cleaning load. Now that the bristles have a diameter of only 0.23 mm, it's most probable that the sharp tips are no longer in contact with the surface. Instead, the bristle's circular portion may rub against the coated glass, which could be less harmful than the sharp tips.

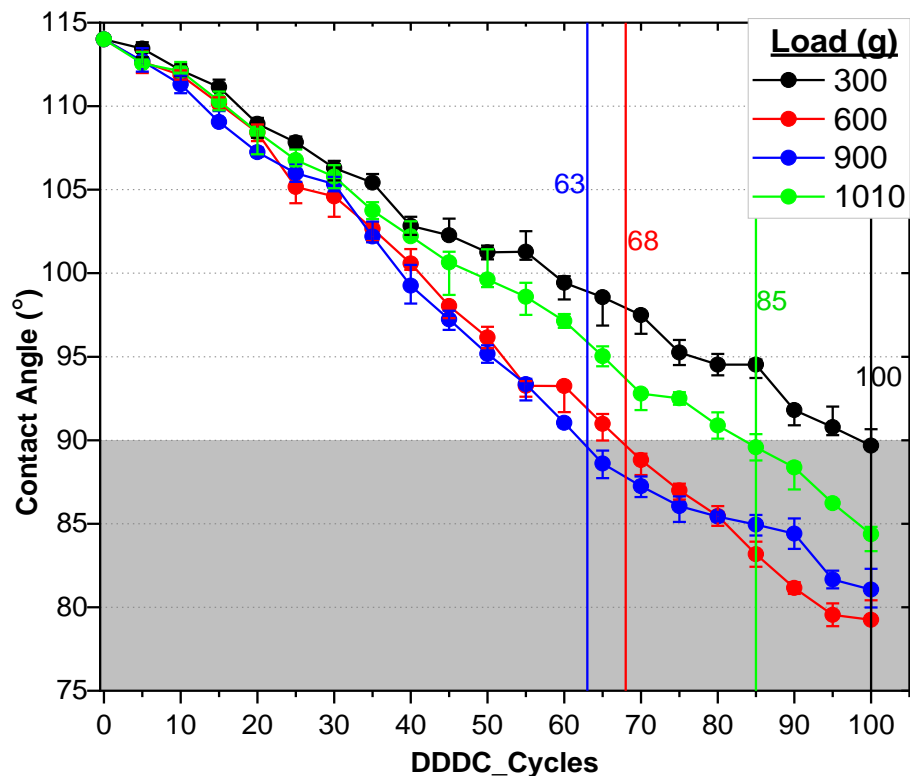


Figure 26: Effect of different cleaning loads on coating. The line connecting the solid circles represents the mean values of 5 samples of respective loads. In vertical error bars extended from the mean values, upper & Lower caps indicating the maximum and minimum values among those 5 samples. Thin coloured vertical line is the coating failure point for the respective loads.

7.3) Statistical Analysis (Hypothesis testing)

Hypothesis testing aims to find out whether the Cleaning Load and DDDC cycles has significant effects on coating durability, for this the nonparametric Wilcoxon Signed Rank Test (WSRT) is taken into consideration. The P-Value determines whether a change in sample data is possibly the result of random fluctuation or a true effect (DDDC + Load). The null hypothesis (H_0) assumes that there is no noticeable distinction between two similar groups or circumstances. The α level determines whether the p-value is sufficient for one to ignore the null hypothesis. A normal significance level is 0.05, which means that if the p-value is smaller than α , the hypothesis can be rejected. with 95% confidence and a different explanation can be taken into consideration.

7.3.1) Wilcoxon Signed Rank Test

Our experimental assumptions for the experiment are:

- Null hypothesis (H_0): The median difference between the paired samples is zero.
- Alternative hypothesis (H_a): There is a significant difference b/w the paired samples.
- Significance level (α) = 0.05
- Sample size (N) = 10
- P-value $< \alpha$ = Reject H_0 with 95% confidence level
- P-value $\geq \alpha$ = advisably do not reject H_0
- Dataset pair1 = Pairs of consecutive cycle intervals, such as (0–5), (5–10), and so forth, are used until the coating for each load degrade.
- Dataset pair2 = Pairs for various loads at respective deterioration stages (e.g., 300-600, 600-900, etc.).

7.3.2) Result and discussion

In the graph horizontal red line is the significance level (0.05 here). This assures us with 95% confidence level, the significant impact of DDDC cycles (figure 27) and Cleaning Load (figure 28) on the coating degradation. Since CA is measured after every five cycles, 65 and 70 DDDC are taken into consideration here rather than 63 and 68 DDDC for pairing dataset.

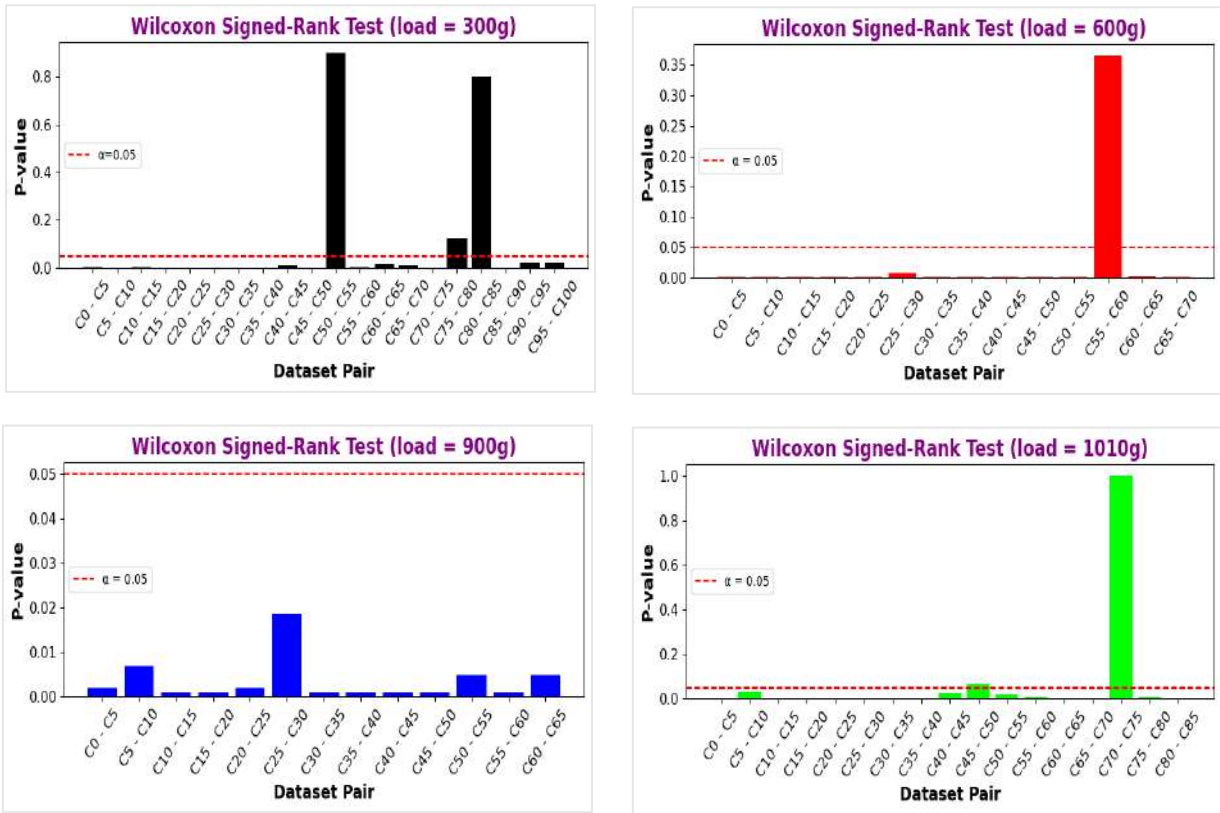


Figure 27: WSRT for Dataset pair1 for loads 300g, 600g, 900g, 1010g (clockwise from top left corner).

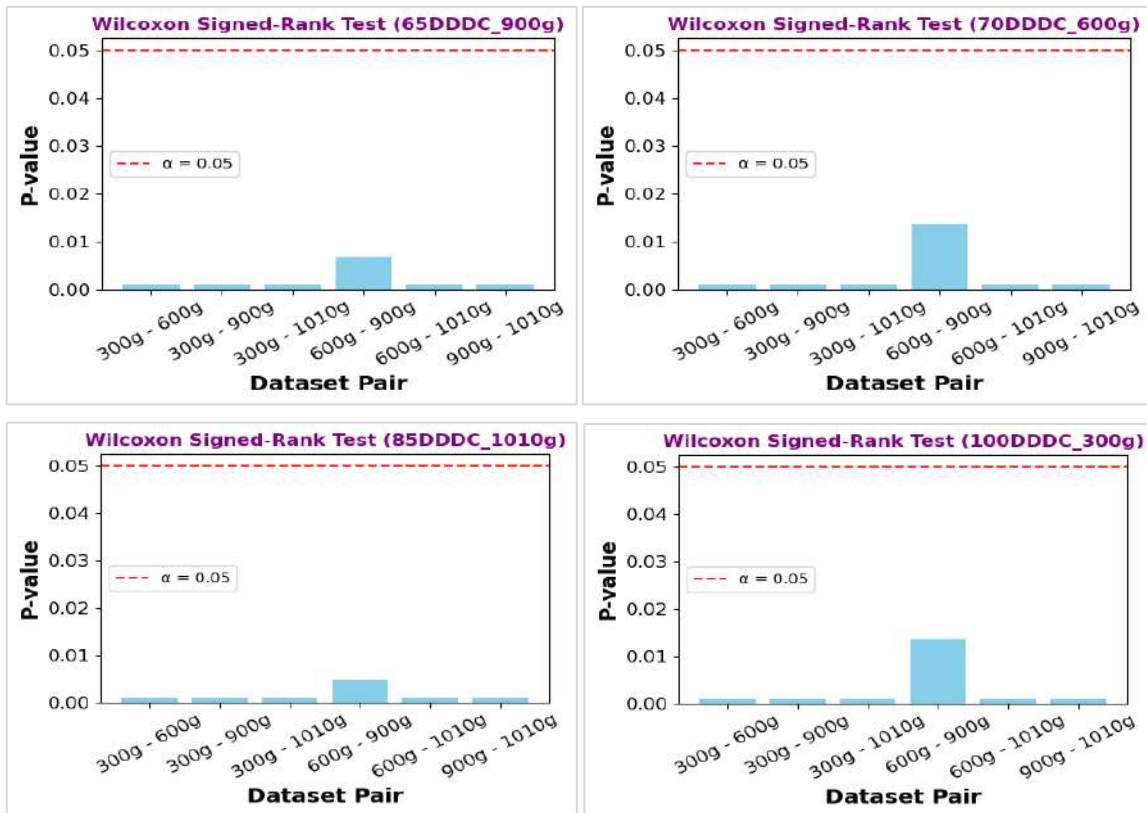


Figure 28: WSRT for Dataset pair2 for loads 300g, 600g, 900g, 1010g compared to their degradation cycle (65, 70, 85 and 100) clockwise from top left corner.

7.4) Efficacy of different cleaning loads

The outcomes of an experiment "Effect of different cleaning loads on coating" have presented us with a challenge. Findings of an experiment indicates that there isn't a direct correlation between the cleaning load and coating degradation at that point. Thus, simply opting any cleaning load, isn't sufficient without considering its efficacy. There's a possibility that despite its favorable impact on coating life, it might require multiple cleaning cycles to achieve pure surface cleaning and this can also be harmful for coating life. Understanding both the efficacy and degradation aspects can provide a balanced approach for selecting the appropriate cleaning load. Which can allow us to compromise between minimizing degradation and ensuring effective cleaning, for the selection of appropriate cleaning load.

7.4.1) Fundamental approach.

We are aware that the short circuit current (I_{SC}) of solar cells is directly correlated with solar radiation. The creation of electron-hole pairs increases with intensity, leading to an increase in I_{SC} . When a dusty glass is placed over a solar cell, less light enters the cell due to dust, forcing the I_{SC} of the cell to decrease. However, when the glass is cleaned, more light enters the cell, improving the I_{SC} . In this case, ΔI_{SC} is the loss of light due to obstruction on solar cell. Here this loss is soiling loss and can be relatable to efficacy of cleaning load.

7.4.2) Experimental setup

In this experiment, we measure the I_{SC} values of a solar cell with and without dust, as well as after dust removal by the brush. For this purpose, we've packaged a mini solar module. The $2 \times 2 \text{ cm}^2$ cell has been cut from a $15.6 \times 15.6 \text{ cm}^2$ polysilicon solar cell using an SLTL LASER cutting equipment (NCPRE lab, IIT Bombay). Following that, this cell is soldered with copper-tin plated as a busbar. The cell is then sandwiched (Backseat, EVA, Cell, EVA, Glass) and laminated with a PV laminator (NCPRE Lab, IIT Bombay). The test glass is $2.5 \times 5 \text{ cm}^2$ textured glass from Borosil Glass Works Limited, India.

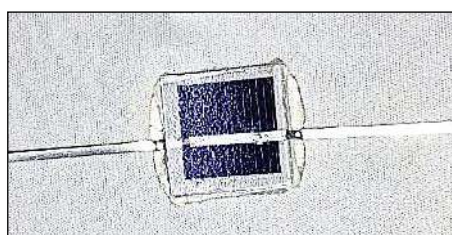
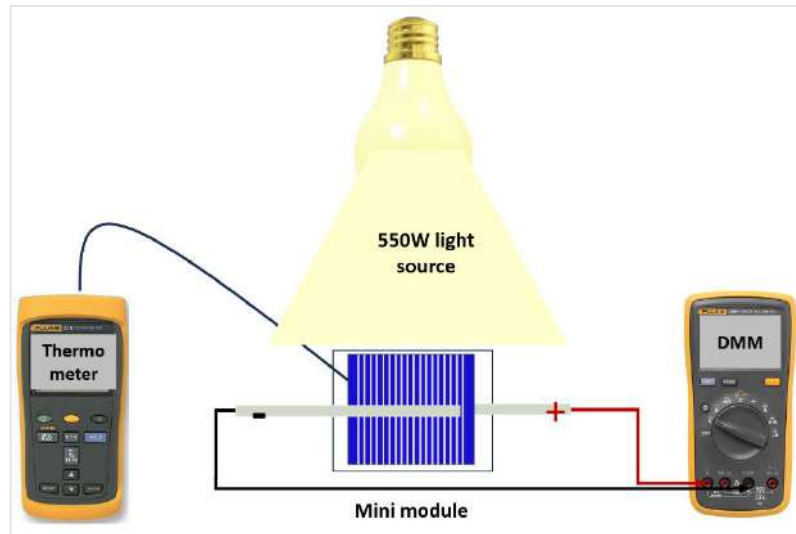
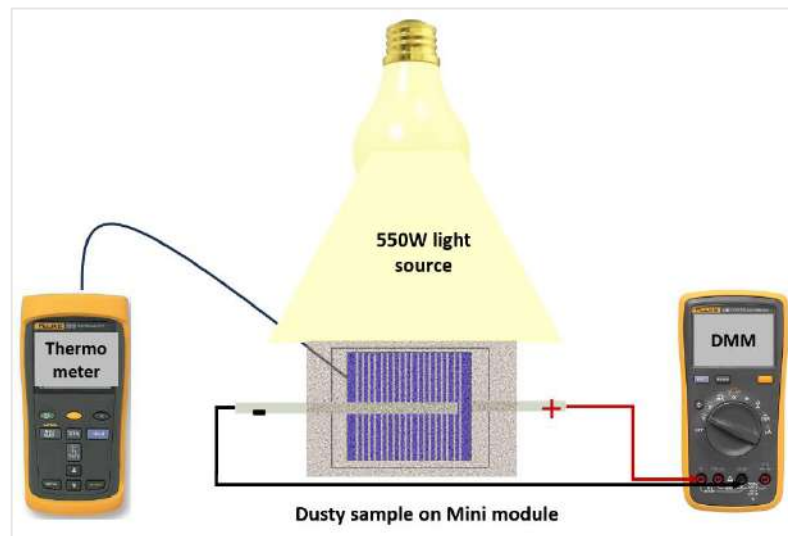


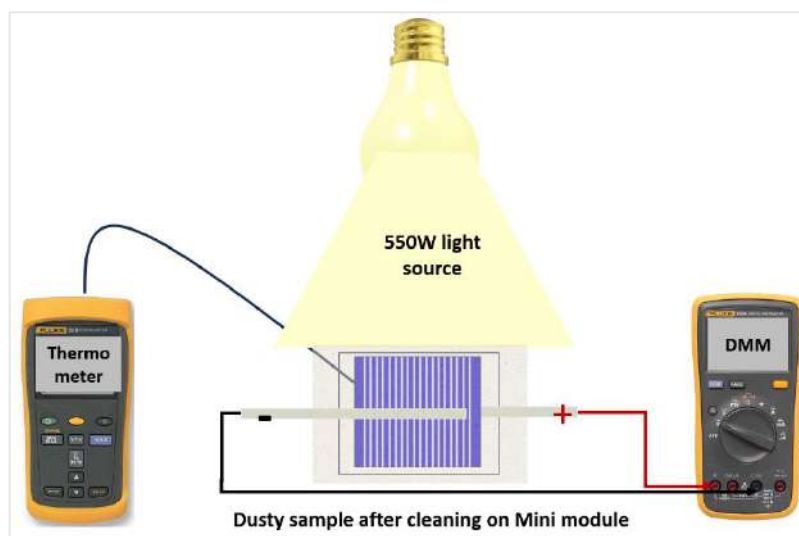
Figure 29: packaged mini solar module



a)



b)



c)

Figure 30: a), b) and c) represents I_{sc} measurement setup without dust, with dust and after cleaning the dust respectively.

The figure 30 shows the solar cell I_{SC} measurement setup, which consists of shining a Halogen (~550W) light source on a mini solar module and measuring the I_{SC} using a FLUKE-107 600V CAT III Digital Multimeter (DMM). A K-type thermocouple has been attached to the backsheet of the mini module, and the temperature is measured using the FLUKE 52 II Thermometer.

Table 4: Current and Temperature References

ABET-Mini module I_{SC}	145.10 mA (25°C, 1000W, Xenon lamp)
Solar Simulator-Mini module I_{SC}	76 mA (28°C, ~550W, Halogen lamp)
Solar Simulator-Mini module + Glass I_{SC}	72.5 mA ((28°C, ~550W, Halogen lamp)
Backsheet Temperature	27.5°C to 28.8°C

7.4.3) Process followed:

We experimented with two different soil gravimetric densities (SGD) to measure efficacy: 0.2mg/cm² and 0.6mg/cm². We deposited 12 glass samples for each SGD, using 3 samples for each cleaning load. We measured the I_{SC} of dusty glass at four distinct sites to ensure homogeneity. We flashed light for only two to three seconds at each site to measure I_{SC} before turning it off to minimize temperature changes.

- 1) In very first step mini modules I_{SC} is measured by flashing a light on it.
- 2) Next, we placed a bare borosil glass (2.5*5 cm²) on the mini module and measured the I_{SC} . This is considered as our reference I_{SC} .
- 3) Now the borosil glass is deposited with 0.2mg/cm² dust then this dusty sample is placed on mini module and I_{SC} is measured.
- 4) After this the dusty sample is cleaned once by applying a 300g cleaning load by the brush and then this cleaned sample is placed on mini module to measure the I_{SC} .
- 5) If the I_{SC} is very close to reference value, we expect that sample has been cleaned at satisfactory level (~71-72.5mA) and further cleaning is not required; if not, then same cleaned dusty sample again subjected to second time cleaning by 300g cleaning load.
- 6) The sample is cleaned till the I_{SC} value is measured to satisfactory level and after each cleaning the I_{SC} value is registered.
- 7) steps 4 to 6 are repeated for different cleaning loads (600g, 900g, and 1010g).
- 8) Step 3 to 7 is repeated for 0.6mg/cm² soil gravimetric density.
- 9) Soiling loss is calculated based on measured I_{SC} .



Figure 31: a) 0.2mg/cm², b) 0.6mg/cm² dust deposition on glass samples

Table 5: Measured average I_{sc} values of mini module

Average I _{sc} of different samples (mA)								
Load	0.2mg/cm ²				0.6mg/cm ²			
	300g	600g	900g	1010g	300g	600g	900g	1010g
D	57.42	57.92	57.75	57.50	38.33	38.42	38.00	38.08
C1	64.75	68.58	69.25	71.08	64.67	68.42	68.92	71.42
C2	67.83	70.50	71.25		66.83	70.92	71.19	
C3	70.83	71.53	71.67		71.00	71.58	71.67	
C4	71.50				71.50			

Here, in the data table, the "D" row represents the I_{sc} readings of the solar panel for dust deposition levels of 0.2mg/cm² or 0.6mg/cm². "C1" indicates the I_{sc} measured after the initial cleaning, and so forth for "C2", "C3" and "C4" after the second, third and fourth cleanings, respectively of the same dusty sample.

Table 6: Soiling Loss

Soiling Loss (%)								
Load	0.2mg/cm ²				0.6mg/cm ²			
	300g	600g	900g	1010g	300g	600g	900g	1010g
D	20.80	20.11	20.34	20.69	47.13	47.01	47.59	47.47
C1	10.69	5.40	4.48	1.95	10.80	5.63	4.94	1.49
C2	6.44	2.76	1.72		7.82	2.18	1.81	
C3	2.30	1.34	1.15		2.07	1.26	1.14	
C4	1.38				1.38			

The soiling loss is calculated by using below formula:

$$\% \text{ Soiling loss} = \frac{I_{sc-clean} - I_{sc-soiled}}{I_{sc-clean}}$$

Here $I_{sc-clean}$ is 72.5 mA which is measurement of I_{sc} from mini module with bare glass on top of it and $I_{sc-soiled}$ is the I_{sc} values taken from Table 5.

7.4.4) Result and discussion

The relationship between cleaning loads and soiling losses is evident: as cleaning loads increase, cleaning efficacy improves. Despite multiple cleaning attempts, achieving zero soiling loss remains challenging. This is because of the dry-cleaning method, which may leave behind fine dust residues on the glass surface. These fine dust residues obstruct light radiation from reaching the active region of the solar cells, thereby reducing overall efficiency.

7.5) Conclusion

If we define efficient cleaning as achieving less than 2% soiling loss, then using a 300g cleaning load requires 4 cleaning cycles, while 600g, 900g, and 1010g cleaning loads require 3, 2, and 1 cleaning cycles, respectively.

An important aspect of the experiment "Effect of Different Cleaning Loads on Coating and Cleaning Efficacy" is that choosing a specific cleaning load for solar panels to balance coating degradation along with effective cleaning may not be accurate at this point. The observation from soiling loss for efficacy indicates that the number of cleaning cycles required for efficient cleaning depends on the cleaning load selected. However, the experiment on the effect of different loads on coating degradation was conducted with only one cleaning cycle. It would be unfair to draw conclusions based only on these results because we don't know how multiple cleaning cycles combined with Dew-Dust-Dry cycles (DDD+C) can degrade the coating.

Chapter 8

Summary and Future Objective

8.1) Summary

Photovoltaic (PV) technology is playing a pivotal role in driving sustainable growth. The performance of a PV power system is influenced by various environmental factors. Soiling, the accumulation of dust on PV modules, is a significant factor that can reduce global solar production by at least 3-4% even in optimized clean up scenarios. This translates into annual revenue losses between €3 billion and €5 billion. To mitigate soiling losses, several techniques are available. One effective approach is the application of ASCs. ASCs are applied to the outer surface of PV modules, but their effectiveness must be validated in actual outdoor field settings. Currently, there is no standardized methodology or test protocol to evaluate the reliability of ASCs for commercial applications. Consequently, there are no pass/fail criteria to assess the performance of commercially available ASCs. To address this issue, a novel accelerated test bed CCS, has been developed at NCPRE, IIT Bombay. This system is modified for enhanced performance, including: Uniform heat-cool operation, Rigid support structure, Real-time temperature measurement using thermocouple and Load cell-based device to measure force applying by brush. The result of the experiment “Effect of different cleaning Load on coating and cleaning efficacy” can be used for better compromise to choose a specific cleaning load for solar panels to balance coating degradation along with effective cleaning.

8.2) Future work

Additional experiments are needed to study the effect of cleaning loads with multiple DDD+C cycles for a fair comparison and informed selection of cleaning loads. The durability of coating should be tested under various stressors faced by module over the year to evaluate the coating performance. This type of evaluation can help manufactures and researchers to work on the weak areas of coating. An experiment has planned to perform by emulating the whole year accelerated test scenario for jodhpur location where the coating undergoes from various stressors (i.e. Rainfall, UV dose, Abrasion).

References

- [1] M. de, *Snapshot of Global PV Markets 2023 Task 1 Strategic PV Analysis and Outreach PVPS*.
- [2] S. W. Glunz, R. Preu, and D. Biro, "1.16 - Crystalline Silicon Solar Cells: State-of-the-Art and Future Developments," in *Comprehensive Renewable Energy*, Elsevier, 2012, pp. 353–387. doi: 10.1016/B978-0-08-087872-0.00117-7.
- [3] A. S. Al-Ezzi and M. N. M. Ansari, "Photovoltaic Solar Cells: A Review," *Applied System Innovation*, vol. 5, no. 4. MDPI, Aug. 01, 2022. doi: 10.3390/asi5040067.
- [4] M. E. Meral and F. Diner, "A review of the factors affecting operation and efficiency of photovoltaic based electricity generation systems," *Renewable and Sustainable Energy Reviews*, vol. 15, no. 5. pp. 2176–2184, Jun. 2011. doi: 10.1016/j.rser.2011.01.010.
- [5] F. Ekinçi, A. Yavuzdeğer, H. Nazlıgül, B. Esenboğa, B. Dođru Mert, and T. Demirdelen, "Experimental investigation on solar PV panel dust cleaning with solution method," *Solar Energy*, vol. 237, pp. 1–10, May 2022, doi: 10.1016/j.solener.2022.03.066.
- [6] L. Micheli *et al.*, "Correlating photovoltaic soiling losses to waveband and single-value transmittance measurements," *Energy*, vol. 180, pp. 376–386, Aug. 2019, doi: 10.1016/j.energy.2019.05.097.
- [7] M. Rylander *et al.*, "Methods to determine recommended feeder-wide advanced inverter settings for improving distribution system performance," in *2017 IEEE 44th Photovoltaic Specialist Conference, PVSC 2017*, Institute of Electrical and Electronics Engineers Inc., 2017, pp. 2799–2803. doi: 10.1109/PVSC.2017.8366289.
- [8] L. L. Kazmerski *et al.*, "Fundamental studies of adhesion of dust to PV module surfaces: Chemical and physical relationships at the microscale," *IEEE J Photovolt*, vol. 6, no. 3, pp. 719–729, May 2016, doi: 10.1109/JPHOTOV.2016.2528409.
- [9] A. K. Yadav and S. S. Chandel, "Tilt angle optimization to maximize incident solar radiation: A review," *Renewable and Sustainable Energy Reviews*, vol. 23. Elsevier Ltd, pp. 503–513, 2013. doi: 10.1016/j.rser.2013.02.027.
- [10] M. F. R. B. L. L. K. S. M. N. S. and A. K. Sonali Bhaduri, "Cleaning efficacy of anti-soiling coatings," *IEEE Photovoltaic specialist conference*, 2020, Accessed: Dec. 03, 2023.
- [11] S. Warade and A. Kottantharayil, *Analysis of Soiling Losses for Different Cleaning Cycles*. 7th World Conf. Photovoltaic. Energy Conv., 2018.
- [12] S. Bhaduri and A. Kottantharayil, "Mitigation of Soiling by Vertical Mounting of Bifacial Modules," *IEEE J Photovolt*, vol. 9, no. 1, pp. 240–244, Jan. 2019, doi: 10.1109/JPHOTOV.2018.2872555.
- [13] K. Ilse *et al.*, "Techno-Economic Assessment of Soiling Losses and Mitigation Strategies for Solar Power Generation," *Joule*, vol. 3, no. 10. Cell Press, pp. 2303–2321, Oct. 16, 2019. doi: 10.1016/j.joule.2019.08.019.
- [14] A. Allouhi, S. Rehman, M. S. Buker, and Z. Said, "Up-to-date literature review on Solar PV systems: Technology progress, market status and R&D," *Journal of Cleaner Production*, vol. 362. Elsevier Ltd, Aug. 15, 2022. doi: 10.1016/j.jclepro.2022.132339.
- [15] J. Cano, G. Tamizhmani, A. Madakannan, and N. Macia, "Photovoltaic Modules: Effect of Tilt Angle on Soiling," 2011.
- [16] R. Asmatulu, W. S. Khan, R. J. Reddy, and M. Ceylan, "Synthesis and analysis of injection-molded nanocomposites of recycled high-density polyethylene incorporated with graphene nanoflakes," *Polym Compos*, vol. 36, no. 9, pp. 1565–1573, Sep. 2015, doi: 10.1002/pc.23063.
- [17] I. Nayshevsky, Q. F. Xu, G. Barahman, and A. M. Lyons, "Fluoropolymer coatings for solar cover glass: Anti-soiling mechanisms in the presence of dew," *Solar Energy Materials and Solar Cells*, vol. 206, Mar. 2020, doi: 10.1016/j.solmat.2019.110281.

- [18] S. Bhaduri, A. Alath, S. Mallick, N. S. Shiradkar, and A. Kottantharayil, "Identification of Stressors Leading to Degradation of Antisoiling Coating in Warm and Humid Climate Zones," *IEEE J Photovolt*, vol. 10, no. 1, pp. 166–172, Jan. 2020, doi: 10.1109/JPHOTOV.2019.2946709.
- [19] G. C. Oehler *et al.*, "Testing the durability of anti-soiling coatings for solar cover glass by outdoor exposure in Denmark," *Energies (Basel)*, vol. 13, no. 2, 2020, doi: 10.3390/en13020299.
- [20] Z. S. Huang *et al.*, "Experimental investigation of the anti-soiling performances of different wettability of transparent coatings: Superhydrophilic, hydrophilic, hydrophobic and superhydrophobic coatings," *Solar Energy Materials and Solar Cells*, vol. 225, Jun. 2021, doi: 10.1016/j.solmat.2021.111053.
- [21] S. Bhaduri, "Dust mitigation strategies for photovoltaic modules: Vertical mounting of bifacial modules and anti-soiling coatings DOCTOR OF PHILOSOPHY," 2023.
- [22] Kenan Isbilir; Fabiana Lisco; Gerald Womack; Ali Abbas; John Michael Walls, "Testing of an Anti-Soiling Coating for PV Module Cover Glass Testing of an Anti-Soiling Coating for PV Module Cover Glass," *IEEE 7th World Conference on Photovoltaic Energy Conversion (WCPEC)*, 2018, Accessed: Dec. 03, 2023.
- [23] F. L. T. B. M. A. T. and J. M. W. S. F. Bukhari, "Development of a Hydrophobic, Anti-soiling coating for PV Module Cover Glass," *IEEE*, 2019. Accessed: Dec. 03, 2023.
- [24] K. Ilse, M. Z. Khan, N. Voicu, V. Naumann, C. Hagendorf, and J. Bagdahn, "Advanced performance testing of anti-soiling coatings – Part I: Sequential laboratory test methodology covering the physics of natural soiling processes," *Solar Energy Materials and Solar Cells*, vol. 202, Nov. 2019, doi: 10.1016/j.solmat.2019.110048.
- [25] S. Bhaduri, R. Bajhal, M. Farkade, S. Mallick, N. Shiradkar, and A. Kottantharayil, "Understanding Multiple Stressors Which Degrade Antisoiling Coatings: Combined Effect of Rain, Abrasion, and UV Radiation," *IEEE J Photovolt*, vol. 13, no. 4, pp. 603–609, Jul. 2023, doi: 10.1109/JPHOTOV.2023.3273812.
- [26] T. Sharma, P. Jain, S. Patel, N. Bhatt, and Prof. K. Kathia, "A Review on Peltier Device and Heat Dissipation of It's Hot Surface Using Fins," *Int J Res Appl Sci Eng Technol*, vol. 10, no. 3, pp. 1084–1094, Mar. 2022, doi: 10.22214/ijraset.2022.40819.
- [27] P. By ALLDATASHEETCOM, "DS18B20 DALLAS | Alldatasheet."
- [28] P. By ALLDATASHEETCOM, "MAX6675 MAXIM | Alldatasheet."
- [29] J. J. John, "Characterization of Soiling Loss on Photovoltaic Modules, and Development of a Novel Cleaning System," 2015.



Arti Parganiha <arti.parganiha@gmail.com>

Your lab has been matched with the PSA Valence-Dominance Study

11 messages

Chris Chartier <cchartie@ashland.edu>
To: Arti Parganiha <arti.parganiha@gmail.com>

Tue, Jan 9, 2018 at 11:45 PM

Dear Arti,

You signed up to be part of the first Accelerator Data Collection Wave, and you have been selected as a data collection laboratory for this project! We are so happy to have you on board!

The most urgent next step is for all data collection labs to obtain ethics approval. Please start this process as soon as possible. Ethics approval has created the longest hold ups in the past for similar projects (such as Many Labs), so we have set the deadline for each lab's submission as 2 weeks from receiving this email. We have attached the final study proposal here if that helps you get started.

Please update your ethics approval status in [this spreadsheet](#) when you have submitted your materials, and again when you have received approval.

The lead authors for this project, Lisa de Bruine and Ben Jones (University of Glasgow), and the PSA Director, Chris Chartier (Ashland University), have submitted their materials for IRB approval, and we will share them when they are approved in the case that their materials may help you prepare yours or that their approval may expedite your own review process.

We anticipate that between 50 and 100 labs will collect data for this project. The included labs were selected based on their data collection capacity as well as geographic location, to allow for an adequate distribution over world regions. We look forward to sharing this exciting journey with you!

All the best,



Dr. Christopher R. Chartier
Associate Professor, Psychology
Director, [Psychological Science Accelerator](#)
Ashland University
cchartie@ashland.edu

Arti Parganiha <arti.parganiha@gmail.com>
To: babita pande <babitatime14@gmail.com>

Thu, Jan 11, 2018 at 12:39 PM

----- Forwarded message -----

From: **Chris Chartier** <cchartie@ashland.edu>
Date: Tue, Jan 9, 2018 at 11:45 PM
Subject: Your lab has been matched with the PSA Valence-Dominance Study
To: Arti Parganiha <arti.parganiha@gmail.com>

Dear Arti,

You signed up to be part of the first Accelerator Data Collection Wave, and you have been selected as a data collection laboratory for this project! We are so happy to have you on board!

PI	Institution	City	Country	Contributing Lab Members	Email Addresses	Collecting data in 2018?	Likely total N in 2018	Other Planned Contributions	Subject Pool Info	Primary language(s) of data collection	Specialized Equipment, Software, or Other Resources	Subfield (Social, Cognitive, Clinical, etc.)
Denis Cousineau	University of Ottawa	Ottawa	Canada		denis.cousineau@u	Yes for me;	300 yearly;	Based on	No subject	French	Computers; CRT screens	Cognitive; visual
wolf vanpaemel	KU Leuven	Leuven	Belgium	francis tuerlinckx	wolf.vanpaemel@ku	yes (in the fall)	100		dutch	dutch		cognitive
Niklas Steffens	University of	Brisbane	Australia	together with Kim Peters	n.steffens@uq.edu.	yes	100		University	English	We have access to labs for	Social, organisational,
Jerome Olsen	University of Vienna,	Vienna	Austria	Jerome Olsen, Martin	jerome.olsen@univi	yes	100		Pool of	German		Social
Olivier Klein	Université Libre de	Brussels	Belgium	Nicolas Van der Linden	nivdind@ulb.ac.be	Yes	I can quite	Translation	First-year	French	For online studies, we use	Social and intercultural
Hause Lin	University of Toronto	Toronto	Canada	Hause Lin, Michael	hause.lin@mail.utor	yes	100		Mix of		PsychoPy, ePrime, MediaLab,	Social, cognitive,
Daniel Ansari	University of Western	London	Canada		Daniel.ansari@gmai	yes	100		University	English	E-prime, PsychoPy	Cognitive, Developmental
Lorne Campbell	University of Western	London	Canada	Lorne Campbell,	lcampb23@uwo.ca	yes	100		Introductor		Qualtrics	
Gorka Navarrete	Universidad Adolfo	Santiago	Chile		gorkang@gmail.co	Yes			University	Spanish	PsychoPy, Limesurvey,	Social & Cognitive
Diego Forero	Universidad Antonio	Bogota	Colombia	Diego Forero, Andrés	diego.forero@uan.e	Yes	200		University			
William Jimenez Leal	Universidad De Los	Bogota	Colombia	William Jiménez,	w.jimenezleal@unia	yes	200	Data	120.	Spanish	8 networked computers, biopac	Thinking and reasoning,
Darko Loncaric	University of Rijeka	Rijeka	Croatia		dloncaric@uniri.hr	Yes	100	Local	Preschool,	Croatian, English	E-Prime; PsychoPy; LimeSurvey;	Developmental and
Marek Vranka	Charles University	Prague	Czech		vranka.marek@gm	yes	100		University	Czech, English (non-native)		Social
Kaminski Gwenaël	Toulouse university,	Toulouse	France		gwenaël.kaminski@	yes	200	Data analysis	University	French	E-prime, MAtlab, Qualtrics, (Eye	Social and Cognitive
Susann Fiedler	Max Planck Institute	Bonn	Germany		susann.fiedler@gm	yes			University	German	Eye-tracking, PsychoPy, z-tree,	Social Psychology,
Balazs Aczel	Eötvös Loránd	Budapest	Hungary	Marton Kovacs, Peter	marcikovacs95@g	Yes	In lab - 200,		Undergrad	Hungarian	Qualtrics, Opensesame	Cognitive
MohammadHasan	University of Tehran	Tehran	Iran	Javad Hatami	hasan.sharifian@ut.	yes			University	Persian		Social and Cognitive
Marco Tullio Liuzza	"Magna Graecia"	Catanzaro	Italy		liuzza@unicz.it	Yes	300		Undergrad	Italian	PsychoPy	Social, Cognitive
Patrizio Tressoldi	Dipartimento di	Padova	Italy		patrizio.tressoldi@u	Yes	100			Italian		
David Clarence	Busara Center for	Nairobi	Kenya		david.clarence@bus	yes	~15000		Low	Swahili, English	zTree, oTree, PsychoPI,	Behavioral Economics,
Vilius Dranseika	Vilnius University	Vilnius	Lithuania	Vilius Dranseika	vilius.dranseika@sf	Yes	100+		Lithuanian			
Steve Janssen	University of	Kuala	Malaysia	Steve MJ Janssen	steve.janssen@notti	Yes	100			English	E-prime, psychopy	
Humberto Nicolini,	Grupo Medico Carracci	Mexico City	Mexico	Humberto Nicolini, Nuria	nicolini_humberto@	Yes	100		Mexican	Spanish	EEG, TMS, CANTAB, biological	Clinical, cognitive,
Joanne M. Chung	Tilburg University	Tilburg	Netherlands		j.m.h.chung@uvt.nl	Yes	100		Dutch	Dutch, English		Developmental,
Dongning Ren	Tilburg University	Tilburg	Netherlands		d.ren@uvt.nl	Yes	100		Dutch	Dutch, English		Social
Mark Brandt	Tilburg University	Tilburg	Netherlands		m.j.brandt@tilburgu	yes	150 for any		Includes	English/Dutch	computers/qualtrics/inquisit	social
Gerit Pfuhl	UiT The Arctic	Tromso	Norway		Gerit.pfuhl@uit.no	yes	100 in		2 year	norwegian but fluent in	access to inquisit, matlab,	cognitive, neurocognitive
Janis Zickfeld	University of Oslo	Oslo	Norway	Janis Zickfeld, Thomas	jhzickfeld@gmail.co	Yes	100		1 year	Norwegian (fluent in English)	E-Prime, Inquisit, Presentation,	Social
Michal Parzuchowski	SWPS University of	Sopot	Poland	Bogdan Wojciszke,	mparzuchowski@s	Yes	>500 for	where	Undergrad	Polish	Inquisit, E-prime, PsychoPy,	Social/Cognitive
Samuel Lins	University of Porto	Porto	Portugal		samuel.bezerra.lins	yes	maximum		University	Portuguese		Social
Ivan Ivanchei	Russian Academy of	Moscow	Russia		ivancheyii@gmail.co	Yes	100		undergradu	Russian	E-prime, PsychoPy, Matlab, R,	Cognitive
Vanja Ković	Laboratory for	Belgrade	Serbia	Vanja Ković, Anđela	vanja.kovic@f.bg.ac	yes	100 in		University	Serbian	ERP - Neuroscan, SMI eye-	cognitive, neurocognitive
Iris Zezelj	University of Belgrade	Belgrade	Serbia		izezelj@f.bg.ac.rs	yes	300	Based on	University	Serbian, Bosnian	Inquisit, OpenSesame, Survey	Social
Gabriel Baník	Institute of	Presov	Slovakia	Gabriel Baník, Ivan	gabriel.banik@gmail	yes	150		undergradu	Slovak		Cognitive, Social,
Miguel Vadillo	Universidad	Madrid	Spain		miguel.vadillo@uam	Yes	100		Undergrad	Spanish	Matlab, PsychToolbox, PsychoPy	Cognitive
Zoltan Kekecs	Lund University	Lund	Sweden		zoltan.kekecs@psy.	yes	100	Methodologic	no	Swedis, but English may		clinical psychology,
Evie Vergauwe	university of Geneva	Geneva	Switzerland	Kim Uittenhove	Evie.Vergauwe@uni	Yes	maximum	Community	first year	French	e-prime, MAtlab	Cognitive, developmental
Sau-Chin Chen	Tzu-Chi University	Hualian	Taiwan		pmsp96@gmail.co	Yes	100	Anywhere	University	Chinese (Written in	Opensesame, Gorilla	Cognitive
Harry Manley	Chulalongkorn	Bangkok	Thailand		harrisonmanley@g	Yes	100		(~300 1st	Thai / English	Inquisit, PsychoPy, E-Prime	Cognitive / Social
Adil Saribay	Bogazici University	Istanbul	Turkey		adil.saribay@boun.e	yes	100		Introductor		Medialab, DirectRT, E-Prime,	

Tara Marshall	Brunel University	London	UK		Tara.Marshall@brun	yes	100		Introductor	English	ePrime, Qualtrics, Inquisit	Social, personality	
Gavin Sullivan	Coventry University	Coventry	UK	Chris Day, Vanessa	Ab7809@coventry.a	Yes	150 or more -	Indonesia is	University				
Benjamin Vincent	University of Dundee	Dundee	UK		b.t.vincent@dundee	Yes	50 (joint with		University	English	Matlab, PsychoPy	Cognitive	
Blair Saunders	University of Dundee	Dundee	UK		b.z.saunders@dund	Yes	50 (joint with			English			
Miroslav Sirota	University of Essex	Colchester	UK		msirota@essex.ac.	yes	100			1st year	English	Qualtrics, Inquisit, (E-prime &	Cognitive/Social
Christopher R.	Ashland University	Ashland	USA	Christopher R. Chartier,	cchartie@ashland.e	yes	300	Project	Traditional	English	ePrime, MediaLab, BioCapture	Social, Meta	
Brady Wiggins	Brigham Young	Idaho	USA	Brady Wiggins	wigginsb@byui.edu	Yes	100 - 300	Where	Psychology	English	Qualtrics, Matlab, OpenSesame,	Clinical, Theoretical and	
Dustin Calvillo	California State	San	USA	Dustin Calvillo	dcalvill@csusm.edu	Yes	~100		Undergrad	English	Computers, Eprime, qualtrics	Cognitive	
Nikki Legate	Illinois Institute of	Chicago	USA	Nikki Legate	nlegate@iit.edu	Yes	In lab - 100,		Undergrad	English			
Jack Arnal	McDaniel College	Westminst	USA		Jarnal@mcdaniel.ed	yes	~100		Liberal	English	SuperLab, Qualtrics	Cognitive (but happy to	
William Chopik	Michigan State	East	USA	William Chopik	chopikwi@msu.edu	Yes	200		Undergrad	English	Psychopy, Qualtrics, could easily	social, personality,	
Randy McCarthy	Northern Illinois	DeKalb	USA		rmccarthy3@niu.ed	yes	200		Introductor	English		Social	
Ernest Baskin	Saint Joseph's	Philadelphi	USA	Ernest Baskin	ebaskin@sju.edu	yes	100		Principles	English			
Kathleen Schmidt	Southern Illinois	Carbondale	USA		kathleenschmidt1@	Yes	200-300	Where I'm	Intro	English	ePrime, MediaLab, Qualtrics;	Social Cognitive	
Justin Robert Keene	Texas Tech University	Lubbock	USA		justin.r.keene@ttu.e	Yes	200		Mass	English	ePrime, MediaLab, Biopac,	Cognitive	
Heather Urry	Tufts University	Medford	USA		heather.urry@tufts.e	yes	100		Undergradu	English	E-Prime, Inquisit, Qualtrics,	Affective Science	
Gwen Gardiner	UC - Riverside	Riverside	USA		ggard001@ucr.edu	Yes	100		Undergrad	English		Personality	
J. Protzko	University of	Santa	USA	J. Protzko	protzko@gmail.com	Yes	60 for 30-		500	English			
Daniel Storage	University of Illinois	Urbana-	USA	Daniel Storage	research@danielsto	yes	100		Undergrad				
Crystal N. Steltenpohl	University of Southern	Evansville	USA	Crystal N. Steltenpohl	cnsteltenp@usi.edu	Possibly	Hopefully 100	Where	Sona	English	Trying to get MediaLab,	Community, social	
Nicholas Coles	University of	Knoxville	USA	Deanna Jordan	colesn@vols.utk.ed	Yes	250	Anywhere	Undergrad	English	E-Prime, Qualtrics, Camtasia,	Social/Affective	
Mike Mensink	University of	Menomonie	USA	Desiree Budd, Sarah	mensinkm@uwstout	Yes	100		Undergrad	English	Qualtrics, E-Prime, Biopac, SMI	Cognitive/Social	
Henrik Danielsson	Linköping University	Linköping	Sweden		henrik.danielsson@l	Possibly		Methodology	Students	Swedish		Cognitive	
Cynthia Fu	University of East	London	UK		c.fu@uel.ac.uk	Possibly							
Liam Satchell	University of West	Ealing	UK		liam.satchell@uwl.a	Possibly	Perhaps 100		No subject	English	Qualtrics	Forensic (legal and	
Tony Buchanan	Saint Louis University	St. Louis	USA		tbuchan7@slu.edu	Possibly			Undergrad	English	E-Prime, Qualtrics, eye tracking,	affective, neuro	
Luis H. Favela	University of Central	Orlando	USA		luis.favela@ucf.edu	Possibly			Undergrad	English		Cognitive, perception-	
Yarrow Dunham	Yale University	New Haven	USA		yarrow.dunham@yal	Possibly			Undergrad	English	Inquisit, Qualtrics	Social/Cognitive/Develop	
Kai Horstmann	Humboldt-Universität	Berlin	Germany	Kai Horstmann	kaitobiashorstmann	No		Methodologic				Psychometrics	
Anna Szabelska	Queen's University	Belfast	Northern		aszabelska01@qub.	No	N/A	data		English, Polish	R, Python, SPSS, Microsoft Azure	Cognition	
Miguel A. Silan	University of the	Quezon	Philippines		MiguelSilan@gmail.	No		Methodologic		English, Tagalog, Bisaya		Social / I/O	
Hannah Moshontz	Duke University	Durham	USA	Hannah Moshontz	hmoshontz@gmail.c	No			Undergrad	English	Qualtrics, can likely get access	Social	
Melissa Kline	MIT	Cambridge	USA		mekline@mit.edu	No	NA					Developmental, Cognitive	
S. Mason Garrison	Vanderbilt University	Nashville	USA	S. Mason Garrison	s.mason.garrison@	No	No	Methodologic		R	R, Mplus, git, computing Cloud,	Quantitive/Differential	
Pekka Santtila	NYU Shanghai	Shanghai	China		pekka.santtila@nyu.	Hopefully			University	Chinese		Legal Psychology	
Jan Antfolk	Åbo Akademi	Turku	Finland		jantfolk@abo.fi	Hopefully			Population-	Finnish, Swedish			
Hans IJzerman	Université Grenoble	Grenoble	France		h.ijzerman@gmail.c	Yes	Unknown for					social	
Michelangelo Vianello	University of Padova	Padova	Italy		michelangelo.vianell	Yes	100		Master	Italian	Inquisit		
Oscar Oviedo-	Centre for Accident	Brisbane	Australia		oscar.oviedotrespal								
Ryan Perry	University of	Melbourne	Australia		ryanmalkmus@gma								
Khandis Blake	University of New	Sydney	Australia		k.blake@unsw.edu.				University	English	Medialab, Qualtrics, Inquisit, Eye-	social/evolutionary	
Tiago Lim	University of Fortaleza	Fortaleza	Brazil		tiago.souzalima@ho								

Jill A. Jacobson	Queen's University	Kingston	Canada		jill.jacobson@queen								
Bernard	Université du Québec	Montreal	Canada		bernard.paquito@uq								
John R. Vokey	University of	Lethbridge	Canada		vokey@uleth.ca								
Patricia Brosseau-	University of Ottawa	Ottawa	Canada		pbrossea@uottawa.								
Ravin Alaei	University of Toronto	Toronto	Canada		ravin.alaei@mail.uto								
Julia zhao	Shanxi Normal	Shaanxi	China		18335181126@163.								
Vojtech Zika	Center for Behavioral	Prague	Czech		vojtech.zika@cebex								
Andero Uusberg	University of Tartu	Tartu	Estonia		andero.uusberg@ut.								
Eric Karlsson	Fakulteten för	Turku	Finland		epa.karlsson@gmail							Psytools, Soile, Eye-tracking,	Evolutionary, Forensic,
Armand Chatard	Université de Poitiers	Poitiers	France		armand.chatard@un								
Christoph Stahl	Department for	Cologne	Germany		christoph.stahl@uni-								
Benjamin Gagl	Goethe Universität	Frankfurt	Germany		gagl@psych.uni-								
Philipp Kanske	Technische	Dresden	Germany		philipp.kanske@tu-								
Johannes Lutz	Universität Potsdam	Potsdam	Germany		jlutz@uni-								
Bettina Schwörer	University of Hamburg	Hamburg	Germany		bettina.schwoerer@					English, German			Motivation and Self-
Lea Hildebrandt	University of	Wurzburg	Germany		lea.k.hildebrandt@g								
DR Abhijit Das	AMRI Institute of	Kolkata	India		abhijit.neuro@gmail.								
Michael Gilead	Ben-Gurion University	Beersheba	Israel		michael.gilead@gm								
Daniel Lakens	Eindhoven University	Eindhoven	Netherlands	Anne Scheel	D.Lakens@tue.nl			Methodologic		Dutch			Meta
Alan KS Nielsen	Max Planck Institute	Nijmegen	Netherlands		alan@languageevol								
Mark Verschoor	University of	Groningen	Netherlands		m.verschoor@rug.nl								
Simon Columbus	Vrije Universiteit	Amsterdam	Netherlands		simon@simoncolum								
Michael Philipp	Massey University	Palmerston	New Zealand		M.Philipp@massey.		≤ 100	university	English		Psychpy, DirectRT, Qualtrics,		
Katarzyna Jasko	Jagiellonian	Krakow	Poland		kasia.jot@gmail.co								
Dmitry Lyusin	Higher School of	Moscow	Russia		ooch@mail.ru								
Ljiljana Lazarevic	Institute of	Belgrade	Serbia		ljiljana.lazarevic@f.								
Taehwan Yoon Ph.D.	ICS, Seoul National	Seoul	South Korea		thyoon93@snu.ac.k								
Oskar Flygare	Karolinska Institutet	Solna	Sweden		oskar.flygare@ki.se								
Peter Edelsbrunner	ETH Zurich	Zurich	Switzerland		peter.edelsbrunner								
Florian Brühlmann	University of Basel	Basel	Switzerland		florian.bruehlmann								
Tim Böttger	University of St. Gallen	St. Gallen	Switzerland		tim.boettger@unisg.								
Hamza Dincer	Boğaziçi University	Istanbul	Turkey		hamzamustakdincer								
Sami Gulgoz	Koc University	Istanbul	Turkey		sgulgoz@ku.edu.tr								
Anıl Şafak Kaçar	Koç University	Istanbul	Turkey		akacar@ku.edu.tr								
İlker Dalğar	Middle East Technical	Ankara	Turkey		ilkerdalgar@gmail.c								
Vera Kempe	Abertay University	Dundee	UK		v.kempe@abertay.a								
Emily S. Cross	Bangor University	Gwynedd	UK		e.cross@bangor.ac.								
Ruth Horry	Swansea University	Swansea	UK		R.horry@swansea.a								
Stephanie Rossit	University of East	Norwich	UK		s.rossit@uea.ac.uk								
Zander Crook	University of Edinburgh	Edinburgh	UK		zander.crook@ed.a								
Alexa Morcom	University of Edinburgh	Edinburgh	UK		Alexa.morcom@ed.								
Lisa DeBruine	University of Glasgow	Glasgow	UK		lisa.debruine@glasg								

Olga Perepelkina	Lomonosov Moscow State University	Moscow	Russia		neptizza@gmail.co							
Adamovich Timofey	Moscow State University	Moscow	Russia		tadamovich11@gm							
Ilya Zakharov	Psychological Institute of the Russian Academy of Sciences	Moscow	Russia		iliazaharov@gmail.c				Students		PsychoPy, EEG, tDCS, ready to	behavioral genetics
Chun-Chia Kung	National Cheng Kung University	Tainan	Taiwan		chunkung@mail.nck							
Kate Gee	Canterbury Christ Church University	Canterbury	UK		kate.gee@canterbur							
David Vernon	Canterbury Christ Church University	Canterbury	UK		david.vernon@cant							
Aimee Chabot	Duke University	Durham	USA		aimee.chabot@duk							
Cody Christopherson	Southern Oregon University	Ashland	USA		christoc1@sou.edu							
Alexander Garinther	University of Oregon	Eugene	USA		agarinth@uoregon.e							
Charlie Ebersole	University of Virginia	Charlottesville	USA		cebersole@virginia.							
Debora I. Burin	Universidad de Buenos Aires	Buenos Aires	Argentina		dburin@psi.uba.ar				Students	Spanish	Experience in trans-cultural test	Cognitive/ Psychometric
Arti Parganiha	Pt. Ravishankar Shukla University	Raipur	India	Babita Pande, Pratibha Kujur, Anshuma	arti.parganiha@gma	Yes	Around 300 (graduate se	Contribute	University	English; Hindi (after translation of questionna	CANTAB (sustained attention, spatial memory), Time	Chronobiology, Cognition

Proposers: Benedict Jones, Lisa DeBruine, Jessica Flake

Title: Does Oosterhof and Todorov's valence-dominance model of social perception of faces generalize across world regions?

Link for demo version: <http://faceresearch.org/project?PSAeng&auto>

Background. Oosterhof and Todorov (2008 PNAS) found that Principal Component Analysis of trait ratings of face images made by students at a US university produced two components (faces were rated for aggressiveness, attractiveness, caringness, confidence, dominance, emotional stability, unhappiness, intelligence, meanness, responsibility, sociability, trustworthiness, weirdness). The first component, which they labeled 'valence', was correlated with all traits except dominance and was particularly highly correlated with trustworthiness. The second component, which they labeled 'dominance', was highly correlated with rated dominance, correlated with aggressiveness and confidence, and largely unrelated to the other traits.

Although this two-component model of social judgments of faces has become very influential, the extent to which it applies to trait ratings of faces made in other regions of the world is not yet known (but see Sutherland et al., in press PSPB for a recent replication in China). The proposed project will test whether the model described in Oosterhof and Todorov (2008 PNAS) can (1) be replicated in a new sample of North American raters and (2) can also explain trait-ratings made in other world regions (United Nations Country Grouping: Africa, Asia, Central America, Eastern Europe, European Union, Middle East, North America, Oceania, South America, The Caribbean).

Participant characteristics. Adult participants. No restriction on sex, sexual orientation, or ethnicity necessary. Data on age, sex, sexual orientation, ethnicity, and country of residence would be collected. Only world region of residence (determined from country of residence) would be used in the proposed analyses. The other factors would be made available for further, exploratory analyses.

Participating labs will be expected to collect data from 50-100 participants during 2018 to earn authorship on the resulting manuscript.

Procedure. Each participant would be allocated to rate 102 faces (49 female and 53 male faces, diverse ethnicity) for one of 14 adjectives (aggressive, attractive, caring, confident, dominant, emotionally stable, unhappy, intelligent, mean, responsible, sociable, trustworthy, weird, old) using a 1 (very low) to 7 (very high) scale. These are the same 13 adjectives used by Oosterhof and Todorov (2008), plus 'old' (shown by Sutherland et al., 2013 Cognition to produce a third component). To mitigate potential problems with translating single-word labels, dictionary definitions for each of the 13 original adjectives would also be provided (following Bainbridge et al., 2013 JEP:G; see appendix for their definitions). Although this departs from Oosterhof and Todorov's methods, we have discussed this change with Todorov who agrees it is sensible. Each

participant would rate all 100 faces for one adjective only (which adjective they rated the faces for would be randomly determined). Based on data collected in our lab (UK), the mediantime to complete this task is ~5 minutes (90th percentile = ~8 minutes). Following Oosterhof and Todorov's original paper, we would require a minimum of 15 participants from each geographic region to rate the faces for each adjective (i.e., a minimum of 210 raters per region).

Our lab can provide a set of 102 faces (49 female, 53 male faces, diverse ethnicity) for the study (https://figshare.com/articles/Face_Research_Lab_London_Set/5047666). We have already made these images open access and they were recently used by Todorov's lab in a replication and extension of their original paper (see Oh et al., 2017 <https://psyarxiv.com/fxvcu>).

Analysis plan. Analyses would be based on those reported by Sutherland et al. (in press PSPB). These analyses use averaged ratings for each face. Ratings from each world region will be analyzed separately. Countries will be allocated to world regions using the United Nations Country Grouping (Africa, Asia, Central America, Eastern Europe, European Union, Middle East, North America, Oceania, South America, The Caribbean).

First, we would identify how many components (i.e., factors) underpin judgments in each geographic region. This will be done using exploratory factor analysis (i.e., principal axis factoring) with a non-orthogonal rotation. Number of factors will be identified from scree plots, number of factors with eigenvalues greater than one, minimum average partial procedure, and parallel analysis. Differences in the outcome of these methods will be reconciled using a procedure described in Flake et al. (2015 Contemporary Educational Psychology).

Second, for each geographic region, we will identify which traits have strong loadings on each factor, which traits have weak loadings on each factor, and which traits crossload between or among factors. Criteria for strong and weak loadings will be set following Flake et al. (2015).

Publication plan. We suggest submitting to Nature Human Behavior as a registered report in the first instance, with Royal Society Open Science as a backup plan (again as a registered report). This would require a list of participating labs. Importantly, each lab would be required to have ethics approval before submitting the registered report for Stage 1 review.

Equipment required: A computer with Internet connection to access online study.

Appendix. Trait definitions used in Bainbridge et al. (2013 JEP:G). Note that Bainbridge et al. did not include dominance or age in their study. We propose defining dominant as "strong; important" and old as "having greater age; not young". Like the Bainbridge et al. definitions, these are adapted dictionary definitions.

Trait	Definition
aggressive	inclined to behave in a hostile fashion
attractive	appealing to the senses through beauty, form, character, etc
caring	feeling or showing compassion
confident	sure of oneself; having no uncertainty about ones own abilities
emotionally stable	not subject to emotional instability or illness; sane; mentally sound
unhappy	not joyful; sad or depressed
intelligent	having a good understanding or a high mental capacity
mean	offensive, selfish, or unaccomodating; nasty; malicious
responsible	able to take rational decisions without supervision; accountable for ones own actions
sociable	friendly or agreeable in company; companionable
trustworthy	deserving of confidence; dependable; reliable
weird	strange or bizarre

Report On
The Workshop “Hands-on Actigraphy”
Date: 28th JULY 2022
Venue: LG-1, GMU
Organized by Odisha Centre for Geriatrics and Gerontology

Odisha Centre for Geriatrics and Gerontology of Gangadhar Meher University, Sambalpur, Odisha organized a workshop on “Hands on Actigraphy” on 28th July 2022 at LG-1 of GMU. The workshop was organized in collaboration with the Centre for Translational Chronobiology (CTC), Pt. Ravishankar Shukla University, Raipur. In the workshop, Prof. Arti Parganiha, the Coordinator of CTC, was present as a resource person and subject expert.

Importance of Workshop

The Odisha Center for Geriatrics and Gerontology (OCGG) at Gangadhar Meher University (GMU), Sambalpur is the first-ever center in the field of Geriatrics and Gerontology in Odisha. The Center was established in 2020 with financial assistance from the World Bank-funded “Odisha Higher Education Programme for Excellence and Equity” (OHEPEE) which focuses on interdisciplinary research on the social, psychological, and biological aspects of the elderly persons of Odisha.

One of the core objectives of the Center is to determine the sleep quality and cognitive abilities of the elderly population in Odisha. Therefore, the workshop has significant importance to the study of sleep quality measurement for the elderly population. Actigraphy is a non-invasive technique that is used to assess objective sleep variables and the rest-activity cycle of human subjects.

Proceeding of the workshop

The workshop began at 11:00 AM along with the introduction of the theme by Prof. Arti Parganiha.

Prof. Arti Parganiha elaborated in her lecture on the Application of Actigraphy-based output in various groups of subjects, such as seemingly healthy humans, cancer patients, and subjects with obstructive sleep apnea in the study area of Raipur. She also elaborated on the different parameters which are associated with the sleep quality in human subjects. She emphasized the importance of two rhythm parameters, i.e., autocorrelation coefficient at 24 hours (r_{24}) and dichotomy index ($I < 0$). She also highlighted the challenges faced during her studies. During the hands-on training session, she explained how to study the sleep-wake rhythms in human subjects using Actiwatch - MotionWatch8. She demonstrated how to configure the MotionWatch8 on a PC for data collection and how to retrieve the data of MotionWatch8 using

the software. She explained in detail the MotionWatch8-derived important sleep variables, Non-Parametric Circadian Rhythm Analysis (NPCRA), and the 24-hour activities of subjects. She explained the uses and operations of MotionWare Software.

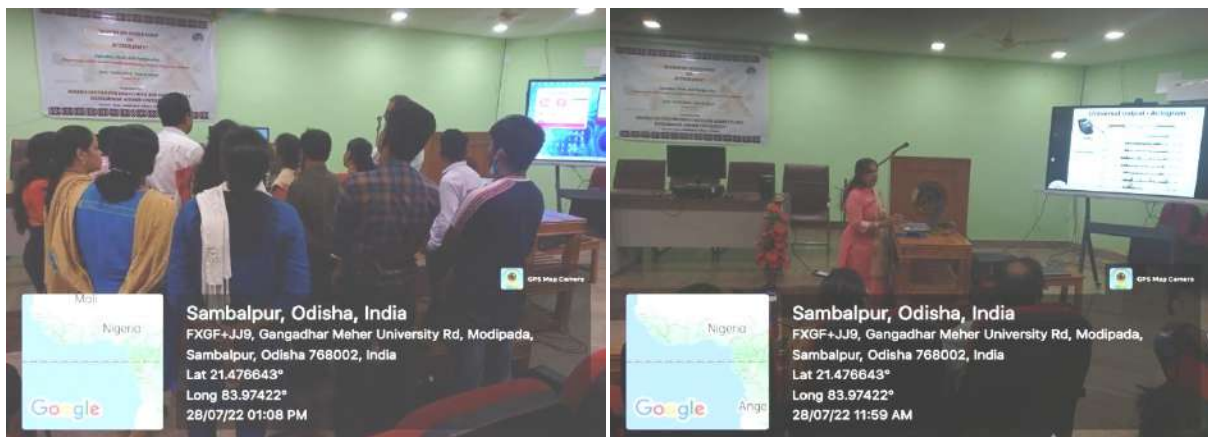
During the deliberation, Prof. Parganiha suggested some points to incorporate into the OCGG study. The points are:

- a) To check the normality and homogeneity of data,
- b) To make a protocol that includes a selection of area, subjects, inclusion and exclusion criteria for Actigraphy study,
- c) Only trained persons should operate the MotionWatch8.

Participants

In the workshop, the participants were PI, Co-PI, Research Associate, Research Assistant, and Office Assistant of OCGG and other faculties from the School of Anthropology and School of Botany.

Some Photographs during the Workshop





साहित्य एवं भाषा-अध्ययनशाला,
समाज शास्त्र एवं समाजकार्य अध्ययनशाला
पं. रविशंकर शुक्ल विश्वविद्यालय, रायपुर (छ.ग.)



का संयुक्त आयोजन

पब्लिक आउटरीच व्याख्यान



विशिष्ट वक्ता

प्रो. डी. आर. साहू

संकायाध्यक्ष, समाज विज्ञान
लखनऊ विश्वविद्यालय, लखनऊ

“Success Blueprint : Building
Your Bright Tomorrow”

स्थान : सेमीनार हॉल, भूतल, कला भवन

दिनांक : 21 अगस्त 2023

समय : पूर्वाह्न 11:00 बजे



विशिष्ट वक्ता

प्रो. अजय कुमार शुक्ला

विभागाध्यक्ष, अंग्रेजी विभाग
डॉ. डी. यू. गोरखपुर विश्वविद्यालय, गोरखपुर

** आयोजक **

प्रो. कल्लोल के. घोष
निदेशक, पब्लिक आउटरीच सेंटर

डॉ. शैल शर्मा
अध्यक्ष, साहित्य एवं भाषा-अध्ययनशाला

डॉ. निस्तर कुजूर
अध्यक्ष, समाजशास्त्र एवं समाजकार्य-अध्ययनशाला

डॉ. शैलेन्द्र पटेल
कुलसचिव

Certificate of Completion

Postgraduate Internship Program
Indian Institute of Technology, Hyderabad

This is to certify that **Ms. Geetanjali Sahu**, 2nd year M.Sc. Physics student at **Pt. Ravishankar Shukla University, Raipur**, has successfully completed his Research Internship on the topic **“Eu³⁺-Activated Novel Red-emitting Phosphor for Solid-State-Lighting Applications”** at the **Department of Chemistry, Indian Institute of Technology, Hyderabad**, under the supervision of **Prof. Sivakumar Vaidyanathan (Advanced Photonics and Electronics Lab)** from **06/03/2024 to 31/03/2024**.

Date: 31/03/2024



Research Supervisor

Certificate of Completion

Postgraduate Internship Program
Indian Institute of Technology, Hyderabad

This is to certify that **Mr. Yash Kumar Sahu**, 2nd year M.Sc. Physics student at **Pt. Ravishankar Shukla University, Raipur**, has successfully completed his Research Internship on the topic **“Eu³⁺-Activated Novel Red-emitting Phosphor for Solid-State-Lighting Applications”** at the **Department of Chemistry, Indian Institute of Technology, Hyderabad**, under the supervision of **Prof. Sivakumar Vaidyanathan (Advanced Photonics and Electronics Lab)** from **06/03/2024 to 31/03/2024**.

Date: 31/03/2024



Research Supervisor

Certificate of Completion

Postgraduate Internship Program

Indian Institute of Technology, Hyderabad

This is to certify that **Ms. Khushi Dewangan**, 2nd year M.Sc. Physics student at **Pt. Ravishankar Shukla University, Raipur**, has successfully completed his Research Internship on the topic **“Eu³⁺-Activated Novel Red-emitting Phosphor for Solid-State-Lighting Applications”** at the Department of Chemistry, Indian Institute of Technology, Hyderabad, under the supervision of **Prof. Sivakumar Vaidyanathan (Advanced Photonics and Electronics Lab)** from **06/03/2024 to 31/03/2024**.

Date: 31/03/2024



Research Supervisor



ISO 9001:2015 Certified

राज्यस्तरीय भौतिकी प्रयोगशाला, दिल्ली
Solid State Physics Laboratory, Delhi



File No. 1805...62..HR/SSPL

Dated 16.04.2024

(Min. of Defence, DRDO)

Lucknow Road, Timarpur, Delhi-110054

प्रशिक्षण प्रमाणपत्र / TRAINING CERTIFICATE

This is to certify that Mr./Ms./ SONAM

Student of SOS IN PHYSICS AND ASTROPHYSICS, P.T.R.S.U. RAIPUR (C.G.) Roll No. 2210190029
Branch M.Sc. (Physics) has completed successfully Summer/~~Winter~~ Internship for
the period from 06/03/2024 to 15/04/2024 Duration Six (06) weeks/~~months~~.

Topic of Internship was Study of Sic and Cutting of Sic Boule into
Wafers using Diamond wire Multi-wire saw machine.

During the training period his/hér conduct at SSPL was good.

MjWshana
Head-HR

SI

ISO 9001:2015 Certified

राजराष्ट्र
भौतिकी प्रयोगशाला, दिल्ली
Solid State Physics Laboratory, Delhi



File No. 1805 61 /HR/SSPL

Dated 16.04.2024

(Min. of Defence, DRDO)

Lucknow Road, Timarpur, Delhi-110054

प्रशिक्षण प्रमाणपत्र / TRAINING CERTIFICATE

This is to certify that Mr./Ms./ YEENA SAHU

Student of SOS IN PHYSICS AND ASTROPHYSICS, Raipur (C.G.) Roll No. 2210190034
Branch M. Sc. (Physics) has completed successfully Summer/Winter Internship for
the period from 06/03/2024 to 15/04/2024 Duration Six (06) weeks / months

Topic of Internship was Study of SiC Material and Growth of
Poly - Crystalline SiC by Physical Vapor Transport Method.

During the training period his/her conduct at SSPL was good.

M. W. Sharma
Head-HR

Certificate

[2]

ISO 9001:2015 Certified

श्री
Solid State Physics Laboratory, दिल्ली
भौतिकी प्रयोगशाला, दिल्ली

SSPL

(Min. of Defence, DRDO)
Lucknow Road, Timarpur, Delhi-110054

प्रशिक्षण प्रमाणपत्र / TRAINING CERTIFICATE

This is to certify that Mr./Ms./ SHRUTI PRAJAPATI
Student of SOS IN PHYSICS AND ASTROPHYSICS, Pt. R.S.D. RAIPUR (C.G.) Roll No. 2310190038
Branch M.Sc. (PHYSICS) has completed successfully Summer/~~Winter~~ Internship for
the period from 06/03/2024 to 15/04/2024 Duration Six (06) weeks/~~months~~.

Topic of Internship was Study of SiC and KOH Vapour Etching

During the training period ~~his~~/her conduct at SSPL was good.

M. Sharma
Head-HR

SI

ISO 9001:2015 Certified

भारतीय भौतिकी प्रयोगशाला, दिल्ली
Solid State Physics Laboratory, Delhi



File No. 1805...60./HR/SSPL

Dated ...16.04.2024

(Min. of Defence, DRDO)

Lucknow Road, Timarpur, Delhi-110054

प्रशिक्षण प्रमाणपत्र / TRAINING CERTIFICATE

This is to certify that Mr./Ms./ BHARAT KUMAR SAHU
Student of SOS IN PHYSICS AND ASTROPHYSICS, P.L.R.S.O. RAIPUR (C.G.) Roll No. 2210190003
Branch M.Sc. (PHYSICS) has completed successfully Summer/Winter Internship for
the period from 06/03/2024 to 15/04/2024 Duration Six (06) weeks / months.

Topic of Internship was Study of SiC and Chemical Mechanical
Polishing : Theory and Experiment

During the training period his/her conduct at SSPL was good.

MjWshans

Head-HR



Letter of Collaboration

To,

Dr. P. Shukla
HOD Psychology
Pt. Ravishankar University
Raipur, CG

Madam,

We would like to extend a collaboration proposal with your prestigious department. If given this opportunity we would like to offer an internship program for your students to create an ongoing community outreach program on mental health awareness & wellbeing .

This program will equip your students to take up responsibility as young citizens in creating awareness in the community.

Here are the details of the internship.

Purpose: To create an outreach internship program to reach out to the high schoolers of our city (and nearby towns in CG) and educate them about mental health awareness and wellbeing.

The volunteers will be given in-person and online training by the team of Project Karuna. The volunteers will be conducting in-person educational sessions in the schools of Raipur and designated / chosen cities.

Timeline : 3-month internship, The trainees can work at their own pace.

Honorarium: The volunteers will be given 800 rupees for each school they cover. This will be provided at the end of their internship.

Process: The internship step-by-step guide is attached to this letter for the details.

Certificate: A collaborative certificate of completion will be provided at the end of the academic year.

We eagerly look forward for a positive response from your end.

Thanks & Regards,

Nidhi Nathaniel

Nidhi Nathaniel
Founder - Project Karuna
info@projectkaruna.org
www.projectkaruna.org
Date: 1/5/2023

Accepted by:

Dr. P. Shukla
HOD (Psychology)
Pt. Ravishankar University
Raipur, CG
Date: 1/5/2023

REVIEW ARTICLE

Concept and Evolution in 3-D Printing for Excellence in Healthcare

Priyank Sinha^{1,#}, Preeti Lahare^{1,#}, Meena Sahu^{1,#}, Richard Cimler², Marek Schnitzer³, Jana Hlubanova³, Radovan Hudak³, Namrata Singh^{2,4,*}, Bhanushree Gupta¹ and Kamil Kuca^{2,5,*}

¹Department of Chemistry, Centre for Basic Sciences, Pt. Ravishankar Shukla University, Raipur 492010, Chhattisgarh, India; ²Faculty of Science, University of Hradec Kralove, Rokitanskeho 62, Hradec Kralove, Czech Republic; ³Department of Biomedical Engineering and Measurement, Faculty of Mechanical Engineering, Technical University of Kosice, Letna 1/9 Kosice, Slovakia; ⁴Department of engineering Sciences, Ramrao Adik Institute of Technology, DY Patil University, Nerul, Navi Mumbai, Maharashtra 400706, India; ⁵Biomedical Research Center, University Hospital Hradec Kralove, Sokolska 581, 50005 Hradec Kralove, Czech Republic

ARTICLE HISTORY

Received: June 14, 2023
Revised: August 05, 2023
Accepted: October 31, 2023

DOI:
[10.2174/0109298673262300231129102520](https://doi.org/10.2174/0109298673262300231129102520)

Abstract: Three-dimensional printing (3DP) has gained popularity among scientists and researchers in every field due to its potential to drastically reduce energy costs for the production of **customised** products by **utilising** less energy-intensive machines as well as **minimising** material waste. The 3D printing technology is an additive manufacturing approach that uses material layer-by-layer fabrication to produce the digitally specified 3D model. The use of 3D printing technology in the pharmaceutical sector has the potential to **revolutionise** research and development by providing a quick and easy means to manufacture **personalised** one-off batches, each with unique dosages, distinct substances, shapes, and sizes, as well as variable release rates. This overview addresses the concept of 3D printing, its evolution, and its operation, as well as the most popular types of 3D printing processes **utilised** in the health care industry. It also discusses the application of these cutting-edge technologies to the pharmaceutical industry, advancements in various medical fields and medical equipment, 3D bioprinting, the most recent initiatives to combat COVID-19, regulatory frameworks, and the major challenges that this technology currently faces. In addition, we attempt to provide some futuristic approaches to 3DP applications.

Keywords: 3D printing techniques, vat photopolymerization, SLS, EMP, inkjet, DOP, EHD, personalized medicines, drug delivery system, COVID-19 treatment, 3D printed equipment, 3D bioprinting.

1. INTRODUCTION

3D printing, also known as additive manufacturing, involves creating a three-dimensional object by depositing successive layers of material in a controlled manner [1]. This process utilises Computer-Aided Design (CAD) software to transmit instructions to a 3D printer. The printer translates the digital model into two-dimensional sections and uses them as a basis to construct the object in layers. Alternative terms for this technology include freedom fabrication manufacturing and additive layer manufacturing [2].

*Address correspondence to these authors at the Faculty of Science, University of Hradec Kralove, Rokitanskeho 62, Hradec Kralove, Czech Republic; Tel: +91-9892723773, E-mail: kamil.kuca@uhk.cz; Tel: +420 493 332 509; E-mail: chemnamrata09@gmail.com

[#]These authors contributed equally to this work.

As the name suggests, additive manufacturing (3D printing) adheres to the opposite principles of fabrication from subtractive manufacturing, which involves the creation of three-dimensional objects through the use of material removal techniques like drilling, milling, sawing, broaching, etc [3]. Both additive and subtractive manufacturing methods can be used for quick prototyping. The decision is dependent on taking into account a variety of elements, including the intricacy of the products to be manufactured, the material used, the required number of copies, and the cost. It is important to note that additive manufacturing has the potential to significantly reduce energy costs for the production of **personalised** products by employing less energy-intensive machines, as well as material waste.

3D printing was discovered back in the late 1980s

when Charles Hull first introduced it in a patent for a technique of successively layering with liquid photopolymer solutions to print objects in three dimensions. This concept was the earliest 3D printing technology, today known as Stereolithography (SLA) [4]. Hull later used this technology to create the SLA-250, the first 3D printer available to the general public [5].

After the discovery of SLA, researchers became very interested in creating 3D printing technology to print products using alternative materials like metal, ceramics, *etc.* Some of the developed alternative print technologies are material jetting, Digital Laser Printing (DLP), Selective Laser Sintering (SLS), Selective Laser Melting (SLM), and Laminated Object Manufacturing (LOM).

The industries of aerospace, mechanical manufacturing, construction, and biomedical engineering have all benefited significantly from the rapid development and wide-ranging uses of 3D printing technologies [6]. However, the pharmaceutical industry started using it very recently. The U.S. Food and Drug Administration (FDA) **authorised** a levetiracetam pill (Spritam®) developed using 3D printing technology in July 2015, indicating the industry's acceptance of this technology [7]. In the pharmaceutical industry, it has been used to create a variety of pharmaceutical products, including microneedles, transdermal patches, orodispersible films, gastro-floating tablets, controlled-release tablets, and polypills [8]. 3D printing techniques were also helpful in the battle against COVID-19 through the development of equipment like face masks, face shields, safety goggles, nasopharyngeal swabs, ventilation devices, and respiratory devices [9-12].

Despite the benefits of 3DP, there are still several barriers that impede the advancement of 3DP technologies. High temperatures are used due to the stability of these products, which is challenging. Low mechanical resistance, low printing resolution and limited material choices are some other aspects confined to the limitations of this technology [13].

This review **summarises** the 3DP concept, its evolution and workings, outlining the most prevalent types of 3D printing technologies and their application in the pharmaceutical field. The relevance of this technology to the various medical fields, including manufacturing of medical equipment, 3D bio-printing and the most recent approach to combating COVID-19, have been discussed in this report. It also covers the regulatory guidelines, the major challenges currently associated with 3-DP technology, and the future outlook toward the advancement of human healthcare (Fig. 1).

2. EVOLUTION FROM CONVENTIONAL TO 3D PRINTING TECHNOLOGIES

The conventional methods of medical treatment were based on the formula “one size fits all”, which means that the same doses of the same drugs were given to every patient for a specific illness [14]. The drugs were made with fixed parameters, which include shape, size, and release type, without considering the patient's needs, such as gender, age, genetic features, and level of the disease. Moreover, drug dosage is generally adult-based in traditional methods, which demands the production of age-specific doses for children and elderly patients [15, 16]. Moreover, conventional methods are heavily based on trial-and-error methods, which leads to uncertainty in the development procedures [17]. In addition to the oral delivery of drugs, other specific dosage forms are also needed depending on the patients, such as a transdermal delivery system [18]. Also, the establishment of new methodologies is desirable for the production of hydrophobic drugs to achieve the time-specific release [19, 20]. Currently, researchers have found that 60% of drugs in research and 40% of commercial drugs are hydrophobic in nature, which causes problems in the formulation of oral drug delivery systems [19, 21, 22]. The conventional method procedures have some drawbacks, such as time consumption for large-scale production, rigid labour work as well as doses that cannot be changed according to the requirements of the patients. As a consequence, of all these aspects, pharmacists need to develop new methods and compounds that have controlled release properties and patient-specific needs [22, 23].

Therefore, the concept of **personalised** medicine has begun, where medicines are fabricated for a patient according to their physiology and genetic features [12]. **Personalised** medicines are more precise, productive, safer, and cost-efficient [24]. Hence, 3D printing is an appealing route for the fabrication of personalized medicine because it is a method that manufactures substances in a solid form by settling the material layer by layer. In pharmaceuticals, 3D printing plays a huge role in the construction of personalized medicine and drug delivery. During the late 1970s, several patents were granted for computer-aided techniques that attempt several platforms of 3-DP [25]. Charles Hull invented the technique that is currently used in 3D printing, *i.e.*, stereolithography (SLA), which involves the process of polymerization of resins by using UV light to get the desired material and his work soon got patented during the mid-1980s [26-28]. This technology was used in non-clinical areas, such as automobiles and consumer products [29]. A student of Texas State

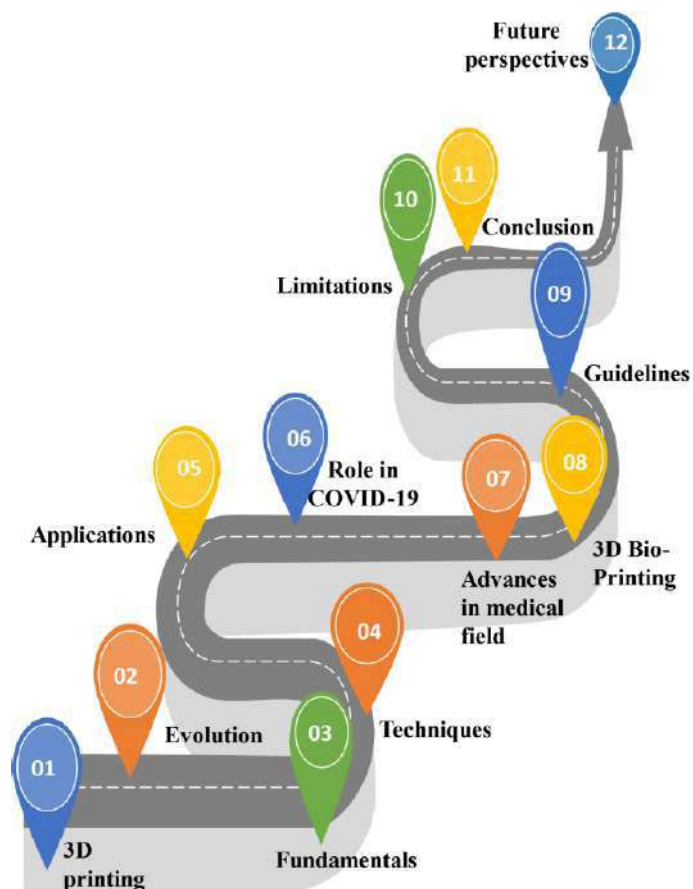


Fig. (1). Roadmap of the review. (A higher resolution / colour version of this figure is available in the electronic copy of the article).

University named Carl Deckard invented another method called Selective laser sintering by fusing the powder through laser operations in 1986. By following this method, in 1989 by Scott and Lisa Crump at Stratasys company, a fused deposition modelling was proposed, involving metal and plastic extrusion by heating. Furthermore, Emanuel Sachs and his team at MIT (Massachusetts Institute of Technology, Cambridge, USA) invented an inkjet printer or binder jetting method based on 3D printing in the early 1990s, which involved binding solutions from the powder surface. This innovation led to the beginning of 3D printing in the drug industry [13]. Hans Langer developed metal laser sintering, which used lasers to generate 3D materials through computer operations [26-30]. Andrew Bowyer from the University of Bath focused on the 3D printers that generate their own materials, and later, they reported their application in various fields [25]. Moreover, implants with active pharmaceutical additives can have the potential for **personalised** medicine [31]. This is how 3D printing technology by using a Magnetic Resonance Image (MRI) or 3D Comput-

er-Aided Design (CAD) has entered the sector of pharmaceuticals for the development of programmed and personalized products [32, 33]. Thereafter, Spritam or Lev- etiracetam, which is the first 3D printed drug, was developed by Aprelia Pharmaceuticals and approved by USFDA in 2015. This drug was constructed by applying the binder jet printing technique. It has the ability for fast oral dissolution due to its highly porous nature and is used for epilepsy treatment [34]. Additionally, 3D printing has a huge application in drug delivery, diagnosis purposes, transdermal therapies, organ and tissue manufacturing, biomedical apparatus, and Additive Manufacturing (AM), such as biorobotics, implants and bioprinted substances for wound healing, *etc.* There are several advantages of 3D printing compared to traditional methods, like rapid and easy, highly accurate solid dosage forms, personalized formulation with adjustable dosage, being more **computerised**, and cost-efficient [35-39]. This innovation can decrease the chances of failure in new pharmaceutical procedures (Fig. 2) [29].

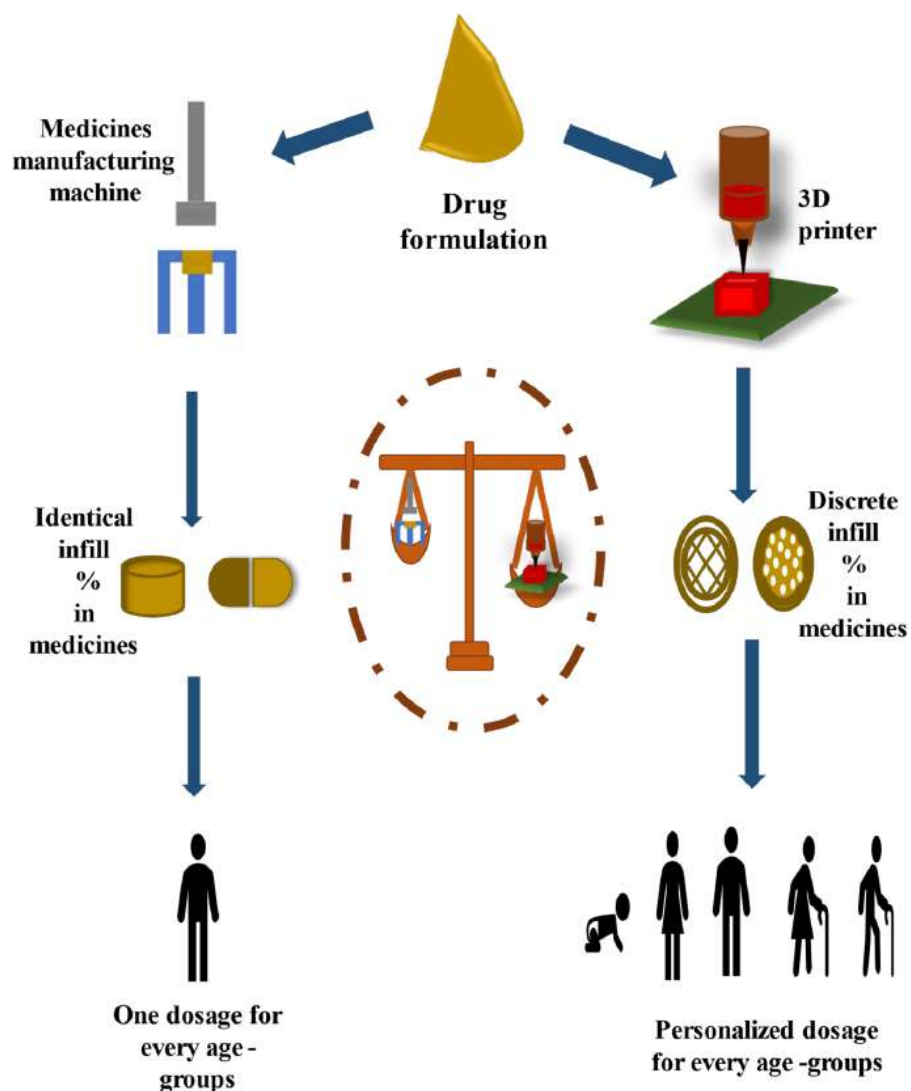


Fig. (2). Comparison of conventional and 3D printing methods. (A higher resolution / colour version of this figure is available in the electronic copy of the article).

3. FUNDAMENTALS OF 3D PRINTING

A cutting-edge technology called 3D printing is assisting designers in rethinking the design of things like **personalised** formulations and leadership development. This is achieved by reducing the design cycle of making decisions through the creation of fresh concepts and ideas, useful feedback, and improved design [40].

Digitally exquisite software, such as Solid Works, Onshape, Creo Parametric, Autocad, Autodesk Tinker Cad, BRL-CAD, Free CAD, Open SCAD, 3D Slash, Wings3D, Sketch UP, Fusion 360, etc., are used to create virtual 3D designs of objects [41]. The 3D model must be converted to the Standard Tessellation Language (STL) file format (from Stereolithography), which records the information about the model's sur-

faces as a table of triangulated section coordinates after it has been constructed [42].

Slicing is the process of converting a three-dimensional model into a stack of flat layers. Software for slicing, such as Matter Control, Ultimaker Cura, Slic3r, Octo Print, Concept Maker, etc., are used to slice objects [43]. These layers appear in slicing software as direct derivatives of the laser or other extruder fixing mechanisms used in 3D printing. The Standard Tessellation Language (STL) file is converted into a G file by slicing the design into a series of 2D horizontal cross-sections with the aid of specialized slicer software installed in the 3D printer. The next step is to select a material that will work well for 3D printing. A vast range of materials, including plastics, ceramics,

resins, metals, sand, fabrics, biomaterials, glass, food, and lunar dust, among others, may be used in 3D printing. The computer sends instructions to the 3D printer for layer-by-layer material deposition as soon as the model is loaded. A 3D printer operates by extruding molten plastic through a tiny nozzle. It moves precisely in accordance with computer instructions. After

printing one layer, the printer waits for it to dry before printing the next layer on top. This process continues until the final product is obtained (Fig. 3) [44].

All types of 3D printing follow a basic work cycle and flow, often referred to as the “three D’s of 3D printing,” even if each has unique features and benefits to offer (Fig. 4) [29].

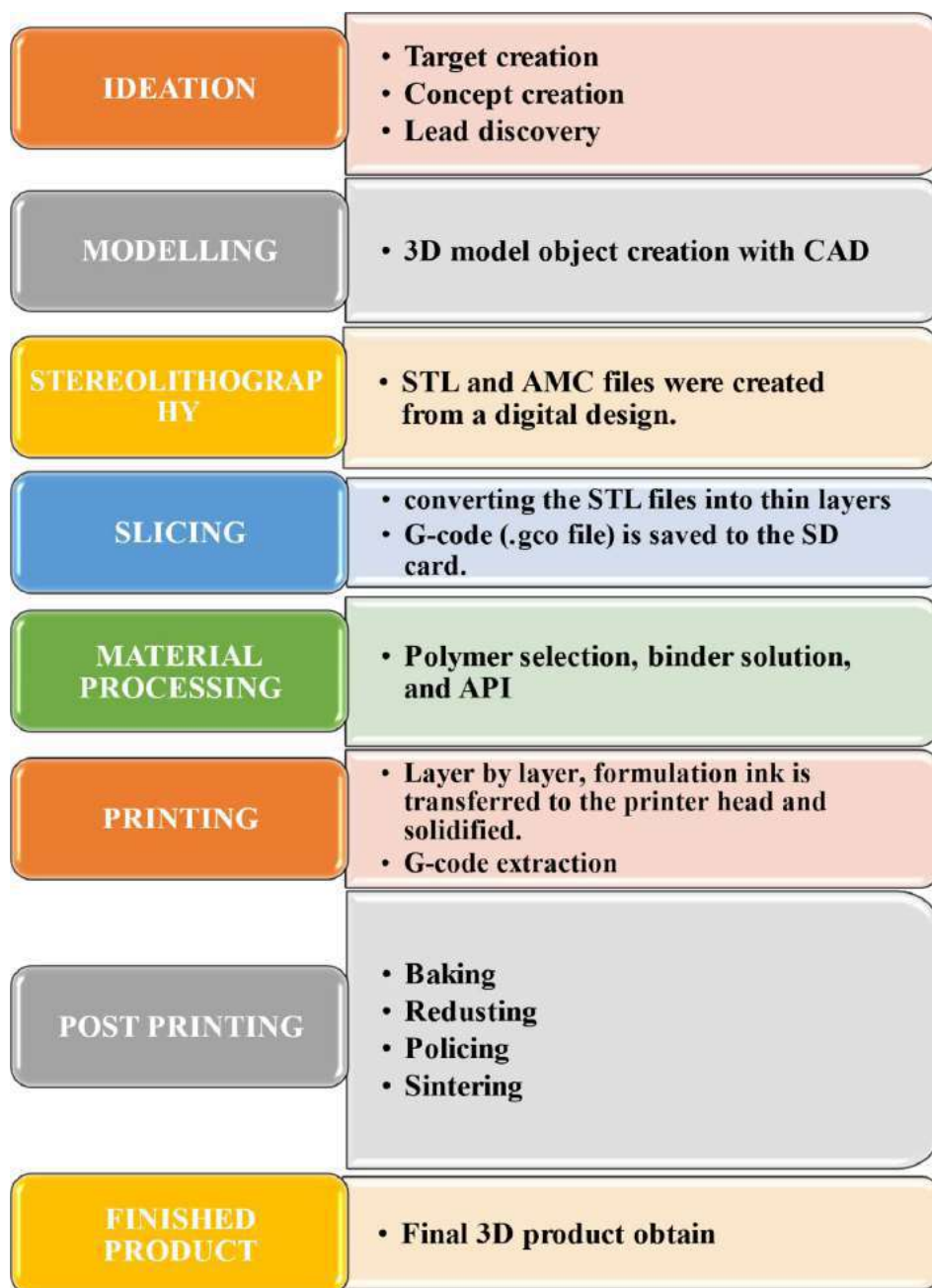


Fig. (3). Step-by-step procedure for 3D printing. (A higher resolution / colour version of this figure is available in the electronic copy of the article).

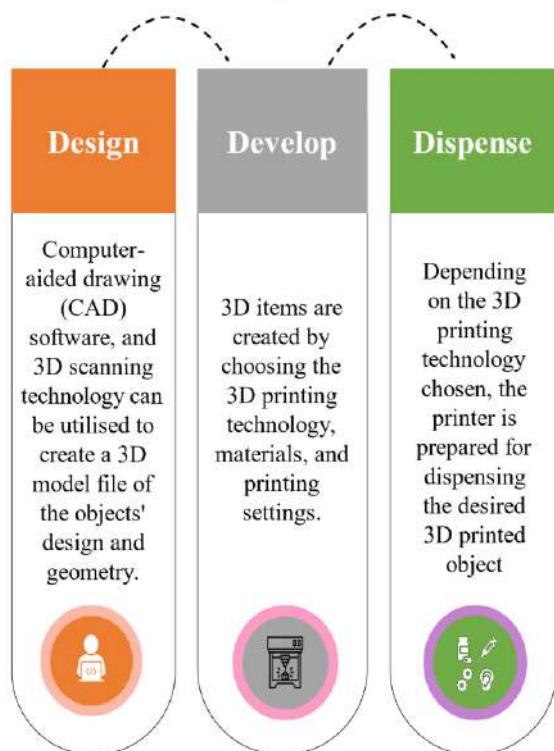


Fig. (4). Three D's of 3D printing. (A higher resolution / colour version of this figure is available in the electronic copy of the article).

The fact that production is carried out layer by layer, as is typical of an additive process, as opposed to more conventional production techniques that employ subtractive procedures or casting processes, is what unites all these 3D processes and technologies [45].

4. TECHNIQUES OF 3D PRINTING

Various 3DPs have been designed, which have the ability to print, extrude, and shape the important dimen-

sions of 3D printing. There are six types of printing methods (Fig. 5) used in the pharmaceutical field based on the energy source, materials, mechanical properties and layer formation, as shown in Table 1. These are Vat photopolymerization, Selective Laser Sintering (SLS), Extrusion Molding Printing (EMP), ink-jet-based printing, Drop On Powder (DOP), and Electrohydrodynamic (EHD) printing techniques.

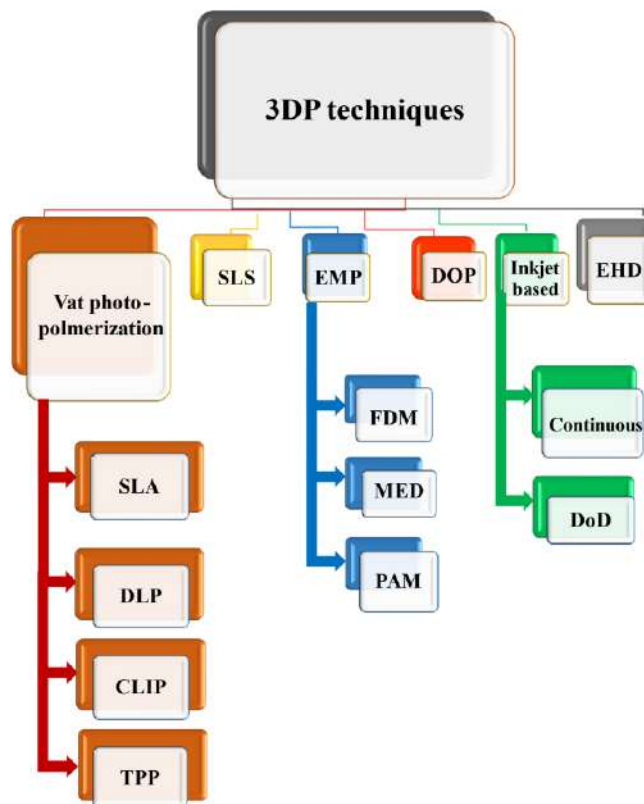


Fig. (5). Various techniques of 3D printing. (A higher resolution / colour version of this figure is available in the electronic copy of the article).

Table 1. Summary of various 3D printing techniques.

3D Printing Techniques	Excipients Used	Advantages	Disadvantages	Configure	References
Vat photo-polymerization	SLA • PEG • pHEMA • PEGDA • GelMA • PEG-DMA • PPF/DEF, etc	• Excellent resolution • Less thermal stress is involved • Less demand for properties and chemical structure of drugs/excipients • Patterning precise structures	• Limited formulation • Toxic material • Costly • Fewer resins present	• Transdermal micro-needle • Modified release tablets • Multi-layer polypills • Drug loaded hydrogels • Bladder devices • Anti-acne patch	[28, 87]

(Table 1) contd....

3D Printing Techniques		Excipients Used	Advantages	Disadvantages	Configure	References
	DLP	<ul style="list-style-type: none"> • PEGDA • PEGDMA • PPF • DEF • PEGMA, etc. 	<ul style="list-style-type: none"> • Fast process • Less usage of resins • Instantly solidify the complete layer 	<ul style="list-style-type: none"> • Possibility of degradation of materials • Unexpected drug-polymer interactions • Time-consuming 	<ul style="list-style-type: none"> • Drug delivery implants • Solid oral dosage forms • Micro-needle arrays 	[47]
	CLIP	<ul style="list-style-type: none"> • PEGDMA • PCL-tMa • PCLDMA • PMA, etc. 	<ul style="list-style-type: none"> • Predictable mechanical features • Consistent molecular structure of 3D object 	<ul style="list-style-type: none"> • Degradation of materials • Accidental drug-polymer reactions 	<ul style="list-style-type: none"> • Transdermal drug delivery devices • Microneedle • Mask devices 	[47]
	TPP	<ul style="list-style-type: none"> • PEGDA • PEGDMA • PLA, etc. 	<ul style="list-style-type: none"> • Control drug release profile • Act as a drug carrier with variable size and shape • Adjustable drug release kinetics 	<ul style="list-style-type: none"> • Unexpected drug-polymer interactions • Degradation of materials 	<ul style="list-style-type: none"> • Microneedle • Drug delivery devices 	[47]
SLS	-	<ul style="list-style-type: none"> • PE • PVA-PEG • PCL, etc 	<ul style="list-style-type: none"> • Solvent-free • High resolution • Single-step method for drug delivery • Less time consuming • Absent of liquid binders 	<ul style="list-style-type: none"> • Degradation of materials due to highly energetic light source • Finite speed of sintering 	<ul style="list-style-type: none"> • Oral dispersible tablets • Cubic porous structure • Pellets loaded with drugs 	[28, 87, 289]
EMP	FDM	<ul style="list-style-type: none"> • PVA • TCP • PLA • HPMCAS • PCL • HPC • PLGA • Eudragit, etc 	<ul style="list-style-type: none"> • Low-cost • Easy operating process • Accurate • Promising parameter properties • Association of HME • Excellent mechanical properties • More flexible in designing complex formulations 	<ul style="list-style-type: none"> • Less drug loading capacity • Causes of thermal degradation 	<ul style="list-style-type: none"> • Immediate, Pulsatile and Enteric drug-release tablet • Vaginal ring suppositories • Microneedle patches • Rectal ring suppositories • Oral dispersible films • Delivery devices for nanocapsules • Uterus devices 	[289]
	MED	<ul style="list-style-type: none"> • PEG • HPC • Glycerol • Kollidon, etc 	<ul style="list-style-type: none"> • Filament-free method • Accurate • Reproducible • Large-scale production • Operating multiple materials • Excellent compatibility with drugs/ excipients • Broad-range excipients can be used • No product degradation • GMP compliance 	-	<ul style="list-style-type: none"> • Multi-component tablets, such as core-shell structured tablets with a delay layer • drug delivery devices 	[17]

(Table 1) contd....

3D Printing Techniques		Excipients Used	Advantages	Disadvantages	Configure	References
	PAM	<ul style="list-style-type: none"> • PVP • HPC • HPMC • MCC, etc 	<ul style="list-style-type: none"> • Appropriate for thermally unstable drugs • A broad range of initial materials can be used 	<ul style="list-style-type: none"> • Post-processing required • Usage of heavy machinery tools, <i>i.e.</i>, hot extruder motor • Low resolution • Organic solvents are used 	<ul style="list-style-type: none"> • Double layer tablet • Suppositories • Floating drug delivery system (FDDS) • Nanocapsules • Gummy drugs 	[29, 87]
Inkjet based	-	<ul style="list-style-type: none"> • Binder fluid like glycerol, deionised water • PVP • Polysorbate, <i>etc.</i> 	<ul style="list-style-type: none"> In continuous inkjet, <ul style="list-style-type: none"> • Rapid droplet ejection • No blockage in the nozzle In DoD, <ul style="list-style-type: none"> • Cost-effective • Easy to use • High precision • Controlled droplet sizes • Less wastage of drugs 	<ul style="list-style-type: none"> In continuous inkjet, <ul style="list-style-type: none"> • Unnecessary dispersion of ink • Costly maintenance • Low resolution In TIJ, <ul style="list-style-type: none"> • Degradation of thermal-sensitive active ingredients 	<ul style="list-style-type: none"> • Implants • Oral wafers • Tablets • Inhaler 	[28, 289]
	-	-	-	-	-	-
DOP/ Binder jet	-	<ul style="list-style-type: none"> • PVP • HPMC • Starch, <i>etc.</i> 	<ul style="list-style-type: none"> • Restoration of unprocessed powder after the activity • High level of porosity • Inexpensive production • Removal of residual volatile solvent through thermal sintering • Normal temperature process • A broad range of materials can be used 	<ul style="list-style-type: none"> • High fragile • Less resolution • Post-processing required • Defects in product • Deficient mechanical features 	<ul style="list-style-type: none"> • Implants • Orally disintegrating tablets (ODTs) • Extended-release and Enteric dual pulsatory tablets 	[28, 87]
EHD	-	<ul style="list-style-type: none"> • CA • PCL • PEO • PVA, <i>etc</i> 	<ul style="list-style-type: none"> • Highly controllable resolution • Provide a suitable atmosphere for polymers/drugs • Controllable digital system for the deposition of materials • Complex geometries fabrication • Single step process • Low-cost production 	<ul style="list-style-type: none"> • Organic solvents are used • Less effective 	<ul style="list-style-type: none"> • Micro/nano-scale fibers • Wound dressings • Cylindrical capsules • Film patches • Composite films • Dual-core matrices 	[87]

4.1. Vat Photopolymerization Printing Technique

Vat photopolymerization 3D printing method is the process in which high energy light is ejected onto the

vat of liquid photopolymer to fabricate the solid objects. The polymer forms due to the reactive species generated from the photoinitiators under the radiation. Recently, researchers have developed novel

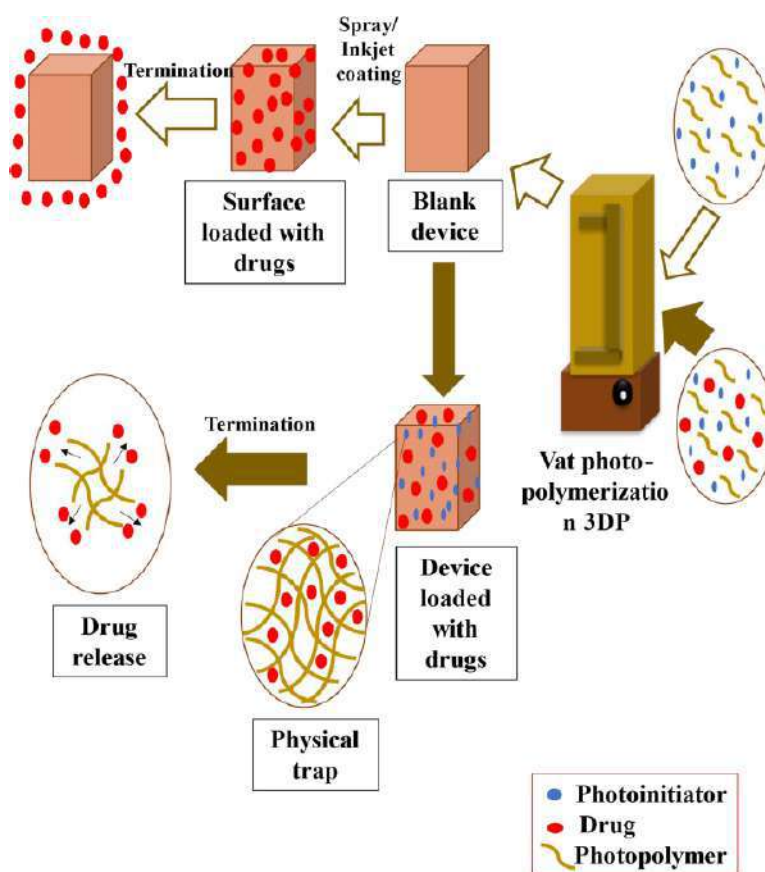


Fig. (6). A schematic illustration of VAT photopolymerization 3D printing technique for drug delivery system preparations. (*A higher resolution / colour version of this figure is available in the electronic copy of the article*).

photopolymers that have shape memory properties. This can be used to tailor the smart devices by formulating the water-responsive shape rearrangement 3D structures with the hydrophilic or hydrophobic complex based on poly (propylene glycol) dimethacrylate (PPGDMA) and poly (ethylene glycol) diacrylate (PEGDA) [46]. It has numerous applications in tissue engineering, versatile drug delivery, and biomedical devices [47]. Fig. (6) shows graphically how vat photopolymerization 3D printing can be used to create devices that are loaded with drugs. This can be done in one of two ways: either by adding the drug directly to the liquid resin before printing or by adding it to a blank device after printing [48]. In the first scenario, magnetic stirring at room temperature is used to completely dissolve or uniformly disperse the medication in a resin made up of a photoinitiator and a photopolymer. The medication is then physically confined in the cross-linked polymeric network after printing. The medicine is released *via* diffusion from the swelling matrix once the device has been disseminated into a dissolving media. For blank devices, conventional drug loading meth-

ods based on adsorption, such as spray coating and dipping, can be used to integrate the medication. Alternatively, by soaking the blank device in a drug-concentrated solution, the drug can be absorbed into the polymer network. Post-loading **minimises** potential drug deterioration while pre-printing or printing, even if it adds an extra production step. Moreover, there are four main types of vat photopolymerization processes, which are as follows: Stereolithography (SLA), Continuous Light Interface Production (CLIP), Two-Photon Polymerization (TPP), and Digital Light Processing (DLP) [49].

4.1.1. Stereolithography (SLA) Printing Technique

SLA technology is the first technology that is available for commercial purposes [4]. SLA printing method uses an ultraviolet laser to photopolymerize the photosensitive liquid resins [50, 51]. The SLA printer system can either be top-down, in which the platform is below, and the UV laser is above, or bottom-up, in which the platform is above, and the UV laser is below [28]. The first step of SLA is scanning a

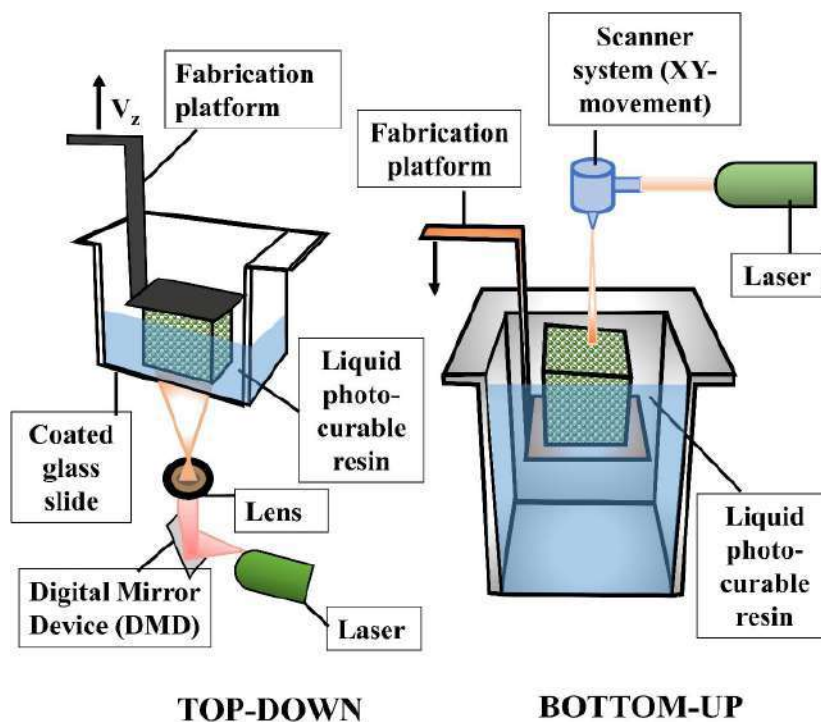


Fig. (7). A schematic illustration of top-down and bottom-up approaches of SLA 3D printing technique. (A higher resolution / colour version of this figure is available in the electronic copy of the article).

thin layer of liquid resin along with the drug for polymerization by using a photoinitiator. The adhesion of the next layer on the basic layer takes place due to the curing depth being a little bit larger than the thickness of a single layer, which results in the polymerization between the resins and unreacted compounds in two adjoining layers. This cycle takes place till the product is formed. After the process, unnecessary resin and photoinitiator should be rinsed with alcohol to avoid the toxicity of resin and to develop the mechanical properties of the object by using a UV oven [28, 52, 53]. Additionally, when drugs, excipients, and resins form a homogeneous mixture with each other, they can be absorbed into it due to polymerization and cross-linking [54]. Hence, it is necessary that materials used in SLA have photo-curable properties for photo-cross-linkage.

The advantages of SLA include excellent resolution (20 μm), less thermal stress involved, less demand for properties and chemical structure of drugs or excipients, and patterning precise structures [28, 55]. Therefore, SLA has applications in hydrogels, microneedle patches, and fabricating oral solid dosages [56-60]. However, it has some drawbacks, like the limited formulation for dosage formation, as SLA can barely use a particular resin formulation at a time of a single printing process, except the earlier formulation is replaced

with the latest formulation if the printing is discontinued. Although some photocrosslinkable polymers have been developed over the past few years, such as Gel-MA and PEGDA, photosensitive polymers are limited and are FDA-approved [61-63]. Hence, SLA is a potential tool for the pharmaceutical industry (Fig. 7).

4.1.2. Digital Light Processing (DLP) Printing System

In this printing system, liquid photopolymers are cured by photon exposure in a layer-by-layer form. The building platform is immersed in resin, and the polymerized resin layer is at the bottom of the vat during the printing process. This method prevents direct contact with the air, making the printing process less vulnerable to oxygen inhibition [64]. The 3D material through the DLP printing system was prepared by Yang *et al.* [65]. It was found that robustness, printability, drug loading capacity and drug release profile were highly dependent on the height of the layer, plasticizer addition, emission time, and concentration of PEGDA. When compared with SLA, the DLP printing system is a fast process, allowing less usage of resin to develop 3D objects and instantly solidify the complete layer [66]. DLP has applications in the construction of drug-delivery devices and personalized medicine (Fig. 8) [47].

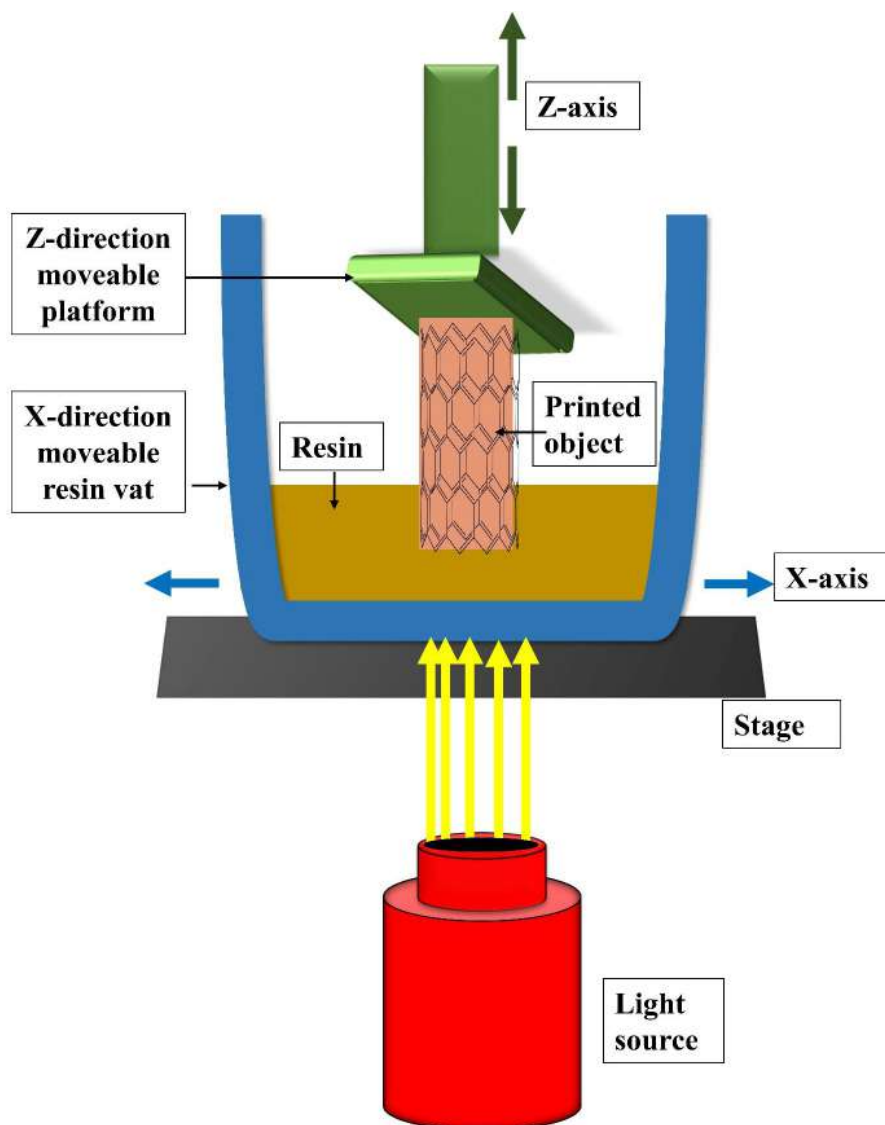


Fig. (8). A schematic illustration of the DLP 3D printing technique. (A higher resolution / colour version of this figure is available in the electronic copy of the article).

4.1.3. Continuous Light Interface Production (CLIP) Printing Technique

In the CLIP printing method, 3D objects are formed by a continuous fabrication process instead of a layer-by-layer manner. In 2014, Joseph DeSimone *et al.* prepared the CLIP printing system [67]. The dead zone is a thin layer of liquid interface between the liquid resin and the printed parts created by the CLIP system using an oxygen-permeable window [68]. This dead zone prevents photopolymerization at the interface, permits resin to flow freely under the window surface, and removes the need for an intermediate resin re-coating step for each layer, which is the most time-con-

suming procedure in DLP printing [69]. It has advantages over the SLA or DLP method, such as predictable mechanical features and consistent molecular structure of a 3D object. The CLIP technique includes the mask device fabrication for the microneedle coating and was developed by Caudill *et al.* [70]. In addition to this, the coated mask was applied for the regulated fast delivery of model proteins (such as bovine serum albumin, lysozyme and ovalbumin) from the microneedles into the skin and also the possibility of co-delivery of various antigens/ proteins through a single microneedle. Therefore, it has applications in the fabrication of transdermal drug delivery devices (Fig. 9).

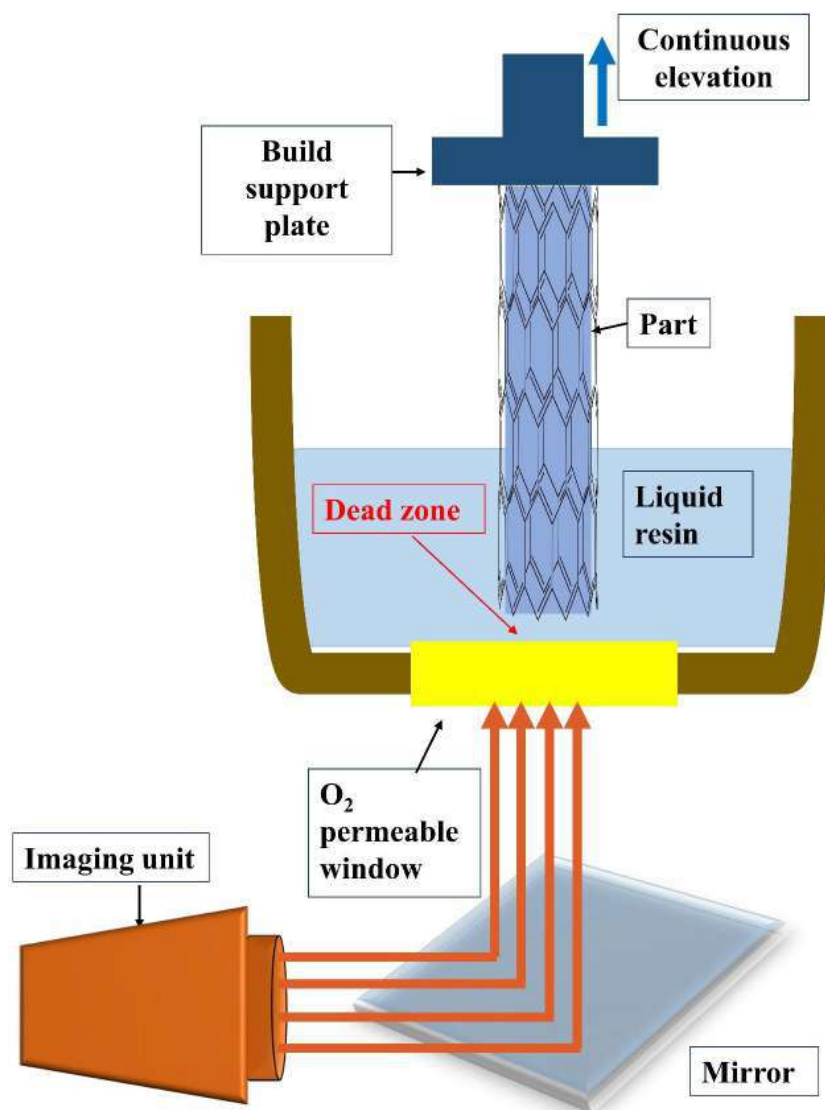


Fig. (9). A schematic illustration of CLIP 3D printing technique. (A higher resolution / colour version of this figure is available in the electronic copy of the article).

4.1.4. Two-Photon Polymerization (TPP) Printing Technique

TPP is a microfabrication technique in which near-infrared femtosecond laser sources are exposed to a photosensitive resin. Photosensitive polymers absorb two or more photons at the same time in the non-linear optical process and later, the regional resins get solidified to form 3D nano/microstructures [71]. Additionally, the resolution of TPP is influenced by the exposure time, photoinitiator ability and laser power density [72]. Furthermore, TPP is capable of developing drug-encapsulated particles from polylactide (PLA) based photocurable polymers. There are several achieve-

ments of the TPP printing process. Shavkuta *et al.* used TPP in conjunction with a micromolding process to design the particles loaded with insulin from methacrylate-functionalized PLA [73], and thus, this combination is useful for drug carriers with a controlled drug release profile, adaptable size and shape. Also, Cordeiro *et al.* used the TPP 3D printing technique to manufacture several designs of microneedle array templates [74]. This microneedle was found to be efficient in drug delivery and better at skin insertion. Besides this, Do *et al.* used the TPP method to construct rhodamine B-loaded poly (ethylene glycol) dimethacrylate (PEGDMA) devices [75]. Therefore, it has applications in the fabrication of drug-delivery devices (Fig. 10) [47].

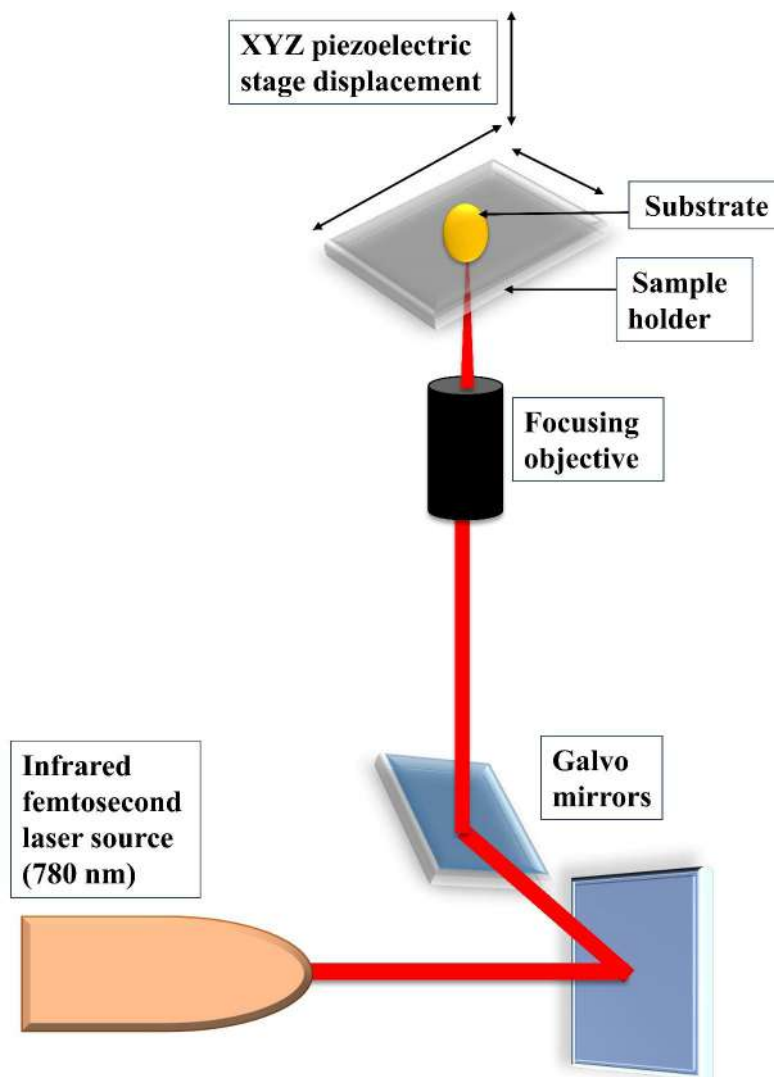


Fig. (10). A schematic illustration of TPP 3D printing technique. (A higher resolution / colour version of this figure is available in the electronic copy of the article).

4.2. Selective Laser Sintering (SLS) Printing Technique

SLS is a laser-based 3D printing technique that uses the laser beam of CO₂ rather than the binders for the accurate sintering of a particular area of powders in every layer. It employs heat through a laser beam and combines the powder to form a 3D structure. There are three main components of SLS, which are the laser system, powder bed, and spreading platform [28]. The first step of SLS is to produce long filaments, which include thermoplastic polymers, by using hot melted extrusion and active pharmaceutical ingredients (APIs) [76]. In SLS, commonly used thermoplastic polymers are as follows: polylactic acid (PLA), polycarbonates (PC), polymethylmethacrylate (PMMA), polyvinyl al-

cohol (PVA), polylactide (PLLA), polyamides (PA), polyurethane (PU) polyethylene (PE), poly(ether-ether-ketone) (PEEK), and polycaprolactone (PCL) [77]. The process chamber is filled with inert gas, commonly nitrogen, to avoid the oxidation of materials. Moreover, the process chamber works at a temperature that generally ranges less than the melting point of raw materials (40-50°C) for the entire printing process, and thereafter, the powder must be cooled to eliminate stress and curl deformation [64, 78]. The excellent sintering process is obtained when the size of powder particles ranges from 58-180 μm, and the thickness of the layer ranges in size around 0.1-0.3 mm [77, 79]. SLS has several advantages, such as solvent-free, high resolution (approx. 30 to 60 μm), single step

method for drug delivery as well as less time consuming due to the absence of liquid binders so that the evaporation of solvents is not required [80].

In recent years, SLS has been widely acknowledged due to the easy disintegration of drugs by using high-energy laser beams. It has been found that SLS has applications in the drug delivery system and tissue engineering [81-85]. In 2017, Fina *et al.* developed paracetamol tablets by using Kollicoat IR, which includes an immediate release feature, as well as Eudragit L100-55, which includes a modified release property [80]. It has been observed that the mechanical properties of this tablet fulfil the need of the US pharmacopeia, and also, no degradation of the drug was found. Additionally, Hamed *et al.* applied SLS printing technology to manufacture amorphous lopinavir (LPV), which is an inhibitor used to treat the HIV virus and study the formulation outcomes [86]. In this way, SLS received huge attention in the pharmaceutical field (Fig. 11).

4.3. Extrusion Molding Printing (EMP) Technique

It is a very often used methodology that is primarily categorised into three types based on the molding substances: Pressure Assisted Microsyringe extrusion moulding method (PAM), Fused Deposition Modeling method (FDM), and Melt Extrusion Deposition (MED) 3D printing method [17, 87].

4.3.1. Fused Deposition Modeling (FDM) Printing Technique

FDM, also known as fused filament fabrication, is a widely used 3D printing technique. This method works by converting the drug-loaded polymers into a semi-fluid state by heating them to a critical state and then ejecting them through the printing nozzle based on the parameters, which solidify over the printing surface, and the product can be achieved [88]. This technique involves several parameters in its working phenomena, such as nozzle diameter, product filled percentage, extrusion speed, temperature, layer width, and head movement printing speed. Moreover, the preparation of drug-loaded filament is the fundamental step in the development of FDM, which is obtained by the passive soaking technique. In this technique, filament substances are placed in the solvent of ethanol or methanol, which contains the drug, and then dried. Nevertheless, due to the less probability of getting drug load through this approach, Hot Melt Extrusion (HME) method, including single or twin screws, is an alternative way for the filament preparation. The filament substances that are mainly used are as follows: Polyvinyl alcohol (PVA), Polycaprolactone (PCL), Polylactic Acid (PLA), polylactide-coglycoside (PLGA), and other derivatives of cellulose [31, 89-93]. Despite this approach, the preparation of drug-loaded filament can be avoided by

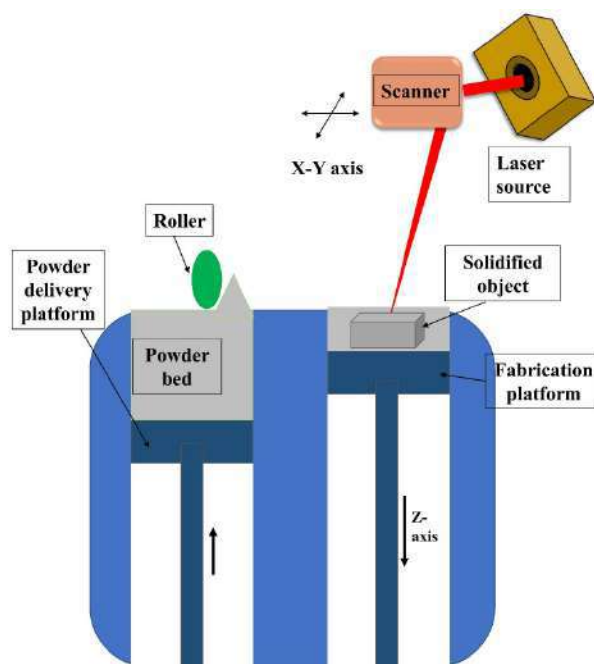


Fig. (11). A schematic illustration of SLS 3D printing technique. (A higher resolution / colour version of this figure is available in the electronic copy of the article).

making the polymer compatible with the 3D printer as well as the original form of the drug as a raw material [94]. Additionally, dosage forms based on TPU, which are loaded with 60% (w/w) crystalline drug, are efficiently developed by Verstraete *et al.*, whereas the HME method linked with the FDM method is also effective in developing a tablet, as discussed by Zhang *et al.* in 2017 [95, 96]. These results demonstrated the potential of FDM technology in the application of solid forms of dosage preparation.

The advantages of the FDM technique include low cost, easy operating process, accuracy, promising parameter properties, an association of HME, excellent mechanical properties of the product and also, it is more flexible to design complex pharmaceutical procedures, such as chamber-like and core-shell structures [97, 98]. However, the disadvantages of the FDM technique include high-temperature heating action in printing, generally greater than 150°C, which is not appropriate for thermally unstable drugs like 4-aminosalicylic acid, which decays over 210°C [99].

Through this study, various modifications are made in FDM technology to **minimise** thermal stress, such as the preparation of drug-loaded filaments by using low-melting point povidone, which was successfully developed by Kollamaram *et al.* [100]. It showed that low-melting point filaments can reduce the temperature of the printing procedure up to 90 °C. Another study showed that the temperature of printing can be diminished by eliminating filament with soft extruded polymer threads as well as preparing filament by using water as a temporary plasticizer that reduces the temperature up to 54 °C [101, 102]. In addition to this, researchers have found that Direct Powder 3D Printing (DPP) is used for tablet tailoring, which is a single-step FDM process with the absence of HME. In this process, after filling the powder into a stainless-steel extrusion cartridge, the powder mixtures were heated, which led to the printing of tablets into honeycomb structures [103]. FDM technology has major significance in the pharmaceutical field (Fig. 12).

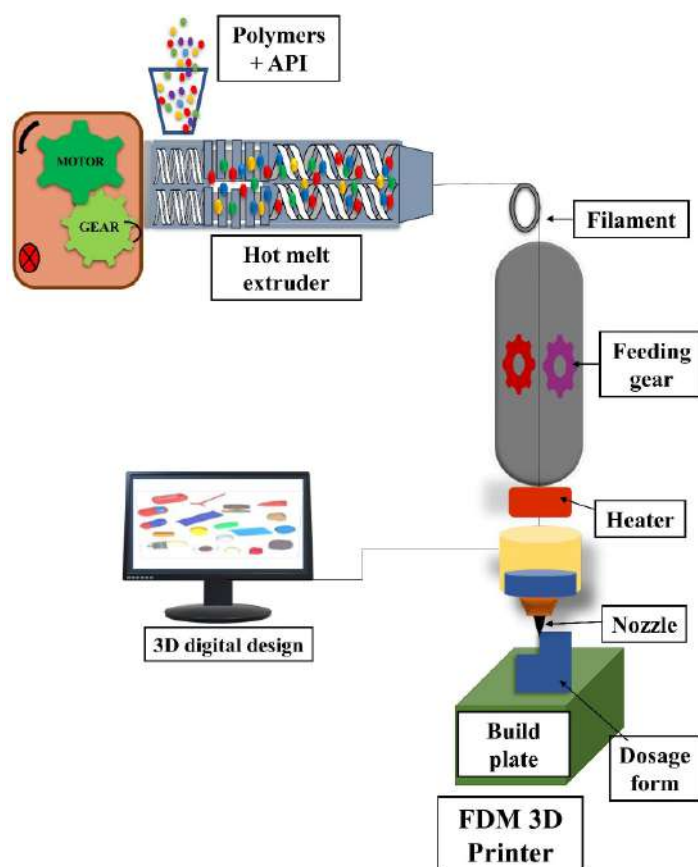


Fig. (12). A schematic illustration of hot melt extrusion coupled with FDM 3D printing technique. (A higher resolution / colour version of this figure is available in the electronic copy of the article).

4.3.2. Melt Extrusion Deposition (MED) Printing Technique

The Melt Extrusion Deposition (MED) 3D printing technique belongs to the extrusion-based category. Unlike FDM technology, it offers a significant advantage by eliminating the need for filament preparations when working with drugs and excipients during the printing process. In this method, the initial materials are active ingredients and excipients in the form of powder. The powder of materials and active pharmaceutical ingredients were directly used for MED without any additional processing. The powder feedstocks were converted into molten states, and layer-by-layer deposition was followed to produce the desired geometries of the object. MED filament-free method is also reliable for the production of high drug loaded (60%) thermoplastic polymers. The nozzle printer array has high throughput, precise control of deposition, and operation of multiple materials that can build the accurate, reproducible and large-scale production of the desired product. Moreover, Good Manufacturing Practice (GMP) compliant MED 3DP technology was developed in which each printing stations contain one nozzle that is

synchronised with each other for the fabrication of certain parts of the structure, such as shell, delay layer, core, filler, etc. Therefore, it leads to the tailoring of multi-component tablets by using compartment models, which provide controlled kinetics, on-set time release, and mode of release and fulfill desired product needs.

The predictability of tablet release serves as the platform for the 3DP Formulation by Design (3DPFbD) approach, which is a novel development approach that provides an effective process of product development. It has several advantages, such as excellent compatibility with drugs or excipients, a broad range of excipients that can be used, no filament preparation, no degradation of product, and GMP compliance. It is crucial for controlled drug delivery. Many desired aspects of current pharmaceutical production are also implemented, resulting in a compact, modular, continuous manufacturing, scalable, versatile, and intelligent MED 3D printing system. The technology enables the efficient production of modified-release medication tablet products at any required scale, suggesting a viable route for next-generation pharmaceutical manufacturing (Fig. 13) [17].

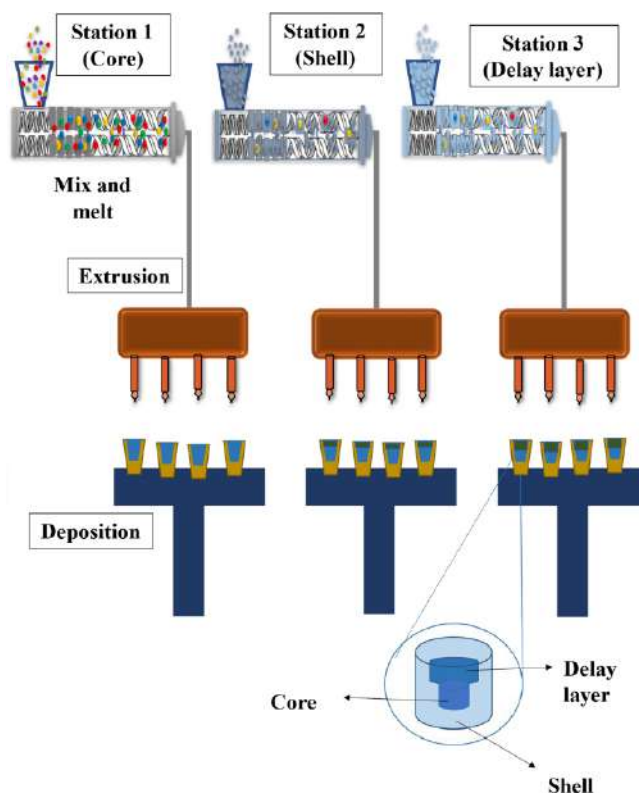


Fig. (13). A schematic illustration of the fabrication of core-shell structured tablet with a delay layer by using MED 3D printing technique. (A higher resolution / colour version of this figure is available in the electronic copy of the article).

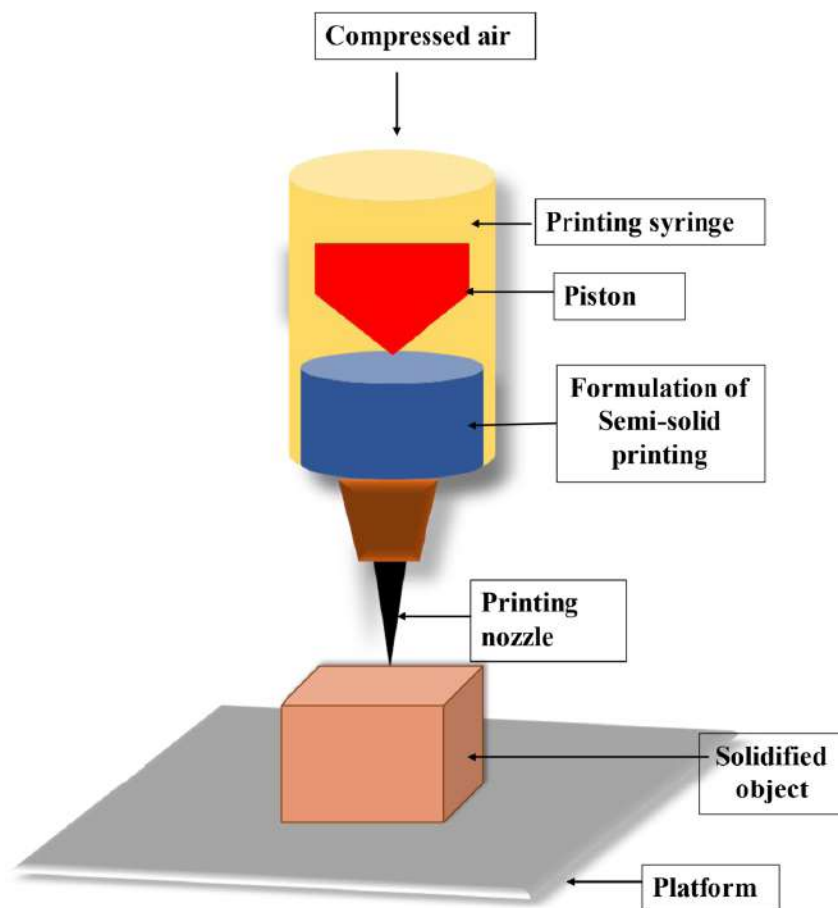


Fig. (14). A schematic illustration of PAM 3D printing technique. (A higher resolution / colour version of this figure is available in the electronic copy of the article).

4.3.3. Pressure-Assisted Microsyringe (PAM) Printing Technique

PAM is a 3D printing technology that is also known as the Semi-Solid Extrusion method (SSE) [104]. The extrusion can be pneumatic, solenoid or mechanical piston based [28]. This method exerts pressure or screw gear rotation on the syringe-based print head for the uniform extrusion of the semi-solid materials and places it on the printing surface layer by layer for the printing process according to the command of the software. The exerted pressure for the printing is required around 0.4-3.8 bar and the syringe print head diameter is around 0.35-0.85 mm. In the PAM technique, raw materials play a significant role in the semi-solid process due to the pressure directly exerted for the extrusion of semi-solid materials into the head of the printer without distortion. It allows the microstructure production, which is around 5-10 μm or less [29]. The PAM method has advantages like no requirement

of heating, so it is appropriate for thermally unstable drugs, for example, guaifenesin [105, 106]. However, it has some drawbacks, such as the usage of heavy machinery tools, *i.e.*, hot extruder motor element for the extrusion process by applying torque, as well as the usage of organic solvent for making semi-solid materials, which may not be suitable for the remaining organic solvents in the tablets [107, 108]. The PAM technique is potentially good for pharmaceutical applications (Fig. 14).

4.4. Inkjet Printing Technique

The inkjet printing method is based on the placing of liquid droplets onto a substrate under the command of a digital controlling system. The combination of drugs and other materials, which are known as ink, are settled as droplets in a layer-by-layer form over the substrate. Inkjet printing is mainly classified into two types, namely Drop on Demand (DoD) and Continuous Inkjet printing (CIJ) (Fig. 15) [63, 109].

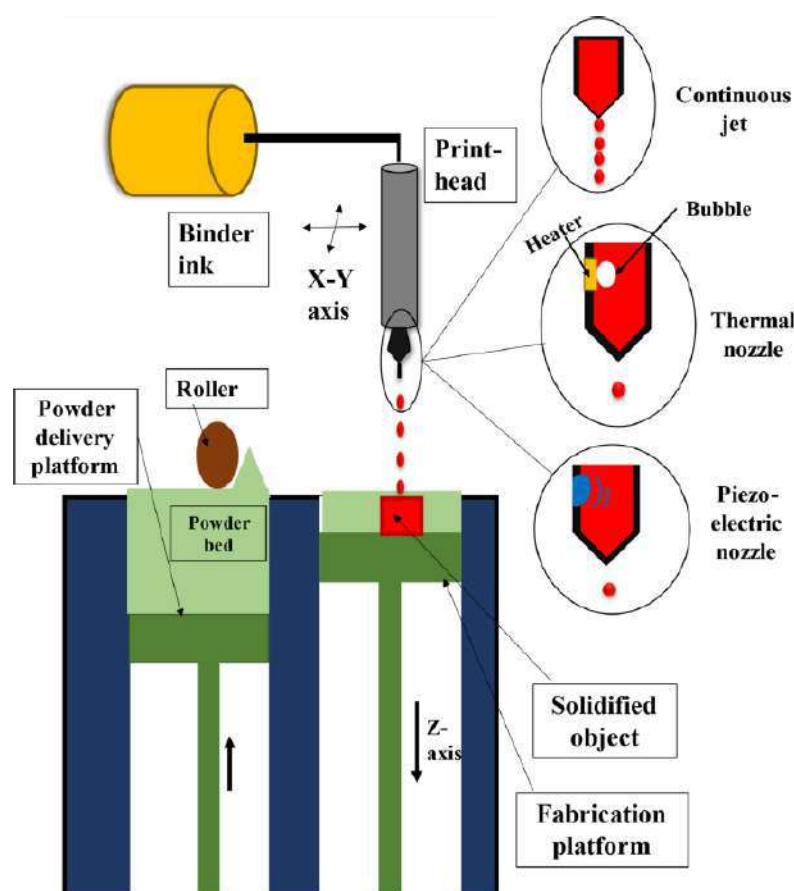


Fig. (15). A schematic illustration of inkjet-based 3D printing technique. (A higher resolution / colour version of this figure is available in the electronic copy of the article).

4.4.1. Continuous Inkjet Printing Technique

This type of printer discharges a jet of droplets of liquid over a substrate in a continuous manner. The evenly sized droplets are formed due to the pressure generated into the inkjet, and thereafter, droplets discharge from the nozzle whose diameter is around 50-80 μm [29]. There are some advantages of continuous inkjet printers, which include rapid droplet ejection and no blockage in the nozzle. However, there are some disadvantages of this technology, which include unnecessary dispersion of ink, inflated maintenance, and low resolution [110].

4.4.2. Drop on Demand (DoD) Inkjet Printing Technique

This method only ejects the liquid droplets (10-50 μm diameter with 1-70 pL volume) when it is necessary over a substrate according to the command of the signal [29]. DoD inkjet printers have sources, which are present in the printhead, which provide kinetic energy to the droplets near every nozzle [111]. Also, this

kind of printer has many nozzles, which are around 100-1000; however, a single specialised printhead is present. There are several advantages of the DoD method, which include cost-effective, easy to use, high précised, controlled droplet sizes, and less wastage of drugs [28]. However, it still gains more attention as compared to the continuous inkjet printing [112, 113]. DoD inkjet printers are categorised on the basis of the printhead, namely thermal inkjet (TIJ) and piezoelectric inkjet (PIJ) printers [52].

In the TIJ technique, thermal energy is the signal used to eject droplets out of the nozzle. Here, printheads carry resistors to gain exposure to the ink (fluid) and induce electric current to generate heat. This thermal energy leads to the bubble formation from the volatile fluid; thereafter, it enlarges and discharges fluid in the form of droplets from the nozzle. However, it has some drawbacks, such as the degradation of thermally sensitive active ingredients due to the usage of resistors with high temperatures of around 200-300 degree Celsius [110, 114].

In the piezoelectric inkjet printer, a certain amount of electric voltage is given to the piezoelectric crystal/element/actuator, which changes its shape to generate a signal that further generates pressure, leading to the discharges of ink from the nozzle. Thereafter, the elements attain their original shape, and the nozzle is again filled with the fluid for the activation [113, 115]. There are some advantages of this technique, which include efficiency at room temperature due to the presence of more biocompatible and less volatile fluids [114]. Hence, the piezoelectric print head is **in** demand for numerous applications.

4.4.3. Miscellaneous Inkjet Printing Technique

4.4.3.1. Valve Jet Printing Method

This method is also known as electromagnetic printing, which is applicable in the pharmaceutical field and is based on small-sized solenoid valves. In contrast to the TIJ or PIJ, this technology is better due to its large orifice sizes, robustness, and ability to print coarser suspensions [116].

4.4.3.2. Glass Inkjet Printing Method

This method discharges the droplets at high frequencies, and it has shown applications in the pharmaceutical field due to the inertness of glass that will stay unreactive with other materials [117].

4.4.3.3. UV-based Inkjet Printing Method

This technology has UV photo-initiation along with inkjet printing, which is useful to harden the substances quickly. In this method, the ink contains cross-linked functional groups that get signals through light, and further, a photo-initiator is involved in the process [118].

4.5. Drop On Powder (DOP) Printing Technique

The DOP printing method is also known as binder jetting, drop on solid, and plaster printing technology [29]. It is an application of the inkjet-based printing method. In this method, the print head ejects the droplets so that it can combine the powder particles in a deposited powder over the surface [119] in layer-by-layer form, which is uniformly placed by using a roller. The nozzle of the printer contains binder fluid, which is operated to jet above the powder bed by moving in the x-y direction [28]. The ejecting droplets with binders, for example, hydroxyl propyl methylcellulose (HPMC) and PVP K30, are deposited on the powder bed at a controlled speed according to a certain pattern designed in the computer. The powder soaked the

liquid drops, which solidifies the layer. The solidification process that takes place in DOP is similar to the wet granulation used in tablet formation [120]. Solid bridges are formed due to the crystallisation of dissolved particles and the evaporation of the solvent. Furthermore, the layers are formed by sliding the previous layer of the surface along the vertical axis and then printing the new layer in place of the previous layer from the feeding cell. Furthermore, this cycle continues until it completes the construction of 3D objects. Many parameters are involved in the preparation process, like the droplet spacing, layer thickness, nozzle diameter, distance between the print head and spread powder, movement of the print head, droplet velocity, line spacing, and frequency of the droplets [121-123]. These parameters facilitate the behavior of drug release and physical properties (viscosity, concentration and surface tension) [124]. The flowing nature of printing ink depends on the physical properties, and it can be altered by adding binders or Active Pharmaceutical Ingredients (APIs), for example, HPMC, CMC-Na, PVP, HPC, and PEO [125-127]. In view of the fact that material integrity totally depends on the weak force rather than the mechanical compression force, the dosage forms are easily tailored with interlinked pores in the micro range for the preparation of tablets [128].

Moreover, DOP is **categorised** into two types based on the printhead, namely thermal and piezoelectric [121]. The thermal printhead allows a smaller number of solvents with high vapour pressure to vaporize. It uses a heater with a temperature of around 200-300 °C to vaporize a small amount of fluid, which forms small bubbles that eject the droplets [129]. It has been found that below 0.5% of the liquid in the print head comes under the influence of high temperature for a few microseconds [130] with no degradation of proteins (insulin and human growth hormone) for the thermal print head [131]. In comparison to piezoelectric print heads, thermal print heads are inexpensive for the fabrication process. The piezoelectric printhead contains piezoelectric crystals, which get charged by providing the voltage. This causes the distortion of the liquid, which ejects the drops from the nozzle. Hence, piezoelectric printheads are in more demand for various substances. Furthermore, there are advantages to the DOP method in post-processing, including the restoration of unprocessed powder and the removal of residual volatile solvent through thermal sintering [28]. Spritam, which is the first 3D printed drug, was constructed by using the binder jet-based zip dose method [34]. It is a novel microfabrication process that has application to construct dosage forms in a layer-wise fashion [132].

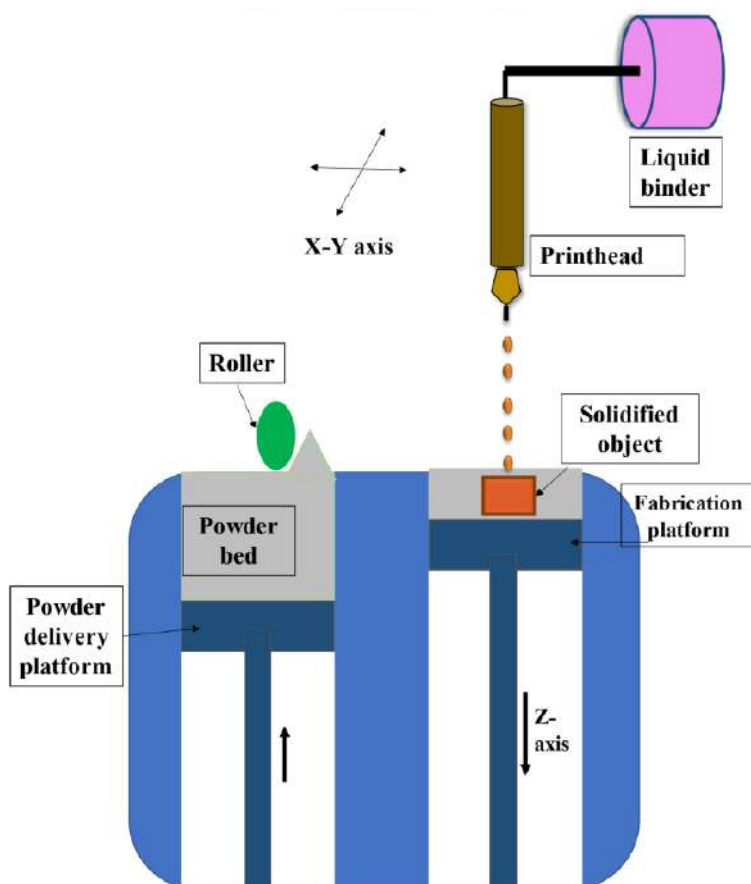


Fig. (16). A schematic illustration of DOP 3D printing technique. (A higher resolution / colour version of this figure is available in the electronic copy of the article).

However, DOP has some drawbacks as it shows defects in the printed product due to high fragility and low resolution. Therefore, further exploration of this method to overcome the problem is still needed (Fig. 16).

4.6. Electrohydrodynamic (EHD) Printing Technique

Electrohydrodynamic 3D printing is a growing technology that can model thread-like materials by placing the materials layer by layer to fabricate a controlled system. EHD has several components, which are required for the printing process: a thin nozzle print head, syringe pumps, a moving platform along the X-Y-Z direction with a controller, and a high-voltage power supply [133]. Several materials having viscosities between 1-10,000 mPa have been processed to develop drug carriers, such as polycaprolactone (PCL), polyvinyl alcohol (PVA), polyethylene oxide (PEO), and cellulose acetate (CA) [134]. There are several ad-

vantages of EHD technology, such as highly controllable resolution, providing a suitable atmosphere for polymers and many drugs like thermally stable drugs, manufacturing **micro-** to nanoscale fibers, a controllable digital system for deposition of materials, and fabrication of systematic complex geometries [135]. The complex geometries formed by this technology include dual-core graphene composite matrices, film patches, wounding dressings, cylindrical capsules, Janus fibers, and coreshells [136-141]. Hence, EHD 3D printing is a flexible approach for drug delivery and the fabrication of **personalised** medicines by printing a specific pattern of therapeutics on a porous film (Fig. 17) [129].

5. APPLICATION OF 3D PRINTING IN THE PHARMACEUTICAL FIELD

The use of 3D printing is expanding quickly across all industrial manufacturing sectors owing to its advantages for improving production efficiency and lowering the cost and quantity of defects by preventing human factors [142, 143]. Given its significant flexibility

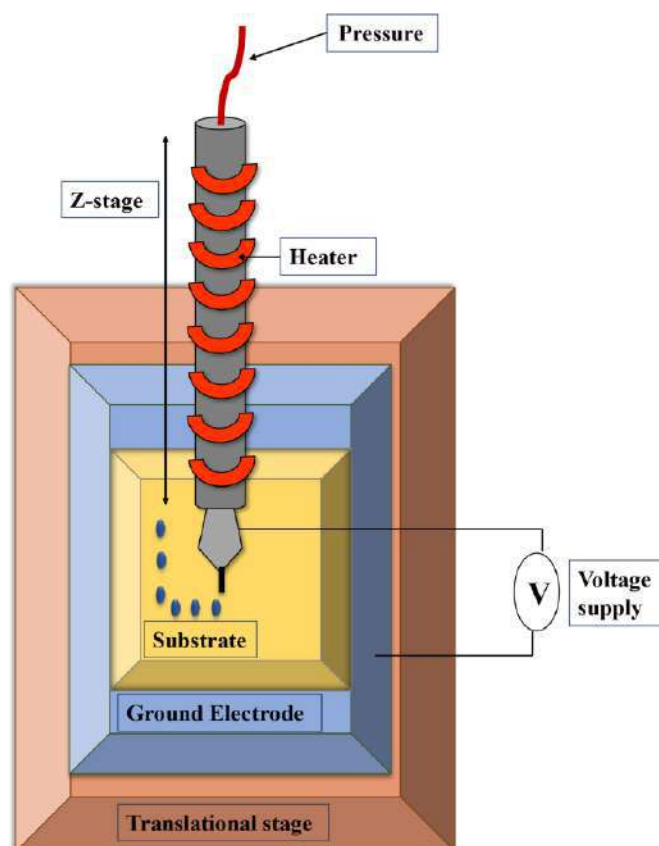


Fig. (17). A schematic illustration of the EHD 3D printing technique. (A higher resolution / colour version of this figure is available in the electronic copy of the article).

and ability to create a variety of simple to complex geometries, 3D printing has altered not only industrial production but also the emphasis on industrial automation. To produce high-quality drug products with improved process robustness, 3D printing is quickly pioneering pharmaceutical manufacturing in the field of biopharmaceutical product development, where there is a reliance on producing medications using conventional manufacturing techniques [13, 144].

Utilizing 3D printing technology to foster drug items has gained critical interest in the pharmaceutical industry and universities as 3D printing innovation becomes more accessible to drug researchers. The assembly of medication delivery systems with precisely engineered constructions and the production of **customised** medications are two expected effects of the use of 3D printing in the pharmaceutical industry that will help bring the development of pharmaceutical products into uncharted territory. Due to its potential benefits, such as improved productivity, complex drug release profiles, multiple dosing, single-step processes at low cost, and customization/personalization of drug deliv-

ery, 3DP has seen widespread use in the pharmaceutical industry. This updated technology is a very helpful tool for more accurate drug dispensing with tailored drug release to meet the particular needs of each patient. Additionally, **personalised** medicine offers 3D printing a previously unheard-of opportunity to address the difficulties associated with treating heterogeneous diseases. Below is a description of the momentous implications of 3D printing in the pharmaceutical field.

5.1. Pre-medical Assessment of New Drugs

Before the approval of any kind of drug for commercial use, the pharmaceutical properties of the active ingredients of the drug are thoroughly examined and **analysed** by scientists for clinical safety and efficacy purposes in the early phase of drug development. To overcome drug failure during early-phase development and fulfil the high demand for promising drugs, it is crucial for companies to rapidly identify suitable drugs at the low expense as early as possible during the drug development process, ideally within preclinical studies [145, 146]. The 3DP technique can be considered for

this purpose, as it has proven its ability to fabricate dosage forms in the early phases of drug development with fewer resources, time and human efforts [147, 148]. 3DP is a very flexible procedure that makes it simple to modify doses to meet the demands of the trial. By physically changing the tablet's size or infill level, doses may be adjusted quickly and easily [91]. Whereas in conventional production, thorough pre-formulation studies, large batch sizes, scaling up and optimising the formula so as to create the desired dosage forms and significant labour costs are required [50, 149].

5.2. Person Specific Drugs (**Personalised** Medicine)

The majority of patients are supported by conventional dosage forms, which are only based on fixed strengths. **Personalised** medicine aims to offer the best medication at the optimum dose for the patient's individual symptoms at the right time according to the patient's genetic, physiological, or pathological background, taking into account additional variables, such as genetic makeup, gender, age, and weight for dose titration and dosage form design [14]. They increase patient compliance and are cost-efficient, more effective, and safer [24]. To provide such **personalised** drugs to treat specific patient populations for all age groups, the 3D printing technique can be a better tool, especially for treating complex diseases like Alzheimer's disease, cancer, and epilepsy [142, 150, 151]. 3D printing offers the preparation of a drug delivery system (DDS) with various doses, geometries, substances, and adjusted release rates considering the patient's personal characteristics [78, 152]. Additionally, it is possible to print pills in a kid-friendly format for kids who have trouble swallowing [98]. The 3D printing method does not require the installation of a comprehensive manufacturing setup with upscale equipment as with conventional methods, and it is flexible for on-site production. In this way, 3D printing techniques encourage a **personalised** drug approach [153-155]. In short, individualising and **personalising** therapies can enhance the therapeutic result, lessen side effects, and boost patient adherence to the regimen.

5.3. Complex Drug Therapies

In order to maintain drug levels in the blood for the desired therapeutic action for extended periods of time, patients frequently need to take conventional dosage forms of multiple pills for a single disease indication [156]. Such a strategy has a number of disadvantages, including low patient compliance, missed doses that cause blood levels to fluctuate, and high costs. With the use of 3D printing technology, it is now feasible to

design complicated, unmoldable dosage forms with distinctive properties and improved efficiency to facilitate long-acting drug therapy. Complicated dosage forms have narrow therapeutic parameters that would not be achievable with traditional manufacturing methods [155-157]. Such complex drugs loaded with high dosages are referred to as Fixed-Dose Combinations (FDCs) or polypills. It is now possible to individually adjust dosages and release patterns as well as the co-formulation of pharmaceuticals with interaction potential by physical separation of medications with the help of layer-by-layer printing [155]. A 3D-printing method of drug delivery would greatly benefit medications, such as asthma, cancer, cardiovascular diseases, TB, and epilepsy, where polypills are advised for patients.

5.4. Fabrication of Novel Drug Delivery Systems

The creation of solid pharmaceutical dosage forms has been significantly influenced by 3D printing. Compared to traditional methods, it offers the design of dosage, providing a great deal of flexibility and efficiency [158]. The process of making solid dosage forms traditionally entails a number of batch-wise operations, including mixing, granulation, milling, compaction, and compression. As a result, conventional multistep manufacturing is linked to increased batch-to-batch variability and decreased process robustness. The development of a variety of dosage forms, including solid dosage forms, implants, stents, and transdermal, rectal, and vaginal devices, can be done quickly and easily with 3D printing due to its high robustness, accuracy, and precision [36, 124, 156]. Additionally, it decreases the number of manufacturing steps, associated costs, failure risks, and quality consistency.

5.4.1. Oral Solid Dosage Forms

The easiest way to administer API is through oral dosage forms, which also have higher patient compliance than any other method. The layer-by-layer formation principle that underlies 3D printing gives the flexibility to produce geometric dimensions that are difficult to achieve using conventional approaches. These dosage forms can contain multiple drugs and excipients to achieve altered drug release properties. 3D printing gives you the freedom to alter the tablet's geometry, use different infill densities, or incorporate multiple medications for a release profile based on the lag phase. By using CAD, these features are obtained by altering the dosage form's geometric size and shape. Additionally, altering the film's characteristics by the use of plasticizers, such as polyethylene glycol (PEG), triethyl citrate, talc, or stearic acid, as well as modifying process variables like the roller printing speed, can

help manage the performance of the drug release [144] [143]. Children's favourite cartoon or animal-shaped tablets can be designed and printed using 3D printing technology by precisely adjusting the geometric shapes of the tablet [159]. Using extrusion-based 3D printing technology, paediatric-friendly chocolate-based chewable tablets were recently fabricated into six shapes resembling the simple structures of cartoon characters [160]. Additionally, 3D printing enhances the pharmacokinetic performance and solubility of poorly water-soluble drugs [122, 156, 161].

For disease indications that demand a quick start to the drug's activity, immediate-release tablets are necessary. These come in a range of dose forms, including buccal and sublingual tablets, orodispersible tablets, tablets for solution, fast-dissolving tablets, etc [13]. The traditional manufacturing of such formulations involves a number of steps, high-end equipment, and the selection of the best excipients in the right amounts to achieve the desired performance. Fabrication of such drugs with 3D printing is more productive. The tablets are typically printed using IJP, which has the medication distributed in a wet binder solution. To construct the entire tablet, the powder mixture for substrate production is applied layer by layer to the surface. Drug-loading filaments can be created using polymers like polyvinyl pyrrolidone (PVP), hydroxypropyl methylcellulose (HPMC), hydroxypropyl cellulose (HPC), and polycaprolactone. The effectiveness of medication loading and release can be changed by adjusting the polymer concentrations in the filament [162-164].

The choice of appropriate excipients or binder materials, as well as manufacturing processes for creating the desired dosage forms, are the main factors influencing dosage form development using 3D printing. Drug delivery systems created using 3D printing should undergo routine testing, including evaluations of hardness, friability, disintegration, and dissolution time, just like conventional dosage forms do.

Modified-release dosage forms offer a typical medication release profile according to the needs of the dis-

ease, in contrast to immediate-release tablets. Enteric release, delayed release, controlled release, and extended-release systems are just a few of the modified-release systems that have been created [98, 165, 166]. Biphasic release systems, multi-active tablets, and pulsatile drug delivery systems are examples of modified-release systems. 3D printing can also be used to create formulations with the complicated geometry necessary to generate a typical medication release profile.

5.4.2. Transdermal Drug Delivery System (TDDS)

Depending on the patient's needs, the 3D printing technique has been effectively used in a number of transdermal formulation strategies, including implants, microneedles, masks, and patches for both systemic and local API administration. Using a 3D printing technique, the geometry of the administered implant can be tuned according to the application site [167]. Dissolvable micro-needles developed using a piezoelectric ink-jet printing technique were fabricated with seasonal influenza vaccine using a drop-on-drop deposition technique, which aids in vaccine stabilization for percutaneous administration [168]. Transdermal films containing indomethacin produced using the piezoelectric ink-jet printing technique demonstrated effective drug penetration as well as better anti-inflammatory action when compared to a higher printing density of 600 Dots Per Inch (DPIs) [169].

6. ADVANCES IN 3D PRINTING FOR THE MEDICAL INDUSTRY

6.1. Branch of Medicines

Emerging as a modern and swift manufacturing method, three-dimensional (3D) printing has shown great potential in the medical and drug delivery fields. In this section, we explore the current advancements of 3D printing technology in healthcare and drug delivery, conveniently presented in Table 2 (Fig. 18).

Table 2. 3D printing technology in the medical field.

3DP technology	Formulation	API	Special characteristics	Medical field	References
SLA	Spherical implant	Ifosfamide, methotrexate, Cisplatin (CDDP)	Transdermal microneedles	Oncology	[290]
Power extrusion	Tablet	Lopinavir+ ritonavir	Mini tablets (6mm)	Paediatrics	[291]
FDM	Orodispersible	Aripiprazole	Personalized medicine	Geriatrics	[292]
Melt-extrusion	Tablet	Levofloxacin	Personalized medicine	Ophthalmology	[184]
DLP	Fast dissolving tablet	Diclofenac	Microneedle	Dermatology	[293]
SSE	Hydrogel patches	Doxorubicin	Solid self-emulsifying formulations	Virology	[294]

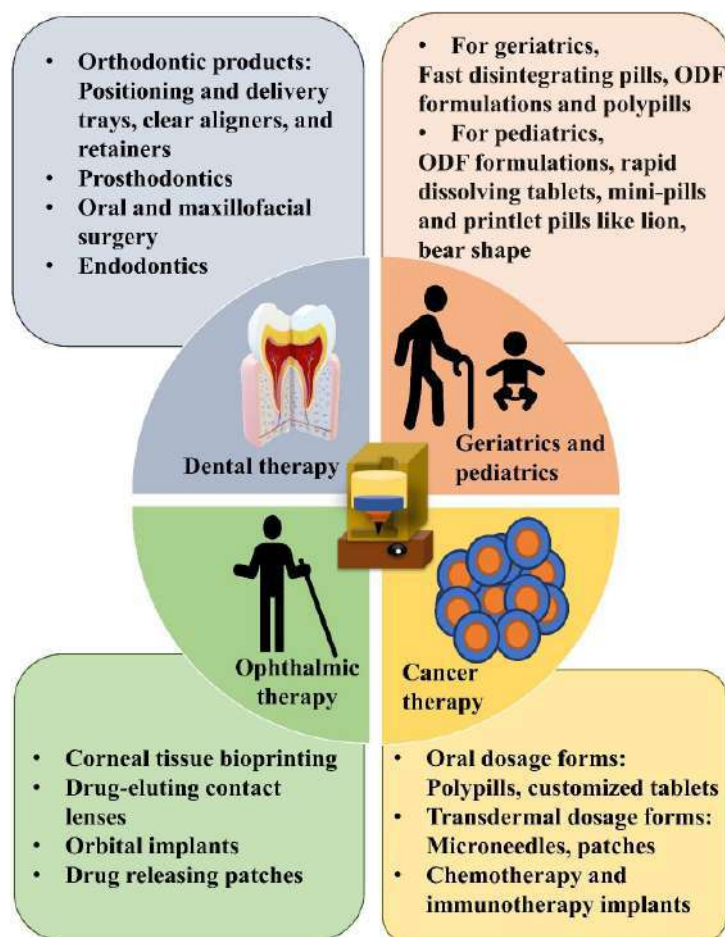


Fig. (18). Application of 3D printing technique in different branches of medicine. (A higher resolution / colour version of this figure is available in the electronic copy of the article).

6.1.1. Pediatrics

Children's unique preferences for dosage form, taste, shape, and scent make them the most challenging segment of the population. Even though oral administration may appear most practical, it can be challenging when dealing with young children. A youngster might simply reject one dose form over another due to petty preferences for shape, colour, or flavour. This is where 3D printing may help and cater to each person's preferences [170]. Orally Dissolving Film (ODF) formulations, rapid dissolving tablets, and mini-pills created using 3D printing seem appropriate for delivery because swallowing is an issue in younger children.

According to a study on children's dosage form preferences, kids preferred mini-tablets with a 4 mm diameter over other formulations [171]. Giving dosage forms in the flavour and colour of their choice to children can boost their adherence to and compliance with their medication [172]. By extruding HPMCAS- and

PEG-based filaments loaded with indomethacin to produce formulations of various forms, such as a heart, ring, bottle, bear, and lion, Scoutaris *et al.* created candy-like formulations for paediatric medications with improved palatability [173]. Wang *et al.* (2020) created taste-masked donut-shaped tablets for pedological uses [174]. As a result, 3D printing has advantages over conventional production methods when producing paediatric dose forms. From the foregoing, it may be inferred that dosage forms can be made with the precise dose, shape, and size that will improve paediatric populations' drug adherence, therapeutic outcomes, and safety.

6.1.2. Geriatrics

Most urbanized nations have greater life expectancies and, as a result, a generally ageing population, with the majority of people anticipated to live above the age of 65. These nations also typically have nutri-

tion, cutting-edge medical facilities, and better patient care. Senior patients suffer from a variety of illnesses, including neurological ones, such as dysphagia and dementia. Compared to adults in the overall adult population (18 to 60 years old), medications and the elderly (those above 65) face far more complex and difficult management issues due to the latter typically requiring different characteristics from adult drugs. As swallowing problems get worse with age in the majority of the senior population, it can be difficult to take medications as prescribed. Fast-disintegrating pills and orodispersible film formulations can be used to treat this issue. The elderly population has a variety of illnesses that necessitate numerous medications, which leads to polypharmacy problems [175]. The problem of polypharmacy can be overcome by using poly-pills that are 3D printed specifically for the needs of the patient. Additionally, some of them experience dementia, which can hinder drug compliance. This can be avoided by using 3D-printed dosage forms with embossed graphics that can be **customised** for each patient and show the date, time, and/or day of the week for administration [176].

6.1.3. Oncology

A CT scan or MRI is the first step in the diagnosis, staging, and planning of a tumour's treatment. The two imaging methods help to determine the shape, volume, size, and extent of tumours as well as reveal information regarding metastasis. In CAD, **customised** tumour models can be created based on a patient's CT or MRI scan. To investigate applications in diagnosis and treatment, these models are further printed and closely match the cancer structure [177].

The process of creating **customised** medications starts with a cancer examination and is largely accomplished through 3D printing. Using an extrusion-based printing approach, a **personalised** anticancer drug delivery prosthesis that enables targeted chemotherapy delivery was created. A polydimethylsiloxane carrier prosthesis that included paclitaxel and doxorubicin successfully delivered the medications for more than 3 weeks. The mice's breast cancer spread and recurrence were prevented by the 3D-printed **personalised** prosthesis [178]. To encourage localised drug distribution, three-dimensional printed microneedles with different anticancer agents have been extensively explored for skin cancer.

In addition to aiding in the delivery of anticancer medications, three-dimensional printing also helps with cancer diagnosis, particularly when using cancer-specific diagnostic tools. Three different cancerous

cell types were successfully isolated using a 3D-jet-printed microfluidic device to separate cancerous cells from blood samples. The device was outfitted with anti-epithelial cell adhesion molecular antibodies that captured the circulating tumour cells (CTCs), which were then used for diagnosis and treatment planning [179]. To isolate CTCs, a similar microfluidic device using the negative enrichment of hybrid cells principle was created using the jet printing technique [180].

This technology can be used in the medical field to lessen the discomfort associated with cancer therapy. It might be compared to employing chemotherapy and radiation therapy as long-lasting cancer treatments. It works well when used for breast cancer [181, 182]. Tumour cells are extracted and printed during this process. This makes it easier to test out various medications and choose the best course of action for the patient [2].

6.1.4. Ophthalmology

Hydrogel-based formulations for 3D-printed medication patches can also enable drug release effectively in the eye, such as the conjunctiva, without impairing vision or making blinking uncomfortable. In order to provide unique dosages that may be tailored to the needs of patients in hospitals, Tagami *et al.* developed lyophilized ophthalmic patches [183]. Levofloxacin was an antibiotic that was present in the drug-releasing patches. A hydrogel-based bio-ink made of hydroxypropyl methylcellulose (HPMC), mannitol, xylitol, and the medication were used to print the 3DP drug-releasing patch. The formulation was created using a freeze-drying method. Additionally, various concentrations of mannitol, xylitol, and HPMC were examined and contrasted. The viscosity property of the bio-ink was determined by the composition of the biomaterials, which, in turn, may have an impact on the printability of the patches [184]. Furthermore, visual impairment raises a number of issues with regard to medicine and treatment, particularly for the elderly population, which frequently takes several different drugs. This causes poor treatment management and medication adherence, which eventually results in therapeutic inefficiency. Orally disintegrating tablets that are ideal for people who are blind or visually impaired were created by Awad *et al.* using SLA. When these printlets are removed from their packaging, patients may recognise the drug because of the braille and moon patterns on their surface. Differently shaped tablets with additional information, such as dosage instructions or drug indications, have been developed. By increasing drug adherence and lowering medication errors, this ground-

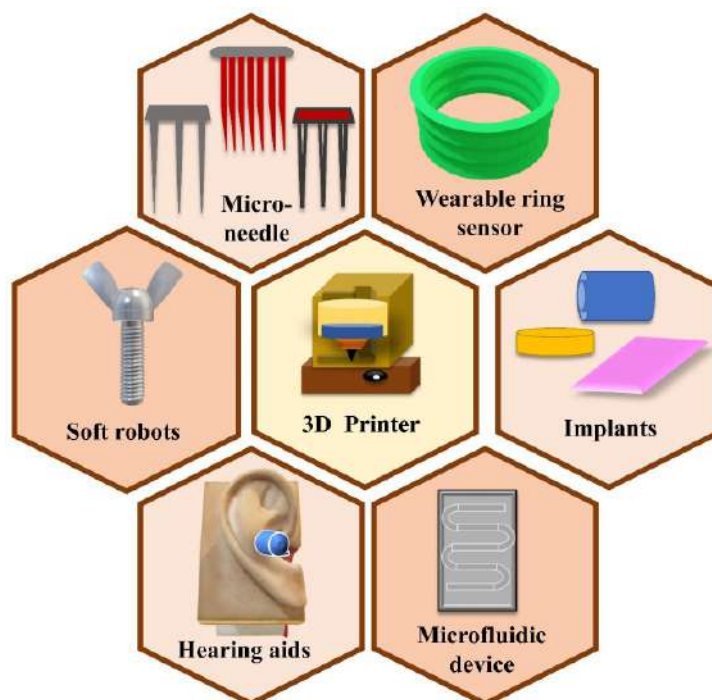


Fig. (19). Medical equipment produced with the help of 3D printing. (A higher resolution / colour version of this figure is available in the electronic copy of the article).

breaking idea can significantly help the management of patients who are blind or visually impaired [185]. Although 3D printing (3DP) in the ophthalmic field is not yet fully comprehended and advanced, its undeniable potential to offer groundbreaking solutions for various eye diseases remains evident. The emergence of bioinks in 3D printing has the potential to address the scarcity of corneal transplantation and facilitate the advancement of tissue regeneration [184, 186].

6.1.5. Dermatology

The largest organ, the skin, is most prone to injuries caused by severe burns and conditions like dermatitis or diabetes. Full-thickness wound patients are physically and financially burdened. Given that they do not trigger allergic or harmful reactions, biodegradable patches have found use in the treatment of wounds [187]. In order to create constructs with customizable features, a hybrid printing method for hydrogel wound dressings was developed. This method combines the deposition of thermoplastic polycaprolactone with hydrogel scaffolds made of alginate and carboxymethylcellulose. The antibacterial properties of alginate are well known, and studies have demonstrated that carboxymethylcellulose can absorb dangerous germs [188]. In order to replicate the upper layers of skin, the epidermis and dermis, respectively, a similar

technology was used to print a bilayer membrane (BLM) made of a poly (lactic-co-glycolic acid) (PLGA) membrane and an alginate hydrogel layer. The membrane had a dual purpose: the multi-porous alginate gel promoted cell attachment and proliferation, while the PLGA prevented bacterial infection and maintained the needed levels of moisture. Electrospinning was used to create the PLGA mat, yielding fibres with a two-micrometre thickness and a ten-millimetre diameter. To create the final scaffold, sodium alginate hydrogels were created by applying the gel to the surface of the PLGA mat [189].

6.1.6. Dentistry

Dental labs may now correctly and quickly construct crowns, bridges, plaster/stone models, and a variety of orthodontic appliances, such as surgical guides and aligners, by combining oral scanning, CAD/CAM (Computer-aided Manufacturing) design, and 3D printing. Instead of making uncomfortable imprints, a 3D scan is obtained, which is eventually converted into a 3D model and sent to be 3D printed. An entire range of orthodontic products, including delivery and positioning trays, clear aligners, and retainers, can be produced using the printed model. As 3D CAD files, the models can also be easily stored digitally. With the use of 3DP, the entire operation may be digitalized, thereby

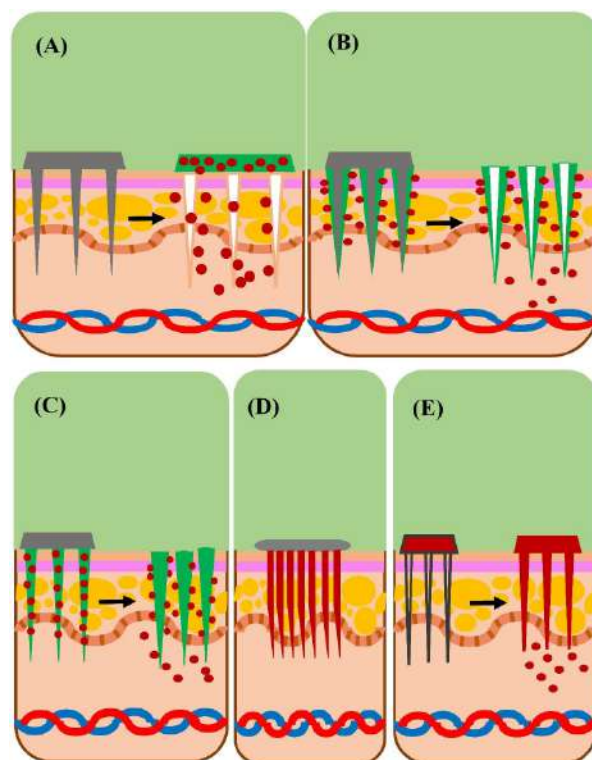


Fig. (20). Transdermal drug delivery using various types of 3D printed microneedle (MN); (A) Solid MN (B) Coated MN (C) Dissolving MN (D) Personalized MN (E) Hollow MN. (A higher resolution / colour version of this figure is available in the electronic copy of the article).

reducing turnaround times and raising output. Additionally, they make it possible to do away with model storage and physical impressions [190].

The product Invisalign®, which consists of 3D-printed clear orthodontic devices that straighten teeth without the use of conventional metal braces, is the most frequently cited example of 3D printing in dentistry [40]. Small intraoral cameras could be used to scan a patient's misaligned teeth in the future rather than requiring them to send moulds to a specialised lab for scanning and retainer fabrication (a procedure that can take weeks) [191].

Recent improvements have been made as a result of 3D printer manufacturers realising the increased demand for machines capable of producing dental parts. As an illustration, Stratasys recently unveiled two CrownWorx™ and FraMEDorx™ semi-solid extrusion printers that were created exclusively for dental applications [192]. In order to enable dental laboratories to produce custom-made crowns and bridges, the printers extrude a type of wax.

6.2. Medical Equipment

3D printing technology has revolutionized medical equipment production by enabling customization, rapid prototyping, and cost-effectiveness. Its ability to create personalized devices tailored to individual patients' needs has improved comfort and patient outcomes (Fig. 19).

6.2.1. Microneedle (MN)

Microneedles are a type of TDDS comprising arrays of micro-sized needles (2D,3D projections) organised on the surface of a matrix that increases the interpenetration of biologically active molecules *via* the stratum corneum by developing microchannels or micropores under the skin [193]. These tiny structures can distribute drugs more effectively because they can pass through the SC barrier without damaging pain-producing nerve terminals [194]. Far-reaching materials seemed to be used for MN fabrication, like silicon, glass, metal, ceramics and different types of polymers [170]. Polymeric MNs are gaining attention because of their biodegradability, biocompatibility, strength and optical clarity [49]. Farias *et al.* used stereolithography to draft a cell-hydrogel having a 3D printed methacry-

late-based custom hollow microneedle assembly (1.3 conical frusta circular array) to figure out the potentiality of cells called human hepatocellular [195]. Economiduo *et al.* plotted 3D-printed microneedle arrays via stereolithography (SLA) using a biocompatible resin for the delivery of transdermal insulin [196]. By comparing the control of the entire skin, intensified penetration of diclofenac diethylamine gel was found after medicamentation with the MN finger splint. Likewise, bioinspired MNs, along with backward-facing barbs, were designed to increase tissue adhesion [197] (Fig. 20).

6.2.2. *Implants/prosthetics*

Implants and prosthetics are necessary to meet isolated patients' requirements and are susceptible to their pathology and unique anatomy. Conventional wrought/casting techniques require additional tools or devices that have inherent drawbacks concerning implant fabrication, like inadequate biomechanical joint reconstruction and inaccurate joint fixation. Correspondingly, more than one-fourth of hip implant revisions are re-revisions [198]. Multi-Material Additive Manufacturing (MMAM) fabricated implants underwent improvements like different kinds of drugs/effective ingredients loaded, maximum mechanical properties, and complicated structure implants in comparison with the conventional 3D printed implants [47]. A dosing structure called an embed, containing effective medications within a supported delivery conveyance grid, offers advantages to patients who require long-haul medication. For example, microstructured embeds of levofloxacin exhibit complicated delivery profiles acquired through a solitary embed. This embed indicates a bimodal profile with pulsatile [29].

A 3DP-based multi-drug implant was recently developed by Wu *et al.*, in which tobramycin (TOB) and levofloxacin (LVFX) as APIs were loaded and multifaceted scaffolds were used for the cure of chronic osteomyelitis [199]. The modelling of implants and prostheses by AM has reorganized the area of developing medical equipment, satisfying the growing need for personalized therapy. 3D printing authorizes the construction of tailor-made products that meet individual requirements resulting from specific patient anatomy as well as pathology. Additionally, it allows the development of structures with site-specific physical and mechanical properties and spatial and temporal control of bioactive components [78]. The individualized prosthetic accessories and tools make it possible to regain lost mobility, functionality, and a natural look. Herbert and colleagues created a prosthetic foot [200].

6.2.3. *Hearing aids*

Hearing aids are an incredible instance of medical devices that have become advanced from the development of VAT photopolymerization and 3D printing. In fact, more than 99% of patient-oriented hearing aids are fabricated using 3D printing nowadays. Prior to 3D printing being established, the fabrication of hearing aids took longer than a week. Today, the entire operation, involving scanning, design and 3D printing, could take less than one day. One of the top manufacturers of hearing aids is Envision TEC, which offers large-scale production and more than 16 biomedically certified materials, both soft and hard, ranging from translucent for ear moulds to skin tones for ear shells [190, 201].

6.2.4. *Biorobotics*

The ability of bio-inspired hybrid devices to simulate different biological activities has recently received a lot of interest. The biorobots are formed of synthetic scaffolds that support soft biological stuff like proteins, live cells, or tissues and are made of polymer elastomers or hydrogels. They can conduct several sorts of movements, such as walking or swimming, and can interact with their surroundings since they are more flexible than typical robots. The most exciting of these robots are the rotary machines, which are typically connected to the conversion of chemical energy from ATP (Adenosine triphosphate) hydrolysis into work [202-204]. Biorobots are in high demand due to the benefits of 3D (bio)printing tissues and organs since they act as little mechanical devices that can take part in tissue regeneration and drug administration. They might also aid in the comprehension of locomotives. To explain the mechanism of microbes, William *et al.* developed the long flagellar swimmer. The swimmer consists of a polydimethylsiloxane filament with a short, rigid head and a long, slender tail [205]. Direct production of soft robots utilizing MMAM offers a method for creating 3D objects out of different materials in a single step. In contrast to traditional robots with rigid bodies, soft robots are devices with compliant and flexible bodies (made of elastomeric materials) that enable complicated motions and actions. This section introduces a few soft robots that are employed as medical devices with the ability to administer drugs. The first example is a hybrid MMAM-made soft actuator with adjustable stiffness. This soft actuator combined an elastomeric body with a pneumatic system, a layer of shape memory polymer for controlling stiffness, and a layer containing silver particles for resistive heating [206].

6.2.5. Wearable Sensors

New wearable sensors, which can be thought of as adaptative electrochemical cells able to monitor chemical species in biological fluids in real-time, have been made viable due to additive manufacturing. The scientists described a 3D-printed device with integrated electronics and a screen-printed electrode that was formed into a ring and connected to a computer through Bluetooth. The electrode was covered with a semi-solid agarose-based electrolyte. The electrochemical device was tested for the detection of 2,4-dinitrotoluene (DN-T), a by-product of peroxide-based explosives' degradation that is frequently linked to the explosives 2,4,6-trinitrotoluene (TNT) and H_2O_2 in liquid and vapour phases. Katseli described a wearable glucose measuring device that was 3D printed, following the idea of a ring-shaped device [207]. After gold electrodeposition on the 3D-printed carbon black/PLA electrode for the electrocatalytic oxidation of glucose, glucose detection was made possible and was identified on perspiration before and after a meal. Without requiring an enzyme, the gadget is adaptable and ready to be used for continuous glucose monitoring.

Intriguing wearable technology for sweat analysis was made possible by 3D printing, as reported by Dias and colleagues [208]. A flexible thermal-printed electrode was positioned at the 3D-printed reservoir at which perspiration was collected from the volunteer's body. The instrument was able to measure zinc ions in sweat using anodic stripping voltammetry and a working electrode that had been modified to contain bismuth. The ability to create flexible devices with an integrated electrochemical system is a key benefit of 3D printing technology in the creation of wearable sensors [209].

6.2.6. Microfluidics

A microfluidic device is a collection of tiny channels made to hold tiny amounts of reagent. Microfluidic devices have been used to accurately examine biological and chemical processes, diagnose diseases at the point of care, and cultivate cells in regulated environments [210, 211]. These devices have a significant reduction in reagent usage, low manufacturing costs, and high throughput. The ability to cast microfluidic devices from a liquid that cures at low temperatures, its surface inertness, its transparent appearance (which makes it ideal for optical detection), its non-toxic nature, its gas permeability, and its ability to chemically modify its surface make poly(dimethyl

siloxane) (PDMS) one of the most frequently used materials [212, 213]. By applying adhesive to seal the tubing or drilling holes, microfluidic devices can be connected with fluidic tubing, although bad tubing connections can result in abrupt device failure, leakage susceptibility, or the generation of dead volumes that impair device performance. To enable label-free and direct measurements of electroactive compounds, these devices can also be integrated with electrochemical detectors. Therefore, 3D printed devices and microfluidic devices both offer certain advantages from a strategic standpoint. However, using a 3D printer to precisely and repeatedly create complicated micromachined components, fluid connectors and junctions, and other parts offers potential benefits [214].

6.3. Role of 3D Printing Techniques to Counter COVID-19

The rapid spread of COVID-19 has strained healthcare systems worldwide, leading to a scarcity of essential supplies, such as N95 respirator masks, face shields, ventilator valves, testing kits, and other vital personal protective equipment (PPE). As the pandemic continues to unfold, ensuring adequate production and distribution of PPE becomes increasingly critical. To address these shortages, an innovative and promising solution lies in the application of 3D printing technology. Renowned for its ability to fabricate complex architectures, 3D printing emerges as a novel approach to meet the pressing demand for essential medical equipment during this unprecedented crisis [12].

In response to the demands for essential services, especially in the healthcare sector, the establishment of adaptable factories capable of manufacturing materials and devices on demand becomes imperative. Within this context, the integration of a robust and advanced manufacturing network, empowered by the distribution of 3D printing facilities, holds significant promise. These small factories can be strategically located at hospitals and transportation hubs, enabling the swift and efficient provision of medical necessities. The COVID-19 crisis has served as a crucible for the redeployment of 3D printing capabilities, showcasing its competitive advantage in meeting emergency requirements [215].

There are various 3D printing applications against COVID-19, as shown in Fig. (21), such as face masks and shields, ventilator circuit splitters and valves, nasopharyngeal swabs, and field respirators. Table 3 presents the equipment associated with 3D printing techniques for COVID-19.

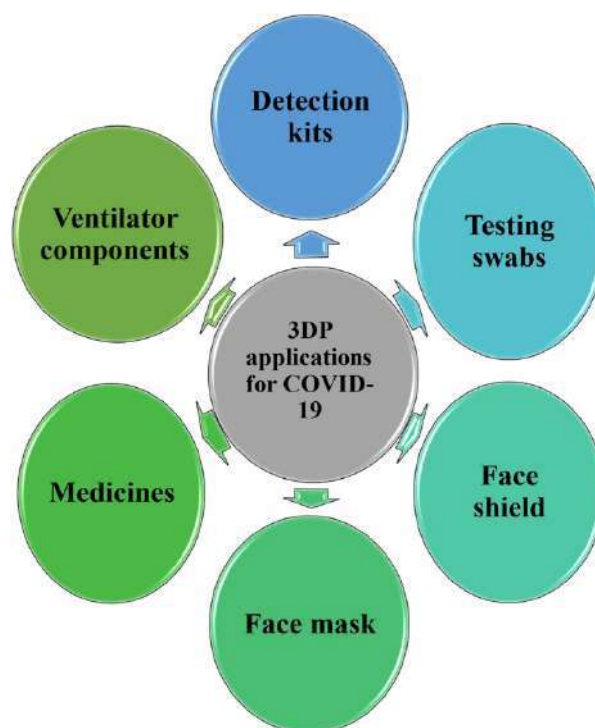


Fig. (21). Use of 3D printing technique against COVID-19. (A higher resolution / colour version of this figure is available in the electronic copy of the article).

Table 3. COVID-19 related equipment associated with 3D printing techniques.

S. No.	Medical Devices/PPE	3D Printing Techniques	References
1.	Facemasks	FDM, SLS	[9]
2.	Respiratory Valves	FDM, SLA	[11]
3.	Face-shield	FDM	[12]
4.	Field Respirators	Not Specified	[10]
5.	Ventilation Devices	FDM	[12]
6.	Mask Fitter	FDM	[10]
7.	Surgery Mask	FDM	[9]
8.	Nasopharyngeal Swabs	FDM, SLA, SLS	[12]
9.	Safety Goggles	FDM, SLS	[10]

6.3.1. Face Mask

The use of 3D printing technology fulfills a significant need for facemasks in the COVID-19 pandemic crisis. As the most effective method of preventing inter-human transmission, facemask use is necessary when in public. A customized 3D protective facemask is possible due to 3D printing. The 3D-printed reusable parts and filter membrane support make up the unique protective facemask. A removable, non-woven particle filter can be used to assemble these parts. With the aid of this specialised 3D protective facemask, the use of dis-

posable surgical masks can be reduced. The reusable cartridge that is inserted between the facemask can also be manufactured using 3D technology [10].

6.3.2. Ventilator Circuit Splitter

Every area of the world has been greatly harmed by the COVID-19 problem, but the health sector has been particularly hit harder. There was a severe global ventilator shortage as a result of the virus uprising. Additionally, the manufacture and movement of medical devices were halted by the interruption of the worldwide

supply chain. Employing six Briggs T-tubes and a Puritan-Bennett 840 Series ventilator, the concept of using a single ventilator for several patients was tested on four sheep to simulate human size. The Briggs T-tube is a sophisticated device that was not always accessible. Due to 3D printing technology, digitized designs are readily accessible online. Briggs T-tubes could now be produced in bulk where they were needed due to 3D printing. The Royal Women's Hospital in Australia has created a splitter and flow restrictor device. Fusion 360 has been used by San Rafael, CA, USA, for computer-aided ideas and design. Several low-cost FDM 3D printers are used to build the ventilator splitter. The desktop 3D printer (Original Prusa i3 MK3S, Prusa Research, Prague, Czech Republic) with one complete set of two splitters, comprising expiratory and inspiratory limbs and one inspiratory flow restrictor, had a production time limit of six hours [11].

6.3.3. Ventilator Valves

For patients with acute respiratory distress, including those with COVID-19, ventilator valves are attachments that provide oxygen at regulated doses. Single-use valve sets can be produced using three-dimensional printing technology *via* a filament extrusion system or a polymer-laser powder bed fusion procedure. Biomaterials like polyamide and polysulfone, polycarbonate, silicone rubber, and stainless steel can be used to design the various valve components on 3D printers. Furthermore, these disposable valves eliminate the need for time-consuming sterilization procedures [12].

6.3.4. Face Shield

Face shields are mostly used in the medical, dental, and veterinary fields to safeguard patients by covering their full faces [216]. Polylactic acid (PLA) was used to quickly produce the face shield using a material extrusion-based 3D printer. Finite Element Analysis (FEA) in ANSYS Workbench was used to simulate head-holding and wearing situations and verify the structural design of the shield. A single face shield (with a mass of less than ten grams) may be created in less than 45 minutes, according to the experiment. Elasticity, comfort, Design for Additive Manufacturing (DfAM), single frame design, biodegradability of filaments, ease of maintenance, lightweight, productivity, quick production, and multi-facility manufacturability were the criteria used to optimise the final face mask design [217]. A face shield is a frame worn on the head that shields the user's eyes, nose, and mouth from respiratory droplets, saliva inhalation, dust, and pollen [218]. A face shield's frame has straightforward geometry and is easily fabricatable with the aid of 3D print-

ing [173]. During the COVID-19 epidemic, Delbarre *et al.* used 3D printing to create cloth shields for slit lamps. The face shield is made using 3D printing with Fused Deposition Modelling (FDM). A headband, a shield, and an elastic strap are all 3D printed in face shields. Utilizing PLA material, 3D printing technology was used to create the face shield structure. The face-shield prototype can be used by the surgeon for protection after assembling the transparent film in the frame [10].

6.3.5. Nasopharyngeal (NP) Swabs

The most accurate and secure method for gathering a patient sample for the diagnosis of COVID-19 is using nasal and NP swabs. NP swabs are flexible sticks that are about 6 inches long and have a bristled end. They are rotated into the space between the nose and mouth to ensure that adequate material is gathered. Then, the swab is put into a container with a culture medium and taken to the lab for analysis. The availability of nasal swabs required for COVID-19 test kits was significantly hampered by the COVID-19 epidemic [9].

6.3.6. Field Respirators

In specific work zones where a patient exhibits respiratory symptoms and when handling the remains of suspected patients who have passed away, full-face respiratory protection equipment is necessary (death due to COVID-19). A tool used for temporary emergency ventilation is a field respirator. These respiratory protection devices are made to prevent patients from breathing in dangerous airborne bacteria. By allowing air to escape and keeping the interior dry, the field respirators facilitate easy breathing for the wearer. Using 3D printing technology, Petsiuk *et al.* created a fully open portable bag-valve mask-based ventilator compression system. As a temporary emergency ventilator, an automatic ventilator can be made available [219].

7. 3D BIO-PRINTING

3D bioprinting concerns the dispensing of cell-loaded biomaterials for the manufacture of complicated functional living tissues or organs. It has been used in medication to fabricate tissues like bone, skin, and cartilage. Therefore, a different technical concept compatible with the deposition of living cells becomes compulsory. Precise cell deposition control, scalability, customization, high resolution, and cost-effectiveness are a few benefits of 3D bioprinting.

Bio-inks are expressions that originate from cells and may comprise bio-materials as well as biologically active components [220].

Table 4. Different tissues, printing methods, and cell responses in terms of 3D bio-printing.

Tissue	Printing Techniques	Cell Response	References
Bone	MED/FDM	<ul style="list-style-type: none"> • After 21 days of cell culture, cells on aligned scaffolds maintained their orientation. • On scaffolds containing Hap and coating, increased cell proliferation and osteogenic differentiation were observed. • <i>in vivo</i> bone production and improved osteogenic differentiation for scaffolds coated with CaSH. 	[295]
Cardiac	MED/Extrusion printing	<ul style="list-style-type: none"> • Favor cell contractions • maturation. 	[28]
Cartilage	FDM	<ul style="list-style-type: none"> • Enhanced chondrogenesis for scaffolds using cytokines. Better cartilage healing for cytokine-loaded scaffolds <i>in vivo</i>	[28]
Cornea	NFES (Near field electrospinning)	Enhanced mineralization, osteoblast differentiation, and extracellular matrix (ECM) deposition on Hap-infused scaffolds.	[295]
Kidney	MED	Rhombus pores with unidirectional cell alignment and elevated gene expression.	[295]

Bioinstructive materials can directly influence cell performance by providing specific biochemical as well as physical cues and direct tissue formation [221]. Bioinstructive materials give multi-scale guidance for cells in a 3D environment by establishing cell signaling to closely imitate specific biological, compositional and mechanical properties of native tissues [222, 223]. The cues can be introduced inside the scaffold matrix or on the scaffold surface, and they are divided into biochemical and physical ones. Physical cues involve electrical, mechanical and topographical stimuli like roughness or hierarchically ordered structure. Biochemical signals involve specific drugs, growth factors, proteins and integrated insoluble particles [224]. They direct cell behaviour by modulating the proliferation, migration patterns, adhesion and differentiation of stem cells [225-227]. For improved performance, both kinds of cues can be mixed in a single material system. Table 4 presents the different tissues, printing methods, and cell responses in terms of 3D bioprinting (Fig. 22).

7.1. 3D Bio-printing Applications

7.1.1. Cardiac Tissue

Mechanical cues used in heart tissue engineering support cell contractions as well as maturation. According to studies, the levels of cardiac markers are increased when using scaffold designs with enhanced elastic characteristics or growing cells in dynamic environments [228, 229]. The most popular technique for creating scaffolds for the regeneration of heart tissue is extrusion bioprinting. However, recently, MED also gained appeal for that application because it could

print flexible scaffolds and had a fresh hydrogel printing alternative [230].

7.1.2. Bone Tissue

Bone tissue engineering is the foremost field implementing bio-instructive materials, mainly based on FDM of PCL as well as PLA, which has high energy and moderate degradation rates [231-233]. To intensify the osteogenic potential of printed scaffolds, biochemical cues like hydroxyapatite (HAP) (insoluble particles) are integrated [234-236]. Additionally, components like Strontium (Sr) particles, bio-glass, or tricalcium phosphate (TCP) are also added to scaffold matrices to promote bone formation [237-239]. Bone substitutes with physical clues, such as modified pore shape and size, are made using MED and FDM [231, 240-244].

7.1.3. Cartilage

FDM and MED printing techniques were used to create fibers that reinforced various hydro-gel matrices for the regeneration of cartilage tissue [245, 246]. The incorporation of soluble cues like growth factors, cartilage-based extracellular matrix (ECM), or proteins into scaffolds is made possible by the use of hydrogels, which enhance regeneration [247-249].

7.1.4. Neural Tissue

Electric stimulation is the main stimulus for brain regeneration. A conductive coating or conductive compounds (such as gold) that promote the differentiation and elongation of neural cells are used to deliver this cue [250]. These results are amplified by electric stimulation [251, 252].

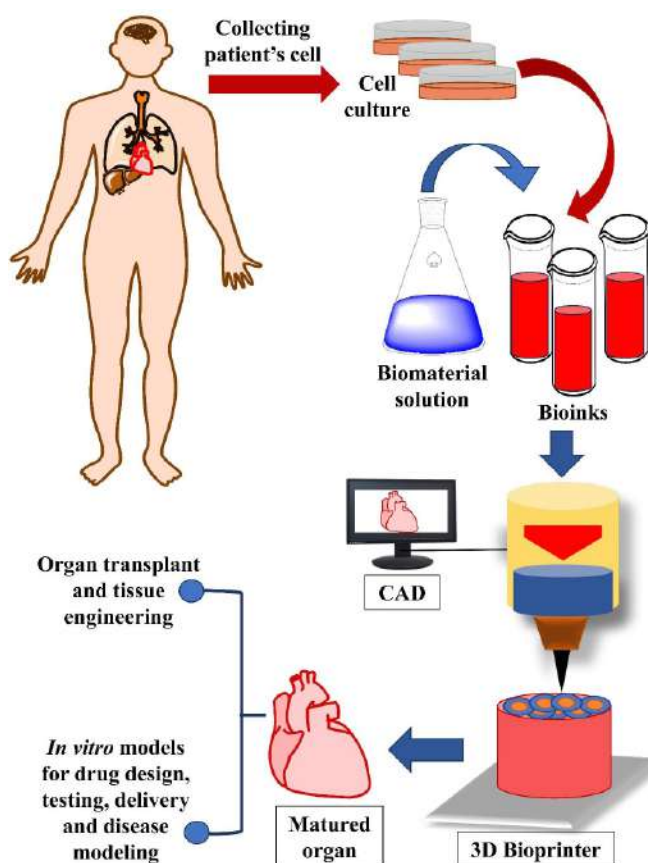


Fig. (22). Pathway of 3D bioprinting. (A higher resolution / colour version of this figure is available in the electronic copy of the article).

7.1.5. Skin Tissue Engineering

For sophisticated skin regeneration techniques, 3D bio-printing has been available for the past ten years [253]. The different methods can now be divided into two categories: bottom-up and top-down. The former tries to create massive tissue blocks that replicate the structure of actual tissue, while the latter aims to create little complicated constructions. Cell aggregates, micro-beads, or hydrogels with cell content are examples of bottom-up technologies. Cells are seeded into biodegradable scaffolds for top-down techniques, and active elements like growth factors are added to encourage cell proliferation and growth. Generally, skin bio-printing has generated a lot of attention, and major cosmetic businesses like *L'Oréal* and Procter and Gamble, as well as printer makers like Rokit, are working to build skin models. For instance, *L'Oréal* has created a unique technology called Episking that can be applied to cosmetics, therefore adhering to the three R's (Replacement, Reduction and Refinement) for enhanced animal welfare and more compassionate animal research [37].

7.1.6. Other Tissues

Hydrogel extrusion printing enables the creation of scaffolds with the appropriate stiffness, and bio-printing is the technique most frequently utilized for the regeneration of soft tissues (such as skin, muscle, or liver). Alginate and gelatin are well-known bio-compatible bio-inks, and stiffness can be controlled, for example, by adjusting the amount of cross-linker used [254-256]. The regeneration of skin can be enhanced, especially by using soluble cues that improve cell differentiation and cell proliferation [257, 258]. Successively, due to its ability to guide cells toward an applied force, mechanical stimulation has been shown to be helpful for tendon and muscle regeneration [259-261]. With approximately 40 different types of cells in the lungs, co-culture can be a crucial trigger for lung regeneration because cells secrete the necessary signalling molecules [262, 263].

7.2. Emerging Perspectives in 3D Bioprinting to Fight COVID-19

The distinct and unexpected pattern of COVID-19 infection and the dearth of potent vaccinations and antivirals have brought the world's human population to the brink. However, the global response to the pandemic was remarkably quick, with early community initiatives and a quick increase in COVID-19-related research. There are now various attempts being made to repurpose existing medications as viable counter measures and produce efficient vaccine technologies. Tissue engineering-based therapies and *in vitro* tissue models created from stem cells can be a blessing in this kind of overwhelming pandemic crisis. Traditionally, tissue engineering has placed a strong emphasis on creating synthetic structures for organ regeneration or replacement. Despite the vast promise, only a small number of engineered constructions have been effective in human clinical trials to date [264]. In this vicious circumstance featuring a constellation of unanswered problems, tissue engineering technologies may offer creative solutions. Both healthy tissue models (such as human hair follicles and cartilage tissue) and diseased tissue models (such as an osteoarthritis model and ocular pathological conditions) can be created using tissue engineering [265, 266]. Even more breakthroughs are made possible by three-dimensional bioprinting, which requires the layer-by-layer precise positioning of living cells, biochemistry, growth factors, ECM orientation, etc. When combined, a 3D structure that mimics the native tissue's ultrastructure can be created [267]. In the pandemic situation caused by SARS-CoV-2, an attempt was made to suggest how organ-on-a-chip, 3D bioprinting, organoids, and advanced bioreactor models made of a coculture of cells from endodermal, mesodermal, and ectodermal origin can be used to create *in vitro* human tissue models that can be used for more effective diagnosis, drug delivery, and customized development of drugs and vaccines as well as the delivery of small molecules at targeted anatomical sites.

8. GUIDELINES IN 3D PRINTING

In 2015, the FDA approved the first 3D printing product, which significantly increased the motivation of biopharmaceutical manufacturers to adopt 3D printing as a new technology for creating pharmaceutical products and biomedical devices. Due to the rapid advancement, questions regarding regulation and liability in the event that a product fails or has a negative effect are some of the most frequently discussed topics with the 3D printing of medications and equipment. In order to provide potential regulatory insights and key chem-

istry, manufacturing, and control requirements for the approval of 3D-printed drug products and medical devices, the FDA published "Technical Considerations for Additive Manufactured Medical Devices" in December 2017 [268]. Following the FDA guidance, Health Canada also issued new guidance in late 2018, including a description of the essential elements of manufacturing operations, a summary of the 3D printing process, and important device design parameters for 3D printing of medical devices to promote high-quality personalized drug therapy and treatment solutions for patients. Discussions are currently being held by the FDA's Office of Testing and Research to find solutions to issues like how to investigate the key parameters of various printing technologies, how to assess the effectiveness of 3D-printed medications, how to study the release of preparations *in vitro* and *in vivo*, and how to regulate the quality of 3D-printed formulations [269]. Under the International Coalition of Medicines Regulatory Authorities (ICMRA), several regulatory organizations, including Health Canada, the Therapeutic Goods Administration (TGA, Australia), the European Medicines Agency (EMA), *Agencia Nacional de Vigilancia Sanitaria* (ANVISA, Brazil), the Health Sciences Authority (HAS, Singapore), and the Pharmaceuticals and Medical Devices Agency (PMDA, Japan), discussed the potential benefits of the developing 3D printing technology in 2019. Three of them began establishing new legal frameworks (Health Canada, HSA, and ANVISA) or developing new regulatory frameworks to promote the creation of novel products, including 3D bio-printed products [270].

9. LIMITATIONS OF 3D PRINTING

Though 3D printing technology has several advantages, there is still a need for modifications as well as exploration in the printing instruments, software, excipients, mechanical strength, false product and clinical practice [28, 87].

9.1. Technology

The printing process includes computer-based operation, which demands that the software programming be constantly reconditioned based on the formulation. In the case of DOP technology, multiple pauses and restarts of the print head are required, which is particularly demanding regarding the print head's stability [121]. Additionally, the performance of printing formulations has been impacted by nozzle blockages, the movement and leakage of binders, and the variation in powder feed [271]. Several print nozzles that are related to extrusion moulding technology have been created and upgraded for compatibility with FDM and PAM

technologies. However, in order to get various formulations, the double nozzle location may be off, which has a significant impact on the product's characteristics, including content homogeneity, hardness, and friability. Devices using lasers and heat may degrade active pharmaceutical ingredients, cause unintended drug-polymer interaction, and resin toxicity [47, 272]. Therefore, it is vitally necessary to further optimise and improve the mechanical apparatus, operational processes, driving control mechanisms, and essential components of 3D printers. Furthermore, the recovery and disposal of unused powders in the case of SLS and DOP, as well as any occupational health risks, should be taken into account [273]. Also, the manufacturing practice (GMP) standard is not fulfilled by the 3D printers used in medicine; thus, it is necessary to validate the production process and the end products to guarantee their safety for human health [87].

9.2. Excipients

All types of 3D printing technologies have specific needs for the qualities of excipients throughout the preparation process. The carrier excipient must be suitable for the drug due to the involvement of melting and heating procedures in some printing technologies, such as FDM, in which PVA is used as an excipient. However, it has a high melting point, which is inappropriate for thermally sensitive drugs [274]. Therefore, 3D printing technology based on low temperatures uses excipients like triethyl citrate, PVP, Kollidon, and HPMC for the enhancement of drug loading capacity and drug degradation [96, 100, 275]. In the SLA and SLS methods, photopolymers are used as excipients, which are unsafe as per the guidelines of the FDA. Moreover, a smaller number of excipients are used mostly because of their bad odour, toxicity, and protection from light for the elimination of premature polymerization. In addition, options in solvents are also finite in the case of DOP and SSE methods [276]. Hence, there is a need to explore the excipients that are suitable for pharmaceutical use, such as non-toxic in nature, stable, biocompatible with drugs, and biodegradable [87].

9.3. Mechanical Strength

The mechanical characteristics of the product act as a quality control criterion that can be used to verify the repeatability and acceptability of the tablets for post-processing. The performance of the product is influenced by factors, such as surface tension, nozzle fineness, and viscosity [277]. Whereas the impact on the look and quality of the products are influenced by the post-processing of printing, which involves drying

methods. In SLA, the loading efficiency of the drug contained in the polymer matrix is decreased due to the post-washing step (washing unreacted resins with isopropanol from the printed material). Hence, the post-curing step is essential to increasing the mechanical robustness of printed structures [47]. Furthermore, the Spritam drug is developed, which is highly porous in nature and provides fast degradation, but it lacks mechanical strength (<40 N). Hence, there is a need to improve the optimization techniques, such as the printing process, computer operations and nozzle refinement, for the betterment of the mechanical properties [87].

9.4. False Product

This challenge arises from the usage of 3D printing technology by neglecting its regulatory aspect, which generates false products that do not meet the quality standards. These fake medications may be obtained at a very reasonable cost; however, they can cause major health issues in humans. Moreover, the WHO estimates that fake medicines affect 10.5% of the low and middle-income nations. This can be prevented by using effective safeguards. One study used FDM 3D printing with piezoelectric 2D inkjet printing to establish a unique track and trace false measure for 3D printed medications. For tracking purposes, QR codes and data matrices were placed on the surface of the 3D-printed printlets for scanning by using a smartphone, which provides information about the unique patient, provider, and medicine. Nevertheless, incorporating a data matrix or QR code onto the surface of the printlet might influence its visual aesthetics and potentially influence patients' willingness to accept the medication. Therefore, it is important to assess this aspect in future clinical investigations. It is worth noting that by expanding the variety of additives and coloring agents present in the material inks, the randomized code could encompass an extensive range of permutations, thereby enhancing the incorporation of personalized medications through an enhanced tracking and authentication system throughout the supply chain [278].

9.5. Clinical Use

Installing 3D printing technology into the health centre may pose additional obstacles as it demands a highly qualified worker to handle the technical components, an expensive budget, as well as maintain quality control of printed drugs. Moreover, to satisfy the criteria of customised medicine in a clinical context, packaging and labelling standards must also be considered. More technical advancements are required to bring the ultimate 3D printer for clinical applications, which must be user-friendly, quick, cost-effective, and have a

high resolution, as current 3D printers have not yet overcome their disadvantages [28].

10. CONCLUSION

3D printing has advantages over conventional methods due to its accuracy, reproducibility, controlled size and shape, patient-specific, controlled release properties, safety, and cost efficiency.

There are various techniques involved in the processes of printing, extrusion and designing, such as ink-jet-based, VAT photopolymerization, SLS, EMP, DOP, and EHD. They have applications in the fabrication of personalized medicines, drug delivery (oral, rectal and vaginal), complex drug formation and suitable dosage forms. Furthermore, advancement in 3D printing is manifested in several branches of the medical field, including paediatrics, geriatrics, oncology, ophthalmology, dermatology, and dentistry because of its development in the production of various medical components, such as microneedles, implants, hearing aids, bio-robotics, wearable sensors, and microfluidics. Moreover, 3D printing technology also aids in the fight against pandemics like COVID-19 by using methods like FDM, SLS and SLA for the development of equipment like face masks, face shields, safety goggles, nasopharyngeal swabs, ventilation devices, and respiratory devices. In addition, integrating 3D printing techniques into biomaterials for the tailoring of living tissues of bone, skin, cartilage, cardiac, etc, is of utmost significance. In short, 3D printing plays an important role in the advancement of the healthcare system.

11. FUTURE PERSPECTIVES

Traditional preparation technology and 3D printing preparation technology work well together in several ways. After years of development, traditional preparation technology has reached a distinct industrial advantage. In contrast, 3D printing, an emerging technique, can achieve the precise sculpting of a variety of materials and can address many of the drawbacks of conventional preparatory technology.

Hybrid living materials are another area that has a great deal of potential to aid in the creation of bio-constructive materials. These substances are made of synthetic materials and living microorganisms (such as cells, bacteria, microalgae, or yeast). Microbes control the physical and chemical characteristics, creating new material qualities like self-regeneration or acclimatisation to their surroundings [279]. The creation of self-sufficient and self-regenerating scaffolds that can produce the proteins or enzymes required for cell proliferation and specific differentiation, which will improve

and speed up tissue regeneration, is what we anticipate will result from the continued development of hybrid living materials.

The field of additive manufacturing has made significant progress, resulting in the creation of smart 3D-printed materials that can change their properties and shape in response to outside stimuli over time, so-called 4D printing technology, which addresses the fabrication of shape memory materials, self-evolving structures, and actuators for biorobotics [280-285]. It is expected that 4D printing technology will allow the construction of smart scaffolds with specialised dimensions and shapes in the future. These scaffolds will vary in shape in accordance with the rate of tissue regeneration and maturation. It will also enable the use of minimally invasive surgical techniques to deliver the scaffolds to difficult-to-reach areas of the body.

The idea of on-demand manufacturing of medicine is that specialized software may produce the patient's own information, which is then utilized to print the prescriptions at a community pharmacy or even at home using a personal 3D printer. Instead of depending solely on healthcare professionals, patients may tailor their own dosage requirements based on their illness [13, 157, 286]. For drugs with a short shelf life, printing at the point of treatment can also be helpful, which may lead to the marketing approval of novel medications [286]. This would be especially important in regions of the world where there are not enough medical professionals to meet the demands of the population. The same strategy could be applied to military operations, disaster relief efforts, and remote villages.

The 3D printing strategy can also be applied to the advancement of clinical pharmacy practise. In the modern world, the pharmacist can use 3D printing technology to quickly deliver medication in a format that is customised according to the doctor's prescription [287]. This would eliminate any drug shortage and make it easier to implement personalised drug therapy into routine clinical practice [98, 165]. Hospital pharmacists must be educated about these advanced technologies since they will play an important role in the future implementation of 3D printing in pharmacy practice [288].

LIST OF ABBREVIATIONS

CA	= Cellulose Acetate
DEF	= Diethyl Fumarate
GelMA	= Gelatin Methacryloyl
HPC	= Hydroxyl Propyl Cellulose

HPMC	= Hydroxyl Propyl Methylcellulose
HPMCAS	= Hydroxyl Propyl Methyl Cellulose Acetate Succinate
MCC	= Microcrystalline Cellulose
PCL	= Polycaprolactone
PCLDMA	= Polycaprolactone Dimethacrylate
PCL-tMa	= Polycaprolactone Trimethacrylate
PE	= Polyethylene
PEG	= Polyethylene Glycol
PEGDA	= Poly (Ethylene Glycol) Diacrylate
PEGDMA	= Poly (Ethylene Glycol) Dimethacrylate
PEGMA	= Poly (Ethylene Glycol) Methacrylate
PEO	= Poly(Ethylene Oxide)
pHEMA	= Poly(2-hydroxyethyl Methacrylate)
PLA	= Polylactic Acid
PLGA	= Poly lactide-co-glycoside
PMA	= Propyl Methacrylate
PPF	= Poly (Ethylene Fumarate)
PVA	= Polyvinyl Alcohol
PVP	= Povidone
TCP	= Tricalcium Phosphate

CONSENT FOR PUBLICATION

Not applicable.

FUNDING

This work was supported by the Excellence project PrF UHK - 2216/2023-2024. It was also supported by projects VEGA 1/0387/22, KEGA 050TUKE-4/2022 and CEMBAM, ITMS2014+: 313011V358 and by 'Mr. Sudhir Krishnaraj Thackersey Research Grant-2021-23 at Sir Vithaldas Thackersey College of Home Science (Autonomous), SNDTWU, Mumbai.

CONFLICT OF INTEREST

The authors declare no conflict of interest.

ACKNOWLEDGMENTS

Priyank Sinha, Preeti Lahare and Meena Sahu are grateful to Pt. Ravishankar Shukla University, Raipur, for providing fellowship. NS is grateful to the institute head and head of the Department of Engineering Sciences, Ramrao Adik Institute of Technology, DY Patil

University, Nerul, Navi Mumbai, for providing research facilities.

REFERENCES

- [1] Gebhardt, A. *In Understanding Additive Manufacturing*; Carl Hanser Verlag GmbH & Co. KG, **2011**, pp. I-IX. <http://dx.doi.org/10.3139/9783446431621.fm>
- [2] Rui, Y.; Gang, X.; Shuang-Shuang, M.; Hua-Yu, Y.; Xin-Ting, S.; Wei, S.; Yi-Lei, M. Three-dimensional printing: review of application in medicine and hepatic surgery. *Cancer Biol. Med.*, **2016**, *13*(4), 443-451. <http://dx.doi.org/10.20892/j.issn.2095-3941.2016.0075> PMID: 28154775
- [3] Davim, J.P. *Machining: Fundamentals and recent advances*, 1st ed.; Springer: London, **2008**.
- [4] Hull, C.W.; Arcadia, C. Apparatus for production of three-dimensional objects by stereolithography. U.S. Patent 4575330A, **1984**.
- [5] Chuck Hull and Stereolithography. **2023**. Available from: <https://spie.org/news/spie-professional--magazine-archive/2013-january/chuck-hull?SSO=1> (Accessed on : 04 Aug 2023).
- [6] Pandey, M.; Choudhury, H.; Fern, J.L.C.; Kee, A.T.K.; Kou, J.; Jing, J.L.J.; Her, H.C.; Yong, H.S.; Ming, H.C.; Bhattamisra, S.K.; Gorain, B. 3D printing for oral drug delivery: A new tool to customize drug delivery. *Drug Deliv. Transl. Res.*, **2020**, *10*(4), 986-1001. <http://dx.doi.org/10.1007/s13346-020-00737-0> PMID: 32207070
- [7] Fitzgerald, S. FDA Approves First 3D-printed epilepsy drug experts assess the benefits and caveats. *Neurol. Today*, **2015**, *15*(18), 26-27. <http://dx.doi.org/10.1097/01.NT.0000472137.66046.b5>
- [8] Chen, G.; Xu, Y.; Chi Lip Kwok, P.; Kang, L. Pharmaceutical Applications of 3D Printing. *Addit. Manuf.*, **2020**, *34*, 101209. <http://dx.doi.org/10.1016/j.addma.2020.101209>
- [9] Kalkal, A.; Allawadhi, P.; Kumar, P.; Sehgal, A.; Verma, A.; Pawar, K.; Pradhan, R.; Paital, B.; Packirisamy, G. Sensing and 3D printing technologies in personalized healthcare for the management of health crises including the COVID-19 outbreak. *Sensors Int.*, **2022**, *3*, 100180. <http://dx.doi.org/10.1016/j.sintl.2022.100180> PMID: 35601184
- [10] Agarwal, R. The personal protective equipment fabricated via 3D printing technology during COVID-19. *Ann. 3D Print. Med.*, **2022**, *5*, 100042.
- [11] Nazir, A.; Azhar, A.; Nazir, U.; Liu, Y.F.; Qureshi, W.S.; Chen, J.E.; Alanazi, E. The rise of 3D Printing entangled with smart computer aided design during COVID-19 era. *J. Manuf. Syst.*, **2021**, *60*, 774-786. <http://dx.doi.org/10.1016/j.jmsy.2020.10.009> PMID: 33106722
- [12] Ishack, S.; Lipner, S.R. Applications of 3D printing technology to address COVID-19-related supply shortages. *Am. J. Med.*, **2020**, *133*(7), 771-773. <http://dx.doi.org/10.1016/j.amjmed.2020.04.002> PMID: 32330492
- [13] El Aita, I.; Ponsar, H.; Quodbach, J. A critical review on 3D-printed dosage forms. *Curr. Pharm. Des.*, **2019**, *24*(42), 4957-4978. <http://dx.doi.org/10.2174/1381612825666181206124206> PMID: 30520369
- [14] Litman, T. Personalized medicine-concepts, technologies,

- and applications in inflammatory skin diseases. *Acta Pathol. Microbiol. Scand. Suppl.*, **2019**, 127(5), 386-424. <http://dx.doi.org/10.1111/apm.12934> PMID: 31124204
- [15] Rajjada, D.; Wac, K.; Greisen, E.; Rantanen, J.; Genina, N. Integration of personalized drug delivery systems into digital health. *Adv. Drug Deliv. Rev.*, **2021**, 176, 113857. <http://dx.doi.org/10.1016/j.addr.2021.113857> PMID: 34389172
- [16] Zhu, X.; Li, H.; Huang, L.; Zhang, M.; Fan, W.; Cui, L. 3D printing promotes the development of drugs. *Biomed. Pharmacother.*, **2020**, 131, 110644. <http://dx.doi.org/10.1016/j.biopha.2020.110644> PMID: 32853908
- [17] Zheng, Y.; Deng, F.; Wang, B.; Wu, Y.; Luo, Q.; Zuo, X.; Liu, X.; Cao, L.; Li, M.; Lu, H.; Cheng, S.; Li, X. Melt extrusion deposition (MED™) 3D printing technology - A paradigm shift in design and development of modified release drug products. *Int. J. Pharm.*, **2021**, 602, 120639. <http://dx.doi.org/10.1016/j.ijpharm.2021.120639> PMID: 33901601
- [18] Raju, S.; Reddy, P.S.; Kumar, V.A.; Deepthi, A.; Reddy, K.S.; Reddy, P.M.J.J.C.P.R. Flash release oral films of metoclopramide hydrochloride for pediatric use: Formulation and *in-vitro* evaluation. *J. Chem. Pharm. Res.*, **2011**, 3(4), 636-646.
- [19] Hsu, M.N.; Luo, R.; Kwek, K.Z.; Por, Y.C.; Zhang, Y.; Chen, C.H. Sustained release of hydrophobic drugs by the microfluidic assembly of multistage microgel/poly (*lactico-glycolic acid*) nanoparticle composites. *Biomicrofluidics*, **2015**, 9(5), 052601. <http://dx.doi.org/10.1063/1.4916230> PMID: 25825623
- [20] Kalepu, S.; Nekkanti, V. Insoluble drug delivery strategies: Review of recent advances and business prospects. *Acta Pharm. Sin. B*, **2015**, 5(5), 442-453. <http://dx.doi.org/10.1016/j.apsb.2015.07.003> PMID: 26579474
- [21] Fuhrmann, K.; Schulz, J.D.; Gauthier, M.A.; Leroux, J.C. PEG nanocages as non-sheddable stabilizers for drug nanocrystals. *ACS Nano*, **2012**, 6(2), 1667-1676. <http://dx.doi.org/10.1021/nn2046554> PMID: 22296103
- [22] Larrañeta, E.; Stewart, S.; Ervine, M.; Al-Kasasbeh, R.; Donnelly, R.F. Hydrogels for hydrophobic drug delivery. Classification, synthesis and applications. *J. Funct. Biomater.*, **2018**, 9(1), 13.
- [23] González, K.; Larraza, I.; Berra, G.; Eceiza, A.; Gabilondo, N. 3D printing of customized all-starch tablets with combined release kinetics. *Int. J. Pharm.*, **2022**, 622, 121872. <http://dx.doi.org/10.1016/j.ijpharm.2022.121872> PMID: 35636631
- [24] Mathur, S.; Sutton, J. Personalized medicine could transform healthcare. *Biomed. Rep.*, **2017**, 7(1), 3-5. <http://dx.doi.org/10.3892/br.2017.922> PMID: 28685051
- [25] Savini, A.; Savini, G.G. A short history of 3D printing, a technological revolution just started. *2015 ICO-HTEC/IEEE International History of High-Technologies and their Socio-Cultural Contexts Conference (HISTELCON)*, Tel-Aviv, Israel 18-19 Aug 2015, pp. 1-8.
- [26] Su, A.; Al'Aref, S.J. *3D Printing Applications in Cardiovascular Medicine*; Al'Aref, S.J.; Mosadegh, B.; Dunham, S.; Min, J.K., Eds.; Academic Press: Boston, **2018**, pp. 1-10.
- [27] Prasad, L.K.; Smyth, H., III 3D Printing technologies for drug delivery: A review. *Drug Dev. Ind. Pharm.*, **2016**, 42(7), 1019-1031. <http://dx.doi.org/10.3109/03639045.2015.1120743> PMID: 26625986
- [28] Vaz, V.M.; Kumar, L. 3D printing as a promising tool in personalized medicine. *AAPS PharmSciTech*, **2021**, 22(1), 49. <http://dx.doi.org/10.1208/s12249-020-01905-8> PMID: 33458797
- [29] Mohapatra, S.; Kar, R.K.; Biswal, P.K.; Bindhani, S. Approaches of 3D printing in current drug delivery. *Sensors Int.*, **2022**, 3, 100146. <http://dx.doi.org/10.1016/j.sintl.2021.100146>
- [30] Jiménez, M.; Romero, L.; Domínguez, I.A.; Espinosa, M.M.; Domínguez, M. Additive manufacturing technologies: An overview about 3D printing methods and future prospects. *Complexity*, **2019**, 2019, 1-30. <http://dx.doi.org/10.1155/2019/9656938>
- [31] Water, J.J.; Bohr, A.; Boetker, J.; Aho, J.; Sandler, N.; Nielsen, H.M.; Rantanen, J. Three-dimensional printing of drug-eluting implants: Preparation of an antimicrobial polylactide feedstock material. *J. Pharm. Sci.*, **2015**, 104(3), 1099-1107. <http://dx.doi.org/10.1002/jps.24305> PMID: 25640314
- [32] Ballard, D.H.; Trace, A.P.; Ali, S.; Hodgdon, T.; Zygmunt, M.E.; DeBenedictis, C.M.; Smith, S.E.; Richardson, M.L.; Patel, M.J.; Decker, S.J.; Lenchik, L. Clinical applications of 3D printing: Primer for radiologists. *Acad. Radiol.*, **2018**, 25(1), 52-65. <http://dx.doi.org/10.1016/j.acra.2017.08.004> PMID: 29030285
- [33] ISO/ASTM 52900:2015 - Additive manufacturing - General principles - Terminology. Available from: <https://www.iso.org/standard/69669.html>
- [34] Trenfield, S.J.; Madla, C.M.; Basit, A.W.; Gaisford, S. Binder jet printing in pharmaceutical manufacturing. In: *3D Printing of Pharmaceuticals*; Basit, A.W.; Gaisford, S., Eds.; Springer: Cham, **2018**; pp. 41-54. http://dx.doi.org/10.1007/978-3-319-90755-0_3
- [35] Hsiao, W.K.; Lorber, B.; Reitsamer, H.; Khinast, J. 3D printing of oral drugs: A new reality or hype? *Expert Opin. Drug Deliv.*, **2018**, 15(1), 1-4. <http://dx.doi.org/10.1080/17425247.2017.1371698> PMID: 28836459
- [36] Chia, H.N.; Wu, B.M. Recent advances in 3D printing of biomaterials. *J. Biol. Eng.*, **2015**, 9(1), 4. <http://dx.doi.org/10.1186/s13036-015-0001-4> PMID: 25866560
- [37] Tabriz, A.G.; Douroumis, D. Recent advances in 3D printing for wound healing: A systematic review. *J. Drug Deliv. Sci. Technol.*, **2022**, 74, 103564. <http://dx.doi.org/10.1016/j.jddst.2022.103564>
- [38] Peterson, G.I.; Larsen, M.B.; Ganter, M.A.; Storti, D.W.; Boydston, A.J. 3D-printed mechanochromic materials. *ACS Appl. Mater. Interfaces*, **2015**, 7(1), 577-583. <http://dx.doi.org/10.1021/am506745m> PMID: 25478746
- [39] Anciaux, S.K.; Geiger, M.; Bowser, M.T. 3D printed micro free-flow electrophoresis device. *Anal. Chem.*, **2016**, 88(15), 7675-7682. <http://dx.doi.org/10.1021/acs.analchem.6b01573> PMID: 27377354
- [40] Ventola, C.L. Medical applications for 3D printing: Current and projected uses. *P T*, **2014**, 39(10), 704-711. PMID: 25336867
- [41] Cho, H-W.; Baek, S-H.; Lee, B-J.; Jin, H-E. Ordispersible polymer films with the poorly water-soluble drug, olanzapine: Hot-melt pneumatic extrusion for single-process

- 3D printing. *Pharmaceutics*, **2020**, *12*(8), 692.
- [42] Ambrosi, A.; Pumera, M. 3D-printing technologies for electrochemical applications. *Chem. Soc. Rev.*, **2016**, *45*(10), 2740-2755. <http://dx.doi.org/10.1039/C5CS00714C> PMID: 27048921
- [43] Mendibil, X.; Tena, G.; Duque, A.; Uranga, N.; Campanero, M.Á.; Alonso, J. Direct powder extrusion of paracetamol loaded mixtures for 3D printed pharmaceuticals for personalized medicine *via* low temperature thermal processing. *Pharmaceutics*, **2021**, *13*(6), 907.
- [44] Gültekin, H.E.; Tort, S.; Acartürk, F. An effective technology for the development of immediate release solid dosage forms containing low-dose drug: Fused deposition modeling 3D printing. *Pharm. Res.*, **2019**, *36*(9), 128. <http://dx.doi.org/10.1007/s11095-019-2655-y> PMID: 31250313
- [45] G, B.O.; S, G.V.; K, S.B.; C, D.R.; A, G.S.; S, G.P. 3D printing & pharmaceutical manufacturing: Opportunities and challenges. *Int. J. Bioassays*, **2016**, *5*(1), 4723. <http://dx.doi.org/10.21746/ijbio.2016.01.006>
- [46] Zhao, Z.; Kuang, X.; Yuan, C.; Qi, H.J.; Fang, D. Hydrophilic/hydrophobic composite shape-shifting structures. *ACS Appl. Mater. Interfaces*, **2018**, *10*(23), 19932-19939. <http://dx.doi.org/10.1021/acsami.8b02444> PMID: 29737169
- [47] Wang, J.; Zhang, Y.; Aghda, N.H.; Pillai, A.R.; Thakkar, R.; Nokhodchi, A.; Maniruzzaman, M. Emerging 3D printing technologies for drug delivery devices: Current status and future perspective. *Adv. Drug Deliv. Rev.*, **2021**, *174*, 294-316. <http://dx.doi.org/10.1016/j.addr.2021.04.019> PMID: 33895212
- [48] Bloomquist, C.J.; Mecham, M.B.; Paradzinsky, M.D.; Januszewicz, R.; Warner, S.B.; Luft, J.C.; Mecham, S.J.; Wang, A.Z.; DeSimone, J.M. Controlling release from 3D printed medical devices using CLIP and drug-loaded liquid resins. *J. Control. Release*, **2018**, *278*, 9-23. <http://dx.doi.org/10.1016/j.jconrel.2018.03.026> PMID: 29596874
- [49] Xu, X.; Awad, A.; Robles-Martinez, P.; Gaisford, S.; Goyanes, A.; Basit, A.W. Vat photopolymerization 3D printing for advanced drug delivery and medical device applications. *J. Control. Release*, **2021**, *329*, 743-757. <http://dx.doi.org/10.1016/j.jconrel.2020.10.008> PMID: 33031881
- [50] Awad, A.; Trenfield, S.J.; Goyanes, A.; Gaisford, S.; Basit, A.W. Reshaping drug development using 3D printing. *Drug Discov. Today*, **2018**, *23*(8), 1547-1555. <http://dx.doi.org/10.1016/j.drudis.2018.05.025> PMID: 29803932
- [51] Voet, V.S.D.; Strating, T.; Schnelting, G.H.M.; Dijkstra, P.; Tietema, M.; Xu, J.; Woortman, A.J.J.; Loos, K.; Jager, J.; Folkersma, R. Biobased acrylate photocurable resin formulation for stereolithography 3d printing. *ACS Omega*, **2018**, *3*(2), 1403-1408. <http://dx.doi.org/10.1021/acsomega.7b01648> PMID: 31458469
- [52] Lamichhane, S.; Bashyal, S.; Keum, T.; Noh, G.; Seo, J.E.; Bastola, R.; Choi, J.; Sohn, D.H.; Lee, S. Complex formulations, simple techniques: Can 3D printing technology be the Midas touch in pharmaceutical industry? *Asian J. Pharmaceut. Sci.*, **2019**, *14*(5), 465-479. <http://dx.doi.org/10.1016/j.ajps.2018.11.008> PMID: 32104475
- [53] Robles Martinez, P.; Basit, A.W.; Gaisford, S. The history, developments and opportunities of stereolithography. In: *3D Printing of Pharmaceuticals*; Basit, A.W.; Gaisford, S., Eds.; Springer: Cham, **2018**; Vol. 31, pp. 55-79. http://dx.doi.org/10.1007/978-3-319-90755-0_4
- [54] Martinez, P.R.; Goyanes, A.; Basit, A.W.; Gaisford, S. Fabrication of drug-loaded hydrogels with stereolithographic 3D printing. *Int. J. Pharm.*, **2017**, *532*(1), 313-317. <http://dx.doi.org/10.1016/j.ijpharm.2017.09.003> PMID: 28888978
- [55] Melchels, F.P.W.; Feijen, J.; Grijpma, D.W. A review on stereolithography and its applications in biomedical engineering. *Biomaterials*, **2010**, *31*(24), 6121-6130. <http://dx.doi.org/10.1016/j.biomaterials.2010.04.050> PMID: 20478613
- [56] Healy, A.V.; Fuenmayor, E.; Doran, P.; Geever, L.M.; Higginbotham, C.L.; Lyons, J.G. Additive manufacturing of personalized pharmaceutical dosage forms *via* stereolithography. *Pharmaceutics*, **2019**, *11*(12), 645.
- [57] Martinez, P.R.; Goyanes, A.; Basit, A.W.; Gaisford, S. Influence of geometry on the drug release profiles of stereolithographic (SLA) 3D-printed tablets. *AAPS Pharm-SciTech*, **2018**, *19*(8), 3355-3361. <http://dx.doi.org/10.1208/s12249-018-1075-3> PMID: 29948979
- [58] Economidou, S.N.; Lamprou, D.A.; Douroumis, D. 3D printing applications for transdermal drug delivery. *Int. J. Pharm.*, **2018**, *544*(2), 415-424. <http://dx.doi.org/10.1016/j.ijpharm.2018.01.031> PMID: 29355656
- [59] Yeung, C.; Chen, S.; King, B.; Lin, H.; King, K.; Akhtar, F.; Diaz, G.; Wang, B.; Zhu, J.; Sun, W.; Khademhosseini, A.; Emaminejad, S. A 3D-printed microfluidic-enabled hollow microneedle architecture for transdermal drug delivery. *Biomicrofluidics*, **2019**, *13*(6), 064125. <http://dx.doi.org/10.1063/1.5127778> PMID: 31832123
- [60] Wang, P.; Berry, D.; Moran, A.; He, F.; Tam, T.; Chen, L.; Chen, S. Controlled growth factor release in 3D-printed hydrogels. *Adv. Healthc. Mater.*, **2020**, *9*(15), 1900977. <http://dx.doi.org/10.1002/adhm.201900977> PMID: 31697028
- [61] Wang, Z.; Kumar, H.; Tian, Z.; Jin, X.; Holzman, J.F.; Menard, F.; Kim, K. Visible light photoinitiation of cell-adhesive gelatin methacryloyl hydrogels for stereolithography 3D bioprinting. *ACS Appl. Mater. Interfaces*, **2018**, *10*(32), 26859-26869. <http://dx.doi.org/10.1021/acsami.8b06607> PMID: 30024722
- [62] Liu, S.; Yeo, D.C.; Wiraja, C.; Tey, H.L.; Mrksich, M.; Xu, C. Peptide delivery with poly(ethylene glycol) diacrylate microneedles through swelling effect. *Bioeng. Transl. Med.*, **2017**, *2*(3), 258-267. <http://dx.doi.org/10.1002/btm2.10070> PMID: 29313035
- [63] Goole, J.; Amighi, K. 3D printing in pharmaceuticals: A new tool for designing customized drug delivery systems. *Int. J. Pharm.*, **2016**, *499*(1-2), 376-394. <http://dx.doi.org/10.1016/j.ijpharm.2015.12.071> PMID: 26757150
- [64] Ligon, S.C.; Liska, R.; Stampfl, J.; Gurr, M.; Mülhaupt, R. Polymers for 3D printing and customized additive manufacturing. *Chem. Rev.*, **2017**, *117*(15), 10212-10290. <http://dx.doi.org/10.1021/acs.chemrev.7b00074> PMID: 28756658
- [65] Yang, Y.; Zhou, Y.; Lin, X.; Yang, Q.; Yang, G. Printability of external and internal structures based on digital light processing 3D printing technique. *Pharmaceutics*, **2020**,

- 12(3), 207.
- [66] Zhang, J.; Hu, Q.; Wang, S.; Tao, J.; Gou, M. Digital light processing based three-dimensional printing for medical applications. *Int. J. Bioprint.*, **1970**, 6(1), 242. <http://dx.doi.org/10.18063/ijb.v6i1.242> PMID: 32782984
- [67] DeSimone, J.M.; Samulski, E.T.; Rolland, J.P. Methods and apparatus for continuous liquid interface production with rotation. U.S. Patent 10589512B2, **2020**.
- [68] Taki, K. A simplified 2D numerical simulation of photopolymerization kinetics and oxygen diffusion-reaction for the continuous liquid interface production (CLIP) system. *Polymers*, **2020**, 12(4), 875. <http://dx.doi.org/10.3390/polym12040875> PMID: 32290249
- [69] Januszewicz, R.; Tumbleston, J.R.; Quintanilla, A.L.; Mecham, S.J.; DeSimone, J.M. Layerless fabrication with continuous liquid interface production. *Proc. Natl. Acad. Sci.*, **2016**, 113(42), 11703-11708. <http://dx.doi.org/10.1073/pnas.1605271113> PMID: 27671641
- [70] Caudill, C.L.; Perry, J.L.; Tian, S.; Luft, J.C.; DeSimone, J.M. Spatially controlled coating of continuous liquid interface production microneedles for transdermal protein delivery. *J. Control. Release*, **2018**, 284, 122-132. <http://dx.doi.org/10.1016/j.jconrel.2018.05.042> PMID: 29894710
- [71] Geng, Q.; Wang, D.; Chen, P.; Chen, S.C. Ultrafast multi-focus 3-D nano-fabrication based on two-photon polymerization. *Nat. Commun.*, **2019**, 10(1), 2179. <http://dx.doi.org/10.1038/s41467-019-10249-2> PMID: 31097713
- [72] Xing, J.F.; Zheng, M.L.; Duan, X.M. Two-photon polymerization microfabrication of hydrogels: an advanced 3D printing technology for tissue engineering and drug delivery. *Chem. Soc. Rev.*, **2015**, 44(15), 5031-5039. <http://dx.doi.org/10.1039/C5CS00278H> PMID: 25992492
- [73] Shavkuta, B.; Bardakova, K.; Khristidis, Y.; Minaev, N.V.; Frolova, A.; Kotova, S.; Aksenova, N.; Heydari, Z.; Semenova, E.; Khlebnikova, T.; Golubeva, E.N.; Kostjuk, S.; Vosough, M.; Timashev, P.S.; Shpichka, A.I. Approach to tune drug release in particles fabricated from methacrylate functionalized polylactides. *Mol. Syst. Des. Eng.*, **2021**, 6(3), 202-213. <http://dx.doi.org/10.1039/D0ME00157K>
- [74] Cordeiro, A.S.; Tekko, I.A.; Jomaa, M.H.; Vora, L.; McAlister, E.; Volpe-Zanutto, F.; Nethery, M.; Baine, P.T.; Mitchell, N.; McNeill, D.W.; Donnelly, R.F. Two-photon polymerisation 3D printing of microneedle array templates with versatile designs: Application in the development of polymeric drug delivery systems. *Pharm. Res.*, **2020**, 37(9), 174. <http://dx.doi.org/10.1007/s11095-020-02887-9> PMID: 32856172
- [75] Do, A.V.; Worthington, K.S.; Tucker, B.A.; Salem, A.K. Controlled drug delivery from 3D printed two-photon polymerized poly(ethylene glycol) dimethacrylate devices. *Int. J. Pharm.*, **2018**, 552(1-2), 217-224. <http://dx.doi.org/10.1016/j.ijpharm.2018.09.065> PMID: 30268853
- [76] Giri, B.R.; Song, E.S.; Kwon, J.; Lee, J-H.; Park, J-B.; Kim, D.W. Fabrication of intragastric floating, controlled release 3D printed theophylline tablets using hot-melt extrusion and fused deposition modeling. *Pharmaceutics*, **2020**, 12(1), 77.
- [77] Awad, A.; Fina, F.; Goyanes, A.; Gaisford, S.; Basit, A.W. 3D printing: Principles and pharmaceutical applications of selective laser sintering. *Int. J. Pharm.*, **2020**, 586, 119594. <http://dx.doi.org/10.1016/j.ijpharm.2020.119594> PMID: 32622811
- [78] Jamróz, W.; Szafraniec, J.; Kurek, M.; Jachowicz, R. 3D printing in pharmaceutical and medical applications - recent achievements and challenges. *Pharm. Res.*, **2018**, 35(9), 176. <http://dx.doi.org/10.1007/s11095-018-2454-x> PMID: 29998405
- [79] Leong, K.F.; Chua, C.K.; Gui, W.S.; Verani Building porous biopolymeric microstructures for controlled drug delivery devices using selective laser sintering. *Int. J. Adv. Manuf. Technol.*, **2006**, 31(5-6), 483-489. <http://dx.doi.org/10.1007/s00170-005-0217-4>
- [80] Fina, F.; Goyanes, A.; Gaisford, S.; Basit, A.W. Selective laser sintering (SLS) 3D printing of medicines. *Int. J. Pharm.*, **2017**, 529(1-2), 285-293. <http://dx.doi.org/10.1016/j.ijpharm.2017.06.082> PMID: 28668582
- [81] Tolochko, N.; Mozzharov, S.; Laoui, T.; Froyen, L. Selective laser sintering of single and two component metal powders. *Rapid Prototyping J.*, **2003**, 9(2), 68-78. <http://dx.doi.org/10.1108/13552540310467077>
- [82] Williams, J.M.; Adewunmi, A.; Schek, R.M.; Flanagan, C.L.; Krebsbach, P.H.; Feinberg, S.E.; Hollister, S.J.; Das, S. Bone tissue engineering using polycaprolactone scaffolds fabricated via selective laser sintering. *Biomaterials*, **2005**, 26(23), 4817-4827. <http://dx.doi.org/10.1016/j.biomaterials.2004.11.057> PMID: 15763261
- [83] Shi, Y.; Pan, T.; Zhu, W.; Yan, C.; Xia, Z. Artificial bone scaffolds of coral imitation prepared by selective laser sintering. *J. Mech. Behav. Biomed. Mater.*, **2020**, 104, 103664. <http://dx.doi.org/10.1016/j.jmbbm.2020.103664> PMID: 32174422
- [84] Shuai, C.; Gao, C.; Nie, Y.; Hu, H.; Zhou, Y.; Peng, S. Structure and properties of nano-hydroxyapatite scaffolds for bone tissue engineering with a selective laser sintering system. *Nanotechnology*, **2011**, 22(28), 285703. <http://dx.doi.org/10.1088/0957-4484/22/28/285703> PMID: 21642759
- [85] Bertrand, P.; Bayle, F.; Combe, C.; Goeriot, P.; Smurov, I. Ceramic components manufacturing by selective laser sintering. *Appl. Surf. Sci.*, **2007**, 254(4), 989-992. <http://dx.doi.org/10.1016/j.apsusc.2007.08.085>
- [86] Hamed, R.; Mohamed, E.M.; Rahman, Z.; Khan, M.A. 3D-printing of lopinavir printlets by selective laser sintering and quantification of crystalline fraction by XRPD-chemometric models. *Int. J. Pharm.*, **2021**, 592, 120059. <http://dx.doi.org/10.1016/j.ijpharm.2020.120059> PMID: 33171261
- [87] Cui, M.; Pan, H.; Su, Y.; Fang, D.; Qiao, S.; Ding, P.; Pan, W. Opportunities and challenges of three-dimensional printing technology in pharmaceutical formulation development. *Acta Pharm. Sin. B*, **2021**, 11(8), 2488-2504. <http://dx.doi.org/10.1016/j.apsb.2021.03.015> PMID: 34567958
- [88] Thakkar, R.; Pillai, A.R.; Zhang, J.; Zhang, Y.; Kulkarni, V.; Maniruzzaman, M. Novel on-demand 3-dimensional (3-D) printed tablets using fill density as an effective release-controlling tool. *Polymers*, **2020**, 12(9), 1872.
- [89] Beck, R.C.R.; Chaves, P.S.; Goyanes, A.; Vukosavljevic, B.; Buanz, A.; Windbergs, M.; Basit, A.W.; Gaisford, S.

- 3D printed tablets loaded with polymeric nanocapsules: An innovative approach to produce customized drug delivery systems. *Int. J. Pharm.*, **2017**, *528*(1-2), 268-279. <http://dx.doi.org/10.1016/j.ijpharm.2017.05.074> PMID: 28583328
- [90] Melocchi, A.; Parietti, F.; Loreti, G.; Maroni, A.; Gazzaniga, A.; Zema, L. 3D printing by fused deposition modeling (FDM) of a swellable/erodible capsular device for oral pulsatile release of drugs. *J. Drug Deliv. Sci. Technol.*, **2015**, *30*, 360-367. <http://dx.doi.org/10.1016/j.jddst.2015.07.016>
- [91] Goyanes, A.; Buanz, A.B.M.; Basit, A.W.; Gaisford, S. Fused-filament 3D printing (3DP) for fabrication of tablets. *Int. J. Pharm.*, **2014**, *476*(1-2), 88-92. <http://dx.doi.org/10.1016/j.ijpharm.2014.09.044> PMID: 25275937
- [92] Khorasani, M.; Edinger, M.; Rajjada, D.; Bøtker, J.; Aho, J.; Rantanen, J. Near-infrared chemical imaging (NIR-CI) of 3D printed pharmaceuticals. *Int. J. Pharm.*, **2016**, *515*(1-2), 324-330. <http://dx.doi.org/10.1016/j.ijpharm.2016.09.075> PMID: 27720877
- [93] Melocchi, A.; Parietti, F.; Maroni, A.; Foppoli, A.; Gazzaniga, A.; Zema, L. Hot-melt extruded filaments based on pharmaceutical grade polymers for 3D printing by fused deposition modeling. *Int. J. Pharm.*, **2016**, *509*(1-2), 255-263. <http://dx.doi.org/10.1016/j.ijpharm.2016.05.036> PMID: 27215535
- [94] Shaqour, B.; Reigada, I.; Górecka, Ż.; Choinńska, E.; Verleije, B.; Beyers, K.; Świąszkowski, W.; Fallarero, A.; Cos, P. 3D-printed drug delivery systems: The effects of drug incorporation methods on their release and antibacterial efficiency. *Materials*, **2020**, *13*(15), 3364.
- [95] Zhang, J.; Feng, X.; Patil, H.; Tiwari, R.V.; Repka, M.A. Coupling 3D printing with hot-melt extrusion to produce controlled-release tablets. *Int. J. Pharm.*, **2017**, *519*(1-2), 186-197. <http://dx.doi.org/10.1016/j.ijpharm.2016.12.049> PMID: 28017768
- [96] Verstraete, G.; Samaro, A.; Grymonpré, W.; Vanhoorne, V.; Van Snick, B.; Boone, M.N.; Hellemans, T.; Van Hoorebeke, L.; Remon, J.P.; Vervaet, C. 3D printing of high drug loaded dosage forms using thermoplastic polyurethanes. *Int. J. Pharm.*, **2018**, *536*(1), 318-325. <http://dx.doi.org/10.1016/j.ijpharm.2017.12.002> PMID: 29217471
- [97] Awad, A.; Trenfield, S.J.; Gaisford, S.; Basit, A.W. 3D printed medicines: A new branch of digital healthcare. *Int. J. Pharm.*, **2018**, *548*(1), 586-596. <http://dx.doi.org/10.1016/j.ijpharm.2018.07.024> PMID: 30033380
- [98] Araújo, M.R.P.; Sa-Barreto, L.L.; Gratieri, T.; Gelfuso, G.M.; Cunha-Filho, M. The digital pharmacies era: How 3D printing technology using fused deposition modeling can become a reality. *Pharmaceutics*, **2019**, *11*(3), 128.
- [99] Goyanes, A.; Buanz, A.B.M.; Hatton, G.B.; Gaisford, S.; Basit, A.W. 3D printing of modified-release aminosalicilate (4-ASA and 5-ASA) tablets. *Eur. J. Pharm. Biopharm.*, **2015**, *89*, 157-162. <http://dx.doi.org/10.1016/j.ejpb.2014.12.003> PMID: 25497178
- [100] Kollamaram, G.; Croker, D.M.; Walker, G.M.; Goyanes, A.; Basit, A.W.; Gaisford, S. Low temperature fused deposition modeling (FDM) 3D printing of thermolabile drugs. *Int. J. Pharm.*, **2018**, *545*(1-2), 144-152. <http://dx.doi.org/10.1016/j.ijpharm.2018.04.055> PMID: 29705104
- [101] Pereira, B.C.; Isreb, A.; Forbes, R.T.; Dores, F.; Habashy, R.; Petit, J.B.; Alhnan, M.A.; Oga, E.F. 'Temporary Plasticiser': A novel solution to fabricate 3D printed patient-centred cardiovascular 'Polypill' architectures. *Eur. J. Pharm. Biopharm.*, **2019**, *135*, 94-103. <http://dx.doi.org/10.1016/j.ejpb.2018.12.009> PMID: 30579852
- [102] Kempin, W.; Domsta, V.; Grathoff, G.; Brecht, I.; Semmling, B.; Tillmann, S.; Weitschies, W.; Seidlitz, A. Immediate release 3D-printed tablets produced via fused deposition modeling of a thermo-sensitive drug. *Pharm. Res.*, **2018**, *35*(6), 124. <http://dx.doi.org/10.1007/s11095-018-2405-6> PMID: 29679157
- [103] Fanous, M.; Gold, S.; Muller, S.; Hirsch, S.; Ogorka, J.; Imanidis, G. Simplification of fused deposition modeling 3D-printing paradigm: Feasibility of 1-step direct powder printing for immediate release dosage form production. *Int. J. Pharm.*, **2020**, *578*, 119124. <http://dx.doi.org/10.1016/j.ijpharm.2020.119124> PMID: 32035253
- [104] El Aita, I.; Breikreutz, J.; Quodbach, J. On-demand manufacturing of immediate release levetiracetam tablets using pressure-assisted microsyringe printing. *Eur. J. Pharm. Biopharm.*, **2019**, *134*, 29-36. <http://dx.doi.org/10.1016/j.ejpb.2018.11.008> PMID: 30439504
- [105] Cheng, Y.; Qin, H.; Acevedo, N.C.; Jiang, X.; Shi, X. 3D printing of extended-release tablets of theophylline using hydroxypropyl methylcellulose (HPMC) hydrogels. *Int. J. Pharm.*, **2020**, *591*, 119983. <http://dx.doi.org/10.1016/j.ijpharm.2020.119983> PMID: 33065220
- [106] Khaled, S.A.; Burley, J.C.; Alexander, M.R.; Roberts, C.J. Desktop 3D printing of controlled release pharmaceutical bilayer tablets. *Int. J. Pharm.*, **2014**, *461*(1-2), 105-111. <http://dx.doi.org/10.1016/j.ijpharm.2013.11.021> PMID: 24280018
- [107] Zema, L.; Melocchi, A.; Maroni, A.; Gazzaniga, A. Three-dimensional printing of medicinal products and the challenge of personalized therapy. *J. Pharm. Sci.*, **2017**, *106*(7), 1697-1705. <http://dx.doi.org/10.1016/j.xphs.2017.03.021> PMID: 28347731
- [108] Dores, F.; Kuźmińska, M.; Soares, C.; Bohus, M.; A Shervington, L.; Habashy, R.; Pereira, B.C.; Peak, M.; Isreb, A.; Alhnan, M.A. Temperature and solvent facilitated extrusion based 3D printing for pharmaceuticals. *Eur. J. Pharm. Sci.*, **2020**, *152*, 105430. <http://dx.doi.org/10.1016/j.ejps.2020.105430> PMID: 32562691
- [109] Kotta, S.; Nair, A.; Alsabeelah, N. 3D printing technology in drug delivery: Recent progress and application. *Curr. Pharm. Des.*, **2019**, *24*(42), 5039-5048. <http://dx.doi.org/10.2174/1381612825666181206123828> PMID: 30520368
- [110] Azizi Machekposhti, S.; Mohaved, S.; Narayan, R.J. Inkjet dispensing technologies: Recent advances for novel drug discovery. *Expert Opin. Drug Discov.*, **2019**, *14*(2), 101-113. <http://dx.doi.org/10.1080/17460441.2019.1567489> PMID: 30676831

- [111] Daly, R.; Harrington, T.S.; Martin, G.D.; Hutchings, I.M. Inkjet printing for pharmaceuticals - A review of research and manufacturing. *Int. J. Pharm.*, **2015**, *494*(2), 554-567. <http://dx.doi.org/10.1016/j.ijpharm.2015.03.017> PMID: 25772419
- [112] İċten, E.; Giridhar, A.; Taylor, L.S.; Nagy, Z.K.; Reklaitis, G.V. Dropwise additive manufacturing of pharmaceutical products for melt-based dosage forms. *J. Pharm. Sci.*, **2015**, *104*(5), 1641-1649. <http://dx.doi.org/10.1002/jps.24367> PMID: 25639605
- [113] Alomari, M.; Mohamed, F.H.; Basit, A.W.; Gaisford, S. Personalised dosing: Printing a dose of one's own medicine. *Int. J. Pharm.*, **2015**, *494*(2), 568-577. <http://dx.doi.org/10.1016/j.ijpharm.2014.12.006> PMID: 25498157
- [114] Acosta-Vélez, G.F.; Wu, B. 3D pharming: Direct printing of personalized pharmaceutical tablets. *Polym. Sci.*, **2016**, *2*(1), 11.
- [115] Vadodaria, S.; Mills, T. Jetting-based 3D printing of edible materials. *Food Hydrocoll.*, **2020**, *106*, 105857. <http://dx.doi.org/10.1016/j.foodhyd.2020.105857>
- [116] Kollamaram, G.; Hopkins, S.C.; Glowacki, B.A.; Croker, D.M.; Walker, G.M. Inkjet printing of paracetamol and indomethacin using electromagnetic technology: Rheological compatibility and polymorphic selectivity. *Eur. J. Pharm. Sci.*, **2018**, *115*, 248-257. <http://dx.doi.org/10.1016/j.ejps.2018.01.036> PMID: 29366961
- [117] Ehtezazi, T.; Dempster, N.M.; Martin, G.D.; Hoath, S.D.; Hutchings, I.M. Development of high-throughput glass inkjet devices for pharmaceutical applications. *J. Pharm. Sci.*, **2014**, *103*(11), 3733-3742. <http://dx.doi.org/10.1002/jps.24192> PMID: 25266398
- [118] Clark, E.A.; Alexander, M.R.; Irvine, D.J.; Roberts, C.J.; Wallace, M.J.; Sharpe, S.; Yoo, J.; Hague, R.J.M.; Tuck, C.J.; Wildman, R.D. 3D printing of tablets using inkjet with UV photoinitiation. *Int. J. Pharm.*, **2017**, *529*(1-2), 523-530. <http://dx.doi.org/10.1016/j.ijpharm.2017.06.085> PMID: 28673860
- [119] Yuan, S.; Shen, F.; Chua, C.K.; Zhou, K. Polymeric composites for powder-based additive manufacturing: Materials and applications. *Prog. Polym. Sci.*, **2019**, *91*, 141-168. <http://dx.doi.org/10.1016/j.progpolymsci.2018.11.001>
- [120] Aulton, M.E.; Taylor, K. *Aulton's pharmaceuticals: The design and manufacture of medicines*; Elsevier, **2013**.
- [121] Yu, D.G.; Zhu, L.M.; Branford-White, C.J.; Yang, X.L. Three-dimensional printing in pharmaceuticals: Promises and problems. *J. Pharm. Sci.*, **2008**, *97*(9), 3666-3690. <http://dx.doi.org/10.1002/jps.21284> PMID: 18257041
- [122] Vithani, K.; Goyanes, A.; Jannin, V.; Basit, A.W.; Gaisford, S.; Boyd, B.J. An overview of 3D printing technologies for soft materials and potential opportunities for lipid-based drug delivery systems. *Pharm. Res.*, **2019**, *36*(1), 4. <http://dx.doi.org/10.1007/s11095-018-2531-1> PMID: 30406349
- [123] Wang, C.-C.; Tejwani Motwani, M.R.; Roach, W.J.; Kay, J.L.; Yoo, J.; Surprenant, H.L.; Monkhouse, D.C.; Pryor, T.J. Development of near zero-order release dosage forms using three-dimensional printing (3-DP) technology. *Drug Dev. Ind. Pharm.*, **2006**, *32*(3), 367-376. <http://dx.doi.org/10.1080/03639040500519300> PMID: 16556541
- [124] Kolakovic, R.; Viitala, T.; Ihalainen, P.; Genina, N.; Peltonen, J.; Sandler, N. Printing technologies in fabrication of drug delivery systems. *Expert Opin. Drug Deliv.*, **2013**, *10*(12), 1711-1723. <http://dx.doi.org/10.1517/17425247.2013.859134> PMID: 24256326
- [125] Buanz, A.B.M.; Saunders, M.H.; Basit, A.W.; Gaisford, S. Preparation of personalized-dose salbutamol sulphate oral films with thermal ink-jet printing. *Pharm. Res.*, **2011**, *28*(10), 2386-2392. <http://dx.doi.org/10.1007/s11095-011-0450-5> PMID: 21544688
- [126] Wilts, E.M.; Ma, D.; Bai, Y.; Williams, C.B.; Long, T.E. Comparison of Linear and 4-Arm Star Poly(vinyl pyrrolidone) for Aqueous Binder Jetting Additive Manufacturing of Personalized Dosage Tablets. *ACS Appl. Mater. Interfaces*, **2019**, *11*(27), 23938-23947. <http://dx.doi.org/10.1021/acsami.9b08116> PMID: 31252452
- [127] Infanger, S.; Haemmerli, A.; Iliev, S.; Baier, A.; Stoyanov, E.; Quodbach, J. Powder bed 3D-printing of highly loaded drug delivery devices with hydroxypropyl cellulose as solid binder. *Int. J. Pharm.*, **2019**, *555*, 198-206. <http://dx.doi.org/10.1016/j.ijpharm.2018.11.048> PMID: 30458260
- [128] Trenfield, S.J.; Awad, A.; Madla, C.M.; Hatton, G.B.; Firth, J.; Goyanes, A.; Gaisford, S.; Basit, A.W. Shaping the future: Recent advances of 3D printing in drug delivery and healthcare. *Expert Opin. Drug Deliv.*, **2019**, *16*(10), 1081-1094. <http://dx.doi.org/10.1080/17425247.2019.1660318> PMID: 31478752
- [129] Elele, E.; Shen, Y.; Susarla, R.; Khusid, B.; Keyvan, G.; Michniak-Kohn, B. Electrodeless electrohydrodynamic drop-on-demand encapsulation of drugs into porous polymer films for fabrication of personalized dosage units. *J. Pharm. Sci.*, **2012**, *101*(7), 2523-2533. <http://dx.doi.org/10.1002/jps.23165> PMID: 22527973
- [130] Meléndez, P.A.; Kane, K.M.; Ashvar, C.S.; Albrecht, M.; Smith, P.A. Thermal inkjet application in the preparation of oral dosage forms: Dispensing of prednisolone solutions and polymorphic characterization by solid-state spectroscopic techniques. *J. Pharm. Sci.*, **2008**, *97*(7), 2619-2636. <http://dx.doi.org/10.1002/jps.21189> PMID: 17876767
- [131] Goodall, S.; Chew, N.; Chan, K.; Auriac, D.; Waters, M.J. Aerosolization of protein solutions using thermal inkjet technology. *J. Aerosol Med.*, **2002**, *15*(3), 351-357. <http://dx.doi.org/10.1089/089426802760292717> PMID: 12396425
- [132] Lee, K.J.; Kang, A.; Delfino, J.J.; West, T.G.; Chetty, D.; Monkhouse, D.C.; Yoo, J. Evaluation of critical formulation factors in the development of a rapidly dispersing captopril oral dosage form. *Drug Dev. Ind. Pharm.*, **2003**, *29*(9), 967-979. <http://dx.doi.org/10.1081/DDC-120025454> PMID: 14606661
- [133] Wang, B.; Wu, S.; Ahmad, Z.; Li, J.; Chang, M.W. Co-printing of vertical axis aligned micron-scaled filaments via simultaneous dual needle electrohydrodynamic printing. *Eur. Polym. J.*, **2018**, *104*, 81-89. <http://dx.doi.org/10.1016/j.eurpolymj.2018.05.005>
- [134] Wu, S.; Ahmad, Z.; Li, J.S.; Chang, M.W. Fabrication of flexible composite drug films via foldable linkages using electrohydrodynamic printing. *Mater. Sci. Eng. C*, **2020**, *108*, 110393. <http://dx.doi.org/10.1016/j.msec.2019.110393> PMID:

- 31923982
- [135] Yao, Z.C.; Wang, J.C.; Ahmad, Z.; Li, J.S.; Chang, M.W. Fabrication of patterned three-dimensional micron scaled core-sheath architectures for drug patches. *Mater. Sci. Eng. C*, **2019**, *97*, 776-783. <http://dx.doi.org/10.1016/j.msec.2018.12.110> PMID: 30678967
- [136] Li, X.; Zhang, C.; Wu, S.; Chen, X.; Mai, J.; Chang, M.W. Precision printing of customized cylindrical capsules with multifunctional layers for oral drug delivery. *ACS Appl. Mater. Interfaces*, **2019**, *11*(42), 39179-39191. <http://dx.doi.org/10.1021/acsami.9b13568> PMID: 31573786
- [137] Wang, B.; Chen, X.; Ahmad, Z.; Huang, J.; Chang, M.W. Engineering on-demand magnetic core-shell composite wound dressing matrices via electrohydrodynamic micro-scale printing. *Adv. Eng. Mater.*, **2019**, *21*(10), 1900699. <http://dx.doi.org/10.1002/adem.201900699>
- [138] Muwaffak, Z.; Goyanes, A.; Clark, V.; Basit, A.W.; Hilton, S.T.; Gaisford, S. Patient-specific 3D scanned and 3D printed antimicrobial polycaprolactone wound dressings. *Int. J. Pharm.*, **2017**, *527*(1-2), 161-170. <http://dx.doi.org/10.1016/j.ijpharm.2017.04.077> PMID: 28461267
- [139] Wang, B.; Chen, X.; Ahmad, Z.; Huang, J.; Chang, M.W. 3D electrohydrodynamic printing of highly aligned dual-core graphene composite matrices. *Carbon*, **2019**, *153*, 285-297. <http://dx.doi.org/10.1016/j.carbon.2019.07.030>
- [140] Wang, J.C.; Zheng, H.; Chang, M.W.; Ahmad, Z.; Li, J.S. Preparation of active 3D film patches via aligned fiber electrohydrodynamic (EHD) printing. *Sci. Rep.*, **2017**, *7*(1), 43924. <http://dx.doi.org/10.1038/srep43924> PMID: 28272513
- [141] Yao, Z.C.; Wang, J.C.; Wang, B.; Ahmad, Z.; Li, J.S.; Chang, M.W. A novel approach for tailored medicines: Direct writing of Janus fibers. *J. Drug Deliv. Sci. Technol.*, **2019**, *50*, 372-379. <http://dx.doi.org/10.1016/j.jddst.2019.02.006>
- [142] Choonara, Y.E.; du Toit, L.C.; Kumar, P.; Kondiah, P.P.D.; Pillay, V. 3D-printing and the effect on medical costs: A new era? *Expert Rev. Pharmacoecon. Outcomes Res.*, **2016**, *16*(1), 23-32. <http://dx.doi.org/10.1586/14737167.2016.1138860> PMID: 26817398
- [143] Palo, M.; Holländer, J.; Suominen, J.; Yliruusi, J.; Sandler, N. 3D printed drug delivery devices: perspectives and technical challenges. *Expert Rev. Med. Devices*, **2017**, *14*(9), 685-696. <http://dx.doi.org/10.1080/17434440.2017.1363647> PMID: 28774216
- [144] Mertz, L. Dream it, design it, print it in 3-D: what can 3-D printing do for you? *IEEE Pulse*, **2013**, *4*(6), 15-21. <http://dx.doi.org/10.1109/MPUL.2013.2279616> PMID: 24233186
- [145] Ku, M.S.; Dulin, W. A biopharmaceutical classification-based Right-First-Time formulation approach to reduce human pharmacokinetic variability and project cycle time from First-In-Human to clinical Proof-Of-Concept. *Pharm. Dev. Technol.*, **2012**, *17*(3), 285-302. <http://dx.doi.org/10.3109/10837450.2010.535826> PMID: 21121705
- [146] Hay, M.; Thomas, D.W.; Craighead, J.L.; Economides, C.; Rosenthal, J. Clinical development success rates for investigational drugs. *Nat. Biotechnol.*, **2014**, *32*(1), 40-51. <http://dx.doi.org/10.1038/nbt.2786> PMID: 24406927
- [147] Kwong, E. *Oral formulation roadmap from early drug discovery to development*; John Wiley & Sons, **2017**. <http://dx.doi.org/10.1002/9781118907894>
- [148] Guvendiren, M.; Molde, J.; Soares, R.M.D.; Kohn, J. Designing biomaterials for 3D printing. *ACS Biomater. Sci. Eng.*, **2016**, *2*(10), 1679-1693. <http://dx.doi.org/10.1021/acsbomaterials.6b00121> PMID: 28025653
- [149] Gioumouxouzis, C.I.; Karavasilis, C.; Fatouros, D.G. Recent advances in pharmaceutical dosage forms and devices using additive manufacturing technologies. *Drug Discov. Today*, **2019**, *24*(2), 636-643. <http://dx.doi.org/10.1016/j.drudis.2018.11.019> PMID: 30503803
- [150] Alhnan, M.A.; Okwuosa, T.C.; Sadia, M.; Wan, K.W.; Ahmed, W.; Arafat, B. Emergence of 3D printed dosage forms: Opportunities and challenges. *Pharm. Res.*, **2016**, *33*(8), 1817-1832. <http://dx.doi.org/10.1007/s11095-016-1933-1> PMID: 27194002
- [151] Gross, B.C.; Erkal, J.L.; Lockwood, S.Y.; Chen, C.; Spence, D.M. Evaluation of 3D printing and its potential impact on biotechnology and the chemical sciences. *Anal. Chem.*, **2014**, *86*(7), 3240-3253. <http://dx.doi.org/10.1021/ac403397r> PMID: 24432804
- [152] Pravin, S.; Sudhir, A. Integration of 3D printing with dosage forms: A new perspective for modern healthcare. *Biomed. Pharmacother.*, **2018**, *107*, 146-154. <http://dx.doi.org/10.1016/j.biopha.2018.07.167> PMID: 30086461
- [153] Alam, M.S.; Akhtar, A.; Ahsan, I.; Shafiq-un-Nabi, S. Pharmaceutical product development exploiting 3D printing technology: Conventional to novel drug delivery system. *Curr. Pharm. Des.*, **2019**, *24*(42), 5029-5038. <http://dx.doi.org/10.2174/1381612825666190206195808> PMID: 30727872
- [154] Warsi, M.H.; Yusuf, M.; Al Robaian, M.; Khan, M.; Muheem, A.; Khan, S. 3D printing methods for pharmaceutical manufacturing: Opportunity and challenges. *Curr. Pharm. Des.*, **2019**, *24*(42), 4949-4956. <http://dx.doi.org/10.2174/1381612825666181206121701> PMID: 30520367
- [155] Robles-Martinez, P.; Xu, X.; Trenfield, S.J.; Awad, A.; Goyanes, A.; Telford, R.; Basit, A.W.; Gaisford, S. 3D printing of a multi-layered polypill containing six drugs using a novel stereolithographic method. *Pharmaceutics*, **2019**, *11*(6), 274. <http://dx.doi.org/10.2174/1381612825666190116104620>
- [156] Lim, S.H.; Kathuria, H.; Tan, J.J.Y.; Kang, L. 3D printed drug delivery and testing systems - a passing fad or the future? *Adv. Drug Deliv. Rev.*, **2018**, *132*, 139-168. <http://dx.doi.org/10.1016/j.addr.2018.05.006> PMID: 29778901
- [157] Norman, J.; Madurawe, R.D.; Moore, C.M.V.; Khan, M.A.; Khairuzzaman, A. A new chapter in pharmaceutical manufacturing: 3D-printed drug products. *Adv. Drug Deliv. Rev.*, **2017**, *108*, 39-50. <http://dx.doi.org/10.1016/j.addr.2016.03.001> PMID: 27001902
- [158] Ameenuzzafar, Alruwaili, N.K.; Rizwanullah, M.; Abbas Bukhari, S.N.; Amir, M.; Ahmed, M.M.; Fazil, M. 3D printing technology in design of pharmaceutical products. *Curr. Pharm. Des.*, **2019**, *24*(42), 5009-5018. <http://dx.doi.org/10.2174/1381612825666190116104620>

- PMID: 30652636
- [159] Wang, X.; Zhou, J.; Yang, W.; Pang, J.; Zhang, W.; Chen, G.; Dong, X.; Zheng, Z.; Lin, W.; Feng, W.; Zhou, G.; Zhu, W.; Yang, F. Wapage optimization and influence factors analysis of 3D printing personalized JJY tablets. *Drug Dev. Ind. Pharm.*, **2020**, *46*(3), 388-394. <http://dx.doi.org/10.1080/03639045.2020.1724129> PMID: 32081054
- [160] Karavasili, C.; Gkaragkounis, A.; Moschakis, T.; Ritzioulis, C.; Fatouros, D.G. Pediatric-friendly chocolate-based dosage forms for the oral administration of both hydrophilic and lipophilic drugs fabricated with extrusion-based 3D printing. *Eur. J. Pharm. Sci.*, **2020**, *147*, 105291. <http://dx.doi.org/10.1016/j.ejps.2020.105291> PMID: 32135271
- [161] Sandler, N.; Preis, M. Printed drug-delivery systems for improved patient treatment. *Trends Pharmacol. Sci. Rep.*, **2016**, *37*(12), 1070-1080.
- [162] Haleem, A.; Javaid, M.; Khan, R.H.; Suman, R. 3D printing applications in bone tissue engineering. *J. Clin. Orthop. Trauma*, **2020**, *11*(Suppl. 1), S118-S124. <http://dx.doi.org/10.1016/j.jcot.2019.12.002> PMID: 31992931
- [163] Huang, W.; Zhang, X. 3D Printing: Print the future of ophthalmology. *Invest. Ophthalmol. Vis. Sci.*, **2014**, *55*(8), 5380-5381. <http://dx.doi.org/10.1167/iovs.14-15231> PMID: 25159591
- [164] Jammalamadaka, U.; Tappa, K. Recent advances in biomaterials for 3D printing and tissue engineering. *J. Funct. Biomater.*, **2018**, *9*(1), 22. <http://dx.doi.org/10.3390/jfb9010022> PMID: 29494503
- [165] Souto, E.B.; Campos, J.C.; Filho, S.C.; Teixeira, M.C.; Martins-Gomes, C.; Zielinska, A.; Carbone, C.; Silva, A.M. 3D printing in the design of pharmaceutical dosage forms. *Pharm. Dev. Technol.*, **2019**, *24*(8), 1044-1053. <http://dx.doi.org/10.1080/10837450.2019.1630426> PMID: 31180272
- [166] Khatri, P.; Shah, M.K.; Vora, N. Formulation strategies for solid oral dosage form using 3D printing technology: A mini-review. *J. Drug Deliv. Sci. Technol.*, **2018**, *46*, 148-155. <http://dx.doi.org/10.1016/j.jddst.2018.05.009>
- [167] Kempin, W.; Franz, C.; Koster, L.C.; Schneider, F.; Bogdahn, M.; Weitschies, W.; Seidlitz, A. Assessment of different polymers and drug loads for fused deposition modeling of drug loaded implants. *Eur. J. Pharm. Biopharm.*, **2017**, *115*, 84-93. <http://dx.doi.org/10.1016/j.ejpb.2017.02.014> PMID: 28232106
- [168] Allen, E.A.; O'Mahony, C.; Cronin, M.; O'Mahony, T.; Moore, A.C.; Crean, A.M. Dissolvable microneedle fabrication using piezoelectric dispensing technology. *Int. J. Pharm.*, **2016**, *500*(1-2), 1-10. <http://dx.doi.org/10.1016/j.ijpharm.2015.12.052> PMID: 26721722
- [169] Arshad, M.S.; Shahzad, A.; Abbas, N.; AlAsiri, A.; Hussain, A.; Kucuk, I.; Chang, M.W.; Bukhari, N.I.; Ahmad, Z. Preparation and characterization of indomethacin loaded films by piezoelectric inkjet printing: A personalized medication approach. *Pharm. Dev. Technol.*, **2020**, *25*(2), 197-205. <http://dx.doi.org/10.1080/10837450.2019.1684520> PMID: 31638453
- [170] Donnelly, R.F.; Singh, T.R.R.; Woolfson, A.D. Microneedle-based drug delivery systems: Microfabrication, drug delivery, and safety. *Drug Deliv.*, **2010**, *17*(4), 187-207. <http://dx.doi.org/10.3109/10717541003667798> PMID: 20297904
- [171] van Riet-Nales, D.A.; de Neef, B.J.; Schobben, A.F.A.M.; Ferreira, J.A.; Egberts, T.C.G.; Rademaker, C.M.A. Acceptability of different oral formulations in infants and preschool children. *Arch. Dis. Child.*, **2013**, *98*(9), 725-731. <http://dx.doi.org/10.1136/archdischild-2012-303303> PMID: 23853004
- [172] Goyanes, A.; Madla, C.M.; Umerji, A.; Duran Piñeiro, G.; Giraldez Montero, J.M.; Lamas Diaz, M.J.; Gonzalez Barcia, M.; Taherali, F.; Sánchez-Pintos, P.; Couce, M.L.; Gaisford, S.; Basit, A.W. Automated therapy preparation of isoleucine formulations using 3D printing for the treatment of MSUD: First single-centre, prospective, crossover study in patients. *Int. J. Pharm.*, **2019**, *567*, 118497. <http://dx.doi.org/10.1016/j.ijpharm.2019.118497> PMID: 31279771
- [173] Scoutaris, N.; Ross, S.A.; Douroumis, D. 3D printed "star-mix" drug loaded dosage forms for paediatric applications. *Pharm. Res.*, **2018**, *35*(2), 34. <http://dx.doi.org/10.1007/s11095-017-2284-2> PMID: 29368113
- [174] Wang, H.; Dumpa, N.; Bandari, S.; Durig, T.; Repka, M.A. Fabrication of taste-masked donut-shaped tablets via fused filament fabrication 3D printing paired with hot-melt extrusion techniques. *AAPS PharmSciTech*, **2020**, *21*(7), 243. <http://dx.doi.org/10.1208/s12249-020-01783-0> PMID: 32856144
- [175] Boateng, J. Drug delivery innovations to address global health challenges for pediatric and geriatric populations (through improvements in patient compliance). *J. Pharm. Sci.*, **2017**, *106*(11), 3188-3198. <http://dx.doi.org/10.1016/j.xphs.2017.07.009> PMID: 28734784
- [176] Fastø, M.M.; Genina, N.; Kaae, S.; Källemark Sporrang, S. Perceptions, preferences and acceptability of patient designed 3D printed medicine by polypharmacy patients: A pilot study. *Int. J. Clin. Pharm.*, **2019**, *41*(5), 1290-1298. <http://dx.doi.org/10.1007/s11096-019-00892-6> PMID: 31444687
- [177] Lee, C.; Abelseth, E.; de la Vega, L.; Willerth, S.M. Bioprinting a novel glioblastoma tumor model using a fibrin-based bioink for drug screening. *Mater. Today Chem.*, **2019**, *12*, 78-84. <http://dx.doi.org/10.1016/j.mtchem.2018.12.005>
- [178] Hao, W.; Zheng, Z.; Zhu, L.; Pang, L.; Ma, J.; Zhu, S.; Du, L.; Jin, Y. 3D printing based drug-loaded implanted prosthesis to prevent breast cancer recurrence post-conserving surgery. *Asian J. Pharmaceut. Sci.*, **2021**, *16*(1), 86-96. <http://dx.doi.org/10.1016/j.ajps.2020.06.002> PMID: 33613732
- [179] Chen, J.; Liu, C.Y.; Wang, X.; Sweet, E.; Liu, N.; Gong, X.; Lin, L. 3D printed microfluidic devices for circulating tumor cells (CTCs) isolation. *Biosens. Bioelectron.*, **2020**, *150*, 111900. <http://dx.doi.org/10.1016/j.bios.2019.111900> PMID: 31767348
- [180] Bhuskute, H.; Shende, P.; Prabhakar, B. 3D printed personalized medicine for cancer: Applications for betterment of diagnosis, prognosis and treatment. *AAPS PharmSciTech*, **2021**, *23*(1), 8.

- <http://dx.doi.org/10.1208/s12249-021-02153-0> PMID: 34853934
- [181] Haleem, A.; Javaid, M. 3D printed medical parts with different materials using additive manufacturing. *Clin. Epidemiol. Glob. Health*, **2020**, *8*(1), 215-223. <http://dx.doi.org/10.1016/j.cegh.2019.08.002>
- [182] Roberts, S.; Peyman, S.; Speirs, V. Current and emerging 3D models to study breast cancer. In: *Breast Cancer Metastasis and Drug Resistance: Challenges and Progress*; Ahmad, A., Ed.; Springer: Cham, **2019**; pp. 413-427. http://dx.doi.org/10.1007/978-3-030-20301-6_22
- [183] Tagami, T.; Goto, E.; Kida, R.; Hirose, K.; Noda, T.; Ozeeki, T. Lyophilized ophthalmologic patches as novel corneal drug formulations using a semi-solid extrusion 3D printer. *Int. J. Pharm.*, **2022**, *617*, 121448. <http://dx.doi.org/10.1016/j.ijpharm.2022.121448> PMID: 35066116
- [184] Tan, G.; Ioannou, N.; Mathew, E.; Tagalakis, A.D.; Lamprou, D.A.; Yu-Wai-Man, C. 3D printing in Ophthalmology: From medical implants to personalised medicine. *Int. J. Pharm.*, **2022**, *625*, 122094. <http://dx.doi.org/10.1016/j.ijpharm.2022.122094> PMID: 35952803
- [185] Awad, A.; Yao, A.; Trenfield, S.J.; Goyanes, A.; Gaisford, S.; Basit, A.W. 3D printed tablets (printlets) with braille and moon patterns for visually impaired patients. *Pharmaceutics*, **2020**, *12*(2), 172.
- [186] Sorkio, A.; Koch, L.; Koivusalo, L.; Deiwick, A.; Miettinen, S.; Chichkov, B.; Skottman, H. Human stem cell based corneal tissue mimicking structures using laser-assisted 3D bioprinting and functional bioinks. *Biomaterials*, **2018**, *171*, 57-71. <http://dx.doi.org/10.1016/j.biomaterials.2018.04.034> PMID: 29684677
- [187] Temirel, M.; Hawxhurst, C.; Tasoglu, S. Shape fidelity of 3D-bioprinted biodegradable patches. *Micromachines*, **2021**, *12*(2), 195.
- [188] Milojević, M.; Harih, G.; Vihar, B.; Vajda, J.; Gradišnik, L.; Zidarič, T.; Stana Kleinschek, K.; Maver, U.; Maver, T. Hybrid 3D printing of advanced hydrogel-based wound dressings with tailorable properties. *Pharmaceutics*, **2021**, *13*(4), 564.
- [189] Wang, S.; Xiong, Y.; Chen, J.; Ghanem, A.; Wang, Y.; Yang, J.; Sun, B. Biotechnology, Three dimensional printing bilayer membrane scaffold promotes wound healing. *Front. Bioeng. Biotechnol.*, **2019**, *7*, 348. <http://dx.doi.org/10.3389/fbioe.2019.00348> PMID: 31803738
- [190] Dodziuk, H. Applications of 3D printing in healthcare. *Kardiochir. Torakochirurgia Pol.*, **2016**, *3*(3), 283-293. <http://dx.doi.org/10.5114/kitp.2016.62625> PMID: 27785150
- [191] Kattadiyil, M.T.; Mursic, Z.; AlRumaih, H.; Goodacre, C.J. Intraoral scanning of hard and soft tissues for partial removable dental prosthesis fabrication. *J. Prosthet. Dent.*, **2014**, *112*(3), 444-448. <http://dx.doi.org/10.1016/j.prosdent.2014.03.022> PMID: 24882595
- [192] Sevenson, B. Stratasys Announces Two New Dental Wax Based 3D Printers, CrownWorx and FrameWorx. Available from: <https://3dprint.com/3711/stratasys-crown-worx-framework/>
- [193] Singh Malik, D.; Mital, N.; Kaur, G. Topical drug delivery systems: A patent review. *Expert Opin. Ther. Pat.*, **2016**, *26*(2), 213-228. <http://dx.doi.org/10.1517/13543776.2016.1131267> PMID: 26651499
- [194] Rzhnevskiy, A.S.; Singh, T.R.R.; Donnelly, R.F.; Anissimov, Y.G. Microneedles as the technique of drug delivery enhancement in diverse organs and tissues. *J. Control. Release*, **2018**, *270*, 184-202. <http://dx.doi.org/10.1016/j.jconrel.2017.11.048> PMID: 29203415
- [195] Farias, C.; Lyman, R.; Hemingway, C.; Chau, H.; Mahacek, A.; Bouzos, E.; Mobed-Miremadi, M. Three-dimensional (3D) printed microneedles for microencapsulated cell extrusion. *Bioengineering*, **2018**, *5*(3), 59.
- [196] Economidou, S.N.; Pere, C.P.P.; Reid, A.; Uddin, M.J.; Windmill, J.F.C.; Lamprou, D.A.; Douroumis, D. 3D printed microneedle patches using stereolithography (SLA) for intradermal insulin delivery. *Mater. Sci. Eng. C*, **2019**, *102*, 743-755. <http://dx.doi.org/10.1016/j.msec.2019.04.063> PMID: 31147046
- [197] Han, D.; Morde, R.S.; Mariani, S.; La Mattina, A.A.; Vignali, E.; Yang, C.; Barillaro, G.; Lee, H. 4D printing of a bioinspired microneedle array with backward-facing barbs for enhanced tissue adhesion. *Adv. Funct. Mater.*, **2020**, *30*(11), 1909197. <http://dx.doi.org/10.1002/adfm.201909197>
- [198] Kärrholm, J. The swedish hip arthroplasty register. *Acta Orthop.*, **2010**, *81*(1), 3-4. <http://dx.doi.org/10.3109/17453671003635918> PMID: 20170435
- [199] Wu, W.; Zheng, Q.; Guo, X.; Sun, J.; Liu, Y. A programmed release multi-drug implant fabricated by three-dimensional printing technology for bone tuberculosis therapy. *Biomed. Mater.*, **2009**, *4*(6), 065005. <http://dx.doi.org/10.1088/1748-6041/4/6/065005> PMID: 19901446
- [200] Herbert, N.; Simpson, D.; Spence, W.D.; Ion, W. A preliminary investigation into the development of 3-D printing of prosthetic sockets. *J. Rehabil. Res. Dev.*, **2005**, *42*(2), 141-146. <http://dx.doi.org/10.1682/JRRD.2004.08.0134> PMID: 15944878
- [201] Banks, J. Adding value in additive manufacturing: Researchers in the United Kingdom and Europe look to 3D printing for customization. *IEEE Pulse*, **2013**, *4*(6), 22-26. <http://dx.doi.org/10.1109/MPUL.2013.2279617> PMID: 24233187
- [202] Nawroth, J.C.; Lee, H.; Feinberg, A.W.; Ripplinger, C.M.; McCain, M.L.; Grosberg, A.; Dabiri, J.O.; Parker, K.K. A tissue-engineered jellyfish with biomimetic propulsion. *Nat. Biotechnol.*, **2012**, *30*(8), 792-797. <http://dx.doi.org/10.1038/nbt.2269> PMID: 22820316
- [203] Feinberg, A.W. Biological soft robotics. *Annu. Rev. Biomed. Eng.*, **2015**, *17*(1), 243-265. <http://dx.doi.org/10.1146/annurev-bioeng-071114-040632> PMID: 26643022
- [204] Phillips, R.; Purohit, P.K.; Kondev, J. *Nanotribology and Nanomechanics: An Introduction*; Bhushan, B., Ed.; Springer: Berlin, Heidelberg, **2005**; pp. 693-729. http://dx.doi.org/10.1007/3-540-28248-3_14
- [205] Williams, B.J.; Anand, S.V.; Rajagopalan, J.; Saif, M.T.A. A self-propelled biohybrid swimmer at low Reynolds number. *Nat. Commun.*, **2014**, *5*(1), 3081. <http://dx.doi.org/10.1038/ncomms4081> PMID: 24435099
- [206] Zhang, Y.F.; Zhang, N.; Hingorani, H.; Ding, N.; Wang, D.; Yuan, C.; Zhang, B.; Gu, G.; Ge, Q. Fast response,

- stiffness□tunable soft actuator by hybrid multimaterial 3D printing. *Adv. Funct. Mater.*, **2019**, 29(15), 1806698. <http://dx.doi.org/10.1002/adfm.201806698>
- [207] Katseli, V.; Thomaidis, N.; Economou, A.; Kokkinos, C. Miniature 3D-printed integrated electrochemical cell for trace voltammetric Hg(II) determination. *Sens. Actuators B Chem.*, **2020**, 308, 127715. <http://dx.doi.org/10.1016/j.snb.2020.127715>
- [208] Dias, A.A.; Chagas, C.L.S.; Silva-Neto, H.A.; Lobo-Junior, E.O.; Sgobbi, L.F.; de Araujo, W.R.; Paixão, T.R.L.C.; Coltro, W.K.T. Environmentally friendly manufacturing of flexible graphite electrodes for a wearable device monitoring zinc in sweat. *ACS Appl. Mater. Interfaces*, **2019**, 11(43), 39484-39492. <http://dx.doi.org/10.1021/acsmi.9b12797> PMID: 31524381
- [209] Silva, A.L.; Salvador, G.M.d.S.; Castro, S.V.F.; Carvalho, N.M.F.; Munoz, R.A.A. A 3D printer guide for the development and application of electrochemical cells and devices. *Front. Chem.*, **2021**, 9, 684256.
- [210] Krejcova, L.; Nejdil, L.; Rodrigo, M.A.M.; Zurek, M.; Matousek, M.; Hynek, D.; Zitka, O.; Kopel, P.; Adam, V.; Kizek, R. 3D printed chip for electrochemical detection of influenza virus labeled with CdS quantum dots. *Biosens. Bioelectron.*, **2014**, 54, 421-427. <http://dx.doi.org/10.1016/j.bios.2013.10.031> PMID: 24296063
- [211] Tasoglu, S.; Cumhur Tekin, H.; Inci, F.; Knowlton, S.; Wang, S.Q.; Wang-Johanning, F.; Johanning, G.; Colevas, D.; Demirci, U. Advances in nanotechnology and microfluidics for human papillomavirus diagnostics. *Proc. IEEE*, **2015**, 103(2), 161-178. <http://dx.doi.org/10.1109/JPROC.2014.2384836>
- [212] Jo, B.H.; Van Lerberghe, L.M.; Motsegood, K.M.; Beebe, D.J. Three-dimensional micro-channel fabrication in polydimethylsiloxane (PDMS) elastomer. *J. Microelectromech. Syst.*, **2000**, 9(1), 76-81. <http://dx.doi.org/10.1109/84.825780>
- [213] Chen, C.; Mehl, B.T.; Munshi, A.S.; Townsend, A.D.; Spence, D.M.; Martin, R.S. 3D-printed microfluidic devices: Fabrication, advantages and limitations—a mini review. *Anal. Methods*, **2016**, 8(31), 6005-6012. <http://dx.doi.org/10.1039/C6AY01671E> PMID: 27617038
- [214] Beebe, D.J.; Mensing, G.A.; Walker, G.M. Physics and applications of microfluidics in biology. *Annu. Rev. Biomed. Eng.*, **2002**, 4(1), 261-286. <http://dx.doi.org/10.1146/annurev.bioeng.4.112601.125916> PMID: 12117759
- [215] Choong, Y.Y.C.; Tan, H.W.; Patel, D.C.; Choong, W.T.N.; Chen, C.H.; Low, H.Y.; Tan, M.J.; Patel, C.D.; Chua, C.K. The global rise of 3D printing during the COVID-19 pandemic. *Nat. Rev. Mater.*, **2020**, 5(9), 637-639. <http://dx.doi.org/10.1038/s41578-020-00234-3> PMID: 35194517
- [216] Davies, A.; Thompson, K.A.; Giri, K.; Kafatos, G.; Walker, J.; Bennett, A. Testing the efficacy of homemade masks: would they protect in an influenza pandemic? *Disaster Med. Public Health Prep.*, **2013**, 7(4), 413-418. <http://dx.doi.org/10.1017/dmp.2013.43> PMID: 24229526
- [217] Ahmed, A.; Azam, A.; Aslam Bhutta, M.M.; Khan, F.A.; Aslam, R.; Tahir, Z. Discovering the technology evolution pathways for 3D printing (3DP) using bibliometric investigation and emerging applications of 3DP during COVID-19. *Cleaner Environmen. Syst.*, **2021**, 3, 100042. <http://dx.doi.org/10.1016/j.cesys.2021.100042>
- [218] Shokrani, A.; Loukaides, E.G.; Elias, E.; Lunt, A.J.G. Exploration of alternative supply chains and distributed manufacturing in response to COVID-19; a case study of medical face shields. *Mater. Des.*, **2020**, 192, 108749. <http://dx.doi.org/10.1016/j.matdes.2020.108749> PMID: 32341616
- [219] Petsiuk, A.; Tanikella, N.G.; Dertinger, S.; Pringle, A.; Oberloier, S.; Pearce, J.M. Partially RepRapable automated open source bag valve mask-based ventilator. *HardwareX*, **2020**, 8, e00131. <http://dx.doi.org/10.1016/j.ohx.2020.e00131> PMID: 32835141
- [220] Mandrycky, C.; Wang, Z.; Kim, K.; Kim, D.H. 3D bioprinting for engineering complex tissues. *Biotechnol. Adv.*, **2016**, 34(4), 422-434. <http://dx.doi.org/10.1016/j.biotechadv.2015.12.011> PMID: 26724184
- [221] Freedman, B.R.; Mooney, D.J. Biomaterials to mimic and heal connective tissues. *Adv. Mater.*, **2019**, 31(19), 1806695. <http://dx.doi.org/10.1002/adma.201806695> PMID: 30908806
- [222] Lutolf, M.P.; Hubbell, J.A. Synthetic biomaterials as instructive extracellular microenvironments for morphogenesis in tissue engineering. *Nat. Biotechnol.*, **2005**, 23(1), 47-55. <http://dx.doi.org/10.1038/nbt1055> PMID: 15637621
- [223] Robb, K.P.; Shridhar, A.; Flynn, L.E. Decellularized matrices as cell-instructive scaffolds to guide tissue-specific regeneration. *ACS Biomater. Sci. Eng.*, **2018**, 4(11), 3627-3643. <http://dx.doi.org/10.1021/acsbomaterials.7b00619> PMID: 33429606
- [224] Gonzalez-Fernandez, T.; Sikorski, P.; Leach, J.K. Bio-instructive materials for musculoskeletal regeneration. *Acta Biomater.*, **2019**, 96, 20-34. <http://dx.doi.org/10.1016/j.actbio.2019.07.014> PMID: 31302298
- [225] Viswanathan, P.; Chirasatitsin, S.; Ngamkham, K.; Engler, A.J.; Battaglia, G. Cell instructive microporous scaffolds through interface engineering. *J. Am. Chem. Soc.*, **2012**, 134(49), 20103-20109. <http://dx.doi.org/10.1021/ja308523f> PMID: 23163574
- [226] Mierke, C.T. Mechanical cues affect migration and invasion of cells from three different directions. *Front. Cell Dev. Biol.*, **2020**, 8, 583226. <http://dx.doi.org/10.3389/fcell.2020.583226>
- [227] Higuchi, A.; Ling, Q.D.; Chang, Y.; Hsu, S.T.; Umezawa, A. Physical cues of biomaterials guide stem cell differentiation fate. *Chem. Rev.*, **2013**, 113(5), 3297-3328. <http://dx.doi.org/10.1021/cr300426x> PMID: 23391258
- [228] Castilho, M.; van Mil, A.; Maher, M.; Metz, C.H.G.; Hochleitner, G.; Groll, J.; Doevendans, P.A.; Ito, K.; Sluijter, J.P.G.; Malda, J. Melt electrowriting allows tailored microstructural and mechanical design of scaffolds to advance functional human myocardial tissue formation. *Adv. Funct. Mater.*, **2018**, 28(40), 1803151. <http://dx.doi.org/10.1002/adfm.201803151>
- [229] Das, S.; Kim, S.W.; Choi, Y.J.; Lee, S.; Lee, S.H.; Kong, J.S.; Park, H.J.; Cho, D.W.; Jang, J. Decellularized extracellular matrix bioinks and the external stimuli to enhance cardiac tissue development *in vitro*. *Acta Biomater.*, **2019**, 95, 188-200. <http://dx.doi.org/10.1016/j.actbio.2019.04.026> PMID: 30986526

- [230] Castilho, M.; Feyen, D.; Flandes-Iparraguirre, M.; Hochleitner, G.; Groll, J.; Doevendans, P.A.F.; Vermonden, T.; Ito, K.; Sluijter, J.P.G.; Malda, J. Melt electrospinning writing of poly(ϵ -hydroxymethylglycolide-co- ϵ -caprolactone)-based scaffolds for cardiac tissue engineering. *Adv. Healthc. Mater.*, **2017**, *6*(18), 1700311. <http://dx.doi.org/10.1002/adhm.201700311>
- [231] Ji, S.; Guvendiren, M. 3D printed wavy scaffolds enhance mesenchymal stem cell osteogenesis. *Micromachines*, **2020**, *11*(1), 31.
- [232] Kim, Y.B.; Kim, G.H. PCL/alginate composite scaffolds for hard tissue engineering: Fabrication, characterization, and cellular activities. *ACS Comb. Sci.*, **2015**, *17*(2), 87-99. <http://dx.doi.org/10.1021/co500033h> PMID: 25541639
- [233] Teixeira, B.N.; Aprile, P.; Mendonça, R.H.; Kelly, D.J.; Thiré, R.M.S.M. Evaluation of bone marrow stem cell response to PLA scaffolds manufactured by 3D printing and coated with polydopamine and type I collagen. *J. Biomed. Mater. Res. B Appl. Biomater.*, **2019**, *107*(1), 37-49. <http://dx.doi.org/10.1002/jbm.b.34093> PMID: 29480562
- [234] He, F.L.; Li, D.W.; He, J.; Liu, Y.Y.; Ahmad, F.; Liu, Y.L.; Deng, X.; Ye, Y.J.; Yin, D.C. A novel layer-structured scaffold with large pore sizes suitable for 3D cell culture prepared by near-field electrospinning. *Mater. Sci. Eng. C*, **2018**, *86*, 18-27. <http://dx.doi.org/10.1016/j.msec.2017.12.016> PMID: 29525092
- [235] Zhang, B.; Wang, L.; Song, P.; Pei, X.; Sun, H.; Wu, L.; Zhou, C.; Wang, K.; Fan, Y.; Zhang, X. 3D printed bone tissue regenerative PLA/HA scaffolds with comprehensive performance optimizations. *Mater. Des.*, **2021**, *201*, 109490. <http://dx.doi.org/10.1016/j.matdes.2021.109490>
- [236] Chen, X.; Gao, C.; Jiang, J.; Wu, Y.; Zhu, P.; Chen, G. 3D printed porous PLA/nHA composite scaffolds with enhanced osteogenesis and osteoconductivity *in vivo* for bone regeneration. *Biomed. Mater.*, **2019**, *14*(6), 065003. <http://dx.doi.org/10.1088/1748-605X/ab388d> PMID: 31382255
- [237] Chen, G.; Chen, N.; Wang, Q. Fabrication and properties of poly(vinyl alcohol)/ β -tricalcium phosphate composite scaffolds *via* fused deposition modeling for bone tissue engineering. *Compos. Sci. Technol.*, **2019**, *172*, 17-28. <http://dx.doi.org/10.1016/j.compscitech.2019.01.004>
- [238] Pierantozzi, D.; Scalzone, A.; Jindal, S.; Stüpniece, L.; Šalma-Ancāne, K.; Dalgarno, K.; Gentile, P.; Mancuso, E. 3D printed Sr-containing composite scaffolds: Effect of structural design and material formulation towards new strategies for bone tissue engineering. *Compos. Sci. Technol.*, **2020**, *191*, 108069. <http://dx.doi.org/10.1016/j.compscitech.2020.108069>
- [239] Kolan, K.C.R.; Li, J.; Roberts, S.; Semon, J.A.; Park, J.; Day, D.E.; Leu, M.C. Near-field electrospinning of a polymer/bioactive glass composite to fabricate 3D biomimetic structures. *Int. J. Bioprinting*, **2018**, *5*(1), 163. <http://dx.doi.org/10.18063/ijb.v5i1.163> PMID: 32782977
- [240] Grémare, A.; Guduric, V.; Bareille, R.; Heroguez, V.; Latour, S.; L'heureux, N.; Fricain, J.C.; Catros, S.; Le Nihouannen, D. Characterization of printed PLA scaffolds for bone tissue engineering. *J. Biomed. Mater. Res. A*, **2018**, *106*(4), 887-894. <http://dx.doi.org/10.1002/jbm.a.36289> PMID: 29105943
- [241] Feng, X.; Ma, L.; Liang, H.; Liu, X.; Lei, J.; Li, W.; Wang, K.; Song, Y.; Wang, B.; Li, G.; Li, S.; Yang, C. Osteointegration of 3D-printed fully porous polyetheretherketone scaffolds with different pore sizes. *ACS Omega*, **2020**, *5*(41), 26655-26666. <http://dx.doi.org/10.1021/acsomega.0c03489> PMID: 33110992
- [242] Gwiazda, M.; Kumar, S.; Świeszkowski, W.; Ivanovski, S.; Vaquette, C. The effect of melt electrospun writing fiber orientation onto cellular organization and mechanical properties for application in Anterior Cruciate Ligament tissue engineering. *J. Mech. Behav. Biomed. Mater.*, **2020**, *104*, 103631. <http://dx.doi.org/10.1016/j.jmbbm.2020.103631> PMID: 32174392
- [243] Paxton, N.C.; Lanaro, M.; Bo, A.; Crooks, N.; Ross, M.T.; Green, N.; Tetsworth, K.; Allenby, M.C.; Gu, Y.; Wong, C.S.; Powell, S.K.; Woodruff, M.A. Design tools for patient specific and highly controlled melt electrospun scaffolds. *J. Mech. Behav. Biomed. Mater.*, **2020**, *105*, 103695. <http://dx.doi.org/10.1016/j.jmbbm.2020.103695> PMID: 32090895
- [244] Su, Y.; Zhang, Z.; Wan, Y.; Zhang, Y.; Wang, Z.; Klausen, L.H.; Huang, P.; Dong, M.; Han, X.; Cui, B.; Chen, M. A hierarchically ordered compacted coil scaffold for tissue regeneration. *NPG Asia Mater.*, **2020**, *12*(1), 55. <http://dx.doi.org/10.1038/s41427-020-0234-7>
- [245] Castilho, M.; Mouser, V.; Chen, M.; Malda, J.; Ito, K. Bilayered micro-fibre reinforced hydrogels for articular cartilage regeneration. *Acta Biomater.*, **2019**, *95*, 297-306. <http://dx.doi.org/10.1016/j.actbio.2019.06.030> PMID: 31233890
- [246] Ross, M.T.; Kilian, D.; Lode, A.; Ren, J.; Allenby, M.C.; Gelinsky, M.; Woodruff, M.A. Using melt-electrowritten microfibres for tailoring scaffold mechanics of 3D bioprinted chondrocyte-laden constructs. *Bioprinting*, **2021**, *23*, e00158. <http://dx.doi.org/10.1016/j.bprint.2021.e00158>
- [247] Li, H.; Liao, Z.; Yang, Z.; Gao, C.; Fu, L.; Li, P.; Zhao, T.; Cao, F.; Chen, W.; Yuan, Z.; Sui, X.; Liu, S.; Guo, Q. 3D printed poly(ϵ -caprolactone)/meniscus extracellular matrix composite scaffold functionalized with kartogenin-releasing PLGA microspheres for meniscus tissue engineering. *Front. Bioeng. Biotechnol.*, **2021**, *9*, 662381. <http://dx.doi.org/10.3389/fbioe.2021.662381> PMID: 33996783
- [248] Han, Y.; Lian, M.; Sun, B.; Jia, B.; Wu, Q.; Qiao, Z.; Dai, K. Preparation of high precision multilayer scaffolds based on Melt Electro-Writing to repair cartilage injury. *Theranostics*, **2020**, *10*(22), 10214-10230. <http://dx.doi.org/10.7150/thno.47909> PMID: 32929344
- [249] Han, Y.; Jia, B.; Lian, M.; Sun, B.; Wu, Q.; Sun, B.; Qiao, Z.; Dai, K. High-precision, gelatin-based, hybrid, bilayer scaffolds using melt electro-writing to repair cartilage injury. *Bioact. Mater.*, **2021**, *6*(7), 2173-2186. <http://dx.doi.org/10.1016/j.bioactmat.2020.12.018> PMID: 33511315
- [250] Vijayavenkataraman, S.; Thaharah, S.; Zhang, S.; Lu, W.F.; Fuh, J.Y.H. 3D-Printed PCL/rGO conductive scaffolds for peripheral nerve injury repair. *Artif. Organs*, **2019**, *43*(5), 515-523. <http://dx.doi.org/10.1111/aor.13360> PMID: 30229979
- [251] Zhang, Z.; Jørgensen, M.L.; Wang, Z.; Amagat, J.; Wang, Y.; Li, Q.; Dong, M.; Chen, M. 3D anisotropic photocatalytic architectures as bioactive nerve guidance conduits for peripheral neural regeneration. *Biomaterials*, **2020**, *253*, 120108. <http://dx.doi.org/10.1016/j.biomaterials.2020.120108>

- PMID: 32428776
- [252] Reitmaier, S.; Kovtun, A.; Schuelke, J.; Kanter, B.; Lemm, M.; Hoess, A.; Heinemann, S.; Nies, B.; Ignatius, A. Strontium(II) and mechanical loading additively augment bone formation in calcium phosphate scaffolds. *J. Orthop. Res.*, **2018**, *36*(1), 106-117. <http://dx.doi.org/10.1002/jor.23623> PMID: 28574614
- [253] Vijayavenkataraman, S.; Lu, W.F.; Fuh, J.Y.H. 3D bioprinting of skin: A state-of-the-art review on modelling, materials, and processes. *Biofabrication*, **2016**, *8*(3), 032001. <http://dx.doi.org/10.1088/1758-5090/8/3/032001> PMID: 27606434
- [254] Lavrentieva, A.; Fleischhammer, T.; Enders, A.; Pirmahboub, H.; Bahnemann, J.; Pepelanova, I. Fabrication of stiffness gradients of GelMA hydrogels using a 3D printed micromixer. *Macromol. Biosci.*, **2020**, *20*(7), 2000107. <http://dx.doi.org/10.1002/mabi.202000107> PMID: 32537875
- [255] Zhang, J.; Wehrle, E.; Adamek, P.; Paul, G.R.; Qin, X.H.; Rubert, M.; Müller, R. Optimization of mechanical stiffness and cell density of 3D bioprinted cell-laden scaffolds improves extracellular matrix mineralization and cellular organization for bone tissue engineering. *Acta Biomater.*, **2020**, *114*, 307-322. <http://dx.doi.org/10.1016/j.actbio.2020.07.016> PMID: 32673752
- [256] Zhang, J.; Wehrle, E.; Vetsch, J.R.; Paul, G.R.; Rubert, M.; Müller, R. Alginate dependent changes of physical properties in 3D bioprinted cell-laden porous scaffolds affect cell viability and cell morphology. *Biomed. Mater.*, **2019**, *14*(6), 065009. <http://dx.doi.org/10.1088/1748-605X/ab3c74> PMID: 31426033
- [257] Hewitt, E.; Mros, S.; Mcconnell, M.; Cabral, J.; Ali, A. Melt-electrowriting with novel milk protein/PCL biomaterials for skin regeneration. *Biomed. Mater.*, **2019**, *14*(5), 055013. <http://dx.doi.org/10.1088/1748-605X/ab3344> PMID: 31318339
- [258] Lin, F.-S.; Lee, J., Jr; Lee, A.K.; Ho, C.-C.; Liu, Y.-T.; Shie, M.-Y. Calcium silicate-activated gelatin methacrylate hydrogel for accelerating human dermal fibroblast proliferation and differentiation. *Polymers*, **2021**, *13*(1), 70.
- [259] Distler, T.; Solisito, A.A.; Schneidereit, D.; Friedrich, O.; Detsch, R.; Boccaccini, A.R. 3D printed oxidized alginate-gelatin bioink provides guidance for C2C12 muscle precursor cell orientation and differentiation *via* shear stress during bioprinting. *Biofabrication*, **2020**, *12*(4), 045005. <http://dx.doi.org/10.1088/1758-5090/ab98e4> PMID: 32485696
- [260] Chae, S.; Sun, Y.; Choi, Y.J.; Ha, D.H.; Jeon, I.; Cho, D.W. 3D cell-printing of tendon-bone interface using tissue-derived extracellular matrix bioinks for chronic rotator cuff repair. *Biofabrication*, **2021**, *13*(3), 035005. <http://dx.doi.org/10.1088/1758-5090/abd159> PMID: 33285539
- [261] Kim, W.; Kim, G. 3D bioprinting of functional cell-laden bioinks and its application for cell-alignment and maturation. *Appl. Mater. Today*, **2020**, *19*, 100588. <http://dx.doi.org/10.1016/j.apmt.2020.100588>
- [262] Berg, J.; Weber, Z.; Fechner-Bitteti, M.; Hocke, A.C.; Hippenstiel, S.; Elomaa, L.; Weinhart, M.; Kurreck, J. Bioprinted multi-cell type lung model for the study of viral inhibitors. *Viruses*, **2021**, *13*(8), 1590.
- [263] Franks, T.J.; Colby, T.V.; Travis, W.D.; Tuder, R.M.; Reynolds, H.Y.; Brody, A.R.; Cardoso, W.V.; Crystal, R.G.; Drake, C.J.; Engelhardt, J.; Frid, M.; Herzog, E.; Mason, R.; Phan, S.H.; Randell, S.H.; Rose, M.C.; Stevens, T.; Serge, J.; Sunday, M.E.; Voynow, J.A.; Weinstein, B.M.; Whitsett, J.; Williams, M.C. Resident cellular components of the human lung: Current knowledge and goals for research on cell phenotyping and function. *Proc. Am. Thorac. Soc.*, **2008**, *5*(7), 763-766. <http://dx.doi.org/10.1513/pats.200803-025HR> PMID: 18757314
- [264] Bhattacharjee, M.; Coburn, J.; Centola, M.; Murab, S.; Barbero, A.; Kaplan, D.L.; Martin, I.; Ghosh, S. Tissue engineering strategies to study cartilage development, degeneration and regeneration. *Adv. Drug Deliv. Rev.*, **2015**, *84*, 107-122. <http://dx.doi.org/10.1016/j.addr.2014.08.010> PMID: 25174307
- [265] Chawla, S.; Ghosh, S. Establishment of *in vitro* model of corneal scar pathophysiology. *J. Cell. Physiol.*, **2018**, *233*(5), 3817-3830. <http://dx.doi.org/10.1002/jcp.26071> PMID: 28657193
- [266] Roy, S.; Yadav, S.; Dasgupta, T.; Chawla, S.; Tandon, R.; Ghosh, S. Interplay between hereditary and environmental factors to establish an *in vitro* disease model of keratoconus. *Drug Discov. Today*, **2019**, *24*(2), 403-416. <http://dx.doi.org/10.1016/j.drudis.2018.10.017> PMID: 30408528
- [267] Das, S.; Pati, F.; Choi, Y.J.; Rijal, G.; Shim, J.H.; Kim, S.W.; Ray, A.R.; Cho, D.W.; Ghosh, S. Bioprintable, cell-laden silk fibroin-gelatin hydrogel supporting multilineage differentiation of stem cells for fabrication of three-dimensional tissue constructs. *Acta Biomater.*, **2015**, *11*, 233-246. <http://dx.doi.org/10.1016/j.actbio.2014.09.023> PMID: 25242654
- [268] Technical Considerations for Additive Manufactured Medical Devices. Guidance for Industry and Food and Drug Administration Staff. **2023**. Available form: <https://www.fda.gov/regulatory-information/search-fda-guidance-documents/technical-considerations-additive-manufactured-medical-devices> (Accessed on : 04 Aug 2023).
- [269] CDER Researchers Explore the Promise and Potential of 3D Printed Pharmaceuticals. Available from: <https://www.fda.gov/drugs/news-events-human-drugs/cder-researchers-explore-promise-and-potential-3d-printed-pharmaceuticals>
- [270] Beg, S.; Almalki, W.H.; Malik, A.; Farhan, M.; Aatif, M.; Rahman, Z.; Alruwaili, N.K.; Alrobaian, M.; Tarique, M.; Rahman, M. 3D printing for drug delivery and biomedical applications. *Drug Discov. Today*, **2020**, *25*(9), 1668-1681. <http://dx.doi.org/10.1016/j.drudis.2020.07.007> PMID: 32687871
- [271] Huang, S.H.; Liu, P.; Mokasdar, A.; Hou, L. Additive manufacturing and its societal impact: A literature review. *Int. J. Adv. Manuf. Technol.*, **2013**, *67*(5-8), 1191-1203. <http://dx.doi.org/10.1007/s00170-012-4558-5>
- [272] Varghese, R.; Sood, P.; Salvi, S.; Karsiya, J.; Kumar, D. 3D printing in the pharmaceutical sector: Advances and evidences. *Sensors Int.*, **2022**, *3*, 100177. <http://dx.doi.org/10.1016/j.sintl.2022.100177>
- [273] Pham, D.T.; Gault, R.S. A comparison of rapid prototyping technologies. *Int. J. Mach. Tools Manuf.*, **1998**, *38*(10-11), 1257-1287. [http://dx.doi.org/10.1016/S0890-6955\(97\)00137-5](http://dx.doi.org/10.1016/S0890-6955(97)00137-5)

- [274] Cui, M.; Pan, H.; Fang, D.; Qiao, S.; Wang, S.; Pan, W. Fabrication of high drug loading levitiracetam tablets using semi-solid extrusion 3D printing. *J. Drug Deliv. Sci. Technol.*, **2020**, *57*, 101683. <http://dx.doi.org/10.1016/j.jddst.2020.101683>
- [275] Naseri, E.; Butler, H.; MacNevin, W.; Ahmed, M.; Ahmadi, A. Low-temperature solvent-based 3D printing of PLGA: A parametric printability study. *Drug Dev. Ind. Pharm.*, **2020**, *46*(2), 173-178. <http://dx.doi.org/10.1080/03639045.2019.1711389> PMID: 31931645
- [276] Annaji, M.; Ramesh, S.; Poudel, I.; Govindarajulu, M.; Arnold, R.D.; Dhanasekaran, M.; Babu, R.J. Application of extrusion-based 3D printed dosage forms in the treatment of chronic diseases. *J. Pharm. Sci.*, **2020**, *109*(12), 3551-3568. <http://dx.doi.org/10.1016/j.xphs.2020.09.042> PMID: 33035541
- [277] Zheng, F.; Huang, S. Advances in study on three-dimensional printing in pharmaceuticals. *Chin. Herb. Med.*, **2016**, *8*(2), 121-125. [http://dx.doi.org/10.1016/S1674-6384\(16\)60020-5](http://dx.doi.org/10.1016/S1674-6384(16)60020-5)
- [278] Trenfield, S.J.; Xian Tan, H.; Awad, A.; Buaz, A.; Gaisford, S.; Basit, A.W.; Goyanes, A. Track-and-trace: Novel anti-counterfeit measures for 3D printed personalized drug products using smart material inks. *Int. J. Pharm.*, **2019**, *567*, 118443. <http://dx.doi.org/10.1016/j.ijpharm.2019.06.034> PMID: 31212052
- [279] Rivera-Tarazona, L.K.; Campbell, Z.T.; Ware, T.H. Stimuli-responsive engineered living materials. *Soft Matter*, **2021**, *17*(4), 785-809. <http://dx.doi.org/10.1039/D0SM01905D> PMID: 33410841
- [280] Khoo, Z.X.; Teoh, J.E.M.; Liu, Y.; Chua, C.K.; Yang, S.; An, J.; Leong, K.F.; Yeong, W.Y. 3D printing of smart materials: A review on recent progresses in 4D printing. *Virtu. Phys. Prototyp.*, **2015**, *10*(3), 103-122. <http://dx.doi.org/10.1080/17452759.2015.1097054>
- [281] Constante, G.; Apsite, I.; Alkhamis, H.; Dulle, M.; Schwarzer, M.; Caspari, A.; Synytska, A.; Salehi, S.; Ionov, L. 4D biofabrication using a combination of 3D printing and melt-electrowriting of shape-morphing polymers. *ACS Appl. Mater. Interfaces*, **2021**, *13*(11), 12767-12776. <http://dx.doi.org/10.1021/acsmi.0c18608> PMID: 33389997
- [282] Wang, Y.; Cui, H.; Wang, Y.; Xu, C.; Esworthy, T.J.; Hann, S.Y.; Boehm, M.; Shen, Y.L.; Mei, D.; Zhang, L.G. 4D printed cardiac construct with aligned myofibers and adjustable curvature for myocardial regeneration. *ACS Appl. Mater. Interfaces*, **2021**, *13*(11), 12746-12758. <http://dx.doi.org/10.1021/acsmi.0c17610> PMID: 33405502
- [283] Huang, J.; Xia, S.; Li, Z.; Wu, X.; Ren, J. Applications of four-dimensional printing in emerging directions: Review and prospects. *J. Mater. Sci. Technol.*, **2021**, *91*, 105-120. <http://dx.doi.org/10.1016/j.jmst.2021.02.040>
- [284] Saska, S.; Pilatti, L.; Blay, A.; Shibli, J.A. Bioresorbable polymers: Advanced materials and 4D printing for tissue engineering. *Polymers*, **2021**, *13*(4), 563.
- [285] Tamay, D.G.; Dursun Usal, T.; Alagoz, A.S.; Yucel, D.; Hasirci, N.; Hasirci, V. 3D and 4D printing of polymers for tissue engineering applications. *Front. Bioeng. Biotechnol.*, **2019**, *7*, 164. <http://dx.doi.org/10.3389/fbioe.2019.00164> PMID: 31338366
- [286] Gu, B.K.; Choi, D.J.; Park, S.J.; Kim, M.S.; Kang, C.M.; Kim, C.H. 3-dimensional bioprinting for tissue engineering applications. *Biomater. Res.*, **2016**, *20*(1), 12. <http://dx.doi.org/10.1186/s40824-016-0058-2> PMID: 27114828
- [287] Paul, G.M.; Rezaenia, A.; Wen, P.; Condoor, S.; Parkar, N.; King, W.; Korakianitis, T. Medical applications for 3D printing: Recent developments. *Mo. Med.*, **2018**, *115*(1), 75-81. PMID: 30228688
- [288] Algahtani, M.S. Assessment of pharmacist's knowledge and perception toward 3D printing technology as a dispensing method for personalized medicine and the readiness for implementation. *Pharmacy*, **2021**, *9*(1), 68. <http://dx.doi.org/10.3390/pharmacy9010068> PMID: 33807103
- [289] Al-Dulimi, Z.; Wallis, M.; Tan, D.K.; Maniruzzaman, M.; Nokhodchi, A. 3D printing technology as innovative solutions for biomedical applications. *Drug Discov. Today*, **2021**, *26*(2), 360-383. <http://dx.doi.org/10.1016/j.drudis.2020.11.013> PMID: 33212234
- [290] Wang, Y.; Sun, L.; Mei, Z.; Zhang, F.; He, M.; Fletcher, C.; Wang, F.; Yang, J.; Bi, D.; Jiang, Y.; Liu, P. 3D printed biodegradable implants as an individualized drug delivery system for local chemotherapy of osteosarcoma. *Mater. Des.*, **2020**, *186*, 108336. <http://dx.doi.org/10.1016/j.matdes.2019.108336>
- [291] Malebari, A.M.; Kara, A.; Khayyat, A.N.; Mohammad, K.A.; Serrano, D.R. Development of advanced 3D-printed solid dosage pediatric formulations for HIV treatment. *Pharmaceuticals*, **2022**, *15*(4), 435.
- [292] Jamróz, W.; Kurek, M.; Łyszczarz, E.; Szafraniec, J.; Knapik-Kowalczyk, J.; Syrek, K.; Paluch, M.; Jachowicz, R. 3D printed orodispersible films with Aripiprazole. *Int. J. Pharm.*, **2017**, *533*(2), 413-420. <http://dx.doi.org/10.1016/j.ijpharm.2017.05.052> PMID: 28552800
- [293] Goyanes, A.; Det-Amornrat, U.; Wang, J.; Basit, A.W.; Gaisford, S. 3D scanning and 3D printing as innovative technologies for fabricating personalized topical drug delivery systems. *J. Control. Release*, **2016**, *234*, 41-48. <http://dx.doi.org/10.1016/j.jconrel.2016.05.034> PMID: 27189134
- [294] Liu, J.; Zheng, X.; Huang, Y.; Shan, H.; Huang, J. Successful use of methylprednisolone for treating severe COVID-19. *J. Allergy Clin. Immunol.*, **2020**, *146*(2), 325-327. <http://dx.doi.org/10.1016/j.jaci.2020.05.021> PMID: 32479759
- [295] Zieliński, P.S.; Gudeti, P.K.R.; Rikmanspoel, T.; Włodarczyk-Biegun, M.K. 3D printing of bio-instructive materials: Toward directing the cell. *Bioact. Mater.*, **2023**, *19*, 292-327. <http://dx.doi.org/10.1016/j.bioactmat.2022.04.008> PMID: 35574057

REVIEW ARTICLE

Prominent Perspective on Existing Biological Hallmarks of Alzheimer's Disease

Namrata Singh^{1,2}, Srishti Sharma³, Kallol K. Ghosh³, Bhanushree Gupta⁴ and Kamil Kuca^{2,5,*}

¹Department of Engineering Science, Ramrao Adik Institute of Technology, DY Patil University, Navi Mumbai, 400706, India; ²Department of Chemistry, Faculty of Science, University of Hradec Kralove, Rokitanskeho 62, 50003, Hradec Kralove, Czech Republic; ³School of Studies in Chemistry, Pt. Ravishankar Shukla University, Raipur, 492010 (C.G.), India; ⁴Centre of Basic Sciences, Pt. Ravishankar Shukla University, Raipur, 492010 (C.G.), India; ⁵Research Institute for Biomedical Science, University of Hradec Králové, Antonína Dvorka 451/1, 500 02 Hradec Kralove, Czech Republic

ARTICLE HISTORY

Received: November 12, 2023
Revised: February 24, 2024
Accepted: March 08, 2024

DOI:
10.2174/0115680266292514240404040341

Abstract: Biomarkers are the most significant diagnosis tools tending towards unique approaches and solutions for the prevention and cure of Alzheimer's Disease (AD). The current report provides a clear perception of the concept of various biomarkers and their prominent features through analysis to provide a possible solution for the inhibition of events in AD. Scientists around the world truly believe that crucial hallmarks can serve as critical tools in the early diagnosis, cure, and prevention, as well as the future of medicine. The awareness and understanding of such biomarkers would provide solutions to the puzzled mechanism of this neuronal disorder. Some of the argued biomarkers in the present article are still in an experimental phase as they need to undergo specific clinical trials before they can be considered for treatment.

Keywords: Alzheimer's disease, biomarkers, β -amyloid peptide, tau protein, neurodegenerative diseases, diagnosis.

1. INTRODUCTION

Hailing from a century-old era, Alzheimer's still holds the position of an unsolved medical mystery. Scientific minds working on this memory impairment are still clueless about its treatment. The sole hold on this situation is therapeutic, which could partially slow down the progression of this disorder. Unfortunately, AD patients can only be comforted by these side effects causing drugs. The answer to this delayed diagnosis of AD lies in the findings of the biomarkers that can pace the research of treatment as well as therapeutics. Biomarkers, also known as neurochemical indicators, give a clear indication of either the risk or the presence of the disease in an organism [1, 2].

AD symptoms precede very slowly. Thus, it is imperative to investigate biomarkers of AD [3]. Some well-known neuropathological indicators of AD have been discussed here and depicted in Fig. (1). The study of biomarkers is prominent in medicine as they lay the foundation for drug development. The effect of the newly designed drugs is first critically measured on volunteers during the clinical trials by examining the specific biological hallmark. This review aims to highlight specific biomarkers of AD that can be targeted for the detection of AD primarily and can result in a hopeful treatment.

Putting an end to something always demands the identification of its specific origin or the multiple causes/reasons behind its emergence. If we are unable to find the cause, it would be impossible to reach the final destination. The search for specific biomarkers for Alzheimer's disease (AD) has been the same story in clinical history for a century. Covering 70% of the pie-chart of dementia, AD is the highest afflicting neurodegenerative dysfunction [4, 5]. The actual cause of its incurability is still unknown as it lacks diagnosis at its earliest onset. Unraveling the clinical hallmarks of AD can not only be helpful in its treatment but also for its early diagnosis and permanent cure. The defining features of AD are the unrequired deposits of amyloid plaques and neurofibrillary tangles [6, 7]. The global prevalence of this disorder is projecting a future plan of hitting a population of only 14 million in the USA by 2050 [8]. Despite a lot of theories and research about the neuropathological events involved in AD, there is neither prevention nor cure available. Efforts are still focused on the slow progressive rate of AD, which is of no help as the incurability is constant till the present [9, 10]. Such a state strongly underscores the necessity to explore the fundamental root cause of the dysfunction development and its prominent clinical markers for sooner diagnosis. Moreover, unsolved mysteries of the mechanism of neurodegeneration initiation need to be unfolded to prevent, delay, or cure AD. The interplay of such responsible causes has been discussed in his mini-review, which triggers the untold story of AD. The understanding of the outline of these clinical markers is important as they hold the baseline for future clinical success. So, this mini-review explores and encompasses the current status of the potential clinical hallmarks

*Address correspondence to these authors at the Department of Engineering science, Ramrao Adik Institute of Technology, DY Patil University, Navi Mumbai, 400706, India; E-mail: chemnamrata09@gmail.com (N. Singh); Department of Chemistry, Faculty of Science, University of Hradec Kralove, Rokitanskeho 62, 50003 Hradec Kralove, Czech Republic; E-mail: kamil.kuca@uhk.cz (K. Kuca)

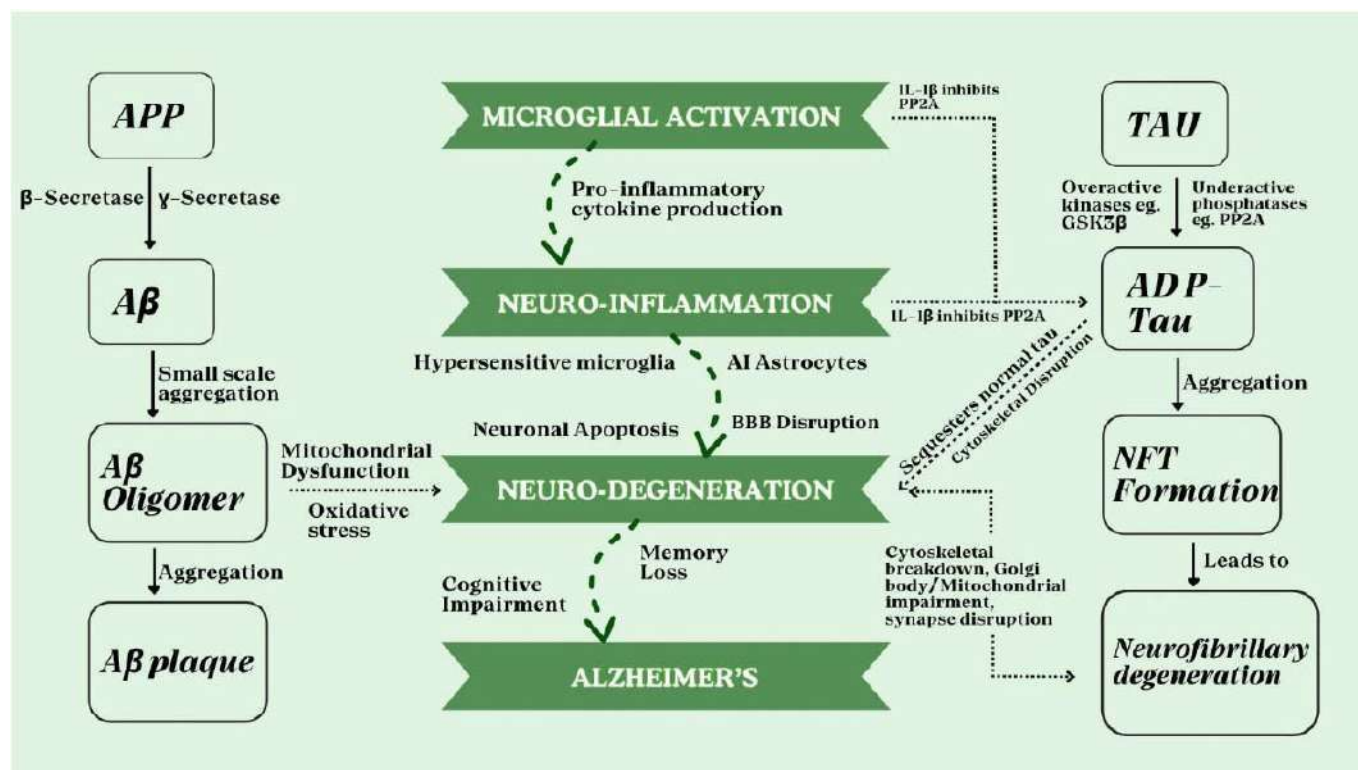


Fig. (1). Biomarkers signaling in Alzheimer's disease. (A higher resolution / colour version of this figure is available in the electronic copy of the article).

of AD. This study could improve clinical studies in a lot of diagnostic and treatment approaches.

The diagnostic pathway proceeds *via*. two different techniques. The techniques used to investigate the biomarkers have been broadly classified into two categories.

1.1. Invasive

Invasive techniques are used to study precise brain areas and cerebrospinal fluid as early biomarkers [11], as shown in Fig. (2). Since these are invasive techniques, they are time-consuming, expensive, and likely to cause discomfort to patients. Hence, minimally invasive techniques and noninvasive techniques are the mandates for early diagnosis of neurodegenerative disorders.

1.2. Non-invasive

The routine diagnosis of AD and mixed forms of dementia from CSF has various limitations, including the invasive nature of lumbar puncture and collection of CSF, the difficulty of patient screening, and the need for multiple-year follow-up on the same patient. To expand the range of AD diagnostic tests, it is crucial to create sensitive and specific ELISA for additional site-specific phosphorylated tau isoforms. It is currently unclear how closely analyte concentration in the blood links to pathological alterations in the brain. Thus, it is obvious that it is necessary to look for biomarkers in other body fluids. With the advent of noninva-

sive neuroimaging techniques that enable the visualization of structures *in vivo* in recent decades, the progress in the diagnosis of AD has been considerably improved. Novel magnetic resonance imaging (MRI), metabolic changes picked up by Positron Emission Tomography (PET), and imaging of amyloid are a few examples. The development of omics technologies over the past few years, including genomes, transcriptomics, proteome, metabolomics, secretomics, *etc.*, has made it possible to analyze a variety of AD hallmarks. These instruments make it easier to analyze human fluid samples of many types, such as blood, tears, urine, or saliva, with easy collection and accessibility under non-invasive techniques. Numerous proteins associated with neurodegenerative diseases, including Tau, amyloid beta, alpha-synuclein, and the huntingtin protein, are known to be abundant in saliva and to reflect physiological activity. These proteins' concentrations in saliva are helpful biomarkers for the kind of diseases they are associated with [12]. Fig. (3) manifests the non-invasive biomarkers of AD.

2. BIOLOGICAL HALLMARKS OF ALZHEIMER'S DISEASE

The elevated exponential rate of people afflicted with AD has highlighted the necessity of taking substantial steps in the direction of finding the neurodiagnostic biomarkers responsible for AD. The prominent biological hallmarks of AD include diffused extracellular amyloid plaques and intraneuronal neurofibrillary tangles in the brain [13]. Apart from

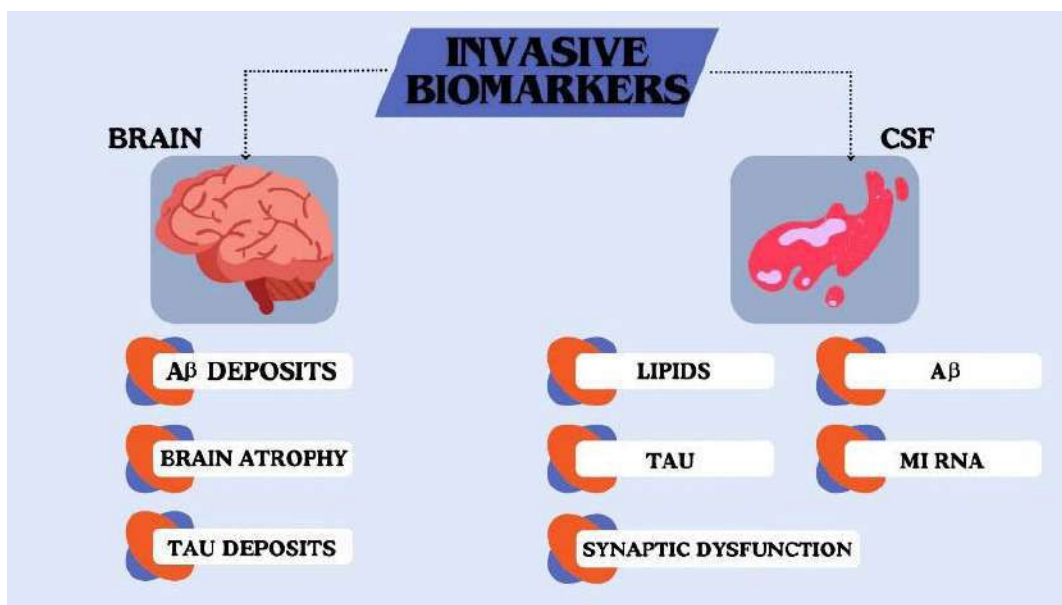


Fig. (2). Invasive biomarkers of Alzheimer's disease. (A higher resolution / colour version of this figure is available in the electronic copy of the article).

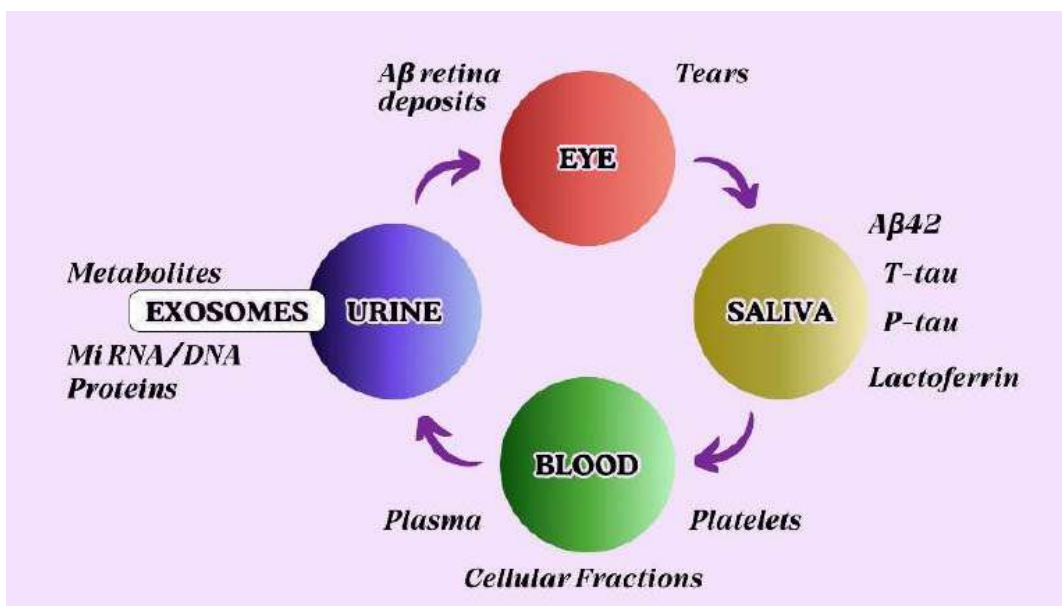


Fig. (3). Non-invasive biomarkers of Alzheimer's disease. (A higher resolution / colour version of this figure is available in the electronic copy of the article).

them, many other clinical factors like cerebrospinal fluid, metal toxicity, mitochondrial dysfunction, neurofilament light chains *etc.*, are proclaimed as promising indicators. With regard to this, Reitz *et al.* and his team in 2011 have critically discussed the prevalence, environmental risk factors, and other protective factors [14]. Therefore, the search

for blood biomarkers that are associated with AD should start with recognized CSF markers, such as biomarkers related to A β and Tau, and also take into account elements related to inflammation, protein aging and cell death, and cerebrovascular dysfunctions. Information regarding crucial AD biomarkers and the changes associated with them has been summarized in Table 1.

Table 1. Essential biomarkers of AD.

S. No.	Biomarkers	Mild AD	Severe AD	References
Amyloid Biomarkers				
1	APP (sAPP β) blood	No change	No change	[15]
2	Three subtypes of APP (106, 110 and 130)	Present in platelets	Present in platelets	[16]
3	APP (sAPP β) blood	Decrease in blood	Decrease in blood	[17]
4	A β peptides (A β 1-42 and A β 1-40 peptides)	Overproduction, accumulation	Overproduction, accumulation, amyloid plaques formation	[18]
5	A β 42/ A β 42	Increase	Increase	[19]
6	Plasma A β (1-42) and A β (1-40)	Elevated, reduced, or remains unchanged	Elevated, reduced, or remains unchanged	[20]
7	A β (1-42)	-	Increase in plasma of women	[21]
8	A β (1-42)	Increase in plasma	Increase in plasma	[22]
9	A β (1-42) autoantibodies	Decrease in serum	Decrease in serum	[23]
Tau Biomarkers				
1	Total tau (t-tau)	Increases in CSF	Increases in CSF	[24]
2	Total tau (t-tau)	Increases in CSF	Increases in CSF	[25]
3	Phospho-tau-231 has shown	Decrease longitudinally from mild to moderate	Elevated	[26]
4	Phosphorylated forms of Tau (phospho-tau-199, -231, -235, -396, and -404)	Elevated	Elevated	[27]
Neuronal Biomarkers				
1	Neurofilament light chain protein (NFL)	Elevated blood and plasma	Elevated blood and plasma	[28]
2	S100b and neuron-specific enolase (NSE) proteins	Reduced	Reduced	[29]
Biomarkers of Neuroinflammation				
1	Glial fibrillary acidic protein (GFAP)	Elevated	Elevated	[30]
2	GSK-3	-	Elevated in white blood cells	[31]
3	Chemokines, cytokines, growth factors, and binding proteins	Elevated in plasma	Elevated in plasma	[32]
4	YKL-40	Increase both in serum and CSF	Increase both in serum and CSF	[33]
5	Neurogranin (synaptic protein)	Increase in the CSF	Increase in the CSF	[34]
Other Biomarkers				
1	Ab toxicity and ubiquitin levels	Elevated in the cerebral cortex	Elevated in the cerebral cortex	[35]
2	telomeres	Smaller in peripheral blood cells	Smaller in peripheral blood cells	[36]
3	C-reactive protein (CRP)	High	High	[37]
4	Level of vasodilator and vasoconstrictor	Increased	Increased	[38]

2.1. Blood-based Biomarkers

Recently, biomarkers of AD research have taken a front seat, especially blood-based biomarkers. Hansoon *et al.* have reviewed blood based biomarkers for clinical trials and practices [39-41]. When identifying AD in patients with cognitive impairment from all other neurodegenerative disorders, phosphorylated Tau (p-tau) in plasma shows excellent diagnostic accuracy [42-44]. There is a need to elucidate the specific research that needs to be conducted before blood-

-based biomarkers can be widely used. Doecke *et al.* [45], with his research team in 2012, have also worked on the identification of plasma biomarkers of AD for the purpose of early diagnosis. For this, they screened AD-afflicted and healthy individuals at the same time. This panel of plasma biomarkers showed an appreciable extent of sensitivity and specificity, which could help in the easy distinction between AD and healthy individuals. This evidence could strongly help in AD diagnosis. Fig. (4) represents crucial plasma biomarkers.

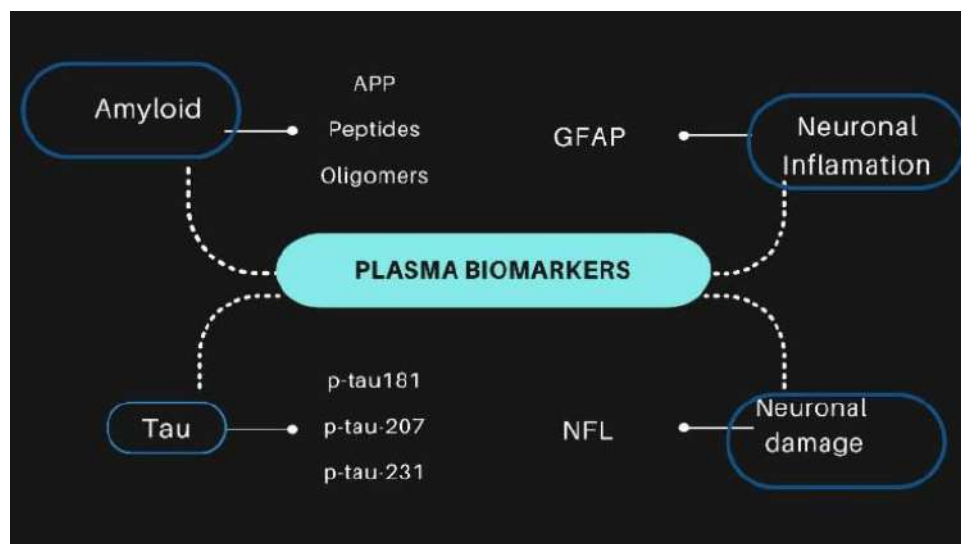


Fig. (4). Plasma biomarkers. (A higher resolution / colour version of this figure is available in the electronic copy of the article).

2.1.1. Plasma Amyloid Beta

Just like the reduction of A β 42/A β 40 in CSF biomarkers, Plasma A β 42/A β 40 biomarkers are strong indicators of AD. A β is isolated from plasma and quantified using mass spectrometry. By using these techniques, it is possible to see group-level decreases in plasma A β 42/A β 40 levels in amyloid PET-positive individuals relative to PET-negative individuals. The fact that plasma A β 42/A β 40 levels are completely altered even in the pre-symptomatic stages of the disease is a significant characteristic. For this reason, this biomarker, similar to CSF A β 42/A β 40, can accurately identify A β pathology in cognitively unimpaired individuals with accuracy levels comparable to those seen in cognitively impaired individuals [46]. For biological reasons, CSF A β 42/A β 40 is a more robust brain A β pathology biomarker than plasma A β 42/A β 40. In clinical laboratory practice, standardizing and maintaining the stability of this kind of test over time with the kind of rigor required to accurately identify the subtle difference between persons who are A β -positive and -negative is a difficult task [47].

2.1.2. Plasma Phosphorylated Tau (P-tau)

Tau phosphorylated at amino acid 181 (p-tau181), 217 (p-tau217), or 231 (p-tau231) have been reported by experts to detect different stages of AD [48, 49]. To evaluate the kinetics of various tau isoforms and fragments in the human Central Nervous System (CNS) and in neurons produced from induced Pluripotent Stem Cells (iPSCs), Sato *et al.* [50] devised stable isotope labeling and mass spectrometry techniques. It was also claimed that both tau tangles and β -amyloid plaques raise the concentration of plasma P-tau217, which is consistent with the theory that P-tau is implicated in the β -amyloid-dependent development of neocortical tau tangles [51]. Recent research on plasma phosphorylated tau has developed methods to study soluble p-tau indicators that have a stronger correlation with cerebral amyloid- β than

with PET-measured tau aggregation [52]. Various reports on plasma phosphorylated Tau are directed toward AD pathology [53, 54].

2.1.3. Plasma Neurofibrillary Tangles (NFL)

Salvado *et al.* [55] carried out a head-to-head comparison between many plasma biomarkers and neuropathological measurements of neurofibrillary tangles and amyloid plaques. They found that while plasma Glial Fibrillary Acidic Protein (GFAP) is uniquely linked to tau pathology, plasma A β 42/40 and plasma p-tau231 are specifically linked to amyloid disease. In individuals with cerebral white matter rarefaction, plasma Neurofilament Light (NfL) is elevated even after taking Alzheimer's disease pathology into consideration. Rodriguez *et al.* [56] reported that A β -positive cognitively impaired groups showed a particular increase in CSF and plasma NTA-tau concentrations. Global uptake and voxel-level correlations between CSF and plasma NTA-tau concentrations and tau PET were found to be stronger than those with A β PET and MRI. Both CSF and plasma NTA-tau are preferentially related to tau disease, according to regression models. Vrillon *et al.* [57] demonstrated in memory clinic settings, CSF NfL, plasma neurofibrillary heavy chain levels, and plasma NfL levels function similarly in positive and differential AD diagnoses. Unlike illnesses affecting motoneuron function, plasma pNfH did not show any additional benefit when compared to plasma NfL. The performance of CSF and PET indicators must be matched by continued research and the creation of reliable tests. In conclusion, blood-based biomarkers are becoming more and more important for AD diagnosis, monitoring, prognostication, assessing treatment response, and population screening-especially in primary care settings. With these advancements, AD diagnostics will be transformed, and more accessible and early detection and management options will be provided [58, 59].

2.1.4. Plasma Glial Fibrillary Acidic Proteins (GFAP)

Pereira *et al.* [60] reported that when compared to persons without amyloid- β pathology, the plasma GFAP concentration was considerably higher in all amyloid- β -positive groups ($P < 0.01$). Furthermore, in all amyloid- β positive groups, there were significant correlations between plasma GFAP and increased amyloid- β -PET signal. Plasma GFAP is a viable candidate to be added to the blood-based biomarker panel for AD because it is linked to AD-type pathology and has the ability to reliably predict clinical progression to AD dementia [61]. It has been demonstrated that the strong predictive value and clinical utility of GFAP as an ideal option to identify high-risk individuals and further prevent early in clinical trials or treatment timely in patients, as it is a highly specific marker of astrocyte activation and a substantial structural element of astrocytes. It is yet unknown, nevertheless, if GFAP is merely a sign of a broader astrocyte activation or even if it is the primary initiator of the inflammatory cascade reactions [62]. Using one-way Analysis Of Variance (ANOVA) and Receiver Operating Characteristic (ROC) curves, it was found that the area under the ROC curve (AUC) of 0.928 for GFAP indicated that it was a more effective diagnostic tool. The two serum indicators for the diagnosis of AD have cut-off values of GFAP >31.40 pg/mL and NfL >40.09 pg/mL. For the diagnosis of AD, the corresponding sensitivity and specificity for NfL were 59.6% and 76.2%, respectively, while the corresponding values for GFAP were 90.4 and 82.1% [63].

2.2. Cerebrospinal Fluid (CSF) Biomarkers

Cerebrospinal Fluid (CSF) is the first call for accessing AD treatment and therapeutic interventions [64]. CSF are most explored due to their ability to spot people with mild cognitive impairment, which can further assist in tracking their AD progression. Seyfried and group have supported this using a novel method known as selected reaction monitoring mass spectrometry, and the findings say that neuronal proteins are capable of differentiating cognitive decline issues [65]. Moreover, bioinformatics methods used by Li [66] *et al.* have led to the identification of six hub proteins in CSF, which could successfully differentiate between AD and other neuronal disorders. CSF biomarkers also aid in the assessment of plaques and tangles accountable for cognitive decline. Recently, many researchers have pointed the importance of CSF biomarkers [67, 68, 69]. Trombetta *et al.* [70] CSF tested a panel of 25 well-validated biomarker assays, and all were elevated in AD patients. Oxidative stress and metabolic markers influenced the multianalyte profile of AD. The authors concluded that it's critical to evaluate several biomarker domains in order to comprehend the heterogeneity of diseases. Mravinacová *et al.* [71] observed that When proteins from various groups were combined in ratios (tau-associated protein/amyloid-associated protein), the proteins' association with cognitive decline as assessed by cognitive scores was dramatically increased. In a discovery cohort with 98 patients, Tao *et al.* [72] conducted tandem mass tag proteomic analysis of matched Cerebrospinal Fluid (CSF) and serum samples. Targeted proteome assays based on par-

allel reaction monitoring were utilized to validate candidate biomarkers in a separate multicenter cohort of 288 individuals. In the discovery cohort, they measured 3,238 CSF and 1,702 serum proteins. Of these, they identified 171 and 860 CSF proteins and 37 and 323 serum proteins, respectively, as possible early diagnostic and staging indicators. Twelve and eighteen serum proteins and fifty-eight CSF proteins were confirmed as early diagnostic and staging indicators in the validation cohort, respectively. Recently [73] the role of neural lipids has been observed in the prediction of mild to AD. Bateman *et al.* [74], in their longitudinal study, revealed very fascinating conclusions. They analyzed 128 participants for cognitive assessments, brain imaging, CSF, and blood tests. The cross-sectional analyses revealed exciting results, such as the concentrations of amyloid-beta 42 decline 25 years before the symptom was revealed. Using positron-emission tomography, A β deposition and Tau protein's presence in the CSF were observed 15 years before AD struck. Hypometabolism of cerebral and fresh memory loss was found to diminish 10 years before the AD diagnosis. Meanwhile, global cognitive impairment was observed 5 years earlier, and the afflicted people met diagnostic criteria only 3 years before. This study concluded that the pathophysiological alterations of the CSF start at least over 20 years before the symptoms are visible. Based on the same biomarkers, Mattson *et al.* [75] and his research group worked to determine their accuracy. For this, an extensive study was conducted involving AD patients and controls from 12 centers in Europe and the US. Here, also follow-up study was done for 2 years till the symptoms progressed for the neurological disorder. The concluding results showed a total number of 271 participants were diagnosed with AD and 59 with other forms of dementia. Fig. (5) summarizes the criteria for establishing a good biomarker for the diagnosis of AD.

Subsequently, Shaw *et al.* [76], again remarked CSF as the most sensitive biomarker for AD, in an experiment performed in the Alzheimer's disease Neuroimaging Initiative (ADNI) cohort with 96.4% detection sensitivity. They also found that CSF can also indicate mild cognitive (MCI) impairment to AD conversion. In 2006, Blennow *et al.* did a follow-up study for 4-6 years of 180 patients having mild cognitive impairment (MCI) in association with CSF biomarkers. Here, the clinical studies clarified that people struck with MCI have a higher chance of encountering with AD in their life. This occurred due to the elevated concentrations of T-tau, position threonine 181 (P-tau181), and A42 in CSF [77].

2.2.1. CSF Amyloid-beta (A β)

The instability of A β (1-42) plasma levels can be attributed to a number of factors [78, 79]. As of right now, the FDA has approved two assays: Roche Elecsys pTau181/A β 42 ratio and Fujirebio Lumipulse G β -Amyloid Ratio (A β 42/40) for assessing these biomarkers in CSF. 2, 3 According to these assays; there is brain amyloid pathology when there is a lower A β 42/40 ratio or a higher pTau181/A β 42 ratio in CSF [80]. Ab levels in the blood fluctuate over time and between individuals and may differ in mild, early, and late stages of

- Reflect physiological aging processes.
- Reflect basic pathophysiological processes of the brain.
- React upon pharmacological intervention.
- Display high sensitivity.
- Display high specificity for the disease as compared with related disorders.
- Allow measurements repeatedly over time.
- Allow reproducibility in laboratories worldwide.
- Should be measurable in non-invasive, easy-to-perform tests.
- Should not cause harm to the individuals being assessed.
- Tests should be inexpensive and rapid.
- Samples should be stable to allow easy and cheap transport.
- Easy collection of fluids not only in hospitals.
- Changes should be at least two-fold to allow differentiation of controls.
- Define good cut-off values to distinguish diseases.
- Data published in peer-reviewed journals.
- Data reproduced by at least two independent researchers.

Fig. (5). Criteria for establishing a good biomarker.

AD. In addition, blood platelets contain high levels of A β , which directly affects plasma levels [81]. The most senile form of AD marker is Amyloid-beta (A β) proteins found in the A β 42, A β 40, and A β 42/40 ratio as detected by positron emission tomography (PET), which eventually uplifts their weightage in comparison to other biomarkers [82]. The CSF also shows their prominent presence [83]. To validate the presence of amyloid in CSF, Queiroz *et al.* used a tandem mass spectrometry technique coupled with fiber-in-tube. It is well known that the alteration caused in amyloidogenic proteins a major reason for these serious neurodegenerative issues [84, 85]. The protein misfolding and resulting structures, such as polymorphic oligomers and fibrils, can often lead to cell death as they are toxic species. Beyer *et al.* have worked for over 17 years to establish the risk associated with the disorder. AD diagnosed around 60 participants and nearly about 200 controls were involved in this study. Their A β abnormal foldings and Ttau biomarkers were studied, revealing that A β is more specific in foretelling the AD risk factor [86].

Gliozzi *et al.* [87] showed the same by performing an interactive study using model membranes, which results in the formation of amyloid aggregates. These aggregates deposit in various tissues and causes AD, but this can still not be detected at the early onset of AD. They have also assumed that environmental conditions may contribute to aggregation and ultimately, to neurodegeneration. A fluorescent probe called Q-OB, which is generated from quinoline, has been created to detect A β oligomers [88]. This was achieved by precisely adjusting the hydrophobicity of the biannulate donor motifs in the donor- π -acceptor structure. When it comes to dynamically monitoring A β oligomerization during amyloid fibrillogenesis *in vitro*, Q-OB has exceptional sensing power. Furthermore, authors utilized this approach to fluorometrically examine the kinetics of A β self-assembly in the cerebrospinal fluids (CSF) of individuals with AD for an early diagnosis method. Various electrochemical immunosensors have

been developed [89] for detecting AD biomarkers (A β and p-tau protein) and their subtypes (A β O, A β ₍₁₋₄₀₎, A β ₍₁₋₄₂₎, t-tau, cleaved-tau (c-tau), p-tau₁₈₁, p-tau₂₃₁, p-tau₃₈₁, and p-tau₄₄₁).

2.2.2. CSF Phosphorylated-tau

One another prominent mechanism involved in AD is Tau pathology [90]. There have been recent reports on biomarkers for moderate cognitive impairment: CSF tau and β -amyloid [91]. A form of protein that is involved in forming neurofibrillary tangles in Alzheimer's patients. Tau is pronounced hyperphosphorylated (39 potential locations) in AD, which causes axonal transport impairment and a lack of function. Authors have reported [52] that the results of PET-assessed tau aggregation are less strongly correlated with soluble p-tau biomarkers than with cerebral amyloid- β . This suggests that p-tau biomarkers should be carefully interpreted within the framework of amyloid/tau/neurodegeneration. The AD group had significantly lower NfL levels but higher total-tau levels. Significant relationships between NfL, p-tau₁₈₁, and total-tau, as well as between NfL and cognitive capabilities, were discovered in the FTD group. A β 42/40 ratio had an inverse correlation with both total-tau and p-tau₁₈₁, but not with NfL. In the AD group, NfL levels were directly connected with both of these measures. The CSF biomarkers p-tau₁₈₁ and p-tau₂₃₁ identified healthy AD, and MCI populations. When matched to controls, AD intensely surges the revealing of Tau that has been phosphorylated at position 181, with a cut-off of >60 pg/ml. PET imaging shows a few Tau-related biomarkers like total tau (t-tau), phosphorylated Tau (p-tau), and tau/A β 42 ratio [92]. Apparently, it was found that Tau emerges peripherally as well as from the brain. Now, it is evident that the brain-related Tau are much more responsible for the neuronal disorder; thus, to distinguish between peripheral and brain-derived Tau, Gonzalez-Ortiz *et al.* brought about an anti-tau antibody that certainly bind to the one that originated from the brain. This is because the former is not a specific biomarker, and may

produce discrepancies [93]. Subsequently, their concentration is also region-defined. This was proved by Dang *et al.*, who, in their study, involved 83 AD patients and 38 normal patients and examined their brain spatial biological patterns. The biomarkers inter-relationship with AD was considered using various tests and algorithms, where they were tagged as the region-specific clinical marker [94]. Rodriguez *et al.* [95] commented on the significance of p-tau 205 in AD biomarking.

According to Braak *et al.* [96], Tau alterations start even 20 years before the A β plaques. The detailed study of Hasegawa on tau pathology has revealed the information that the tau fibrils are characteristically distinct in every other disease. In fact, plaques are only found with the tau tangles in the brain. Thus, it may be the tau alterations may be the reason for the A β plaques [97]. Medina *et al.* observed Tau as a protein that binds to microtubules and then regulates its morphology and activities in the brain. When the pathological alterations occur, they form neurofibrillary tangles. They have reviewed developments in AD and tauopathies [98]. Subsequently in the same year, Serpell *et al.* pondered the cellular distribution, its nuclear location, and functions of Tau and how this alteration varies or changes drastically in the disorder state. Globally, it has been accepted that the Tau is a prominent hallmark of AD [99]. In fact, tau Tau has also been assessed separately by researchers for novel drug development in correspondence with them. The tau accumulation and their regional distribution in a human brain and the aging of Tau has all been taken into concern. The review of Harada *et al.*, helps in the critical understanding of how the tau Tau fibrils interact with amyloid plaques in an AD brain and how their combination assists to the disorder early diagnosis [100].

Šimić *et al.*, have mentioned in their article that the abnormal extra neuronal deposition of aggregated proteins/plaques and the intraneuronal aggregation tau protein are the most common reasons for AD. It is now completely accepted that misfolded or abnormally structured proteins are the reason for AD [101].

2.2.3. CSF-Neurofilament Light Chain (NfL)

In 2019, a new kind of biomarker came under notice: Neurofilament light chain (NfL), which has been marked as a prominent fluid clinical marker by Preische *et al.* for AD. The generation of this chain has been noticed upon the progression of neurodegeneration into CSF [102]. Their presence has been confirmed *via*. Immunoassay. This cytoskeletal protein comes into existence upon neuronal damage; thus, it is not specific to AD.

It has been observed in their research that CSF and serum are correlated and elevated at the primary stage of AD. This elevation of serum NfL was revealed from the longitudinal analysis of people, and surprisingly, it was estimated that this elevation occurred almost a decade earlier before the estimated onset of AD. The elevation was also accompanied by cortical thinning, diagnosed by magnetic reso-

nance imaging (MRI). The study conducted at Mini-Mental State Examination and Logical Memory test shows that assessing NfL dynamics in serum can help in early prediction of AD, indicating that it is a prominent biomarker [103]. Another bioindicator is the Phosphorylated neurofilament heavy chain. They show a resemblance to NFT and mark the axonal damage relating to neurodegeneration [104]. The elevated levels lead to the progression of disease by their presence in CSF.

2.3. Disguised Factors Targeting Alzheimer's Disease

With time, other factors have also been explored which, in disguised form, act as biomarkers of this neuronal disorder. Other important etiological factors responsible for AD are oxidative stress, excess metal ions, *etc.* Again, in 2014, Mitra *et al.* focused on a potential cause of AD *i.e.*, the presence of excess metal ions causing toxicity, but the pathological mechanism is less known than how it affects neurons. Their studies have shown that elevated levels of redox metal ions (iron and copper) in the brain could irreversibly damage neurons. As their repair was inhibited by metal chelators and reducing agents. In their review, they have laid interest in the oxidative genome damage repair pathway, which could help prevent AD [105]. Eventually, in 2014, Hane *et al.*, studied the role of metal ions like (copper and zinc) in the AD pathological pathway. They highlighted the point that the metal ions plausibly change the kinetic path of the A β peptide, forming toxic oligomeric end-products. Here, the authors have critically reviewed how these metals severely affect the reaction path and lead to more neuro-toxic species. Studies have shown that the excess of copper ions can serve the purpose of neurotoxicity [106]. Few by-products, like oxysterols (formed by cholesterol biosynthesis), have a spectrum of biological reactions corresponding to AD pathology. Some oxysterols bear cytotoxic and pro-apoptotic properties. They can induce inflammatory responses and are potent enough to interfere with the lateral domain organization. Studies done on them by Olkkonen *et al.* in 2012 have unraveled that their physiological functions assist as signaling molecules involved in maintaining cellular and body lipid homeostasis. Still, to claim oxysterols as a specific biomarker, their role in the mechanisms of AD is less investigated [107]. The study of clinical hallmarks got an entirely new platform when Fisar and his group studied mitochondrial dysfunctions in co-relation with AD in 2014. Mitochondrial dysfunctions are also indicators of neurodegenerative dysfunction like AD as the impairment in mitochondria may result in AD. In this review, Hroudová *et al.* discussed concepts like reactive oxygen species, impaired mitochondrial dynamics, and apoptosis. Mitochondrial dysfunction also tends to damage the electron transport chain, which is again a responsible factor for the pathogenesis of AD [108]. Moreover, in 2019 a novel factor was underscored, which is also responsible for triggering AD. Mansour *et al.* have reviewed the evidence that air pollution can trigger AD. People with hearing and encoding disability for complex sounds may also be victims of AD. This happens as the auditory brain-

stem's nuclei are sensitive to neurodegenerative disorders. People who regularly encounter air pollution are found to show an accumulation of Tau, senile amyloid plaques, and suffer oxidative stress. Thus, it concludes that the physiological assessment of such people's brain-stem can help in prior indication of AD [109]. In AD, there is an abnormality in the lysosomal pathway-mediated autophagic breakdown of intracellular components. While cells from healthy individuals vigorously internalize A β , macrophages and monocytes from AD patients typically have limited A β phagocytic activity.

3. LIMITATIONS OF BIOMARKERS OF AD

Despite the full coverage of the background story of biological hallmarks of AD, some important questions remain unanswered. These need to be clarified to access AD at its early onset. It is necessary to determine their possible predictive usefulness with respect to the duration of recovery and the likelihood of incomplete recovery or CTE. There is still very less information on the mechanism of biomarkers and how blood concentrations relate to blood-brain barrier dysfunction¹. Moreover, serum and plasma are already highly enriched in a number of proteins (~50-70 g/L), which makes it difficult to detect and leads to less successful results when using biomarkers in blood as opposed to CSF. As of now, there is insufficient data to demonstrate the superiority of biomarkers over other diagnostic techniques for AD (such as CSF/imaging). Therefore, compared to blood-based biomarkers, CSF has fewer difficulties with availability and diagnosis in A/T/N framework-based biomarkers. A major limitation in the field is that markers discovered by one group cannot be reproduced by other groups. The predictive value of the existing biochemical and neuroimaging markers is quite low. Although the prognostic importance is currently limited to the latter stages of the disease, combining neuroimaging investigations with the detection of some CSF proteins improves diagnostic sensitivity and specificity, particularly in AD. The fact that markers found by one group cannot be replicated by other studies is a significant constraint in the field.

CONCLUSION

We have reviewed the prominent hallmarks of AD and discussed various plasma and fluid biomarkers that are relevant to clinical investigations and early predictions with recent insights. Alzheimer's disease (AD) is characterized by neurofibrillary tangles (NFTs) of Tau protein in patients' brains and senile plaques made of A β . Four CSF biomarkers-A β 42, A β 42/40, Tau, and pTau181-have undergone in-depth analysis and have been established as essential markers for AD. Apart from the direct role of biomarkers, the importance of the correct protocol of sample collection has been an area of interest. More information is required on biological variation (*e.g.*, the impact of renal function, body mass index (BMI), and peripheral neuropathy) as well as biomarker performance in a variety of groups. Clinical laboratory practice already uses plasma NfL analysis in several labo-

ratories worldwide. The biomarkers for AD diagnosis that have been explored and used the most include CSF A β 42, CSF A β 42/A β 40, CSF p-tau, tau PET, amyloid PET, structural MRI, *etc.* It has been well established that Tau and A β 42 levels are significantly lower in plasma than in CSF. There is no doubt that once the biomarkers of AD are identified from its core origin, they will projectile in the direction of instant early detection and treatment of the disease. To conclude, a precise clinical diagnosis is crucial when looking for a biomarker. Future research work may help identify more and more highly specific clinical insights for unraveling the biomarkers of this neuronal disorder. With this, drug efficacy can be modified, and novel therapeutic approaches may be introduced. Great insights into biomarkers can give possible solutions when it comes to curing AD. The identification of promising biomarkers can be a truly fascinating finding, which could completely open new ways in the prevention of the most dreadful form of dementia. Hitting the biomarkers of AD at an early stage represents a way better solution than prescribing anti-AD drugs.

LIST OF ABBREVIATIONS

AD	=	Alzheimer's Disease
APP	=	Amyloid Precursor Protein
A β	=	Aymoid Beta
CRP	=	C-reactive Protein
CSF	=	Cerebro Spinal Fluid
GFAP	=	Glial Fibrillary Acidic Protein
MRI	=	Magnetic Resonance Imaging
NFL	=	Neurofilament Light Chain
NFT	=	Neurofibrillary Tangles
NSE	=	Neuron-Specific Enolase
PET	=	Positron Emission Tomography
p-Tau	=	Phosphorylated Tau

CONSENT FOR PUBLICATION

Not applicable.

FUNDING

None.

CONFLICT OF INTEREST

The authors declare no conflict of interest, financial or otherwise.

ACKNOWLEDGEMENTS

NS and KK express their gratitude to the University of Hradec Kralove (project Excellence 2205/2024-2025) for their support. NS is grateful to the Department of Engineering Sciences, Ramrao Adik Institute of Technology, DY Patil University, for its research support and facilities.

REFERENCES

- [1] Kodintsev, A.N.; Izmozherova, N.V.; Popov, A.A.; Volkova, L.I.; Antropova, I.P.; Ryabinina, A.V. Biochemical platelet markers of cognitive impairments in Alzheimer's disease. *Neurochem. J.*, **2023**, *17*(1), 10-18.
<http://dx.doi.org/10.1134/S1819712423010105>
- [2] Wang, S.; Liu, Y.; Zhu, A.; Tian, Y. *in vivo* electrochemical biosensors: Recent advances in molecular design, electrode materials, and electrochemical devices. *Anal. Chem.*, **2023**, *95*(1), 388-406.
<http://dx.doi.org/10.1021/acs.analchem.2c04541> PMID: 36625112
- [3] Sharma, S.; Singh, N. Exploration of neurodiagnostic biomarkers of Alzheimer's. *Rivista Medicina*, **2021**, (2), 31-33.
- [4] Li, J.; Ni, W.; Jin, D.; Yu, Y.; Xiao, M.M.; Zhang, Z.Y.; Zhang, G.J. Nanosensor-driven detection of neuron-derived exosomal AB₄₂ with graphene electrolyte-gated transistor for Alzheimer's disease diagnosis. *Anal. Chem.*, **2023**, *95*(13), 5719-5728.
<http://dx.doi.org/10.1021/acs.analchem.2c05751> PMID: 36943894
- [5] Sharma, S.; Singh, N.; Nepovimova, E.; Korabečný, J.; Kuca, K.; Satnami, M.L.; Ghosh, K.K. Interaction of synthesized nitrogen enriched graphene quantum dots with novel anti-Alzheimer's drugs: spectroscopic insights. *J. Biomol. Struct. Dyn.*, **2020**, *38*(6), 1822-1837.
PMID: 31096863
- [6] Xu, L.; Lai, L.; Wen, Y.; Lin, J.; Chen, B.; Zhong, Y.; Cheng, Y.; Zhang, X.; Guan, J.; Mikulis, D.J.; Lin, Y.; Yan, G.; Wu, R. Angiopep-2, an MRI biomarker, dynamically monitors amyloid deposition in early Alzheimer's disease. *ACS Chem. Neurosci.*, **2023**, *14*(2), 226-234.
<http://dx.doi.org/10.1021/acschemneuro.2c00513> PMID: 36599050
- [7] Sharma, S.; Banjare, M.K.; Singh, N.; Korábečný, J.; Kuca, K.; Ghosh, K.K. Multi-spectroscopic monitoring of molecular interactions between an amino acid-functionalized ionic liquid and potential anti-Alzheimer's drugs. *RSC Advances*, **2020**, *10*(64), 38873-38883.
<http://dx.doi.org/10.1039/D0RA06323A> PMID: 35518436
- [8] Duan, R.; Hong, C.G.; Chen, M.L.; Wang, X.; Pang, Z.L.; Xie, H.; Liu, Z.Z. Targeting autophagy receptors OPTN and SQSTM1 as a novel therapeutic strategy for osteoporosis complicated with Alzheimer's disease. *Chem. Biol. Interact.*, **2023**, *377*, 110462.
<http://dx.doi.org/10.1016/j.cbi.2023.110462> PMID: 36958424
- [9] Leng, H.; Yang, J.; Long, L.; Yan, Y.; Shi, W.J.; Zhang, L.; Yan, J. GFP-based red-emissive fluorescent probes for dual imaging of β -amyloid plaques and mitochondrial viscosity. *Bioorg. Chem.*, **2023**, *136*, 106540.
<http://dx.doi.org/10.1016/j.bioorg.2023.106540> PMID: 37084586
- [10] Sharma, S.; Banjare, M.K.; Singh, N.; Korábečný, J.; Fišar, Z.; Kuca, K.; Ghosh, K.K. Exploring spectroscopic insights into molecular recognition of potential anti-Alzheimer's drugs within the hydrophobic pockets of β -cycloamylose. *J. Mol. Liq.*, **2020**, *311*, 113269.
<http://dx.doi.org/10.1016/j.molliq.2020.113269>
- [11] Ausó, E.; Gómez-Vicente, V.; Esquivá, G. Biomarkers for Alzheimer's disease early diagnosis. *J. Pers. Med.*, **2020**, *10*(3), 114.
<http://dx.doi.org/10.3390/jpm10030114> PMID: 32899797
- [12] Thomas, E.A. Salivary Biomarkers and Neurodegenerative Conditions. *Salivary Bioscience: Foundations of Interdisciplinary Saliva Research and Applications*, **2020**, 263-286.
http://dx.doi.org/10.1007/978-3-030-35784-9_12
- [13] Wang, M.; Tang, G.; Zhou, C.; Guo, H.; Hu, Z.; Hu, Q.; Li, G. Revisiting the intersection of microglial activation and neuroinflammation in Alzheimer's disease from the perspective of ferroptosis. *Chem. Biol. Interact.*, **2023**, *375*, 110387.
<http://dx.doi.org/10.1016/j.cbi.2023.110387> PMID: 36758888
- [14] Reitz, C.; Brayne, C.; Mayeux, R. Epidemiology of Alzheimer disease. *Nat. Rev. Neurol.*, **2011**, *7*(3), 137-152.
<http://dx.doi.org/10.1038/nrneuro.2011.2> PMID: 21304480
- [15] Yun, S.M.; Cho, S.J.; Jo, C.; Park, M.H.; Han, C.; Koh, Y.H. Elevation of plasma soluble amyloid precursor protein beta in Alzheimer's disease. *Arch. Gerontol. Geriatr.*, **2020**, *87*, 103995.
<http://dx.doi.org/10.1016/j.archger.2019.103995> PMID: 31874328
- [16] Tang, K.; Hynan, L.S.; Baskin, F.; Rosenberg, R.N. Platelet amyloid precursor protein processing: A bio-marker for Alzheimer's disease. *J. Neurol. Sci.*, **2006**, *240*(1-2), 53-58.
<http://dx.doi.org/10.1016/j.jns.2005.09.002> PMID: 16256140
- [17] Perneckzy, R.; Guo, L.H.; Kagerbauer, S.M. Soluble amyloid precursor protein β as blood-based biomarker of Alzheimer's disease. *Transl Psychiatry*, **2013**, *3*(2), e227.
<http://dx.doi.org/10.1038/tp.2013.11>
- [18] Delaby, C.; Hirtz, C.; Lehmann, S. Overview of the blood biomarkers in Alzheimer's disease: Promises and challenges. *Rev. Neurol.*, **2022**.
PMID: 36371265
- [19] Sunderland, T.; Mirza, N.; Putnam, K.T.; Linker, G.; Bhupali, D.; Durham, R.; Soares, H.; Kimmel, L.; Friedman, D.; Bergeson, J.; Csako, G.; Levy, J.A.; Bartko, J.J.; Cohen, R.M. Cerebrospinal fluid β -amyloid₁₋₄₂ and tau in control subjects at risk for Alzheimer's disease: The effect of APOE $\epsilon 4$ allele. *Biol. Psychiatry*, **2004**, *56*(9), 670-676.
<http://dx.doi.org/10.1016/j.biopsych.2004.07.021> PMID: 15522251
- [20] Cedazo-Minguez, A.; Winblad, B. Biomarkers for Alzheimer's disease and other forms of dementia: Clinical needs, limitations and future aspects. *Exp. Gerontol.*, **2010**, *45*(1), 5-14.
<http://dx.doi.org/10.1016/j.exger.2009.09.008> PMID: 19796673
- [21] Assini, A.; Cammarata, S.; Vitali, A.; Colucci, M.; Giliberto, L.; Borghi, R.; Inglese, M.L.; Volpe, S.; Ratto, S.; Dagna-Bricarelli, F.; Baldo, C.; Argusti, A.; Odetti, P.; Piccini, A.; Tabaton, M. Plasma levels of amyloid β -protein 42 are increased in women with mild cognitive impairment. *Neurology*, **2004**, *63*(5), 828-831.
<http://dx.doi.org/10.1212/01.WNL.0000137040.64252.ED> PMID: 15365131
- [22] Borroni, B.; Di Luca, M.; Padovani, A. Predicting Alzheimer dementia in mild cognitive impairment patients. *Eur. J. Pharmacol.*, **2006**, *545*(1), 73-80.
<http://dx.doi.org/10.1016/j.ejphar.2006.06.023> PMID: 16831417
- [23] Brettschneider, S.; Morgenthaler, N.G.; Teipel, S.J.; Fischer-Schulz, C.; Bürger, K.; Dodel, R.; Du, Y.; Möller, H.J.; Bergmann, A.; Hampel, H. Decreased serum amyloid β 1-42 autoantibody levels in Alzheimer's disease, determined by a newly developed immuno-precipitation assay with radiolabeled amyloid β 1-42 peptide. *Biol. Psychiatry*, **2005**, *57*(7), 813-816.
<http://dx.doi.org/10.1016/j.biopsych.2004.12.008> PMID: 15820240
- [24] Olsson, B.; Lautner, R.; Andreasson, U.; Öhrfelt, A.; Portelius, E.; Bjerke, M.; Hölttä, M.; Rosén, C.; Olsson, C.; Strobel, G.; Wu, E.; Dakin, K.; Petzold, M.; Blennow, K.; Zetterberg, H. CSF and blood biomarkers for the diagnosis of Alzheimer's disease: a systematic review and meta-analysis. *Lancet Neurol.*, **2016**, *15*(7), 673-684.
[http://dx.doi.org/10.1016/S1474-4422\(16\)00070-3](http://dx.doi.org/10.1016/S1474-4422(16)00070-3) PMID: 27068280
- [25] Sjögren, M.; Vanderstichele, H.; Ågren, H.; Zachrisson, O.; Edsberg, M.; Wikkelsø, C.; Skoog, I.; Wallin, A.; Wahlund, L.O.; Marcusson, J.; Nägga, K.; Andreassen, N.; Davidsson, P.; Vanmechelen, E.; Blennow, K. Tau and A β 42 in cerebrospinal fluid from healthy adults 21-93 years of age: establishment of reference values. *Clin. Chem.*, **2001**, *47*(10), 1776-1781.
<http://dx.doi.org/10.1093/clinchem/47.10.1776> PMID: 11568086
- [26] Hampel, H.; Blennow, K.; Shaw, L.M.; Hoessler, Y.C.; Zetterberg, H.; Trojanowski, J.Q. Total and phosphorylated tau protein as biological markers of Alzheimer's disease. *Exp. Gerontol.*, **2010**, *45*(1), 30-40.
<http://dx.doi.org/10.1016/j.exger.2009.10.010> PMID: 19853650
- [27] Blennow, K. CSF biomarkers for Alzheimer's disease: use in early diagnosis and evaluation of drug treatment. *Expert Rev. Mol. Diagn.*, **2005**, *5*(5), 661-672.
<http://dx.doi.org/10.1586/14737159.5.5.661> PMID: 16149870
- [28] Olsson, B.; Portelius, E.; Cullen, N.C.; Sandelius, Å.; Zetterberg, H.; Andreasson, U.; Höglund, K.; Irwin, D.J.; Grossman, M.; Weintraub, D.; Chen-Plotkin, A.; Wolk, D.; McCluskey, L.; Elman, L.; Shaw, L.M.; Toledo, J.B.; McBride, J.; Hernandez-Con, P.; Lee, V.M.Y.; Trojanowski, J.Q.; Blennow, K. Association of

- cerebrospinal fluid neurofilament light protein levels with cognition in patients with dementia, motor neuron disease, and movement disorders. *JAMA Neurol.*, **2019**, *76*(3), 318-325.
<http://dx.doi.org/10.1001/jamaneurol.2018.3746> PMID: 30508027
- [29] Chaves, M.L.; Camozzato, A.L.; Ferreira, E.D.; Piazenski, I.; Kochhann, R.; Dall'Igna, O.; Mazzini, G.S.; Souza, D.O.; Portela, L.V. Serum levels of S100B and NSE proteins in Alzheimer's disease patients. *J. Neuroinflammation*, **2010**, *7*(1), 6.
<http://dx.doi.org/10.1186/1742-2094-7-6> PMID: 20105309
- [30] Elahi, F.M.; Casaletto, K.B.; La Joie, R. Plasma biomarkers of astrocytic and neuronal dysfunction in early-and late-onset Alzheimer's disease. *Alzheimers Dement.*, **2019**. PMID: 31879236
- [31] Hye, A.; Kerr, F.; Archer, N.; Foy, C.; Poppe, M.; Brown, R.; Hamilton, G.; Powell, J.; Anderton, B.; Lovestone, S. Glycogen synthase kinase-3 is increased in white cells early in Alzheimer's disease. *Neurosci. Lett.*, **2004**, *373*(1), 1-4.
<http://dx.doi.org/10.1016/j.neulet.2004.10.031> PMID: 15555766
- [32] de Barry, J.; Liègeois, C.M.; Janoshazi, A. Protein kinase C as a peripheral biomarker for Alzheimer's disease. *Exp. Gerontol.*, **2010**, *45*(1), 64-69.
<http://dx.doi.org/10.1016/j.exger.2009.10.015> PMID: 19895879
- [33] Llorens, F.; Thüne, K.; Tahir, W.; Kanata, E.; Diaz-Lucena, D.; Xanthopoulos, K.; Kovatsi, E.; Pleschka, C.; Garcia-Esparcia, P.; Schmitz, M.; Ozbay, D.; Correia, S.; Correia, A.; Milosevic, I.; Andréoletti, O.; Fernández-Borges, N.; Vorberg, I.M.; Glatzel, M.; Sklaviadis, T.; Torres, J.M.; Krasemann, S.; Sánchez-Valle, R.; Ferrer, I.; Zerr, I. YKL-40 in the brain and cerebrospinal fluid of neurodegenerative dementias. *Mol. Neurodegener.*, **2017**, *12*(1), 83.
<http://dx.doi.org/10.1186/s13024-017-0226-4> PMID: 29126445
- [34] Kvarnberg, H.; Portelius, E.; Andreasson, U.; Brinkmalm, G.; Hellwig, K.; Lelental, N.; Kornhuber, J.; Hansson, O.; Minthon, L.; Spitzer, P.; Maler, J.M.; Zetterberg, H.; Blennow, K.; Lewczuk, P. Characterization of the postsynaptic protein neurogranin in paired cerebrospinal fluid and plasma samples from Alzheimer's disease patients and healthy controls. *Alzheimers Res. Ther.*, **2015**, *7*(1), 40.
<http://dx.doi.org/10.1186/s13195-015-0124-3> PMID: 26136856
- [35] Wang, G.P.; Khatoon, S.; Iqbal, K.; Grundke-Iqbal, I. Brain ubiquitin is markedly elevated in Alzheimer disease. *Brain Res.*, **1991**, *566*(1-2), 146-151.
[http://dx.doi.org/10.1016/0006-8993\(91\)91692-T](http://dx.doi.org/10.1016/0006-8993(91)91692-T) PMID: 1814531
- [36] Lukens, J.N.; Van Deerlin, V.; Clark, C.M.; Xie, S.X.; Johnson, F.B. Comparisons of telomere lengths in peripheral blood and cerebellum in Alzheimer's disease. *Alzheimers Dement.*, **2009**, *5*(6), 463-469.
<http://dx.doi.org/10.1016/j.jalz.2009.05.666> PMID: 19896585
- [37] Hochstrasser, T.; Weiss, E.; Marksteiner, J.; Humpel, C. Soluble cell adhesion molecules in monocytes of Alzheimer's disease and mild cognitive impairment. *Exp. Gerontol.*, **2010**, *45*(1), 70-74.
<http://dx.doi.org/10.1016/j.exger.2009.10.005> PMID: 19836440
- [38] Clarke, R.; Smith, A.D.; Jobst, K.A.; Refsum, H.; Sutton, L.; Ueland, P.M. Folate, vitamin B12, and serum total homocysteine levels in confirmed Alzheimer disease. *Arch. Neurol.*, **1998**, *55*(11), 1449-1455.
<http://dx.doi.org/10.1001/archneur.55.11.1449> PMID: 9823829
- [39] Hansson, O.; Blennow, K.; Zetterberg, H.; Dage, J. Blood biomarkers for Alzheimer's disease in clinical practice and trials. *Nature Aging*, **2023**, *3*(5), 506-519.
<http://dx.doi.org/10.1038/s43587-023-00403-3> PMID: 37202517
- [40] Hansson, O.; Edelmayer, R.M.; Boxer, A.L.; Carrillo, M.C.; Mielke, M.M.; Rabinovici, G.D.; Salloway, S.; Sperling, R.; Zetterberg, H.; Teunissen, C.E. The Alzheimer's Association appropriate use recommendations for blood biomarkers in Alzheimer's disease. *Alzheimers Dement.*, **2022**, *18*(12), 2669-2686.
<http://dx.doi.org/10.1002/alz.12756> PMID: 35908251
- [41] Garcia-Escobar, G.; Manero, R.M.; Fernández-Lebrero, A.; Ois, A.; Navalpotro-Gómez, I.; Puente-Periz, V.; Contador-Muñana, J.; Estragués-Gazquez, I.; Puig-Pijoan, A.; Jiménez-Balado, J. Blood biomarkers of Alzheimer's disease and cognition: a literature review. *Biomolecules*, **2024**, *14*(1), 93.
<http://dx.doi.org/10.3390/biom14010093> PMID: 38254693
- [42] Smirnov, D.S.; Ashton, N.J.; Blennow, K.; Zetterberg, H.; Simrén, J.; Lantero-Rodriguez, J.; Karikari, T.K.; Hiniker, A.; Rissman, R.A.; Salmon, D.P.; Galasko, D. Plasma biomarkers for Alzheimer's Disease in relation to neuropathology and cognitive change. *Acta Neuropathol.*, **2022**, *143*(4), 487-503.
<http://dx.doi.org/10.1007/s00401-022-02408-5> PMID: 35195758
- [43] Johansson, C.; Thordardottir, S.; Laffita-Mesa, J.; Rodriguez-Vieitez, E.; Zetterberg, H.; Blennow, K.; Graff, C. Plasma biomarker profiles in autosomal dominant Alzheimer's disease. *Brain*, **2023**, *146*(3), 1132-1140.
<http://dx.doi.org/10.1093/brain/awac399> PMID: 36626935
- [44] Álvarez-Sánchez, L.; Peña-Bautista, C.; Ferré-González, L.; Cubas, L.; Balaguer, A.; Casanova-Estruch, B.; Baquero, M.; Cháfer-Pericás, C. Early Alzheimer's disease screening approach using plasma biomarkers. *Int. J. Mol. Sci.*, **2023**, *24*(18), 14151.
<http://dx.doi.org/10.3390/ijms241814151> PMID: 37762457
- [45] Doecke, J.D.; Laws, S.M.; Faux, N.G.; Wilson, W.; Burnham, S.C.; Lam, C.P.; Mondal, A.; Bedo, J.; Bush, A.I.; Brown, B.; De Ruyck, K.; Ellis, K.A.; Fowler, C.; Gupta, V.B.; Head, R.; Macaulay, S.L.; Pertile, K.; Rowe, C.C.; Remback, A.; Rodrigues, M.; Rumble, R.; Szoek, C.; Taddei, K.; Taddei, T.; Trounson, B.; Ames, D.; Masters, C.L.; Martins, R.N. Alzheimer's Disease Neuroimaging Initiative; Australian Imaging Biomarker and Lifestyle Research Group. Blood-based protein biomarkers for diagnosis of Alzheimer disease. *Arch. Neurol.*, **2012**, *69*(10), 1318-1325.
<http://dx.doi.org/10.1001/archneurol.2012.1282> PMID: 22801742
- [46] Palmqvist, S.; Janelidze, S.; Stomrud, E.; Zetterberg, H.; Karl, J.; Zink, K.; Bittner, T.; Mattsson, N.; Eichenlaub, U.; Blennow, K.; Hansson, O. Performance of fully automated plasma assays as screening tests for Alzheimer disease-related β -amyloid status. *JAMA Neurol.*, **2019**, *76*(9), 1060-1069.
<http://dx.doi.org/10.1001/jamaneurol.2019.1632> PMID: 31233127
- [47] Li, Y.; Schindler, S.E.; Bollinger, J.G.; Ovod, V.; Mawuenyega, K.G.; Weiner, M.W.; Shaw, L.M.; Masters, C.L.; Fowler, C.J.; Trojanowski, J.Q.; Korecka, M.; Martins, R.N.; Janelidze, S.; Hansson, O.; Bateman, R.J. Validation of plasma amyloid- β 42/40 for detecting Alzheimer disease amyloid plaques. *Neurology*, **2022**, *98*(7), e688-e699.
<http://dx.doi.org/10.1212/WNL.0000000000013211> PMID: 34906975
- [48] Lantero Rodriguez, J.; Karikari, T.K.; Suárez-Calvet, M.; Troakes, C.; King, A.; Emersic, A.; Aarsland, D.; Hye, A.; Zetterberg, H.; Blennow, K.; Ashton, N.J. Plasma p-tau181 accurately predicts Alzheimer's disease pathology at least 8 years prior to post-mortem and improves the clinical characterisation of cognitive decline. *Acta Neuropathol.*, **2020**, *140*(3), 267-278.
<http://dx.doi.org/10.1007/s00401-020-02195-x> PMID: 32720099
- [49] Ashton, N.J.; Pascoal, T.A.; Karikari, T.K.; Benedet, A.L.; Lantero-Rodriguez, J.; Brinkmalm, G.; Snellman, A.; Schöll, M.; Troakes, C.; Hye, A.; Gauthier, S.; Vanmechelen, E.; Zetterberg, H.; Rosa-Neto, P.; Blennow, K. Plasma p-tau231: a new biomarker for incipient Alzheimer's disease pathology. *Acta Neuropathol.*, **2021**, *141*(5), 709-724.
<http://dx.doi.org/10.1007/s00401-021-02275-6> PMID: 33585983
- [50] Sato, C.; Barthélemy, N.R.; Mawuenyega, K.G.; Patterson, B.W.; Gordon, B.A.; Jockel-Balsarotti, J.; Sullivan, M.; Crisp, M.J.; Kasten, T.; Kirmess, K.M.; Kanaan, N.M.; Yarasheski, K.E.; Baker-Nigh, A.; Benzinger, T.L.S.; Miller, T.M.; Karch, C.M.; Bateman, R.J. Tau kinetics in neurons and the human central nervous system. *Neuron*, **2018**, *97*(6), 1284-1298.e7.
<http://dx.doi.org/10.1016/j.neuron.2018.02.015> PMID: 29566794
- [51] Mattsson-Carlsson, N.; Janelidze, S.; Bateman, R.J.; Smith, R.; Stomrud, E.; Serrano, G.E.; Reiman, E.M.; Palmqvist, S.; Dage, J.L.; Beach, T.G.; Hansson, O. Soluble P-tau217 reflects amyloid and tau pathology and mediates the association of amyloid with tau. *EMBO Mol. Med.*, **2021**, *13*(6), e14022.
<http://dx.doi.org/10.15252/emmm.202114022> PMID: 33949133
- [52] Theriault, J.; Vermeiren, M.; Servaes, S.; Tissot, C.; Ashton, N.J.; Benedet, A.L.; Karikari, T.K.; Lantero-Rodriguez, J.; Brum, W.S.; Lussier, F.Z.; Bezgin, G.; Stevenson, J.; Rahmouni, N.; Kunach, P.; Wang, Y.T.; Fernandez-Arias, J.; Soculaya, K.Q.; Macedo, A.C.; Ferrari-Souza, J.P.; Ferreira, P.C.L.; Bellaver, B.; Leffa, D.T.; Zimmer, E.R.; Vitali, P.; Soucy, J.P.; Triana-Baltzer, G.;

- Kolb, H.C.; Pascoal, T.A.; Saha-Chaudhuri, P.; Gauthier, S.; Zetterberg, H.; Blennow, K.; Rosa-Neto, P. Association of phosphorylated tau biomarkers with amyloid positron emission tomography vs. tau positron emission tomography. *JAMA Neurol.*, **2023**, *80*(2), 188-199.
<http://dx.doi.org/10.1001/jamaneurol.2022.4485> PMID: 36508198
- [53] Ashton, N.J.; Brum, W.S.; Di Molfetta, G.; Benedet, A.L.; Arslan, B.; Jonaitis, E.; Langhough, R.E.; Cody, K.; Wilson, R.; Carlsson, C.M.; Vanmechelen, E.; Montoliu-Gaya, L.; Lantero-Rodriguez, J.; Rahmouni, N.; Tissot, C.; Stevenson, J.; Servaes, S.; Therriault, J.; Pascoal, T.; Lleó, A.; Alcolea, D.; Fortea, J.; Rosa-Neto, P.; Johnson, S.; Jeromin, A.; Blennow, K.; Zetterberg, H. Diagnostic Accuracy of a Plasma Phosphorylated Tau 217 Immunoassay for Alzheimer Disease Pathology. *JAMA Neurol.*, **2024**, *81*(3), 255-263.
<http://dx.doi.org/10.1001/jamaneurol.2023.5319> PMID: 38252443
- [54] Ferreira, P.C.L.; Therriault, J.; Tissot, C.; Ferrari-Souza, J.P.; Benedet, A.L.; Povala, G.; Bellaver, B.; Leffa, D.T.; Brum, W.S.; Lussier, F.Z.; Bezgin, G.; Servaes, S.; Vermeiren, M.; Macedo, A.C.; Cabrera, A.; Stevenson, J.; Triana-Baltzer, G.; Kolb, H.; Rahmouni, N.; Klunk, W.E.; Lopez, O.L.; Villemagne, V.L.; Cohen, A.; Tudorascu, D.L.; Zimmer, E.R.; Karikari, T.K.; Ashton, N.J.; Zetterberg, H.; Blennow, K.; Gauthier, S.; Rosa-Neto, P.; Pascoal, T.A. Plasma p-tau231 and p-tau217 inform on tau tangles aggregation in cognitively impaired individuals. *Alzheimers Dement.*, **2023**, *19*(10), 4463-4474.
<http://dx.doi.org/10.1002/alz.13393> PMID: 37534889
- [55] Salvadó, G.; Ossenkoppele, R.; Ashton, N.J.; Beach, T.G.; Serano, G.E.; Reiman, E.M.; Zetterberg, H.; Mattsson-Carlsson, N.; Janelidze, S.; Blennow, K.; Hansson, O. Specific associations between plasma biomarkers and postmortem amyloid plaque and tau tangle loads. *EMBO Mol. Med.*, **2023**, *15*(5), e17123.
<http://dx.doi.org/10.15252/emmm.202217123> PMID: 36912178
- [56] Lantero-Rodriguez, J.; Tissot, C.; Snellman, A.; Servaes, S.; Benedet, A.L.; Rahmouni, N.; Montoliu-Gaya, L.; Therriault, J.; Brum, W.S.; Stevenson, J.; Lussier, F.Z.; Bezgin, G.; Macedo, A.C.; Chamoun, M.; Mathotaarachi, S.S.; Pascoal, T.A.; Ashton, N.J.; Zetterberg, H.; Neto, P.R.; Blennow, K. Plasma and CSF concentrations of N-terminal tau fragments associate with *in vivo* neurofibrillary tangle burden. *Alzheimers Dement.*, **2023**, *19*(12), 5343-5354.
<http://dx.doi.org/10.1002/alz.13119> PMID: 37190913
- [57] Vrillon, A.; Ashton, N.J.; Karikari, T.K.; Götze, K.; Cognat, E.; Dumurgier, J.; Lilamand, M.; Zetterberg, H.; Blennow, K.; Paquet, C. Comparison of CSF and plasma NfL and pNfH for Alzheimer's disease diagnosis: a memory clinic study. *J. Neurol.*, **2023**, 1-4.
 PMID: 37950758
- [58] Arslan, B.; Zetterberg, H.; Ashton, N.J. Blood-based biomarkers in Alzheimer's disease—moving towards a new era of diagnostics. *Clin. Chem. Labora. Med. (CCLM)*, **2024**.
<http://dx.doi.org/10.1515/cclm-2023-1434>
- [59] Lehmann, S.; Schraen-Maschke, S.; Vidal, J.S.; Blanc, F.; Paquet, C.; Allinquant, B.; Bombois, S.; Gabelle, A.; Delaby, C.; Hanon, O. BALTAZAR Study Group. Blood neurofilament levels predict cognitive decline across the Alzheimer's disease continuum. *Int. J. Mol. Sci.*, **2023**, *24*(24), 17361.
<http://dx.doi.org/10.3390/ijms242417361> PMID: 38139190
- [60] Pereira, J.B.; Janelidze, S.; Smith, R.; Mattsson-Carlsson, N.; Palmqvist, S.; Teunissen, C.E.; Zetterberg, H.; Stomrud, E.; Ashton, N.J.; Blennow, K.; Hansson, O. Plasma GFAP is an early marker of amyloid- β but not tau pathology in Alzheimer's disease. *Brain*, **2021**, *144*(11), 3505-3516.
<http://dx.doi.org/10.1093/brain/awab223> PMID: 34259835
- [61] Cicognola, C.; Janelidze, S.; Hertz, J.; Zetterberg, H.; Blennow, K.; Mattsson-Carlsson, N.; Hansson, O. Plasma glial fibrillary acidic protein detects Alzheimer pathology and predicts future conversion to Alzheimer dementia in patients with mild cognitive impairment. *Alzheimers Res. Ther.*, **2021**, *13*(1), 68.
<http://dx.doi.org/10.1186/s13195-021-00804-9> PMID: 33773595
- [62] Zheng, X.; Yang, J.; Hou, Y.; Shi, X.; Liu, K. Prediction of clinical progression in nervous system diseases: plasma glial fibrillary acidic protein (GFAP). *Eur. J. Med. Res.*, **2024**, *29*(1), 51.
<http://dx.doi.org/10.1186/s40001-023-01631-4> PMID: 38216970
- [63] Fang, T.; Dai, Y.; Hu, X.; Xu, Y.; Qiao, J. Evaluation of serum neurofilament light chain and glial fibrillary acidic protein in the diagnosis of Alzheimer's disease. *Front. Neurol.*, **2024**, *15*, 1320653.
<http://dx.doi.org/10.3389/fneur.2024.1320653> PMID: 38352136
- [64] Schindler, S.E.; Atri, A. The role of cerebrospinal fluid and other biomarker modalities in the Alzheimer's disease diagnostic revolution. *Nature Aging*, **2023**, *3*(5), 460-462.
<http://dx.doi.org/10.1038/s43587-023-00400-6> PMID: 37202514
- [65] Watson, C.M.; Dammer, E.B.; Ping, L.; Duong, D.M.; Modeste, E.; Carter, E.K.; Johnson, E.C.B.; Levey, A.I.; Lah, J.J.; Roberts, B.R.; Seyfried, N.T. Quantitative mass spectrometry analysis of cerebrospinal fluid protein biomarkers in Alzheimer's disease. *Sci. Data*, **2023**, *10*(1), 261.
<http://dx.doi.org/10.1038/s41597-023-02158-3> PMID: 37160957
- [66] Li, Y.; Chen, Z.; Wang, Q.; Lv, X.; Cheng, Z.; Wu, Y.; Tang, F.; Shen, Y.; Gao, F. Identification of hub proteins in cerebrospinal fluid as potential biomarkers of Alzheimer's disease by integrated bioinformatics. *J. Neurol.*, **2023**, *270*(3), 1487-1500.
<http://dx.doi.org/10.1007/s00415-022-11476-2> PMID: 36396814
- [67] Rocha, NP.; Teixeira, AL.; de Souza, LC. Fluid-Based Biomarkers of Alzheimer's Disease. In: *Biomarkers in Neuropsychiatry: A Primer*; Springer International Publishing: Cham, **2023**; pp. 153-161.
http://dx.doi.org/10.1007/978-3-031-43356-6_10
- [68] McGettigan, S.; Nolan, Y.; Ghosh, S.; O'Mahony, D. The emerging role of blood biomarkers in diagnosis and treatment of Alzheimer's disease. *Eur. Geriatr. Med.*, **2023**, *14*(5), 913-917.
<http://dx.doi.org/10.1007/s41999-023-00847-1> PMID: 37648817
- [69] Gao, P.Y.; Ou, Y.N.; Huang, Y.M.; Wang, Z.B.; Fu, Y.; Ma, Y.H.; Li, Q.Y.; Ma, L.Y.; Cui, R.P.; Mi, Y.C.; Tan, L.; Yu, J.T. Associations between liver function and cerebrospinal fluid biomarkers of Alzheimer's disease pathology in non-demented adults: The CABLE study. *J. Neurochem.*, **2024**, *168*(1), 39-51.
<http://dx.doi.org/10.1111/jnc.16025> PMID: 38055867
- [70] Trombetta, B.A.; Wu, C.Y.; Kuo, E.; de Geus, M.B.; Dodge, H.H.; Carlyle, B.C.; Kivisäkk, P.; Arnold, S.E. Cerebrospinal fluid biomarker profiling of diverse pathophysiological domains in Alzheimer's disease. *Alzheimers Dement.*, **2024**, *10*(1), e12440.
<http://dx.doi.org/10.1002/trc2.12440> PMID: 38356471
- [71] Mravinacová, S.; Alanko, V.; Bergström, S.; Bridel, C.; Pijnenburg, Y.; Hagman, G.; Kivipelto, M.; Teunissen, C.; Nilsson, P.; Matton, A.; Månberg, A. CSF protein ratios with enhanced potential to reflect Alzheimer's disease pathology and neurodegeneration. *Mol. Neurodegener.*, **2024**, *19*(1), 15.
<http://dx.doi.org/10.1186/s13024-024-00705-z> PMID: 38350954
- [72] Tao, Q.Q.; Cai, X.; Xue, Y.Y.; Ge, W.; Yue, L.; Li, X.Y.; Lin, R.R.; Peng, G.P.; Jiang, W.; Li, S.; Zheng, K.M.; Jiang, B.; Jia, J.P.; Guo, T.; Wu, Z.Y. Alzheimer's disease early diagnostic and staging biomarkers revealed by large-scale cerebrospinal fluid and serum proteomic profiling. *Innovation*, **2024**, *5*(1), 100544.
<http://dx.doi.org/10.1016/j.xinn.2023.100544> PMID: 38235188
- [73] Dakterzada, F.; Jové, M.; Huerto, R.; Carnes, A.; Sol, J.; Pamploña, R.; Piñol-Ripoll, G. Cerebrospinal fluid neutral lipids predict progression from mild cognitive impairment to Alzheimer's disease. *Geroscience*, **2023**, *46*(1), 683-696.
<http://dx.doi.org/10.1007/s11357-023-00989-x> PMID: 37999901
- [74] Bateman, R.J.; Xiong, C.; Benzinger, T.L.S.; Fagan, A.M.; Goate, A.; Fox, N.C.; Marcus, D.S.; Cairns, N.J.; Xie, X.; Blazey, T.M.; Holtzman, D.M.; Santacruz, A.; Buckles, V.; Oliver, A.; Moulder, K.; Aisen, P.S.; Ghetti, B.; Klunk, W.E.; McDade, E.; Martins, R.N.; Masters, C.L.; Mayeux, R.; Ringman, J.M.; Rossor, M.N.; Schofield, P.R.; Sperling, R.A.; Salloway, S.; Morris, J.C. Dominantly Inherited Alzheimer Network. Clinical and biomarker changes in dominantly inherited Alzheimer's disease. *N. Engl. J. Med.*, **2012**, *367*(9), 795-804.
<http://dx.doi.org/10.1056/NEJMoa1202753> PMID: 22784036
- [75] Mattsson, N.; Zetterberg, H.; Hansson, O.; Andreasen, N.; Parnetti, L.; Jonsson, M.; Herukka, S.K.; van der Flier, W.M.; Blankenstein, M.A.; Ewers, M.; Rich, K.; Kaiser, E.; Verbeek, M.; Tsolaki, M.; Mulugeta, E.; Rosén, E.; Aarsland, D.; Visser, P.J.; Schröder, J.; Marcusson, J.; de Leon, M.; Hampel, H.; Scheltens,

- P.; Pirttilä, T.; Wallin, A.; Jönhagen, M.E.; Minthon, L.; Winblad, B.; Blennow, K. CSF biomarkers and incipient Alzheimer disease in patients with mild cognitive impairment. *JAMA*, **2009**, *302*(4), 385-393.
<http://dx.doi.org/10.1001/jama.2009.1064> PMID: 19622817
- [76] Shaw, L.M.; Vanderstichele, H.; Knapik-Czajka, M.; Clark, C.M.; Aisen, P.S.; Petersen, R.C.; Blennow, K.; Soares, H.; Simon, A.; Lewczuk, P.; Dean, R.; Siemers, E.; Potter, W.; Lee, V.M.Y.; Trojanowski, J.Q. Alzheimer's Disease Neuroimaging Initiative. Cerebrospinal fluid biomarker signature in Alzheimer's disease neuroimaging initiative subjects. *Ann. Neurol.*, **2009**, *65*(4), 403-413.
<http://dx.doi.org/10.1002/ana.21610> PMID: 19296504
- [77] Hansson, O.; Zetterberg, H.; Buchhave, P.; Londos, E.; Blennow, K.; Minthon, L. Association between CSF biomarkers and incipient Alzheimer's disease in patients with mild cognitive impairment: a follow-up study. *Lancet Neurol.*, **2006**, *5*(3), 228-234.
[http://dx.doi.org/10.1016/S1474-4422\(06\)70355-6](http://dx.doi.org/10.1016/S1474-4422(06)70355-6) PMID: 16488378
- [78] Papaliagkas, V.; Kalinderi, K.; Varelzits, P.; Moraitou, D.; Pampitsou, T.; Chatzidimitriou, M. CSF Biomarkers in the Early Diagnosis of Mild Cognitive Impairment and Alzheimer's Disease. *Int. J. Mol. Sci.*, **2023**, *24*(10), 8976.
<http://dx.doi.org/10.3390/ijms24108976> PMID: 37240322
- [79] Alexopoulos, P.; Werle, L.; Roesler, J.; Thierjung, N.; Gleixner, L.S.; Yakushev, I.; Laskaris, N.; Wagenpfeil, S.; Gourzis, P.; Kurz, A.; Perneczky, R. Alzheimer's Disease Neuroimaging Initiative (ADNI). Conflicting cerebrospinal fluid biomarkers and progression to dementia due to Alzheimer's disease. *Alzheimers Res. Ther.*, **2016**, *8*(1), 51.
<http://dx.doi.org/10.1186/s13195-016-0220-z> PMID: 27931251
- [80] Algeciras-Schimmich, A.; Bornhorst, J.A. Importance of cerebrospinal fluid (CSF) collection protocol for the accurate diagnosis of Alzheimer's disease when using CSF biomarkers. *Alzheimers Dement.*, **2024**, *alz.13721*.
<http://dx.doi.org/10.1002/alz.13721> PMID: 38288880
- [81] Humpel, C. Identifying and validating biomarkers for Alzheimer's disease. *Trends Biotechnol.*, **2011**, *29*(1), 26-32.
<http://dx.doi.org/10.1016/j.tibtech.2010.09.007> PMID: 20971518
- [82] Hölttä, M.; Hansson, O.; Andreasson, U.; Hertz, J.; Minthon, L.; Nägga, K.; Andreasen, N.; Zetterberg, H.; Blennow, K. Evaluating amyloid- β oligomers in cerebrospinal fluid as a biomarker for Alzheimer's disease. *PLoS One*, **2013**, *8*(6), e66381.
<http://dx.doi.org/10.1371/journal.pone.0066381> PMID: 23799095
- [83] Guillén, N.; Contador, J.; Buongiorno, M.; Álvarez, I.; Culell, N.; Alcolea, D.; Lleó, A.; Fortea, J.; Piñol-Ripoll, G.; Carnes-Vendrell, A.; Lourdes Ispuerto, M.; Vilas, D.; Puig-Pijoan, A.; Fernández-Lebrero, A.; Balasa, M.; Sánchez-Valle, R.; Lladó, A. Agreement of cerebrospinal fluid biomarkers and amyloid-PET in a multicenter study. *Eur. Arch. Psychiatry Clin. Neurosci.*, **2023**, *1-0*.
<http://dx.doi.org/10.1007/s00406-023-01701-y> PMID: 37898567
- [84] Souza, I.D.; Anderson, J.L.; Tumas, V.; Queiroz, M.E.C. Direct coupling of fiber-in-tube solid-phase microextraction with tandem mass spectrometry to determine amyloid beta peptides as biomarkers for Alzheimer's disease in cerebrospinal fluid samples. *Talanta*, **2023**, *254*, 124186.
<http://dx.doi.org/10.1016/j.talanta.2022.124186> PMID: 36521326
- [85] Athaide Rocha, K.M.; Machado, F.R.; Poetini, M.; Giacomeli, R.; Boeira, S.P.; Jesse, C.R.; Gomes de Gomes, M. Assessment of suberoylanilide hydroxamic acid on a Alzheimer's disease model induced by β -amyloid₍₁₋₄₂₎ in aged female mice: Neuromodulatory and epigenetic effect. *Chem. Biol. Interact.*, **2023**, *375*, 110429.
<http://dx.doi.org/10.1016/j.cbi.2023.110429> PMID: 36870467
- [86] Beyer, L.; Stocker, H.; Rujescu, D.; Holleczek, B.; Stockmann, J.; Nabers, A.; Brenner, H.; Gerwert, K. Amyloid-beta misfolding and GFAP predict risk of clinical Alzheimer's disease diagnosis within 17 years. *Alzheimers Dement.*, **2023**, *19*(3), 1020-1028.
<http://dx.doi.org/10.1002/alz.12745> PMID: 35852967
- [87] Relini, A.; Marano, N.; Gliozzi, A. Misfolding of amyloidogenic proteins and their interactions with membranes. *Biomolecules*, **2013**, *4*(1), 20-55.
<http://dx.doi.org/10.3390/biom4010020> PMID: 24970204
- [88] An, J.; Kim, K.; Lim, H.J.; Kim, H.Y.; Shin, J.; Park, I.; Cho, I.; Kim, H.Y.; Kim, S.; McLean, C.; Choi, K.Y.; Kim, Y.; Lee, K.H.; Kim, J.S. Early onset diagnosis in Alzheimer's disease patients via amyloid- β oligomers-sensing probe in cerebrospinal fluid. *Nat. Commun.*, **2024**, *15*(1), 1004.
<http://dx.doi.org/10.1038/s41467-024-44818-x> PMID: 38307843
- [89] Sharma, A.; Angnes, L.; Sattarahmady, N.; Negahdary, M.; Heli, H. Electrochemical immunosensors developed for amyloid-beta and Tau proteins, leading biomarkers of Alzheimer's disease. *Biosensors*, **2023**, *13*(7), 742.
<http://dx.doi.org/10.3390/bios13070742> PMID: 37504140
- [90] Li, Z.; Fan, Z.; Zhang, Q. The Associations of Phosphorylated Tau 181 and Tau 231 Levels in Plasma and Cerebrospinal Fluid with Cognitive Function in Alzheimer's Disease: A Systematic Review and Meta-Analysis. *J. Alzheimer's Disease*, **2024**, *1-20*.
- [91] Hampel, H.; Blennow, K. CSF tau and β -amyloid as biomarkers for mild cognitive impairment. *Dialogues Clin. Neurosci.*, **2004**, *6*(4), 379-390.
<http://dx.doi.org/10.31887/DCNS.2004.6.4/hhampel> PMID: 22034251
- [92] Blennow, K.; Zetterberg, H. Biomarkers for Alzheimer's disease: current status and prospects for the future. *J. Intern. Med.*, **2018**, *284*(6), 643-663.
<http://dx.doi.org/10.1111/joim.12816> PMID: 30051512
- [93] Gonzalez-Ortiz, F.; Turtton, M.; Kac, P.R.; Smirnov, D.; Premi, E.; Ghidoni, R.; Benussi, L.; Cantoni, V.; Saraceno, C.; Rivolta, J.; Ashton, N.J.; Borroni, B.; Galasko, D.; Harrison, P.; Zetterberg, H.; Blennow, K.; Karikari, T.K. Brain-derived tau: a novel blood-based biomarker for Alzheimer's disease-type neurodegeneration. *Brain*, **2023**, *146*(3), 1152-1165.
<http://dx.doi.org/10.1093/brain/awac407> PMID: 36572122
- [94] Dang, M.; Chen, Q.; Zhao, X.; Chen, K.; Li, X.; Zhang, J.; Lu, J.; Ai, L.; Chen, Y.; Zhang, Z. Tau as a biomarker of cognitive impairment and neuropsychiatric symptom in Alzheimer's disease. *Hum. Brain Mapp.*, **2023**, *44*(2), 327-340.
<http://dx.doi.org/10.1002/hbm.26043> PMID: 36647262
- [95] Lantero-Rodriguez, J.; Montoliu-Gaya, L.; Benedit, A.L.; Vrillon, A.; Dumurgier, J.; Cognat, E.; Brum, W.S.; Rahmouni, N.; Stevenson, J.; Servaes, S.; Therriault, J.; Becker, B.; Brinkmalm, G.; Snellman, A.; Huber, H.; Kvarnstrom, H.; Ashton, N.J.; Zetterberg, H.; Paquet, C.; Rosa-Neto, P.; Blennow, K. CSF p-tau205: a biomarker of tau pathology in Alzheimer's disease. *Acta Neuropathol.*, **2024**, *147*(1), 12.
<http://dx.doi.org/10.1007/s00401-023-02659-w> PMID: 38184490
- [96] Braak, H.; Del Tredici, K. The pathological process underlying Alzheimer's disease in individuals under thirty. *Acta Neuropathol.*, **2011**, *121*(2), 171-181.
<http://dx.doi.org/10.1007/s00401-010-0789-4> PMID: 21170538
- [97] Hasegawa, M. Molecular mechanisms in the pathogenesis of Alzheimer's disease and tauopathies-prion-like seeded aggregation and phosphorylation. *Biomolecules*, **2016**, *6*(2), 24.
<http://dx.doi.org/10.3390/biom6020024> PMID: 27136595
- [98] Medina, M.; Hernández, F.; Avila, J. New features about tau function and dysfunction. *Biomolecules*, **2016**, *6*(2), 21.
<http://dx.doi.org/10.3390/biom6020021> PMID: 27104579
- [99] Bukar Maina, M.; Al-Hilaly, Y.; Serpell, L.; Bukar Maina, M.; Al-Hilaly, Y.K.; Serpell, L.C. Nuclear tau and its potential role in Alzheimer's disease. *Biomolecules*, **2016**, *6*(1), 9.
<http://dx.doi.org/10.3390/biom6010009> PMID: 26751496
- [100] Harada, R.; Okamura, N.; Furumoto, S.; Tago, T.; Yanai, K.; Arai, H.; Kudo, Y. Characteristics of tau and its ligands in PET imaging. *Biomolecules*, **2016**, *6*(1), 7.
<http://dx.doi.org/10.3390/biom6010007> PMID: 26751494
- [101] Šimić, G.; Babić Leko, M.; Wray, S.; Harrington, C.; Delalle, I.; Jovanov-Milošević, N.; Bažadona, D.; Buée, L.; de Silva, R.; Di Giovanni, G.; Wischik, C.; Hof, P. Tau protein hyperphosphorylation and aggregation in Alzheimer's disease and other tauopathies, and possible neuroprotective strategies. *Biomolecules*, **2016**, *6*(1), 6.
<http://dx.doi.org/10.3390/biom6010006> PMID: 26751493
- [102] Preische, O.; Schultz, S.A.; Apel, A.; Kuhle, J.; Kaeser, S.A.; Barro, C.; Gräber, S.; Kuder-Buletta, E.; LaFougere, C.; Laske, C.; Vöglein, J. Serum neurofilament dynamics predicts neurodegeneration and clinical progression in presymptomatic Alzheimer's disease. *Nature Medicine*, **2016**, *25*(2), 277-283.

- <http://dx.doi.org/10.1212/WNL.0000000000003246> PMID: 27694257
- [103] Preische, O.; Schultz, S.A.; Apel, A.; Kuhle, J.; Kaeser, S.A.; Barro, C.; Gräber, S.; Kuder-Buletta, E.; LaFougere, C.; Laske, C.; Vöglein, J.; Levin, J.; Masters, C.L.; Martins, R.; Schofield, P.R.; Rossor, M.N.; Graff-Radford, N.R.; Salloway, S.; Ghetti, B.; Ringman, J.M.; Noble, J.M.; Chhatwal, J.; Goate, A.M.; Benzinger, T.L.S.; Morris, J.C.; Bateman, R.J.; Wang, G.; Fagan, A.M.; McDade, E.M.; Gordon, B.A.; Jucker, M. Dominantly Inherited Alzheimer Network. Serum neurofilament dynamics predicts neurodegeneration and clinical progression in presymptomatic Alzheimer's disease. *Nat. Med.*, **2019**, *25*(2), 277-283. <http://dx.doi.org/10.1038/s41591-018-0304-3> PMID: 30664784
- [104] Leitão, M.J.; Baldeiras, I.; Herukka, S.K. Phosphorylated tau/amyloid beta 1-42 ratio in ventricular cerebrospinal fluid reflects outcome in idiopathic normal pressure hydrocephalus. *Fluids Barriers CNS*, **2015**, *12*(1), 1-11.
- [105] Mitra, J.; Guerrero, E.; Hegde, P.; Wang, H.; Boldogh, I.; Rao, K.; Mitra, S.; Hegde, M. New perspectives on oxidized genome damage and repair inhibition by pro-oxidant metals in neurological diseases. *Biomolecules*, **2014**, *4*(3), 678-703. <http://dx.doi.org/10.3390/biom4030678> PMID: 25036887
- [106] Hane, F.; Leonenko, Z. Effect of metals on kinetic pathways of amyloid- β aggregation. *Biomolecules*, **2014**, *4*(1), 101-116. <http://dx.doi.org/10.3390/biom4010101> PMID: 24970207
- [107] Olkkonen, V.M.; Béaslas, O.; Nissilä, E. Oxysterols and their cellular effectors. *Biomolecules*, **2012**, *2*(1), 76-103. <http://dx.doi.org/10.3390/biom2010076> PMID: 24970128
- [108] Hroudová, J.; Singh, N.; Fišar, Z. Mitochondrial dysfunctions in neurodegenerative diseases: relevance to Alzheimer's disease. *BioMed Res. Int.*, **2014**, *2014*, 1-9. <http://dx.doi.org/10.1155/2014/175062> PMID: 24900954
- [109] Mansour, Y.; Blackburn, K.; González-González, L.O.; Calderon-Garciduenas, L.; Kulesza, R.J. Auditory brainstem dysfunction, non-invasive biomarkers for early diagnosis and monitoring of Alzheimer's disease in young urban residents exposed to air pollution. *Am. J. Alzheimer's Dis.*, **2019**, 1-9.

DISCLAIMER: The above article has been published, as is, ahead-of-print, to provide early visibility but is not the final version. Major publication processes like copyediting, proofing, typesetting and further review are still to be done and may lead to changes in the final published version, if it is eventually published. All legal disclaimers that apply to the final published article also apply to this ahead-of-print version.

Extraction, Characterisation, Biological Properties and Applications of Essential Oils: A Review

Nikita Raghuvanshi^{a,b}, Bhanushree Gupta^a

^aCenter for Basic Sciences, Pt. Ravishankar Shukla University, Raipur, India-492010

^bSchool of Studies in Chemistry, Pt. Ravishankar Shukla University, Raipur, India-492010

*Corresponding Author: bgupta1517@gmail.com

Abstract

In recent decades, essential oils have emerged as natural supplements to synthetic substances in medicine, agriculture, food industries etc. The modern techniques for extraction of essential oils have significantly reduced the time consumption and increased the yield in comparison to the conventional techniques that have been in use for so long. Advanced characterisation techniques like Gas chromatography (GC), Liquid Chromatography (LC), Mass Spectrometry (MS) etc., provide high accuracy in characterisation depending upon the nature of essential oils or other major phytoconstituents. Studies have shown essential oils to possess biologically significant activities like antibacterial, antifungal, anti-inflammatory, antioxidant, antihistamine, anticholinesterase, anti-cancer, antiaging etc. These activities of essential oils have made them eligible for their application in food preservation, medicines, industries, agriculture etc. Thus, the traditional knowledge of plants and extraction of essential oils from their different parts of significance can contribute to a healthy society if efforts are made towards enhancing their natural properties for maximum utilisation. The present review discusses different sources and compositions of essential oils, common extraction and characterisation techniques, some biological properties of essential oils and their applications in various industries.

Keywords: Essential oils, Mass spectrometry, antifungal, anticholinesterase, phytoconstituents.

1. Introduction

Essential oils are volatile odorous oils extracted from various parts (leaves, bark, roots, etc.) of plants. The essential oils extracted from different aromatic plants (like spices or medicinal plants) differ in their odour and flavour owing to the variety in the type and amount of constituents present in them. Some common plants and their parts used for essential oil extraction along with their major chemical constituent(s) are listed in Table 1. The organoleptic compounds, responsible for the aroma and flavour are present at varied concentrations in different parts of the plant depending on the part of the plant chosen for extraction and also on some growth parameters like climate and soil characteristics. Their molecular weights are usually less than 300 and they have some characteristic properties in common. These properties are optical activity, high refractive index, immiscibility with water, sufficient solubility to impart aroma to water, and solubility in most organic solvents such as alcohol and ether. Several methods can be utilized for the extraction of essential oils e.g., effleurage, expression, hydro distillation, steam distillation etc. However, steam distillation is the most used technique for commercial-scale production in related industries. Essential oils are considered secondary metabolites functional in plant defence against microbes (Tajkarimi et al., 2010). The essential oils and their phytoconstituents that have been investigated are known to possess several biological properties including antioxidant (Tit & Bungau, 2023), antimicrobial (Garzoli, 2023), antiparasitic (AlGabbani et al., 2023),

antimutagenic(Rasgele & Altin, 2023), anticancer(Sharma et al., 2022a), anti-inflammatory (Zhao et al., 2023), anti-ageing s(Raina et al., 2023), anticholinesterase(Raina et al., 2023)etc.

Table 1. List of common plants and their parts with major component(s) of essential oil

Common name	Scientific name	Part of plant	Major compound(s)	References
Basil	<i>Ocimum basilicum L</i>	Flowers, leaves, stem	Linalool, estragole, eugenol, methyl chavicol	(da Silva et al., 2021)
Turmeric	<i>Curcuma longa L</i>	Leaves, rhizomes	Turmerone, phellandrene, curcumin	(Ray et al., 2022)
Clove	<i>Syzygium aromaticum L.</i>	Buds	Eugenol, caryophyllene	(Abadi et al., 2022)
Peppermint	<i>Mentha piperita</i>	Leaves	Methanol, methanone	(Pérez-Vázquez et al., 2022)
Ginger	<i>Zingiber officinale</i>	Rhizomes	Citral, zingiberene	(Kalhor et al., 2022)
Bay leaf	<i>Laurus nobilis L.</i>	Leaves, flowers	1,8-cineole, linalool, methyleugenol	(Ordoudi et al., 2022)
Cinnamon	<i>Cinnamomum zeylanicum</i>	Leaves, bark	Cinnamaldehyde, eugenol	(Stevens & Allred, 2022)
Tea tree	<i>Melaleuca alternifolia</i>	Leaves, bark	Terpin-4-ol, terpene, 1,8-cineole, p-cymene	(Borotová et al., 2022)
Thyme	<i>Thymus vulgaris L.</i>	Leaves	Thymol, p-cymene, Terpinene	(Ghafarifarsani et al., 2022)
Orange	<i>Citrus aurantium var.</i>	Fruit	D-limonene, β -myrcene	(Radünz et al., 2021)
Nutmeg	<i>Myristica fragrans Houtt.</i>	Seed	Sabinene, limonene, methyl eugenol, myristicin	(Nikolic et al., 2021)
Black pepper	<i>Piper nigrum L.</i>	Leaves, seeds	β -caryophyllene, limonene	(Ashokkumar, Murugan, et al., 2021)
Lavender	<i>Lavanda angustifolia L</i>	Flowers, leaves	Linalool, Linalyl acetate, β -Caryophyllene	(Ciocarlan et al., 2021)
Ajowain	<i>Trachyspermum ammi L.</i>	Seeds, fruits	Thymol, p-cymene, γ -terpinene, carvacrol	(Mazzara et al., 2021)
Fenugreek	<i>Trigonella foenum-graecum L.</i>	Seeds	Linoleic acid, palmitic acid	(Akbari et al., 2019)

Fennel	<i>Foeniculum vulgare</i> Mill.	Seeds	<i>trans</i> -anethole, estragole, limonene, and fenchone	(Sabzi Nojadeh et al., 2021)
Cumin	<i>Cuminum cyminum</i>	Seeds	Cuminaldehyde, γ -terpinene, β -pinene	(Padilla-Camberos et al., 2022)
Allspice	<i>Pimenta dioica</i>	Berries	Eugenol, 1,8-cineole	(Padilla-Camberos et al., 2022)
Coriander	<i>Coriandrum sativum</i> L.	Aerial parts, seeds	Linalool, 2-decenal	(Raveau et al., 2021)
Clary Sage	<i>Salvia sclarea</i> L.	Aerial parts	Linalool, linalyl acetate, Germacrene-D	(Raveau et al., 2021)
Cardamom	<i>Elettaria cardamomum</i> L.	Seeds	α -terpinyl acetate, 1,8-cineole	(Vellaikumar, et al., 2021)
Mint	<i>Mentha piperita</i> L.	Leaves	Piperitenone oxide, 1,8-cineole	(Ilić et al., 2022)
Oregano	<i>Origanum vulgare</i> , L	Leaves	Thymol, bergamol, terpineol	(Radünz et al., 2021)
Sandalwood	<i>Santalum album</i> L.	Bark	α -and β -santalenes	(Raghavendra & Mahesh, 2022)
Rosewood	<i>Aniba rosaeodora</i>	Bark	Linalool, α -terpineol	(Teles et al., 2020)
Cedarwood	<i>Cedar atlantica</i>	Bark	δ -cadinene, β -farnesene	(Kačániová et al., 2022)
Parsley	<i>Petroselinum crispum</i>	Seed	Myristicin, sabinene, β -myrcene	(Foudah et al., 2022)
Star Anise	<i>Illicium verum</i>	Fruit	Trans-anethole, limonene, estragole	(Yu et al., 2021)

Conventionally, the extraction of essential oil was done through expression methods like enfleurage, effleurage and defleurage, hot maceration process, pelatrice method, cold press, dry press method, etc. but they carried some limitations as well. Modern technologies have been developed over the years to overcome these limitations and to enhance the efficiency of extraction. The modern methods are mostly based on the distillation process and solvent extraction. Hydro-distillation, hydro-diffusion and steam distillation methods are collectively called azeotropic distillation.

It is crucial to perform chemical profiling of essential oils to determine their composition and variation in concentration of different constituents present in essential oils extracted from different plants or different plant parts of the same plant or plant parts of different varieties of the same species. This distinction helps in determining the phytoconstituents responsible for

the biological activities of essential oils. The characterization of essential oils for their composition is done through chromatographic techniques like gas chromatography (GC), Liquid Chromatography (LC) etc. coupled with a detection technique like mass spectrometry (MS), flame ionization detection (FID) etc.

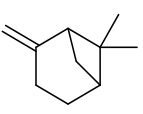
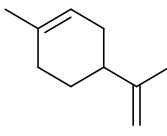
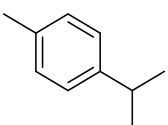
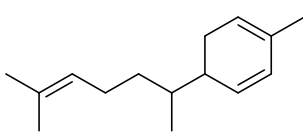
The biological properties of essential oils have generated a wide range of applications. These implications are relevant to both industries and the medicinal fields. The use of synthetic food preservatives has laid roots for skin allergies, cancer, intoxication, and other degenerative conditions. Essential oils have been known to possess antioxidant and antimicrobial activities, and their ability to protect food from pathogenic and spoilage microorganisms raises their eligibility to be used as natural additives in foods and food products. These can also be used as active compounds in packaging materials, by improving their water vapor barrier property associated with their hydrophobic nature. Essential oils are being sought as an alternative to these non-natural products in food preservation(Hussain et al., 2021).

Apart from food preservation, essential oils have also been applied in the field of therapeutics and medicine. Cosmetics and aromatherapy are the leading heads in utilizing the benefits of essential oils. Owing to their insecticidal and plant growth-enhancing properties essential oils have been utilized in the field of agriculture.

2. Sources and Composition

Several plants can be utilized for the extraction of essential oil. However, the part of a plant which acts as the major source of essential oil can always be different. Also, the quantity of different components present in essential oils extracted from different parts of the same plant may vary. The essential oils are mainly composed of low molecular weight (<1000 Da) volatile components, around 85-99%. Essential oils contain over 300 compounds. The chemical composition of essential oils is mostly contributed by secondary metabolites (like terpenes, terpenoids, flavonoids, alkaloids, polyphenols, indigenous pigments, etc.), other aromatic compounds and aliphatic constituents. Terpenes and terpenoids have a structural backbone made up of isoprene units. The structural representation of common terpenes and terpenoids is presented in Table 2. The major compounds found in essential oils are mainly divided into two classes: Terpene hydrocarbons and oxygenated hydrocarbons.

Table 2. Structural representation of common terpenes, terpenoids and flavonoids found in various essential oils

Terpenes					
	pinene	α-terpinene	limonene	p-cymene	zingiberene

Terpenoids	 α -terpineol	 turmerone	 eugenol	 borneol
	 nerol	 geraniol	 linalool	 carvone
	 citronellal	 citronellol	 cinnamaldehyde	 thymol
Flavonoids	 quercetin	 myricetin	 kaempferol	
	 apigenin	 curcumin		

2.1 Terpene Hydrocarbons

Terpenes are a class of aromatic compounds that have a general formula of $(C_5H_8)_n$ and a basic structure formed from 5-carbon-based isoprene (C_5H_8) units. Based on the number of C-units present in the terpenes molecules, they are divided into six classes: hemiterpenes (C_5), monoterpenes (C_{10}), sesquiterpenes (C_{15}), diterpenes (C_{20}), triterpenes (C_{30}) and tetraterpenes (C_{40}). Further higher classes of terpenes are known as carotenoids. Monoterpenes are made up of two isoprene units and are the major components (around 90%) in essential oils.

2.2 Oxygenated Hydrocarbons

These compounds are derived from terpenes and are termed terpenoids (or isoprenoids). Terpenes are modified by the addition of functional groups like alcohol, aldehyde, ketones etc. to form terpenoids. Some examples of terpenoids are represented in Table 3.

Table 3. Examples of Terpenoids

Class	Examples
-------	----------

Phenols	thymol, eugenol, carvacrol, chavicol
Alcohols	borneol, isopulegol, nerolidol, α -santalol, lavanduol, α -terpineol, santalol
Aldehydes	citral, myrtenal, cumin aldehyde, citronellal, cinnamaldehyde, benzaldehyde
Ketones	carvone, menthone, pulegone, fenchone, camphor, thujone, verbenone
Esters	bornyl acetate, linalyl acetate, citronellyl acetate, geranyl acetate
Ethers	1,8-cineole, anethole, elemicin, myristicin
Oxides	1,8-cineole, bisabolone oxide, linalool oxide, sclareol oxide
Lactones	bergaptene, nepetalactone, psoralen, aesculatine, citroptene

3. Extraction of Essential Oils

The process of extraction is crucial in case studies based on essential oils as it defines the quality and quantity of the yield. The extraction method is selected based on the type, state, and form of the plant material. Inappropriate selection of extraction methods may result in loss of bioactivity, natural characteristics, or physical properties. Discolouration, off-odour/flavour, increased viscosity, etc. might also take place. In the worst cases, even alteration of the chemical signature of essential oil may occur. Almost any part of a suitable plant can act as a source and essential oil can be extracted from it to be utilized in applications like food preservation and others. The modern methods are mostly based on the distillation process and solvent extraction.

3.1 Steam Distillation

This method is a common and efficient choice for the extraction of essential oils. The process of steam distillation involves passing steam through crushed or chopped plant material in upward direction. The vapours flowing through the plant material carry the volatile components along with them. The heat carried by steam bursts and breaks the cell structure of plant material and causes the release of phytochemicals. The temperature of steam must always be sufficient for this rupture. The vaporized mixture is then condensed and collected, where the aqueous and non-aqueous components get separated based on their lipophilicity. Figure 1 shows a diagrammatical representation of the steam distillation process. The steam distillation method is efficient in extracting 93% of essential oil and the remaining 7% can be extracted by further processing(Masango, 2005). This method can be coupled with hydrodistillation for better yields(El Kharraf et al., 2021).

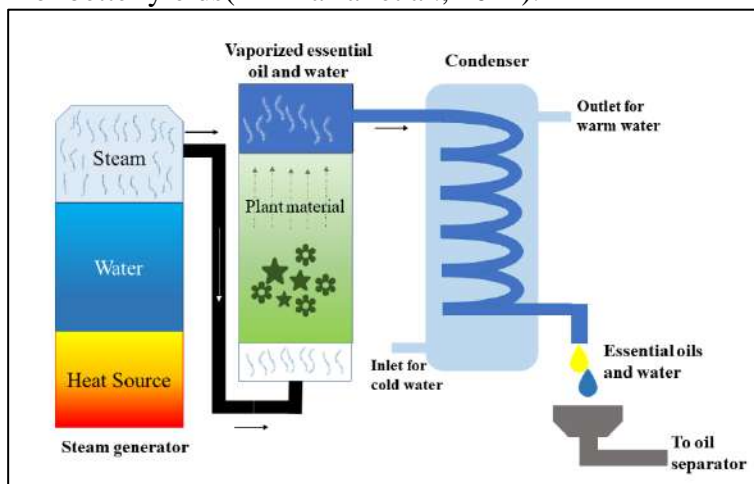


Figure 1. Schematic diagram of steam distillation process.

3.2 Hydro-distillation

Hydro-distillation method for extraction of essential oils involves boiling plant materials completely immersed in water. This method is suitable for capturing the hydrophobic phytochemicals having a high boiling point. The water surrounding plant materials protects them from overheating, which might cause damage to the desired outcome. Upon boiling the essential oil vapors move along with steam and the mixture is allowed to condense. The separation of aqueous and non-aqueous phases takes place upon condensing. Figure 2 shows a diagrammatic representation of the hydro-distillation process. Hydro-distillation method is utilized after coupling it with heating techniques in modern extraction procedures. Microwave-assisted Hydrodistillation(MAHD)(Elyemni et al., 2019), Ultrasonic-assisted hydro-distillation (UAHD)(Sneha et al., 2022) and ohmic-assisted hydrodistillation(Sharifi et al., 2022) are three such cases.

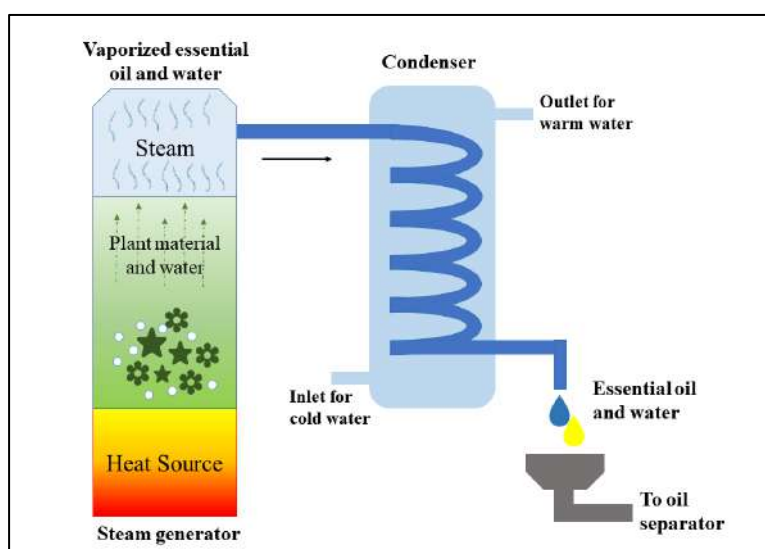


Figure 2. Diagrammatic representation of hydro-distillation.

3.3 Hydro-diffusion

The hydro-diffusion method is similar to the steam-distillation method, as it involves steam as the carrier of heat. In this method, steam is passed from the top of the plant material. This process also protects the plant materials from the damage caused by boiling. Hydro-diffusion method is advantageous over the hydro-distillation method as the processing time is lesser and the yield obtained for a given amount of steam is higher. The traditional hydro-diffusion method has been modified to perform hydro-diffusion and gravity methods(Bousbia et al., 2009).

3.4 Solvent extraction using an organic solvent

Organic solvents like methanol, petroleum ether, ethanol, dimethyl sulphoxide etc. can be utilized for the extraction of essential oils in place of water. Because of the non-aqueous nature of essential oils, this method provides a better yield. This procedure involves mixing plant material with the organic solvent and heating the mixture. This method can be operated efficiently at low temperatures. The mixture is then filtered and the solvent is separated from essential oil by evaporation.

3.5 Solvent extraction using supercritical carbon dioxide

Evaporation of the solvent in the case of organic solvent may lead to the loss of volatile components from essential oil. If not evaporated then the solvent residue may affect the activity of essential oils. Carbon dioxide (CO₂) is capable of forming supercritical fluid at high-pressure conditions. As soon as the room temperature is attained, CO₂ vaporizes leaving no solvent residue. Thus, using supercritical CO₂ is a better option when compared to organic solvents

4. Characterisation Techniques

The modern analytical techniques for the characterisation of essential oils are based on chromatography principles. The essential oil contains both volatile and non-volatile components. The volatile components are analyzed by Gas Chromatography (GC), while non-volatile components are analyzed by Liquid Chromatography (LC).

In both techniques, the components are eluted by the mobile phase and are separated based on their affinity with the stationary phase. In GC, the mobile phase is a carrier gas containing vaporized analytes, while in LC, the mobile phase is a solvent or mixture of solvents. The separated analytes are recorded, and a chromatogram (signal v/s time) is generated following a Gaussian distribution curve scheme. The chromatogram delivers both qualitative and quantitative information. The peak area and height determine the amount of analyte present; the peak width determines the band spreading, and the solute is identified by characteristic retention time, which is also a function of the nature of the solvent.

4.1 Gas Chromatography-Mass Spectrometry (GC-MS)

Mass spectrometry involves the ionization of analytes to generate the gaseous ions, with or without fragmentation. The ions are then analyzed for their mass-to-charge ratios and relative abundances (Todd, 1995). The analytes can be ionized by exposing them to electric fields or energetic species (like electrons, ions, or photons) or thermal methods. Although destructive, this technique is susceptible, requires a small sample size, is lower in expense, simple in design, and caters to fast data acquisition rates.

Gas chromatography coupled with mass spectrometry has great potential in determining the volatile compounds, which hold a significant share in the chemical constitution of essential oils. The mass spectrum of unknown compounds acquired from the GC-MS hyphenated technique is compared against the MS reference library created with standardized protocols of compound analysis. The incorporation of retention indices with MS libraries enhances the accuracy in the identification of compounds (Costa et al., 2007).

4.2 Fast Gas Chromatography

Compared to traditional GC, fast GC provides sufficient resolving power in less time by combining appropriate columns and instrumentation. With improved run conditions, analysis times can be reduced by 3–10 times (Korytár et al., 2002). This technique is more analytically sensitive and efficient in terms of speed. The objective of Fast GC is accomplished by altering some analytical parameters like length and internal diameter (ID) of the column, carrier gas, linear velocity, stationary phase, film thickness, oven temperature, and ramp rate. This method necessitates instruments equipped with high split ratio injection systems to aid smaller sample column capacities, increased inlet pressures, rapid oven heating rates, and fast electronics for detection and data collection.

4.3 GC – Olfactometry

Fuller et al. first modified the gas chromatography to determine the volatile odour activity. The standard GC is incorporated with an olfactory port along with or in place of other detectors. GC-O is utilized in addition to a flame ionization detector (FID), thermal conductivity detector (TCD), mass spectrometer, or photoionization detector.

4.4 Enantioselective GC:

The primary objective of Es-GC is to characterize the enantiomeric excess (ee) and enantiomeric ratio (ER) in chiral compounds. This technique requires a small sample size and provides high separation efficiency and selectivity along with high precision and reproducibility. The resultant information is crucial in characterizing essential oils and is considered equal to ‘fingerprint.’ Es-GC can be hyphenated to MS for more efficiency.

4.5 Liquid Chromatography-Mass Spectrometry (LC-MS)

Although non-volatile components of essential oils hold a small share in their chemical constitution, they are significant when analyzing samples like citrus essential oil obtained by cold pressing methods. Thus, information gathered from GC techniques is not sufficient. Such non-volatile compounds are analyzed using LC, referred to as High-performance LC (HPLC). In normal phase (NP-HPLC) applications, the slightly polar analytes are separated based on their affinities towards an opposite stationary phase and a non-polar mobile phase, and the result is obtained in terms of elution time of analyte, which is highly influenced by the degree of adsorption of the analyte on the stationary phase. In reversed-phase (RP-HPLC) applications, a non-polar stationary phase and a moderately polar aqueous mobile phase are involved. The purified fractions obtained from HPLC or LC techniques are analyzed by coupled mass spectrometry. UV detection and spectrofluorimetric detections have been engaged as analyzing tools.

5. Biological Activities

Essential oils are known to possess various biological activities that can prove to be a boon to humankind if utilized properly.

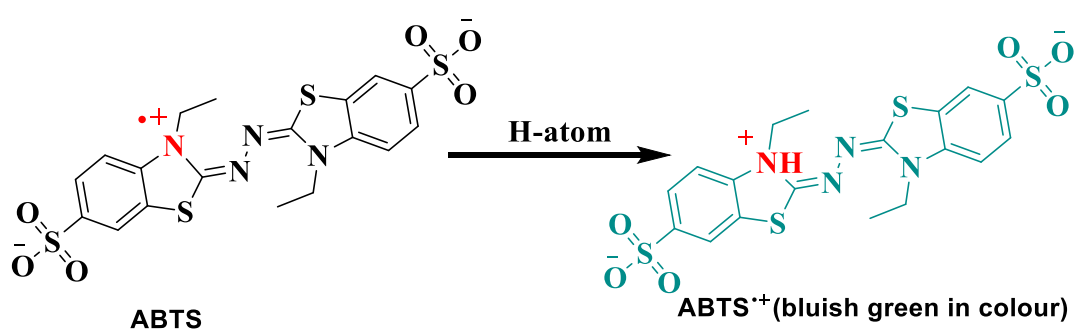
5.1 Antioxidant activity

The production of reactive oxygen species (ROS) and reactive nitrogen species (RNS) as byproducts of various biological processes occurring within the human body is harmful and deteriorating in nature. Studies have bridged the relationship between the oxidative damages caused by ROS and multiple diseases that include ageing (Head, 2008), cancer (Paz-Elizur et al., 2008), diabetes (Jain, 2006), and Parkinson’s disease (Blesa et al., 2015) among many others. To counter these ROS, our body requires antioxidants. Antioxidants are defined as compounds capable of inhibiting or de-escalating an oxidation process. Natural antioxidants, like Vitamin C, Vitamin E, polyphenols/flavonoids, etc., are molecules capable of preventing oxidation of a substrate even when it is present in a lower concentration than the substrate. Studies have reported their effectiveness in preventing the above-mentioned diseases. The antioxidant activities of essential oils can be evaluated through various Hydrogen Atom Transfer (HAT) and Electron Transfer (ET) methods. Some antioxidant assays are categorically listed in Table 4. A schematic representation of some popular assays has been depicted in Figure 3.

Table 4. List of antioxidant assays

Category	List of antioxidant assays
Hydrogen Atom Transfer	Oxygen radical absorbance capacity (ORAC) method
	Lipid peroxidation inhibition capacity (LPIC) assay

methods (HAT)	Total radical trapping antioxidant parameter (TRAP)
	Inhibited oxygen uptake (IOC)
	Crocin bleaching nitric oxide radical inhibition activity
	Scavenging of H ₂ O ₂ radical
	1,2'-azinobis(3-ethylbenzothiazoline-6-sulfonic acid) (ABTS) radical scavenging method
	Scavenging of superoxide radical formation by alkaline
Electron Transfer methods (ET)	Trolox equivalent antioxidant capacity (TEAC)
	Ferric reducing antioxidant power (FRAP)
	2,2-diphenylpicrylhydrazyl (DPPH) free radical scavenging assay
	Copper (II) reduction capacity
	N,N-dimethyl-p-Phenylenediamine (DMPD) assay
Other assays	Total oxidant scavenging capacity (TOSC)
	Inhibition of Briggs-Rauscher oscillation reaction
	Chemiluminescence
	Electrochemiluminescence
	Fluorometric Analysis
	Enhanced chemiluminescence
	TLC bioautography
	Cellular antioxidant (CAA) assay
	Dye-substrate oxidation method



(a) ABTS radical scavenging method

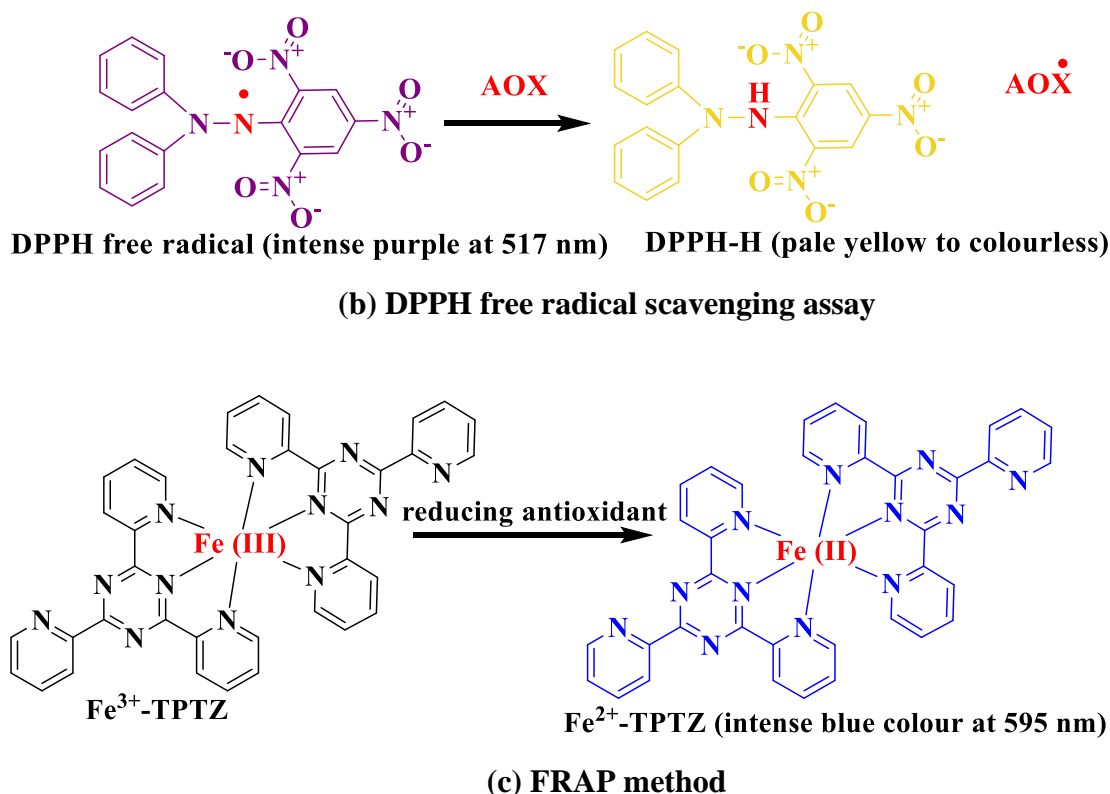


Figure 3. Mechanism of some antioxidant assays (a) ABTS radical scavenging methods, (b) DPPH free radical scavenging assay and (c) FRAP method.

5.2 Anticholinesterase activity

Alzheimer's disease (AD) is a slowly progressive neurodegenerative disease. It is a disorder that causes degeneration of brain cells and is the leading cause of dementia (Cipriani et al., 2011). AD is characterized by neurotic plaques and neurofibrillary tangles, that result from the accumulation of amyloid-beta (A β) peptide in affected areas of the brain, the medial temporal lobe, and neocortical structures (Selkoe, 2001). Disorders like Alzheimer's disease may cause a progressive loss of cognitive functions, which may further result in reduced oxygen supply to the brain, tumours, vitamin B₁₂ deficiency, other nutritional deficiencies, and so on (Nakaizumi et al., 2018). There is currently no widely effective treatment that can stop or slow the progression of Alzheimer's disease. Natural ingredients are expected to play an important role in the emergence of potentially neurodegenerative disorder therapeutic avenues. The utilization of secondary metabolites is beneficial (Sweeney et al., 2018). The inhibition of cholinesterase by essential oils has been investigated using Ellman's colourimetric method (Kamli et al., 2022). The mechanism followed in Ellman's method has been depicted in Figure 4.

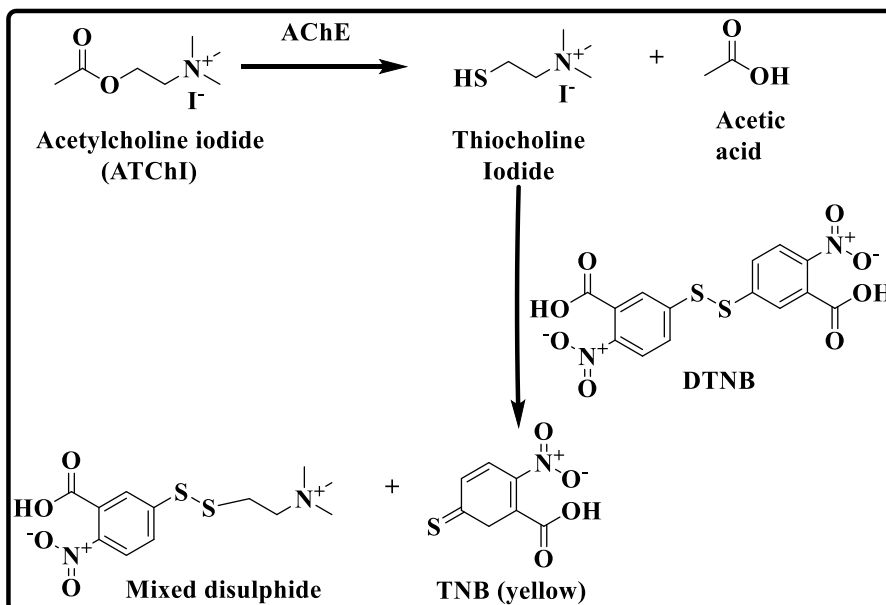


Figure 4. Mechanism of Ellman's method.

5.3 Antimicrobial activity

The bioactive components present in essential oils cause disruption in the cell wall of pathogens. Because of their hydrophobic nature, components of essential oil move rapidly across the lipids of bacterial cell membranes, disrupting cell wall structures and making them more permeable (Figure 5). Essential oils extracted from the plant parts of turmeric(Joshi et al., 2021), pepper(Le et al., 2022), clove(Yoo et al., 2021) etc. have been investigated for their antimicrobial activities.

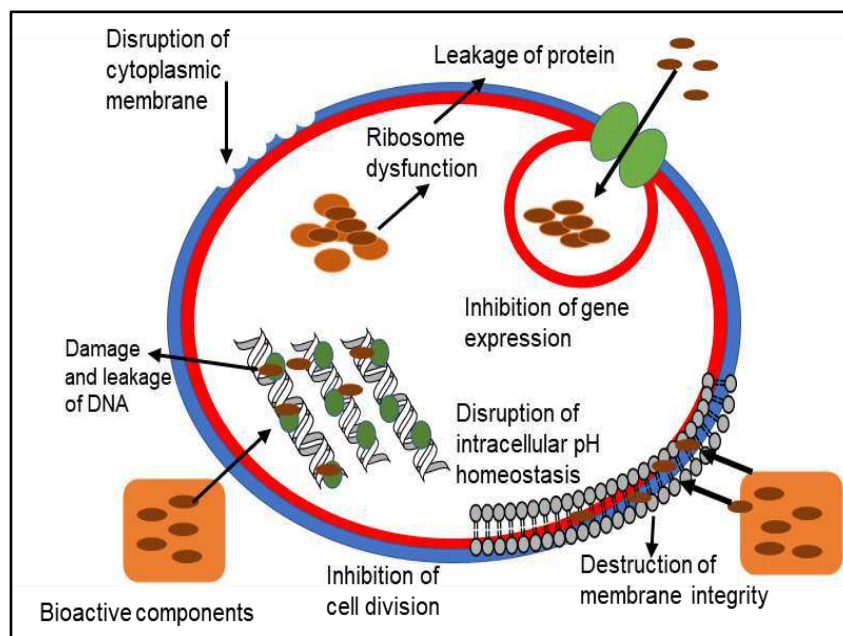


Figure 5. Schematic representation of the antimicrobial action of essential oils(Wang et al., 2020).

5.4 Anti-inflammatory activity

Inflammation is a defense process of human body involving the recognition and removal of foreign stimuli by the immune system. Immune-responsive compounds, cytokines and interleukins are produced by macrophages, keratinocytes and lymphocytes in the human body (Jacob et al., 2013). The components of essential oils like thyme, chamomile, eucalyptus, lavender etc. modulate the transcription of the pro-inflammatory cytokines to reduce inflammation (Pandur et al., 2021).

6. Applications

Essential oils have a wide range of applicability. Different sectors where essential oils have been applied include the Food and beverage industries, paper and printing industries, paint and textiles industries, medical sector, agriculture sector etc. These have also been applied to adhesives, cosmetics and toiletries. The major applications of essential oils are discussed below.

6.1 Food Preservation

Owing to their antimicrobial activity against common food-borne bacteria and fungi, essential oils have been studied and employed for food preservation and increasing their shelf life (Tongnuanchan & Benjakul, 2014). The food industry has utilized several essential oils in the form of flavouring agents and they also have shown potential as food-grade preservatives (Angane et al., 2022). Essential oils have been modified in the form of capsules (Yang et al., 2023), bioactive films (Mohamad et al., 2022), edible coatings (Ju et al., 2019), chitosan-based membranes (Maleki et al., 2022), food packaging (Mukurumbira et al., 2022) etc. to enhance their role as preservatives. Essential oils extracted from herbs and spices have proved to be better than synthetic chemical additives. Essential oils have been applied for the preservation of meat and meat products (Smaoui et al., 2022), bread (Rahman et al., 2022), dairy products (Badola et al., 2023), aquatic food (Shahidi & Hossain, 2022), fruits and vegetables (Pandey et al., 2022). Active packaging of food products using essential oils is highly advantageous as essential oils possess antioxidant and antimicrobial properties that help in shelf-life improvement. Also, the food waste in the case of such packaging can be reused as a source of essential oil. However, the usage of essential oils in food preservation is accompanied by some limitations due to their high volatility, low lipophilicity and easy degradation. These limitations can be resolved by encapsulating essential oils (Carpena et al., 2021).

6.2 Medicines and therapeutics

Essential oils are being studied for their biological properties and have shown results significant to the field of medicine and health care. Aromatherapy is a traditional and most popular application of essential oils in this field and utilizes them to treat several diseases. Aromatherapy utilizes the antiseptic and skin permeability properties of essential oils. Some plants whose essential oils are used in aromatherapy include clary sage, eucalyptus, lavender, lemon, peppermint, rosemary, tea tree etc. The utilization of essential oils in aromatherapy has been reviewed (Ali et al., 2015). The effect of clove essential oil on memory function has also been studied through aromatherapy (Ansariniaki et al., 2022). The application of essential oil to treating skin anomalies (Lee et al., 2022) and dermatological hair problems (Abelan et al., 2022) has been studied recently. Anticancer (Sharma et al., 2022b), anti-inflammatory (Jaradat et al., 2022), antiaging (Lohani & Verma, 2022), and neuroprotective (Rashed et al., 2021) potential of several essential oils have been investigated and they can be employed in the formulation of drugs to counter the aforesaid human-related problems.

6.3 Agriculture

Essential oils can prove to be beneficial in the field of sustainable agriculture. They have shown significant activities against plant pathogens, weeds and a broad spectrum of microorganisms in different *in vitro* and *in planta* studies carried out (Raveau et al., 2020). Due to their remarkable phytotoxic activities, essential oils are suitable candidates for the development of novel bio-herbicides (Wan & Rengasamy, 2022). They also have a potential role as pesticides to play in integrated pest management and organic farming as they are environment-friendly. The biological activities of essential oils have been applied to control plant pests and diseases (Basaid et al., 2021). The insecticidal properties of essential oils have also been studied (Bravim dos Santos et al., 2021). Essential oils have a potential role in extending fruit shelf life by fighting against postharvest pathogens (El Khetabi et al., 2022).

6.4 Cosmetics and Toiletries

Essential oils have emerged as natural ingredients in cosmetics and toiletries due to their odorous character and beneficial biological properties like antioxidant, anti-inflammatory, antimicrobial etc. They have been utilized in the manufacturing of fragrances and perfumes. These oils are used as active ingredients or preservatives in various skin and hair care products like moisturizers, lotions, cleansers, conditioners etc. The application of essential oils and their components in cosmetic products have been properly reviewed recently (Guzmán & Lucia, 2021).

7. Conclusion

Essential oils can be extracted from different parts of a variety of plants. Aromatic plants like spices, flowers, herbs, etc. possessing medicinal properties are chosen for the purpose. The extraction process can be properly chosen to maximize the yield. These oils can be utilized in their natural form or modified into capsules, bio-active films, etc. for their applicability in food preservation. Essential oils and their active agents can act as natural medicine or an alternative to commercially available medicines in the treatment of diseases associated with pathogens and metabolism. If studied properly the essential oils may prove to have the potential to deliver a synergistic effect with the drugs used in the treatment of different diseases. If properly explored to their full potential, essential oils can be a boon to humankind.

8. Future prospects

Owing to the global developments in recent years, the antiviral properties of essential oils can be peculiarly studied and applied for prevention and treatment. The use of natural aromatics for inhalation and their interaction with the central nervous system is an interesting field and can be further explored. Work can still be done to maximize their already existing potential in various fields of food preservation, medicine etc. by enhancing their activities through molecular size-modification, structural rearrangement of components etc. Despite considerable applications, essential oils also showcase some limitations. Firstly, being lipophilic they show less to no interaction with the polar moieties. Secondly, due to their high volatility and instability, their effects are acute. Another important aspect of essential oils is their chemical variability. Being majorly composed of secondary metabolites they are considerably affected by external factors which may degrade their quality over time. Recent studies have suggested the applicability of nanotechnology in the field of essential oils. Preparation of nano formulations of essential oils like nano emulsions, and nano-hydrogels not only promote hydrophilicity but also have the potential to mould essential oils into the desired frame of applications with enhanced stability and bio interaction. Essential oils can

also be encapsulated using nanocontainers and studied for their kinetics and release mechanism. Such methods and studies would intensify their biological applications.

Acknowledgement

The financial support from the Chhattisgarh Council of Science and Technology (CCOST), Raipur (C.G.) is highly acknowledged (1258/CCOST/MRP/2021).

References

- Abadi, A. V. M., Karimi, E., Oskoueian, E., Mohammad, G. R. K. S., and Shafaei, N. (2022). Chemical investigation and screening of anti-cancer potential of *Syzygium aromaticum* L. bud (clove) essential oil nanoemulsion. *3 Biotech*, **12**(2), 1–10. <https://doi.org/10.1007/S13205-022-03117-2>
- Abelan, U. S., de Oliveira, A. C., Cacoci, É. S. P., Martins, T. E. A., Giaccon, V. M., Velasco, M. V. R., and Lima, C. R. R. de C. (2022). Potential use of essential oils in cosmetic and dermatological hair products: A review. *Journal of Cosmetic Dermatology*, **21**(4), 1407–1418. <https://doi.org/10.1111/JOCD.14286>
- Akbari, S., Abdurahman, N. H., Yunus, R. M., Alara, O. R., and Abayomi, O. O. (2019). Extraction, characterization and antioxidant activity of fenugreek (*Trigonella-Foenum Graecum*) seed oil. *Materials Science for Energy Technologies*, **2**(2), 349–355. <https://doi.org/10.1016/J.MSET.2018.12.001>
- AlGabbani, Q., Shater, A. F., Assiri, R., Assiri, G. A., Assiri, A. A., Makhlof, R. T. M., Alsaad, M. A., Alkhalil, S. S., Almuhimed, R. M., Almohaimeed, H. M., and AlDughaisheem, H. (2023). Differential effects of methanolic extracts of clove, ginger, garlic and eucalyptus essential oils on anti-parasitic partivities of *G. lamblia* and *E. histolytica*: an in vitro study. *Rendiconti Lincei*, **34**(3), 853–866. <https://doi.org/10.1007/S12210-023-01173-1>
- Ali, B., Al-Wabel, N. A., Shams, S., Ahamad, A., Khan, S. A., and Anwar, F. (2015). Essential oils used in aromatherapy: A systemic review. *Asian Pacific Journal of Tropical Biomedicine*, **5**(8), 601–611. <https://doi.org/10.1016/J.APJT.2015.05.007>
- Angane, M., Swift, S., Huang, K., Butts, C. A., and Quek, S. Y. (2022). Essential Oils and Their Major Components: An Updated Review on Antimicrobial Activities, Mechanism of Action and Their Potential Application in the Food Industry. *Foods*, **11**(3), 464. <https://doi.org/10.3390/FOODS11030464>
- Ansariniaki, M., Behnam, B., Keyghobady, S., Izadisabet, F., Mirmohammadkhani, M., Abdollahi, M., and Soleimani, M. (2022). The effects of aromatherapy with clove essential oil on memory function of patients during electroconvulsive therapy: A randomized controlled trial. *European Journal of Integrative Medicine*, **51**, 102121. <https://doi.org/10.1016/J.EUJIM.2022.102121>
- Ashokkumar, K., Murugan, M., Dhanya, M. K., Pandian, A., and Warkentin, T. D. (2021). Phytochemistry and therapeutic potential of black pepper [*Piper nigrum* (L.)] essential oil and piperine: a review. *Clinical Phytoscience*, **7**(1), 1–11. <https://doi.org/10.1186/S40816-021-00292-2>
- Ashokkumar, K., Vellaikumar, S., Murugan, M., Dhanya, M. K., Ariharasutharsan, G., Aiswarya, S., Akilan, M., Warkentin, T. D., and Karthikeyan, A. (2021). Essential Oil

- Profile Diversity in Cardamom Accessions From Southern India. *Frontiers in Sustainable Food Systems*, **5**, 639619. <https://doi.org/10.3389/FSUFS.2021.639619>
- Badola, R., Prasad, W., Panjagari, N. R., Singh, R. R. B., Singh, A. K., & Hussain, S. A. (2023). Khoa and khoa based traditional dairy products: preparation, spoilage and shelf life extension. *Journal of Food Science and Technology*, **60**(4), 1209–1221. <https://doi.org/10.1007/S13197-022-05355-X>
- Basaid, K., Chebli, B., Mayad, E. H., Furze, J. N., Bouharroud, R., Krier, F., Barakate, M., and Paulitz, T. (2021). Biological activities of essential oils and lipopeptides applied to control plant pests and diseases: a review. *International Journal of Pest Management*, **67**(2), 155–177. <https://doi.org/10.1080/09670874.2019.1707327>
- Blesa, J., Trigo-Damas, I., Quiroga-Varela, A., and Jackson-Lewis, V. R. (2015). Oxidative stress and Parkinson's disease. *Frontiers in Neuroanatomy*, **9**(July), 147963. <https://doi.org/10.3389/FNANA.2015.00091>
- Borotová, P., Galovičová, L., Vukovic, N. L., Vukic, M., Tvrdá, E., and Kačániová, M. (2022). Chemical and Biological Characterization of Melaleuca alternifolia Essential Oil. *Plants*, **11**(4), 558. <https://doi.org/10.3390/PLANTS11040558>
- Bousbia, N., Abert Vian, M., Ferhat, M. A., Petitcolas, E., Meklati, B. Y., and Chemat, F. (2009). Comparison of two isolation methods for essential oil from rosemary leaves: Hydrodistillation and microwave hydrodiffusion and gravity. *Food Chemistry*, **114**(1), 355–362. <https://doi.org/10.1016/J.FOODCHEM.2008.09.106>
- Bravim dos Santos, A. T., Zanuncio Junior, J. S., Parreira, L. A., Pedra de Abreu, K. M., de Oliveira Bernardes, C., Romário de Carvalho, J., and Menini, L. (2021). Chemical identification and insecticidal effect of Tephrosia vogelii essential oil against Cerosipha forbesi in strawberry crop. *Crop Protection*, **139**, 105405. <https://doi.org/10.1016/J.CROPRO.2020.105405>
- Carpena, M., Nuñez-Estevez, B., Soria-Lopez, A., Garcia-Oliveira, P., and Prieto, M. A. (2021). Essential Oils and Their Application on Active Packaging Systems: A Review. *Resources*, **10**(1), 7. <https://doi.org/10.3390/RESOURCES10010007>
- Ciocarlan, A., Lupascu, L., Aricu, A., Dragalin, I., Popescu, V., Geana, E. I., Ionete, R. E., Vornicu, N., Dului, O. G., Hristozova, G., and Zinicovscaia, I. (2021). Chemical Composition and Assessment of Antimicrobial Activity of Lavender Essential Oil and Some By-Products. *Plants*, **10**(9), 1829. <https://doi.org/10.3390/PLANTS10091829>
- Cipriani, G., Dolciotti, C., Picchi, L., and Bonuccelli, U. (2011). Alzheimer and his disease: A brief history. *Neurological Sciences*, **32**(2), 275–279. <https://doi.org/10.1007/S10072-010-0454-7>
- Costa, R., Fina, M. R. De, Valentino, M. R., Dugo, P., and Mondello, L. (2007). Reliable Identification of Terpenoids and Related Compounds by using Linear Retention Indices Interactively with Mass Spectrometry Search. *Natural Product Communications*, **2**(4), 413–418. <https://doi.org/10.1177/1934578X0700200412>
- da Silva, W. M. F., Kringel, D. H., de Souza, E. J. D., da Rosa Zavareze, E., and Dias, A. R. G. (2021). Basil Essential Oil: Methods of Extraction, Chemical Composition, Biological Activities, and Food Applications. *Food and Bioprocess Technology*, **15**(1), 1–27. <https://doi.org/10.1007/S11947-021-02690-3>
- El Kharraf, S., El-Guendouz, S., Farah, A., Bennani, B., Mateus, M. C., El Hadrami, E. M., and Miguel, M. G. (2021). Hydrodistillation and simultaneous hydrodistillation-steam

- distillation of *Rosmarinus officinalis* and *Origanum compactum*: Antioxidant, anti-inflammatory, and antibacterial effect of the essential oils. *Industrial Crops and Products*, **168**, 113591. <https://doi.org/10.1016/J.INDCROP.2021.113591>
- El Khetabi, A., Lahlali, R., Ezrari, S., Radouane, N., Lyousfi, N., Banani, H., Askarne, L., Tahiri, A., El Ghadraoui, L., Belmalha, S., and Barka, E. A. (2022). Role of plant extracts and essential oils in fighting against postharvest fruit pathogens and extending fruit shelf life: A review. *Trends in Food Science & Technology*, **120**, 402–417. <https://doi.org/10.1016/J.TIFS.2022.01.009>
- Elyemni, M., Louaste, B., Nechad, I., Elkamli, T., Bouia, A., Taleb, M., Chaouch, M., and Eloutassi, N. (2019). Extraction of Essential Oils of *Rosmarinus officinalis* L. by Two Different Methods: Hydrodistillation and Microwave Assisted Hydrodistillation. *Scientific World Journal*, <https://doi.org/10.1155/2019/3659432>
- Foudah, A. I., Alqarni, M. H., Alam, A., Salkini, M. A., Ross, S. A., and Yusufoglu, H. S. (2022). Phytochemical Screening, In Vitro and In Silico Studies of Volatile Compounds from *Petroselinum crispum* (Mill) Leaves Grown in Saudi Arabia. *Molecules*, **27(3)**, 934. <https://doi.org/10.3390/MOLECULES27030934>
- Garzoli, S. (2023). Chemical Composition and Antimicrobial Activity of Essential Oils. *Plants*, **12(4)**, 800. <https://doi.org/10.3390/PLANTS12040800>
- Ghafariarsani, H., Hoseinifar, S. H., Javahery, S., Yazici, M., and Van Doan, H. (2022). Growth performance, biochemical parameters, and digestive enzymes in common carp (*Cyprinus carpio*) fed experimental diets supplemented with vitamin C, thyme essential oil, and quercetin. *Italian Journal of Animal Science*, **21(1)**, 291–302. <https://doi.org/10.1080/1828051X.2021.1965923>
- Guzmán, E., and Lucia, A. (2021). Essential Oils and Their Individual Components in Cosmetic Products. *Cosmetics*, **8(4)**, 114. <https://doi.org/10.3390/COSMETICS8040114>
- Head, E. (2008). Oxidative Damage and Cognitive Dysfunction: Antioxidant Treatments to Promote Healthy Brain Aging. *Neurochemical Research*, **34(4)**, 670–678. <https://doi.org/10.1007/S11064-008-9808-4>
- Hussain, M. A., Sumon, T. A., Mazumder, S. K., Ali, M. M., Jang, W. J., Abualreesh, M. H., Sharifuzzaman, S. M., Brown, C. L., Lee, H. T., Lee, E. W., and Hasan, M. T. (2021). Essential oils and chitosan as alternatives to chemical preservatives for fish and fisheries products: A review. *Food Control*, **129**, 108244. <https://doi.org/10.1016/J.FOODCONT.2021.108244>
- Ilić, Z. S., Milenković, L., Tmušić, N., Stanojević, L., Stanojević, J., and Cvetković, D. (2022). Essential oils content, composition and antioxidant activity of lemon balm, mint and sweet basil from Serbia. *LWT*, **153**, 112210. <https://doi.org/10.1016/J.LWT.2021.112210>
- Jacob, J. N., Badyal, D. K., and Bala, S. (2013). Evaluation of the In Vivo Anti-Inflammatory and Analgesic Activity of a Highly Water-Soluble Aspirin Conjugate. *Basic & Clinical Pharmacology & Toxicology*, **112(3)**, 171–174. <https://doi.org/10.1111/BCPT.12006>
- Jain, S. K. (2006). Superoxide dismutase overexpression and cellular oxidative damage in diabetes: A commentary on “Overexpression of mitochondrial superoxide dismutase in mice protects the retina from diabetes-induced oxidative stress.” *Free Radical Biology and Medicine*, **41(8)**, 1187–1190. <https://doi.org/10.1016/J.FREERADBIOMED.2006.07.017>

- Jaradat, N., Qneibi, M., Hawash, M., Al-Maharik, N., Qadi, M., Abualhasan, M. N., Ayesh, O., Bsharat, J., Khadir, M., Morshed, R., Yaaqbeh, S., Marei, S., Hamayel, S., Mousa, A., Daqqa, M., and Bdir, S. (2022). Assessing *Artemisia arborescens* essential oil compositions, antimicrobial, cytotoxic, anti-inflammatory, and neuroprotective effects gathered from two geographic locations in Palestine. *Industrial Crops and Products*, **176**, 114360. <https://doi.org/10.1016/J.INDCROP.2021.114360>
- Joshi, P., Joshi, S., Semwal, D. K., Bisht, A., Sharma, S., and Dwivedi, J. (2021). Chemical composition, antioxidative and antimicrobial activities of turmeric spent oleoresin. *Industrial Crops and Products*, **162**, 113278. <https://doi.org/10.1016/J.INDCROP.2021.113278>
- Ju, J., Xie, Y., Guo, Y., Cheng, Y., Qian, H., and Yao, W. (2019). Application of edible coating with essential oil in food preservation. *Critical Reviews in Food Science and Nutrition*, **59(15)**, 2467–2480. <https://doi.org/10.1080/10408398.2018.1456402>
- Kačániová, M., Galovičová, L., Valková, V., Ďuranová, H., Štefániková, J., Čmiková, N., Vukic, M., Vukovic, N. L., and Kowalczewski, P. Ł. (2022). Chemical Composition, Antioxidant, In Vitro and In Situ Antimicrobial, Antibiofilm, and Anti-Insect Activity of Cedar atlantica Essential Oil. *Plants* 2022, **11(3)**, 358. <https://doi.org/10.3390/PLANTS11030358>
- Kalhor, M. T., Zhang, H., Kalhor, G. M., Wang, F., Chen, T., Faqir, Y., and Nabi, F. (2022). Fungicidal properties of ginger (*Zingiber officinale*) essential oils against *Phytophthora colocasiae*. *Scientific Reports*, **12(1)**, 1–10. <https://doi.org/10.1038/s41598-022-06321-5>
- Kamli, M. R., Sharaf, A. A. M., Sabir, J. S. M., and Rather, I. A. (2022). Phytochemical Screening of *Rosmarinus officinalis* L. as a Potential Anticholinesterase and Antioxidant–Medicinal Plant for Cognitive Decline Disorders. *Plants*, **11(4)**, 514. <https://doi.org/10.3390/PLANTS11040514/S1>
- Korytár, P., Janssen, H. G., Matisová, E., and Brinkman, U. A. T. (2002). Practical fast gas chromatography: methods, instrumentation and applications. *TrAC Trends in Analytical Chemistry*, **21(9–10)**, 558–572. [https://doi.org/10.1016/S0165-9936\(02\)00811-7](https://doi.org/10.1016/S0165-9936(02)00811-7)
- Le, N. V., Sam, L. N., Huong, L. T., and Ogunwande, I. A. (2022). Chemical Compositions of Essential Oils and Antimicrobial Activity of *Piper albispicum* C. DC. from Vietnam. *Journal of Essential Oil Bearing Plants*, **25(1)**, 82–92. <https://doi.org/10.1080/0972060X.2022.2032840>
- Lee, S. H., Chow, P. S., and Yagnik, C. K. (2022). Developing Eco-Friendly Skin Care Formulations with Microemulsions of Essential Oil. *Cosmetics*, **9(2)**, 30. <https://doi.org/10.3390/COSMETICS9020030>
- Lohani, A., and Verma, A. (2022). Lipid vesicles: potential nanocarriers for the delivery of essential oils to combat skin aging. *Nanotechnology for the Preparation of Cosmetics Using Plant-Based Extracts*, 131–156. <https://doi.org/10.1016/B978-0-12-822967-5.00006-0>
- Maleki, G., Woltering, E. J., and Mozafari, M. R. (2022). Applications of chitosan-based carrier as an encapsulating agent in food industry. *Trends in Food Science & Technology*, **120**, 88–99. <https://doi.org/10.1016/J.TIFS.2022.01.001>
- Masango, P. (2005). Cleaner production of essential oils by steam distillation. *Journal of Cleaner Production*, **13(8)**, 833–839. <https://doi.org/10.1016/J.JCLEPRO.2004.02.039>

- Mazzara, E., Scortichini, S., Fiorini, D., Maggi, F., Petrelli, R., Cappellacci, L., Morgese, G., Morshedloo, M. R., Palmieri, G. F., and Cespi, M. (2021). A design of experiment (Doe) approach to model the yield and chemical composition of ajowan (*trachyspermum ammi* L.) essential oil obtained by microwave-assisted extraction. *Pharmaceuticals*, **14**(8), 816. <https://doi.org/10.3390/PH14080816>
- Mohamad, N., Mazlan, M. M., Tawakkal, I. S. M. A., Talib, R. A., Kian, L. K., and Jawaid, M. (2022). Characterization of Active Polybutylene Succinate Films Filled Essential Oils for Food Packaging Application. *Journal of Polymers and the Environment*, **30**(2), 585–596. <https://doi.org/10.1007/S10924-021-02198>
- Mukurumbira, A. R., Shellie, R. A., Keast, R., Palombo, E. A., and Jadhav, S. R. (2022). Encapsulation of essential oils and their application in antimicrobial active packaging. *Food Control*, **136**, 108883. <https://doi.org/10.1016/J.FOODCONT.2022.108883>
- Nakaizumi, K., Ouchi, Y., Terada, T., Yoshikawa, E., Kakimoto, A., Isobe, T., Bunai, T., Yokokura, M., Suzuki, K., and Magata, Y. (2018). In vivo Depiction of $\alpha 7$ Nicotinic Receptor Loss for Cognitive Decline in Alzheimer's Disease. *Journal of Alzheimer's Disease*, **61**(4), 1355–1365. <https://doi.org/10.3233/JAD-170591>
- Nikolic, V., Nikolic, L., Dinic, A., Gajic, I., Urosevic, M., Stanojevic, L., Stanojevic, J., and Danilovic, B. (2021). Chemical Composition, Antioxidant and Antimicrobial Activity of Nutmeg (*Myristica fragrans* Houtt.) Seed Essential Oil. *Journal of Essential Oil Bearing Plants*, **24**(2), 218–227. <https://doi.org/10.1080/0972060X.2021.1907230>
- Ordoudi, S. A., Papapostolou, M., Nenadis, N., Mantzouridou, F. T., and Tsimidou, M. Z. (2022). Bay Laurel (*Laurus nobilis* L.) Essential Oil as a Food Preservative Source: Chemistry, Quality Control, Activity Assessment, and Applications to Olive Industry Products. *Foods*, **11**(5), 752. <https://doi.org/10.3390/FOODS11050752>
- Padilla-Camberos, E., Sanchez-Hernandez, I. M., Torres-Gonzalez, O. R., Gallegos-Ortiz, M. del R., Méndez-Mona, A. L., Baez-Moratilla, P., and Flores-Fernandez, J. M. (2022). Natural essential oil mix of sweet orange peel, cumin, and allspice elicits anti-inflammatory activity and pharmacological safety similar to non-steroidal anti-inflammatory drugs. *Saudi Journal of Biological Sciences*, **29**(5), 3830–3837. <https://doi.org/10.1016/J.SJBS.2022.03.002>
- Pandey, V. K., Islam, R. U., Shams, R., and Dar, A. H. (2022). A comprehensive review on the application of essential oils as bioactive compounds in Nano-emulsion based edible coatings of fruits and vegetables. *Applied Food Research*, **2**(1), 100042. <https://doi.org/10.1016/J.AFRES.2022.100042>
- Pandur, E., Balatináč, A., Micalizzi, G., Mondello, L., Horváth, A., Sipos, K., and Horváth, G. (2021). Anti-inflammatory effect of lavender (*Lavandula angustifolia* Mill.) essential oil prepared during different plant phenophases on THP-1 macrophages. *BMC Complementary Medicine and Therapies*, **21**(1), 1–17. <https://doi.org/10.1186/S12906-021-03461-5>
- Paz-Elizur, T., Sevilya, Z., Leitner-Dagan, Y., Elinger, D., Roisman, L. C., and Livneh, Z. (2008). DNA repair of oxidative DNA damage in human carcinogenesis: Potential application for cancer risk assessment and prevention. *Cancer Letters*, **266**(1), 60–72. <https://doi.org/10.1016/J.CANLET.2008.02.032>
- Pérez-Vázquez, M. A. K., Pacheco-Hernández, Y., Lozoya-Gloria, E., Mosso-González, C., Ramírez-García, S. A., Romero-Arenas, O., and Villa-Ruano, N. (2022). Peppermint

- Essential Oil and Its Major Volatiles as Protective Agents against Soft Rot Caused by *Fusarium sambucinum* in Cera Pepper (*Capsicum pubescens*). *Chemistry and Biodiversity*, **19**(1). <https://doi.org/10.1002/CBDV.202100835>
- Radünz, M., Mota Camargo, T., Santos Hackbart, H. C. dos, Inchauspe Correa Alves, P., Radünz, A. L., Avila Gandra, E., and da Rosa Zavareze, E. (2021). Chemical composition and in vitro antioxidant and antihyperglycemic activities of clove, thyme, oregano, and sweet orange essential oils. *LWT*, **138**, 110632. <https://doi.org/10.1016/J.LWT.2020.110632>
- Raghavendra, N. R., and Mahesh, H. B. (2022). *Sandalwood Essential Oil and Its Phyto-Chemistry*. 83–88. <https://doi.org/10.1007/978-3-030-93394-4>
- Rahman, M., Islam, R., Hasan, S., Zzaman, W., Rana, M. R., Ahmed, S., Roy, M., Sayem, A., Matin, A., Raposo, A., Zandonadi, R. P., Botelho, R. B. A., and Sunny, A. R. (2022). A Comprehensive Review on Bio-Preservation of Bread: An Approach to Adopt Wholesome Strategies. *Foods*, **11**(3), 319. <https://doi.org/10.3390/FOODS11030319>
- Raina, K., Kumari, R., Thakur, P., Sharma, R., Singh, R., Thakur, A., Anand, V., Sharma, R., and Chaudhary, A. (2023). Mechanistic role and potential of Ayurvedic herbs as anti-aging therapies. *Drug Metabolism and Personalized Therapy*. <https://doi.org/10.1515/DMDI-2023-0024>
- Rasgele, P. G., and Altin, N. (2023). Characterization of Essential Oils from Medicinal Plants and Assessment of Their Antimutagenic Effects Using Ames Salmonella/Microsomal Test. *Proceedings of the Bulgarian Academy of Sciences*, **76**(2), 192–202. <https://doi.org/10.7546/CRABS.2023.02.03>
- Rashed, A. A., Rahman, A. Z. A., and Rathi, D. N. G. (2021). Essential Oils as a Potential Neuroprotective Remedy for Age-Related Neurodegenerative Diseases: A Review. *Molecules*, **26**(4), 1107. <https://doi.org/10.3390/MOLECULES26041107>
- Raveau, R., Fontaine, J., and Lounès-Hadj Sahraoui, A. (2020). Essential Oils as Potential Alternative Biocontrol Products against Plant Pathogens and Weeds: A Review. *Foods*, **9**(3), 365. <https://doi.org/10.3390/FOODS9030365>
- Raveau, R., Fontaine, J., Verdin, A., Mistrulli, L., Laruelle, F., Fourmentin, S., and Sahraoui, A. L. H. (2021). Chemical Composition, Antioxidant and Anti-Inflammatory Activities of Clary Sage and Coriander Essential Oils Produced on Polluted and Amended Soils-Phytomanagement Approach. *Molecules*, **26**(17), 5321. <https://doi.org/10.3390/MOLECULES26175321>
- Ray, A., Mohanty, S., Jena, S., Sahoo, A., Acharya, L., Panda, P. C., Sial, P., Duraisamy, P., and Nayak, S. (2022). Drying methods affects physicochemical characteristics, essential oil yield and volatile composition of turmeric (*Curcuma longa* L.). *Journal of Applied Research on Medicinal and Aromatic Plants*, **26**, 100357. <https://doi.org/10.1016/J.JARMAP.2021.100357>
- Sabzi Nojadeh, M., Pouresmaeil, M., Younessi-Hamzekhanlu, M., and Venditti, A. (2021). Phytochemical profile of fennel essential oils and possible applications for natural antioxidant and controlling *Convolvulus arvensis* L. *Natural Product Research*, **35**(21), 4164–4168. <https://doi.org/10.1080/14786419.2020.1741580>
- Selkoe, D. J. (2001). Alzheimer's disease results from the cerebral accumulation and cytotoxicity of amyloid beta-protein. *Journal of Alzheimer's Disease: JAD*, **3**(1), 75–81. <https://doi.org/10.3233/JAD-2001-3111>

- Shahidi, F., and Hossain, A. (2022). Preservation of aquatic food using edible films and coatings containing essential oils: a review. *Critical Reviews in Food Science and Nutrition*, **62**(1), 66–105. <https://doi.org/10.1080/10408398.2020.1812048>
- Sharifi, A., Hamidi-Esfahani, Z., Ahmadi Gavlighi, H., and Saberian, H. (2022). Assisted ohmic heating extraction of pectin from pomegranate peel. *Chemical Engineering and Processing - Process Intensification*, **172**, 108760. <https://doi.org/10.1016/J.CEP.2021.108760>
- Sharma, M., Grewal, K., Jandrotia, R., Batish, D. R., Singh, H. P., and Kohli, R. K. (2022a). Essential oils as anticancer agents: Potential role in malignancies, drug delivery mechanisms, and immune system enhancement. *Biomedicine & Pharmacotherapy*, **146**, 112514. <https://doi.org/10.1016/J.BIOPHA.2021.112514>
- Sharma, M., Grewal, K., Jandrotia, R., Batish, D. R., Singh, H. P., and Kohli, R. K. (2022b). Essential oils as anticancer agents: Potential role in malignancies, drug delivery mechanisms, and immune system enhancement. *Biomedicine & Pharmacotherapy*, **146**, 112514. <https://doi.org/10.1016/J.BIOPHA.2021.112514>
- Smaoui, S., Ben Hlima, H., Tavares, L., Ennouri, K., Ben Braiek, O., Mellouli, L., Abdelkafi, S., and Mousavi Khaneghah, A. (2022). Application of essential oils in meat packaging: A systemic review of recent literature. *Food Control*, **132**, 108566. <https://doi.org/10.1016/J.FOODCONT.2021.108566>
- Sneha, K., Narayanankutty, A., Job, J. T., Olatunji, O. J., Alfarhan, A., Famurewa, A. C., and Ramesh, V. (2022). Antimicrobial and Larvicidal Activities of Different Ocimum Essential Oils Extracted by Ultrasound-Assisted Hydrodistillation. *Molecules*, **27**(5), 1456. <https://doi.org/10.3390/MOLECULES27051456>
- Stevens, N., and Allred, K. (2022). Antidiabetic Potential of Volatile Cinnamon Oil: A Review and Exploration of Mechanisms Using In Silico Molecular Docking Simulations. *Molecules*, **27**(3), 853. <https://doi.org/10.3390/MOLECULES27030853>
- Sweeney, M. D., Sagare, A. P., and Zlokovic, B. V. (2018). Blood–brain barrier breakdown in Alzheimer disease and other neurodegenerative disorders. *Nature Reviews Neurology*, **14**(3), 133–150. <https://doi.org/10.1038/nrneurol.2017.188>
- Tajkarimi, M. M., Ibrahim, S. A., and Cliver, D. O. (2010). Antimicrobial herb and spice compounds in food. *Food Control*, **21**(9), 1199–1218. <https://doi.org/10.1016/J.FOODCONT.2010.02.003>
- Teles, A. M., Silva-Silva, J. V., Fernandes, J. M. P., Calabrese, K. da S., Abreu-Silva, A. L., Marinho, S. C., Mouchrek, A. N., Filho, V. E. M., and Almeida-Souza, F. (2020). Aniba rosaedora (Var. amazonica Ducke) Essential Oil: Chemical Composition, Antibacterial, Antioxidant and Antitrypanosomal Activity. *Antibiotics*, **10**(1), 24. <https://doi.org/10.3390/ANTIBIOTICS10010024>
- Tit, D. M., and Bungau, S. G. (2023). Antioxidant Activity of Essential Oils. *Antioxidants*, **12**(2), 383. <https://doi.org/10.3390/ANTIOX12020383>
- Todd, J. F. J. (1995). Recommendations for nomenclature and symbolism for mass spectroscopy. *International Journal of Mass Spectrometry and Ion Processes*, **142**(3), 209–240. [https://doi.org/10.1016/0168-1176\(95\)93811](https://doi.org/10.1016/0168-1176(95)93811)
- Tongnuanchan, P., and Benjakul, S. (2014). Essential Oils: Extraction, Bioactivities, and Their Uses for Food Preservation. *Journal of Food Science*, **79**(7), R1231–R1249. <https://doi.org/10.1111/1750-3841.12492>

- Wan, C., and Rengasamy, K. R. R. (2022). Editorial: Application of Plant Natural Products and New Emerging Technologies for the Postharvest Storage of Fruits. *Frontiers in Nutrition*, **9**, 884438. <https://doi.org/10.3389/FNUT.2022.884438>
- Wang, X., Shen, Y., Thakur, K., Han, J., Zhang, J. G., Hu, F., and Wei, Z. J. (2020). Antibacterial Activity and Mechanism of Ginger Essential Oil against *Escherichia coli* and *Staphylococcus aureus*. *Molecules*, **25(17)**, 3955. <https://doi.org/10.3390/MOLECULES25173955>
- Yang, T., Qin, W., Zhang, Q., Luo, J., Lin, D., and Chen, H. (2023). Essential-oil capsule preparation and its application in food preservation: A review. *Food Reviews International*, **39(7)**, 4124–4158. <https://doi.org/10.1080/87559129.2021.2021934>
- Yoo, J. H., Baek, K. H., Heo, Y. S., Yong, H. I., and Jo, C. (2021). Synergistic bactericidal effect of clove oil and encapsulated atmospheric pressure plasma against *Escherichia coli* O157:H7 and *Staphylococcus aureus* and its mechanism of action. *Food Microbiology*, **93**, 103611. <https://doi.org/10.1016/J.FM.2020.103611>
- Yu, C. Y., Zhang, J. F., and Wang, T. (2021). Star anise essential oil : chemical compounds, antifungal and antioxidant activities: a review. *Journal of Essential Oil Research*, **33(1)**, 1–22. <https://doi.org/10.1080/10412905.2020.1813213>
- Zhao, Q., Zhu, L., Wang, S., Gao, Y., and Jin, F. (2023). Molecular mechanism of the anti-inflammatory effects of plant essential oils: A systematic review. *Journal of Ethnopharmacology*, **301**, 115829. <https://doi.org/10.1016/J.JEP.2022.115829>